PNWD-3677
WTP-RPT-127 Rev. 0

Overview of the Pulse Jet Mixer Non-Newtonian Scaled Test Program

P. A. Meyer
D. E. Kurath
C. W. Stewart

December 2005

Prepared for Bechtel National, Inc.
under Contract No. 24590-101-TSA-W000-00004

LEGAL NOTICE

This report was prepared by Battelle – Pacific Northwest Division (Battelle) as an account of sponsored research activities. Neither Client nor Battelle nor any person acting on behalf of either:

MAKES ANY WARRANTY OR REPRESENTATION, EXPRESS OR IMPLIED, with respect to the accuracy, completeness, or usefulness of the information contained in this report, or that the use of any information, apparatus, process, or composition disclosed in this report may not infringe privately owned rights; or

Assumes any liabilities with respect to the use of, or for damages resulting from the use of, any information, apparatus, process, or composition disclosed in this report.

References herein to any specific commercial product, process, or service by trade name, trademark, manufacturer, or otherwise, does not necessarily constitute or imply its endorsement, recommendation, or favoring by Battelle. The views and opinions of authors expressed herein do not necessarily state or reflect those of Battelle.

Overview of the Pulse Jet Mixer Non-Newtonian Scaled Test Program

P. A. Meyer
D. E. Kurath
C. W. Stewart

December 2005

	PNWD	SRNL
Test Specification	24590-WTP-TSP-RT-03-006 Rev. 0	24590-WTP-TSP-RT-03-007 Rev. 0
	24590-WTP-TSP-RT-03-008 Rev. 0	24590-HLW-TSP-RT-03-008 Rev. 0
	24590-WTP-TSP-RT-03-010 Rev. 0	
	24590-WTP-TSP-RT-04-0002 Rev. 0	
Test Plan	TP-RPP-WTP-385 Rev. 0	SRT-RPP-2003-00174 Rev 0
	TP-RPP-WTP-290 Rev. 0	WSRC-TR-2003-00410
	TP-RPP-WTP-296, Rev. 0	
	TP-RPP-WTP-326 Rev. 0	
Test Exceptions	24590-WTP-TEF-RT-04-002	24590-WTP-TEF-RT-03-059
	24590-WTP-TEF-RT-04-00004	24590-WTP-TEF-RT-03-085
	24590-WTP-TEF-RT-04-00005	24590-WTP-TEF-RT-04-001
	24590-WTP-TEF-RT-04-00008	24590-WTP-TEF-RT-04-006
	24590-WTP-TEF-RT-04-00020	
	24590-WTP-TEF-RT-04-00029	
	24590-WTP-TEF-RT-04-00033	
	24590-WTP-TEF-RT-04-00037	
	24590-WTP-TEF-RT-03-052	
	24590-WTP-TEF-RT-03-053	
	24590-WTP-TEF-RT-03-058	
	24590-WTP-TEF-RT-03-060	
	24590-WTP-TEF-RT-03-081	
	24590-WTP-TEF-RT-03-082	
	24590-WTP-TEF-RT-03-083	
	24590-WTP-TEF-RT-03-090	
R&T focus area	Pretreatment & Vitrification	Pretreatment & Vitrification
Test Scoping Statement(s)	B-100	

ACCEPTED FOR
WTP PROJECT USE

Battelle – Pacific Northwest Division
Richland, Washington, 99352

Completeness of Testing

This report summarizes the results of work and testing specified by the Test Specifications and Test Plans listed on the inside title page. The work and any associated testing followed the quality assurance requirements outlined in the Test Specifications/Plans. The descriptions provided in this test report are an accurate account of both the conduct of the work and the data collected. A summary of the test plan results is reported. Also reported are any unusual or anomalous occurrences that are different from expected results. The test results and this report have been reviewed and verified.

Approved:

Gordon H. Beeman, Manager
WTP R&T Support Project

12/20/05
Date

Testing Summary

The U.S. Department of Energy (DOE) Office of River Protection's Waste Treatment Plant (WTP) will process and treat radioactive waste that is stored in underground tanks at the Hanford Site. Pulse jet mixers (PJMs), along with air spargers and steady jets generated by recirculation pumps, have been selected for mixing the high-level waste (HLW) slurries in the HLW lag storage (LS) vessels, the HLW blend vessel, and the ultrafiltration feed process (UFP) vessels. These mixing technologies are collectively called PJM/hybrid mixing systems.

This report provides a summary of an extensive effort spanning more than two years to develop and demonstrate mixing systems for implementation in the WTP vessels expected to contain non-Newtonian waste slurries.

Objectives

Table S.1 summarizes the objectives and results of this testing. Because this report covers a broad range of work and a number of different test specifications, the objective statements are provided in a summary manner. A complete discussion of all of the test objectives may be found in the reports referenced at the end of this summary.

Table S.1. Summary of Test Objectives and Results

Test Objective	Objective Met?	Discussion
Develop non-Newtonian simulants for testing in PJM and PJM/hybrid systems.	Yes	A transparent simulant based on Laponite was developed and used in the early phases of testing. Transparency made this simulant especially useful for visual observation of flow patterns. An existing kaolin-bentonite clay simulant was tailored for the PJM mixing program and used extensively in the later phases of testing. Simulant development efforts are summarized in Section 4 and in Poloski et al. (2004a).
Develop and implement assessment methods for non-Newtonian mixing of simulants in PJM/hybrid test stands.	Yes	Methods for assessing mixing that were developed for the PJM mixing program include chemical tracer techniques, passive integrated transponder (PIT) tags, neutrally buoyant beads, and ultrasonic velocity probes. These methods are summarized in Section 5. Chemical tracer techniques are described in Poloski et al. (2004b).
Provide information for assessing PJM and PJM/hybrid mixing systems using scaled prototypes.	Yes	Several hundred tests were conducted in scaled prototype vessels representing the LS/blend and UFP vessels and HLW concentrate receipt vessel (CRV). The tests included mixing, off-bottom suspension, solids uniformity, gas retention and release, and velocity mapping. Results of the scaled prototype PJM-only tests (Phase I) are summarized in Section 7 and reported in Bates et al. (2004) and Guerrero and Eberl (2004a). Results of scaled prototype PJM/hybrid tests (Phase II) are summarized in Section 8 and reported in Johnson et al. (2005) and Guerrero and Eberl (2004a).
Provide a technical basis for testing scaled PJM systems for non-Newtonian slurries.	Yes	Tests were conducted in three scaled 4PJM test stands using Laponite and kaolin-bentonite simulants at large-, ¼-, and 1/9-scale. A theoretical frame-work for scale-up of PJM systems is presented in Section 3, equipment and methods in Section 5, and experimental validation in Section 6. The technical basis for testing scaled PJM systems with non-Newtonian slurries is reported in Bamberger et al. (2005) and Wilson et al. (2004).

Table S.1. Summary of Test Objectives and Results

Test Objective	Objective Met?	Discussion
Provide a technical basis for scaling of air sparging systems for mixing non-Newtonian slurries.	Yes	Tests were conducted in the large-scale cone bottom tank (CBT) with single and multiple sparge tube arrays to provide a technical basis for scaling air sparging systems for mixing non-Newtonian slurries. The theory of air sparge systems is summarized in Section 3, equipment and experimental methods in Section 5, and experimental validation in Section 6. The technical basis for scaling air sparging systems for mixing in non-Newtonian slurries is reported in Poloski et al. (2005).
Provide a technical basis for scaling gas retention and release (GR&R) in PJM/hybrid mixed tanks containing non-Newtonian slurries.	Yes	GR&R tests were conducted in three scaled 4PJM test stands, three scaled prototypes with PJM/hybrid mixing systems, and the large CBT to provide a technical basis for scaling GR&R in PJM/hybrid mixed tanks containing non-Newtonian slurries. The theory of GR&R is presented in Section 3, equipment and experimental methods in Section 5, and experimental validation in Section 6. The technical basis is reported in Russell et al. (2005) and Guerrero at al. (2004b).
Demonstrate mixing and GR&R in a half-scale lag storage (HSLS) test with plant prototypical cyclic mixing operations.	Yes	Mixing and GR&R tests were conducted in a half-scale replica of the LS vessel with plant prototypical cyclic mixing operations. The data obtained were fit to a GR&R scaling model in a Monte Carlo uncertainty analysis to create probability distributions for gas release rate constants for various plant operations. A mass balance model suitable for predicting plant-scale GR&R behavior was developed. This approach was extended to scale up ¼-scale UFP test data. The results of the HSLS demonstration are summarized in Section 9 and reported in Russell et al. (2005). The model is summarized in Section 10 and reported in Russell et al (2005).

Test Exceptions

A complete discussion of all test exceptions may be found in the reports referenced at the end of this summary.

Results and Performance Against Success Criteria

Table S.2 summarizes the success criteria. Because this report covers a broad range of work and several different test specifications, the success criteria statements are provided in a summary manner. A complete discussion of all test success criteria can be found in the reports referenced at the end of this summary.

Table S.2. Success Criteria

List Success Criteria	How the Tests Did or Did Not Meet the Success Criteria
Develop nonhazardous, inexpensive simulants that mimic the pertinent rheological and physical properties for use in scaled testing of the PJM, PJM/hybrid, and air-sparged mixing systems.	A transparent simulant based on Laponite was developed and used in the early phases of testing. Laponite properties were varied by changing the concentration. Shear strengths ranged from 30–120 Pa and consistency from 10–20 cP. An existing kaolin-bentonite clay simulant was tailored for the PJM program by varying the concentration of the clay components in the 20–30 wt% range. Most of the testing was conducted near the upper-bound rheological properties of 30 Pa for yield stress and 30 cP for consistency. Over the course of all testing, yield stress varied from about 5 to 47 Pa and consistency from about 14 to 41 cP. Simulant development efforts are summarized in Section 4 and Poloski et al. (2004a). Simulants representing chemical, rheological, and physical properties of pretreated waste samples from Hanford tanks AZ-101 and AZ-102 were also used.
Obtain experimental data using non-Newtonian simulants to demonstrate the scaling of mixing behavior in PJM vessels.	Tests were conducted in three scaled 4PJM test stands using Laponite and kaolin-bentonite simulants at large-, ¼-, and 1/9-scale. PJM cavern heights, breakthrough velocities, and upwell velocities were obtained. These results were used to provide a technical basis for scaled testing. A theoretical framework for scale-up of PJM systems is presented in Section 3, test equipment and methods in Section 5, and experimental validation in Section 6. The technical basis for testing scaled PJM systems with non-Newtonian slurries is reported in Bamberger et al. (2005) and Wilson et al. (2004).
Determine the mixing and GR&R characteristics of air sparging in non-Newtonian slurries. Specifically, determine: 1. Zone of influence (ZOI) and region of bubble (ROB) dimensions as a function of air-flow rate 2. ZOI circulation time 3. Time to establish steady-state flow profiles 4. Aerosol entrainment during air sparging 5. Retained gas release characteristics.	Tests were conducted in the large-scale CBT using a kaolin-bentonite clay simulant. Test equipment and experimental methods are summarized in Section 5 and some experimental results in Section 6. All of the results are reported in Poloski et al. (2005). 1. ZOI and ROB dimensions were determined for air flow rates from 5 to 40 acfm. Measurement methods included ultrasonic velocity probes, a laser reference system coupled with video analysis, and PIT tags. 2. ZOI circulation time was established with dye and tracer tests. 3. The time to establish steady-state flow profiles was determined with velocity probes. 4. Aerosol measurements were obtained using impaction plates to collect samples. 5. Retained gas release characteristics were determined by generating oxygen in situ by hydrogen peroxide decomposition followed by sparging.
1) Measure gas holdup levels during steady-state PJM operation using vessels that have demonstrated sufficient mobilization of simulants under prototypic PJM operating conditions. 2) Measure gas release characteristics after simulated loss-of-power event.	Several gas holdup and release tests were conducted in the LS, UFP, and CRV scaled prototypes. Various combinations of PJMs, spargers, and recirculation pumps were tested using a kaolin-bentonite clay simulant. Retained oxygen gas was generated in situ by decomposition of hydrogen peroxide. The theory of GR&R is presented in Section 3, equipment and experimental methods in Section 5, and experimental validation in Section 6. The technical basis is reported in Russell et al. (2005) and Guerrero and Eberl (2004b).

Table S.2. Success Criteria

List Success Criteria	How the Tests Did or Did Not Meet the Success Criteria
Demonstrate PJM/hybrid mixing configurations for the LS/blend vessels, the UFP vessels and the CRV that provide full mobilization of the vessel contents subject to the WTP design requirements.	Several hundred tests were conducted in scaled prototype vessels representing the LS/blend and UFP vessels and HLW CRV. Tests conducted included mixing, off-bottom suspension, solids uniformity, GR&R, and velocity mapping. Results of the scaled prototype PJM-only tests (Phase I) are summarized in Section 7 and reported in Bates et al. (2004) and Guerrero and Eberl (2004a). Results of scaled prototype PJM/hybrid tests (Phase II) are summarized in Section 8 and reported in Johnson et al. (2005) and Guerrero and Eberl (2004b).
Demonstrate mixing and gas retention and release characteristics in a half-scale lag storage test with plant prototypical cyclic mixing operations.	A series of tests was conducted in a half-scale replica of the lag storage vessel. These tests were conducted using the kaolin-bentonite clay simulant. Retained oxygen gas was generated in situ by the decomposition of hydrogen peroxide. These tests demonstrated 1) a normal operating mode consisting of continuous PJM mixing and intermittent sparging, 2) post-design basis event (DBE) operations consisting of intermittent PJM and sparger mixing, and 3) near-term accident response (NTAR) operations consisting of intermittent sparging (no PJMs). The 95% time to mix was also determined using the chloride tracer method. The results of the half-scale LS demonstration are summarized in Section 9 and reported in Russell et al. (2005).

Quality Requirements

The Battelle – Pacific Northwest Division (PNWD) Quality Assurance (QA) Program is based on the requirements as defined in the U.S. Department of Energy (DOE) Order 414.1A, Quality Assurance, and 10 CFR 830, Energy/Nuclear Safety Management, Subpart A – Quality Assurance Requirements (a.k.a. the Quality Rule). PNWD has chosen to implement the requirements of DOE Order 414.1A and 10 CFR 830, Subpart A by integrating them into the Laboratory's management systems and daily operating processes. The procedures necessary to implement the requirements are documented through PNWD's Standards-Based Management System (SBMS).

PNWD implements the RPP-WTP quality requirements by performing work in accordance with the PNWD WTP Support Project quality assurance project plan (QAPjP) approved by the RPP-WTP QA organization. This work was performed to the quality requirements of NQA-1-1989 Part I, Basic and Supplementary Requirements, NQA-2a-1990 Part 2.7 and DOE/RW-0333P Rev. 13, Quality Assurance Requirements and Description (QARD). These quality requirements are implemented through PNWD's WTP Support Project (WTPSP) Quality Assurance Requirements and Description Manual. The analytical requirements are implemented through WTPSP's Statement of Work (WTPSP-SOW-005) with the Radiochemical Processing Laboratory (RPL) Analytical Service Operations (ASO).

Experiments that were not method-specific were performed in accordance with PNWD's procedure QA-RPP-WTP-1101, "Scientific Investigations," and QA-RPP-WTP-1201, "Calibration Control System," ensuring that sufficient data were taken with properly calibrated measuring and test equipment to obtain quality results.

Reportable measurements of distance were made using standard commercially available equipment (e.g., tape measure, scale) and required no traceable calibration requirements. All other test equipment generating reportable data were calibrated according to the PNWD WTPSP QA program. The DASYLab software used to acquire data from the sensors was verified and validated by PNWD WTPSP staff before use, and BNI conducted an acceptance surveillance of the verification and validation activities with no problems noted.

PNWD addresses internal verification and validation activities by conducting an independent technical review of the final data report in accordance with PNWD procedure QA-RPP-WTP-604. This review verifies that the reported results are traceable, that inferences and conclusions are soundly based, and that the reported work satisfies the Test Plan objectives. This review procedure is part of PNWD's WTPSP Quality Assurance Requirements and Description Manual.

Research and Technology Test Conditions

A list and discussion of the research and technology test conditions is too lengthy to include here. A complete discussion of all test research and technology test conditions can be found in the reports referenced at the end of this summary.

Simulant Use

Simulants were used extensively due to the high cost and safety issues associated with actual wastes in the quantities required for the PJM mixing program. Accordingly, two nonhazardous, relatively inexpensive simulants were developed and used for the majority of the testing: Laponite and kaolin-bentonite clay. The simulants were selected based on limited actual waste slurry rheology measurements that indicate the WTP non-Newtonian waste stream can be represented by a Bingham plastic rheology model (Poloski et al. 2004a). The WTP specified bounding values of 30 Pa for yield stress (τ_y) and 30 cP for consistency (κ) for the Bingham plastic parameters. Other important physical parameters for the simulants are density and shear strength.

Laponite is a synthetic smectite clay mineral consisting of nanoscale crystals in the form of platelets that makes a transparent solution when dispersed in water due to the small particle size. A range of rheological properties can be obtained by varying the concentration slightly. The shear strength ranged from 30 to 120 Pa with consistency in the range of 10 to 20 cP. The Laponite concentration was typically about 2 wt% and the density slightly greater than that of water. Laponite was used primarily to represent the gelled-state conditions encountered by PJMs upon restart from idle periods. As such, shear strength was considered the important yield parameter. For low-strength Laponite (30 Pa shear strength) that has been fully sheared, the yield stress is essentially zero, and the material behaves like a Newtonian fluid. For higher-strength Laponite (80–120 Pa), the yield stress was typically in the 10-Pa range.

A simulant developed by Rassat et al. (2003) for Hanford tank retrieval studies was 80% kaolin and 20% bentonite powder mixed to various solids concentrations in water. This simulant has Bingham plastic properties near the target of 30 Pa yield stress and 30 cP consistency. Additionally, the simulant also developed shear strength when at rest that was 1.5 to 2 times the yield stress. Typical density was about 1200 kg/m^3. The rheological properties of the kaolin-bentonite clay simulant were characterized extensively for solids loadings in the 20 to 30 wt% range (Poloski et al. 2004a). This simulant was used

extensively in the PJM program. Significant applications included the final all-in tests for Phase I scaled prototype work, all of the Phase II scaled prototype tests, demonstration of the PJM scaling laws, single and multiple sparge tube testing, and half-scale LS (HSLS) testing.

A limited amount of testing was conducted with simulants representing pretreated AZ-101 and/or AZ-102 waste slurry. These materials are precipitated hydroxide simulants that mimic the chemical, rheological, and physical properties of pretreated waste samples from Hanford tanks AZ-101 and AZ-102 (Eibling et al. 2003). A pretreated AZ-102 simulant was used in single-PJM cavern tests; a pretreated AZ-101/102 simulant was used in bench-scale GR&R tests and gas holdup/mass transfer tests in a bubble column. More use of this simulant was precluded by higher procurement costs, relatively large lead time for procurement, and the hazardous characteristics of the material.

Summary of the PJM Test Program and Results

The DOE Office of River Protection's WTP is being designed and built to pretreat and then vitrify a large portion of the wastes in Hanford's 177 underground waste storage tanks. The WTP process streams significant to this report are those containing relatively high concentrations of solids. These concentrated waste slurries are expected to exhibit non-Newtonian rheology, which requires that a certain amount of shear must be applied before the material begins to move. Seven tanks were projected to contain non-Newtonian slurries.

PJM technology was planned for mixing most vessels in the WTP because PJMs have no moving mechanical parts that require maintenance. PJM technology had been used successfully in the past for mixing Newtonian fluids in radioactive environments; however, application of the technology to non-Newtonian slurries was new with the WTP, and an adequate supporting technical basis was not available. Accordingly, an integrated scaled testing approach was developed and implemented for the WTP vessels expected to contain non-Newtonian slurries.

A robust scaling theory was developed to describe PJM mixing of non-Newtonian fluids (Section 3). Based on rheological measurements of pretreated tank waste samples, the Bingham yield stress model was selected that represents the non-Newtonian fluid with a yield stress, τ_y, and a consistency factor, κ. Gelled slurry also exhibits shear strength, τ_s, which must be exceeded before the slurry begins to move. The PJM mixing theory was based on the concept of intermittent mixing within the PJM "cavern," a region near the PJM nozzles where the yielded slurry experiences turbulent flow that is bounded by unmobilized, gelled slurry. Gas retention and release scaling theory assumes gas is retained as bubbles that rise through the slurry in a well-mixed region but are fixed when mixing ceases.

Several important nondimensional groups and dimensional parameters were derived to characterize PJM mixing and gas retention and release processes. These groups and the associated scaling laws are summarized as follows:

Yield Reynolds number: $$\mathrm{Re}_\tau = \frac{\rho u_0^2}{\tau}$$

Here, ρ is the density, u_0 is the PJM discharge velocity, and τ is the relevant rheological stress parameter (either shear strength, τ_s, for a gelled slurry or yield stress, τ_y, for a slurry with Bingham-type behavior).

Physically, the yield Reynolds number is the ratio of the jet dynamic stress to the non-Newtonian resistive stress of the slurry. This ratio directly affects the size of the mixing cavern. The yield Reynolds number will be the same at both large and small scales as long as the same simulant is used.

Jet Reynolds number: $$Re_0 = \frac{\rho u_0 d_0}{\kappa}$$

Here, d_0 is the PJM nozzle diameter and κ is the consistency of the slurry. The jet Reynolds number is the ratio of jet dynamic stress to viscous stress. It affects the degree of turbulence in the mixed region as well as transitional flow regimes associated with nonsteady mixing. It also affects cavern height. Because the yield Reynolds number was held constant, the jet Reynolds number was reduced at smaller scale. This resulted in a conservative testing approach because testing at reduced jet Reynolds numbers results in generally reduced mixing phenomena such as cavern heights, magnitude of velocity, and degree of turbulence. The quality of mixing is therefore expected to improve at the large scale.

Strouhal number: $$S_0 = \frac{t_D u_0}{d_0}$$

The Strouhal number is the ratio of PJM drive time to the jet flow time scale. It affects the degree to which the jet approaches steady behavior. In the limit of steady jet flows, the Strouhal number becomes infinite, and the effects of pulsation are no longer present. For small Strouhal numbers, the mixing behavior is highly dominated by pulsation effects. If the drive time is reduced by the scale factor at small scale, the Strouhal number is held constant and the essential nonsteady behavior of the mixing process is preserved.

Bubble rise time: $$\tau_R = \frac{V_s}{AU_R} = \frac{H}{U_R}$$

The bubble rise time, τ_R, is the time constant of the gas-release process in the well-mixed slurry bubble migration model. Because the bubble rise velocity, U_R, is roughly constant with scale, the bubble rise time is reduced in proportion to the vessel fill level, H; hence at small scale it is reduced in proportion to the geometric scale factor. The bubble rise time can be nondimensionalized by any characteristic time scale as follows:

Gas holdup number: $$N_\alpha = \frac{g_v V_s}{AU_R} = \frac{g_v H}{U_R} = g_v \tau_R$$

The gas holdup number represents the ratio of gas generated to gas leaving by virtue of bubble rise. It is equal to the theoretical holdup (volume of retained gas per volume of slurry) predicted by the bubble migration theory. If the gas generation rate, g_v, is increased by the geometric scale factor in the small-scale tests, the gas holdup and therefore the gas holdup number remain the same at large and small scale.

Gas-release number: $$N_R = \frac{t_C U_R}{H} = \frac{t_C}{\tau_R}$$

The ratio of PJM cycle time, t_C, or any relevant system time to bubble rise time is defined as the gas release number. It directly affects gas release rates and other transients. The gas release number is preserved at small scale.

Practical scaled testing required a nonhazardous, easily disposable simulant to represent the radioactive waste slurry in the plant. Based on the properties of actual pretreated waste samples, the simulant was designed to a target upper-bound yield stress of 30 Pa and a consistency of 30 cP. Laponite, a transparent simulant, was selected to visualize the mixing process based on comparisons with AZ-102 simulant in cavern tests and initial shear strength. However, because Laponite has significant time-dependent behavior and other nonrepresentative physical properties, the kaolin-bentonite clay mixture was selected for quantitative testing (Section 4).

Hydrogen peroxide decomposition was used to simulate uniform, constant gas generation in plant waste slurries. Laponite simulant required adding a manganese dioxide catalyst to induce decomposition. The clay simulant was sufficiently catalytic without additives (Section 4). GR&R tests were planned carefully because hydrogen peroxide has a relatively high decomposition rate and must be mixed uniformly in the simulant to produce a uniform gas generation rate. However, hydrogen peroxide can be placed into only those regions that participate in mixing. Methods to deal with these challenges for intermittently mixed systems are discussed in conjunction with HSLS testing in Section 9.

Nine different test stands were constructed for all phases of the scaled testing. These are listed in Table S.3. Tests performed in these test stands included cavern size and breakthrough (where the top of cavern reaches the surface), mixing, sparging (introducing air bubbles at a low level through multiple points), and GR&R. Mixing tests investigated mixing effectiveness, time to mix, solids suspension, and slurry velocity distribution. Sparging tests included determination of the size of the ROB, ZOI, aerosol generation, and velocity distributions. Tests were also conducted in a bench-scale bubble column investigating the holdup characteristics of different gases and simulants and mass transfer stripping during sparging. Many novel instrumentation methods and analysis approaches were deployed for these tests (see Section 5).

The three scaled prototype vessels represented plant vessels as outlined in Table S.4. The actual plant LS and blend vessels are not exactly the same size and geometry but were judged similar enough that a single LS prototype was a suitable representation for both vessel types.

The scaled testing strategy was validated by testing in geometrically similar 4PJM mixing systems at three different scales, large, ~¼, and ~1/9 scale. The data were compared nondimensionally to demonstrate the validity of testing prototypic PJM mixing systems at reduced scales. Data from the 4PJM tests at three scales clearly indicate that the yield Reynolds number is the dominant nondimensional parameter governing mixing in non-Newtonian slurries. The jet Reynolds number has a secondary effect, which is to generally reduce velocities and cavern heights at smaller test scales due to the high consistency of the simulant. Therefore, the scaled testing approach is conservative in that the quality of mixing will improve at full scale. While uncertainty and fluctuations in the gas volume fraction during

Table S.3. Summary of PJM Test Vessels and Applications

Vessel	Internals	Description	Scale	Approximate Volume (gal)
APEL single PJM	1PJM	Single pulse tube in clear acrylic vessel	NA	250
336 supernatant tank (SNT)	4PJM	Four pulse tubes in stainless steel vessel	1	10,000
APEL 4PJM	4PJM	Four pulse tubes in clear acrylic vessel	¼ scale of 336 4PJM SNT	250
SRNL 4PJM	4PJM	Four pulse tubes in clear acrylic vessel	1/9 scale of 336 4PJM SNT	30
UFP scaled prototype	Variable PJMs, spargers, recirculation pump	Scaled prototype representing UFP vessel	1/4.94 scale of full-scale UFP vessel	350
LS scaled prototype	Variable PJMs, spargers, recirculation pumps	Scaled prototype representing LS and blend vessels	1/4.29 scale of full-scale LS vessel	1,000
CRV scaled prototype	Variable PJMs, spargers, recirculation pump	Scaled prototype representing CRV	¼-scale of full-scale CRV	230
HSLS vessel	8 PJM cluster (7 around 1), 7 spargers	Half-scale LS vessel	½-scale of full-scale LS vessel	10,000
Cone bottom tank	spargers	Nine spargers in tank with cone shaped bottom	Similar to 336 SNT	10,000

Table S.4. Relationship of WPT Vessels to Test Vessels

Scaled Prototype Nomenclature	WTP Vessel Identification
Lag Storage (LS)	HLW Lag Storage: HLP-VSL-00027A/B HLW Blend: HLP-VSL-00028
Ultrafiltration Process (UFP) Vessel	UFP-VSL-00002A/B
Concentrate Receipt Vessel (CRV)	HCP-VSL-00001/00002

holdup tests makes comparison difficult, the holdup scaling law was qualitatively verified by test results from the three 4PJM systems. Though the results of scaled release tests were less conclusive, the simple gas and hydrogen peroxide mass conservation model predicted gas volume fractions that matched data from three-stage tests including holdup, accumulation, and the initial gas release periods. This result supports the gas bubble migration model as the fundamental description of the GR&R process.

Phase I of the test program was established In June 2003. The PJM Task Team developed an integrated strategy for scaled testing to demonstrate mixing in WTP vessels containing non-Newtonian fluids. The initial scaled tests in October 2003 demonstrated that the baseline pulse jet designs did not mix the non-Newtonian slurries to WTP requirements. Several PJM design features were varied to develop alternative configurations with better mixing performance. The design variables and a summary of the findings are provided below and in Section 7.

- A **Recirculation pump** was found to be effective and was implemented in Phase II testing.

- The **PJM cluster configuration** was found to be ideal combined with sparging and/or recirculation pumps and was implemented in Phase II testing.
- **Outward-angled PJM nozzles** improved mixing and were implemented in Phase II testing.
- **Increased nozzle velocity** improved mixing but decreased drive time and increased air demand. Nozzle velocities up to 12 m/s were implemented in Phase II testing.
- **Larger pulse tubes** improved mixing but increased air demand.
- **Larger-diameter pulse tube nozzles** improved mixing but greatly increased air demand.
- **Additional pulse tubes** placed at a higher levels increased mixing in some regions but blocked the flow of the central upwell and increased air demand.
- **Multiple nozzles** (e.g., rams heads) promoted regional mixing but may be prone to abrasive wear and may be somewhat more difficult to fabricate.
- **Asychronous PJM operations** were not found to be effective.

In November 2003, Phase I of the PJM program developed an alternative "PJM-only" configuration that mixed the vessels containing non-Newtonian slurries. Complete mixing of the vessel contents was demonstrated by testing in scaled prototypes. However, the alternative PJM-only mixing systems were not acceptable because of their effect on the WTP facility designs and their greatly increased compressed air consumption. Accordingly, Phase II of the program investigated PJM hybrid mixing systems with spargers and recirculation pumps added to minimize the impact to overall project cost and schedule. The PJMs were generally arranged in the cluster configuration and used angled nozzles operating at a velocity up to 12 m/s. This design retained the baseline number of PJMs and the baseline nozzle size to limit demand on the air supply. The sparge systems and recirculation jets operated continuously.

Phase II testing demonstrated that PJM hybrid systems mixed non-Newtonian slurries in accordance with WTP requirements and provided safe flammable gas retention and control (Section 8). However, an engineering evaluation indicated that a recirculation pump was infeasible in the LS vessel and that full-time sparging would exceed the allowable vent system air capacity by a factor of 3. This difficulty was resolved by introducing intermittent sparging to release retained gas after a quiescent period. The tests clearly released most of the retained gas in about 5 minutes and all of the gas in 10–15 minutes, which showed that intermittent, full-flow sparging was feasible. One-third-flow tests released gas much more slowly, indicating that continuous low-flow sparging might be adequate but would provide a reduced degree of mixing. Based on these successful sparger gas release results, the recirculation pumps were deleted from the LS and blend vessel designs.

Sparger design methodology was developed by conducting single and multiple sparge tube tests. Sparger mixing was found not to scale in the same way as PJM mixing, but single sparge tube performance data provided the basis for specifying multiple sparge tube arrays for PJM-hybrid mixing systems. Correlations were developed for the size of the upwelling ROB and the downward flow in the ZOI. Adequate mixing is ensured if sparge tubes are arranged so there is adequate overlap of the individual sparging-induced mixing regions (Section 3). This sparge array scaling approach is conservative because full-scale vessels have a greater sparge submergence, hence more effective mixing from a given sparge mixing zone.

While Phase II testing covered most of the issues associated with management and scale up of mixing and flammable gas retention, a confirmatory demonstration of a large, correctly scaled hybrid mixing system was determined to be necessary. This large-scale demonstration became Phase III of the test program. Testing was performed in a half-scale vessel representing the plant LS vessel during normal operations, post-design basis event (post-DBE) operations, and near term accident response (NTAR) operations. In each test a repeating periodic state was achieved with moderate fluctuations of the maximum and minimum cyclic retained gas volume fractions. Mixing was reestablished early in each mixing cycle, and the retained gas accumulated during the off cycle was released with no measurable long-term buildup. Tests showed that full-flow, sparger-only (no PJMs) operation mixed more than 60% of the simulant volume with an unmixed heel of approximately 35%, including the PJM pulse tube volume. Mixing with both full-flow sparging and PJMs operating at half-stroke provided essentially 100% mixing of the vessel contents (see Section 9).

Phase III tests demonstrated that the selected hybrid design provided mixing and flammable gas control meeting WTP requirements during the normal and post-DBE operating scenarios. The larger unmixed volume associated with NTAR (sparging-only operation) would limit the time during which this scenario could be used to avoid excessive gas accumulation. Phase III was completed by applying the test results via a mass balance model to the plant-scale LS and blend vessels and extending the scale-up methodology to the plant-scale UFP vessels. The scaling laws for gas holdup and release were embodied in a gas inventory model that was fit to the HSLS data in a Monte Carlo uncertainty analysis to create probability distributions for gas release rate constants representing four mixing modes: PJMs and full sparging, PJMs and idle sparging, full sparging only, and idle sparging only. The accumulated ¼- and ½-scale test data showed that gas release constants varied with both slurry yield stress and the product of volumetric gas generation rate and simulant depth, g_vH. A methodology was developed to account for these variations in the four parameters and apply them via the mass balance model to predict plant-scale GR&R behavior. The result includes both the uncertainty in the reduced data and the uncertainty in the scaling process itself. This process was also extended to scale up ¼-scale UFP test data (see Section 10).

The WTP non-Newtonian PJM Test Program was planned and executed to provide a significant design margin for the mixing systems. Conservative approaches were taken at each stage of the program. The kaolin-bentonite clay simulant was conservative because its Bingham plastic behavior bounds actual waste rheology, which exhibits shear-thinning behavior (i.e., the consistency is reduced with higher shear rates). Additionally, the yield stress of the simulant used in the scaled tests generally exceeded the design-basis upper bound of 30 Pa. The scaled test approach identifies three key nondimensional parameters governing PJM mixing behavior. Two of these were preserved during testing (Strouhal and yield Reynolds numbers), and the third (jet Reynolds number) was smaller in the reduced-scale tests. This introduced another degree of conservatism because mixing performance is reduced at lower jet Reynolds numbers. This effect was confirmed by mixing tests that clearly demonstrated increased cavern height and fluid velocity with increasing vessel scale. Testing with sparge systems was also conservative. Tests were performed in vessels that were approximately one-half the depth of the full-scale vessel. The sparge ZOI increases somewhat with submergence depth, and the overall energy input increases non-linearly with submergence depth. Therefore, the mixing performance of sparge systems will be improved in plant-scale vessels. Additionally, sparge tube spacing involved significant ZOI overlap, and synergism between adjacent sparge mixing zones was not credited. The removal of hydrogen by mechanisms other than bubble migration (e.g., stripping by the sparge air or from the slurry surface) should be relatively larger (compared with bubble rise at the lower generation rates found in the plant. This and the increased effectiveness of sparger mixing at full scale imply that the measured holdup in the small-scale tests is

higher than the WTP will experience. These factors, as well as others documented in the supporting test reports, ensure a significant degree of conservatism in the test results on which the WTP will base its designs. However, the gas retention and release behavior of clay simulant may be different from that of radioactive waste slurry containing anti-foaming agent and the difference has not yet been quantified.

The WTP Non-Newtonian Test Program was a highly accelerated, integrated effort to develop new knowledge as the technical basis for a revised process vessel mixing system. The test program evolved rapidly in response to engineering requirements and ultimately demonstrated a satisfactory final design. This report provides a summary of the work, including the various options tested, the new theory derived to scale up test data, and the major programmatic decisions made in response to test results.

Discrepancies and Follow-on Tests

While the current test data using a clay simulant provides an adequate basis to account for physical scale-up to plant operation, the difference in GR&R behavior between clay with gas generated by hydrogen peroxide decomposition and radioactive waste slurry containing anti-foaming agent with gas generated by a radiothermal process is not known. Small-scale GR&R tests using clay and AZ-101 chemical simulant with and without an anti-foaming agent are planned to quantify the difference.

The uncertainty in the UFP scale-up predictions is higher relative to LS vessel scale-up due to a lack of test data for intermittent cyclic operations. Performing cyclic operational tests in the 1:4.9-scale APEL UFP prototype test vessel with a clay simulant could reduce the uncertainty in scaling up this vessel.

Due to the need to reduce the number of PJM overblows in the WTP, it is possible that the PJMs will be operated at half-stroke. There was some evidence from the HSLS testing that this may lead to an unmixed slug in the pulse tubes. Additional testing in the HSLS vessel is underway to define the rate of mixing in pulse tubes operated at half-stroke.

References

Bamberger JA, PA Meyer, JR Bontha, CW Enderlin, DA Wilson, AP Poloski, JA Fort, ST Yokuda, HD Smith, F Nigl, M Friedrich, DE Kurath, GL Smith, JM Bates, and MA Gerber. 2005. *Technical Basis for Testing Scaled Pulse Jet Mixing Systems for non-Newtonian Slurries*. WTP-RPT-113 Rev. 0 (PNWD-3551), Battelle – Pacific Northwest Division, Richland, Washington.

Bates JM, JW Brothers, JM Alzheimer, and DE Wallace. 2004. *Test Results for Pulse Jet Mixers in Prototypic Ultrafiltration Feed Process and High-Level Waste Lag Storage Vessels*. WTP-RPT-110 Rev. 0 (PNWD-3496), Battelle – Pacific Northwest Division, Richland Washington.

Bontha JR, CW Stewart, DE Kurath, PA Meyer, ST Arm, CE Guzman-Leong, MS Fountain, M Friedrich, SA Hartley, LK Jagoda, CD Johnson, KS Koschik, DL Lessor, F Nigl, RL Russell, GL Smith, W Yantasee, and ST Yokuda. 2005. *Technical Basis for Predicting Mixing and Flammable Gas Behavior in the Ultrafiltration Feed Process and High-Level Waste Lag Storage Vessels with Non-Newtonian Slurries*. WTP-RPT-132 Rev. 0, Battelle – Pacific Northwest Division, Richland, Washington.

Eibling RE, RF Schumacher, and EK Hansen. 2003. *Development of Simulants to Support Mixing Tests for High Level Waste and Low Activity Waste.* WSRC-TR-2003-00220 Rev. 0 (SRT-RPP-2003-00098 Rev. 0), Westinghouse Savannah River Company, Aiken South Carolina.

Guerrero HN and KR Eberl. 2004a. *Final Report – Hybrid-Mixing Tests Supporting the Concentrate Receipt Vessel (CRV-VSL-00002A/2B) Configuration*. WSRC-TR-2004-00398 Rev. 0 (SRNL-RPP-2004-00060 Rev. 0), Savannah River National Laboratory, Aiken, South Carolina.

Guerrero HN and KR Eberl. 2004b. *Final Report – Gas Retention and Release Tests Supporting the Concentrate Receipt Vessel (CRV-VSL-00002A/2B) Configuration*. WSRC-TR-2004-00399 Rev. 0 (SRNL-RPP-2004-00062 Rev. 0), Savannah River National Laboratory, Aiken, South Carolina.

Johnson MD, MA Gerber, JR Bontha, AP Poloski, RT Hallen, SK Sundaram, and DE Wallace. 2005. *Hybrid Mixing System Test Results for Prototype Ultrafiltration Feed Process and High-Level Waste Lag Storage Vessels.* WTP-RPT-128 Rev. 0, Battelle – Pacific Northwest Division, Richland, Washington.

Poloski A. 2004. *Technical Basis for HLW Vitrification Stream Physical and Rheological Property Bounding Conditions*. WTP-RPT-100 Rev. 0, Battelle – Pacific Northwest Division, Richland, Washington.

Poloski AP, PA Meyer, LK Jagoda, and PR Hrma. 2004a. *Non-Newtonian Slurry Simulant Development and Selection for Pulsed Jet Mixer Testing.* WTP-RPT-111 Rev. 0 (PNWD-3495), Battelle – Pacific Northwest Division, Richland, Washington.

Poloski AP, LA Snow, and ST Arm. 2004b. *Chemical Tracer Techniques for Assessing Mixing Performance in non-Newtonian Slurries for WTP Pulsed Jet Mixer Systems.* WTP-RPT-121 Rev. 0 (PNWD-3494), Battelle – Pacific Northwest Division, Richland, Washington.

Poloski AP, ST Arm, JA Bamberger, B Barnett, R Brown, BJ Cook, CW Enderlin, MS Fountain, M Friedrich, BG Fritz, RP Mueller, F Nigl, Y Onishi, LA Schienbein, LA Snow, S Tzemos, M White, and JA Vucelik. 2005. *Technical Basis for Scaling of Air Sparging Systems for Mixing in Non-Newtonian Slurries*. WTP-RPT-129 Rev. 0 (PNWD-3541), Battelle – Pacific Northwest Division, Richland, Washington.

Russell RL, SD Rassat, ST Arm, MS Fountain, BK Hatchell, CW Stewart, CD Johnson, PA Meyer, and CE Guzman-Leong. 2005. *Final Report: Gas Retention and Release in Hybrid Pulse Jet-Mixed Tanks Containing Non-Newtonian Waste Simulants*. WTP-RPT-114 Rev. 1 (PNWD-3552), Battelle – Pacific Northwest Division, Richland, Washington.

Wilson DA, ML Restivo, HN Guerrero, TJ Steeper, RE Eibling, EK Hansen, TM Jones, and KR Eberl. November 2004. *One-Eighth Scale Pulse Jet Mixer (PJM) – Design Parameters Scale Law Testing*. WSRC-TR-2004-00430 Rev. 0 (SRNL-RPP-2004-00069 Rev. 0), Westinghouse Savannah River Company, Aiken, South Carolina.

Acknowledgments

The authors want to thank the individuals who contributed to the success of this task. Because several hundred individuals contributed to this effort, we may have overlooked someone. We regret any omissions.

- PNWD Task managers, test engineers and principle investigators: Jim Alzheimer, Stuart Arm, Judith Bamberger, Jim Bates, Jagan Bontha, Joe Brothers, Carl Enderlin, Michele Friedrich, Rich Hallen, Mark Gerber, Lynette Jagoda, Mike Johnson, Gary Josephson, Yasuo Onishi, Adam Poloski, Scot Rassatt, Renee Russell, Lawrence Schienbein, and Harry Smith
- SRNL task managers and principle investigators: Hector Guerrero and David Wilson
- Test crew members for putting in long days and many all night shifts: Brent Barnett, Dave Blanchard, Bill Buchmiller, Teresa Carlon, Bill Combs, Abby Capatillo-Isenberg Bryan Cook, Jarrod Crum Kate Deters, Mike Dodson, Carl Enderlin, Stephanie Felch, Bob Fulton, Mike Hall, Don Hartshorn, Chris Johnson, Consuelo Guzman-Leong, Theresa Koehler, Eric Mast, Royce Mathews, Mike McKinnon, Ron Myers, Jackie Newell Franz Nigl, Keith Peterson, Sergei Sinkov, Lanee Snow, Dan Tano, Spyro Tzemos, Dale Wallace, Mike White, Wayne Wilcox, and Mac Zumhoff
- Analytical Services Organization, for providing rapid analyses of the tracer samples, including Karl Pool, Mike Urie, and Marilyn Steele
- Outstanding crafts support: Tom Loftus, Richard Ehlers, Don Cravens, Frank Felix, Rod Bechtol, and Mike Longaker
- Data analysis team members: Jim Fort (data analysis principle investigator), Matt Fountain, Wassanna Yantasee, Stacey Hartley, Sato Yokuda, S. K. Sundaram, Del Lessor, and Pavel Hrma
- Large-scale test stand design and construction crew, which included Vic Epperly, Dale Flowers, Rod Jones, Bob Turner, and Ken Koschik
- Editor: Sheila Bennett
- Project office support: Chrissy Charron
- Procurements support: Teri Claphan, Diane Leitch, Laurie Martin, Kim Collins, and Kathy Whelan
- Quality Assurance support: Barry Sachs and Kirsten Meier.

Finally, we would like to thank the PJM Steering Committee for evaluating the testing results as they became available and providing direction on the conduct of testing. The PJM Steering Committee consisted of Steve Barnes (Committee Chairman, WTP R&T), Hani Abodishish (WTP R&T), Aaron Bronner (WTP Engineering), Clarence Corriveau (WTP Engineering), Gerry Chiaramonte (Pretreatment Engineering), Eric Slaathaug (Pretreatment Engineering), Karen Hornbuckle (WTP R&T), Don Larson (WTP R&T), Walt Tamosaitis (Manager WTP R&T), Don Alexander (DOE-ORP), Paul Fallows (AEA),Hector Guerrero (SRNL), Gary Smith (PNWD), Gordon Beeman (PNWD, Project Manager, WTPSP), and Art Etchells (Du Pont Consultant).

The authors of this report were also members of the steering committee: Dean Kurath (PNWD, Task Manager, PJM Testing), Perry Meyer (PNWD, Chief Scientist, PJM Testing), and Chuck Stewart (PNWD, Principal Investigator, Gas Holdup and Release Testing).

Nomenclature

4PJM	Four pulse jet mixers
A	area of the slurry surface
A_g	Hydrogen peroxide decay rate constant
A_R	Gas release rate constant
acfm	Actual cubic feet per minute
AFA	Anti-foaming agent
APEL	Applied Process Engineering Laboratory
atm	Atmosphere (unit of pressure)
BNI	Bechtel National, Inc.
C_L	Nozzle loss coefficient
CBT	Cone bottom tank
CFD	Computational fluid dynamics
cP	Centipoise
CRV	Concentrate receipt vessel
DACS	Data acquisition and control system
DBE	Design basis event
D_c	Diameter of breakthrough region
DOE	U.S. Department of Energy
d_0	PJM nozzle diameter (m)
D_{0e}	Effective PJM nozzle diameter
D_{ROB}	Diameter of region of bubbles
D_S	Sparge tube spacing
D_{ZOI}	Diameter of zone of influence
D_{PT}	Pulse tube diameter
D_T	Tank diameter
g_m	Specific molar gas generation rate
g_v	Volumetric gas generation rate
GR&R	Gas retention and release
H	Slurry level (height) or tank operating level
H_C	Cavern height

H_e	Hedstrom number
H/D	Height-to-diameter ratio
HLW	High-level waste
HSLS	Half-scale lag storage
IC	Ion chromatography
ID	Inside diameter
ISE	Ion-selective electrodes
ITS	Important to safety
JPP	Jet pump pair
K	Kelvin (unit of absolute temperature)
L	Liter (unit of volume)
LAW	Low-activity waste
LS	HLW lag storage vessel
min	Minute (unit of time)
M_p	Molecular weight of hydrogen peroxide
N	Number of PJMs
N_g	Number of moles of gas
N_R	Gas release number
N_s	Number of sparge tubes
n_s	Sparge tube number density
nm	Nanometer
NTAR	Near-term accident response
OD	Outside diameter
p	Average in situ pressure
p_D	Drive pressure
p_e	Pressure of PJM nozzle
Pa	Pascal
PIT	Passive integrated transponder (tag)
PJM	Pulse jet mixer
PNWD	Battelle – Pacific Northwest Division
ppm	Parts per million
psi	Pounds per square inch

PVC	Polyvinyl chloride
QA	Quality assurance
QAPjP	PNWD Waste Treatment Plant Support Project Quality Assurance Project Plan
Q_{ps}	Volume flow rate of hydrogen peroxide solution
Q_s	Actual air flow rate for a single sparge tube
Q_T	Total sparge system actual air flow rate
R	Gs constant
R&D	Research and development
R&T	Research and technology
R_0	Initial (maximum) volumetric gas release rate from the slurry
R_v	Volumetric gas-release rate from the slurry at the headspace pressure (m^3 gas/s)
Re_τ	Yield Reynolds number
Re_0	Jet Reynolds number
RF	Radio frequency
RFD	Reverse flow diverter
RMS	Root-mean-square
ROB	Region of bubbles
s	Scale factor, S = test dimension/full-scale dimension
S_0	Strouhal number
scfm	Standard cubic feet per minute—14.7 lb per square inch absolute (psia), 68°F, and 0% relative humidity
SRNL	Savannah River National Laboratory
t_C	Total cycle time
t_D	Drive time
T_{DA}	Actual drive time
t_m	Time of maximum discharge
t_S	Suction time
t_{ss}	Jet flow establishment time
t_V	Pulse tube vent time
T	Slurry and gas bubble temperature
TSP	Total suspended particulates
u_a	Average PJM velocity
u_0	Nominal PJM nozzle velocity

u_p	Peak average nozzle velocity
U_R	Average bubble rise velocity at the slurry surface (m/s)
U_s	Sparge air superficial velocity
UFP	Ultrafiltration feed process vessel
UV-vis	Ultraviolet-visible
UVP	Ultrasonic velocity probe
u_{uw}	Upwell velocity
V_{bs}	Total bubbly-slurry volume
v_{bH}	Average bubble volume of the slurry surface (m^3)
V_{PT}	Pulse tube volume
V_P	Volume of fluid that is discharged during a pulse
V_R	Total gas release volume
V_s	Gas-free or initial slurry volume (m^3)
V_T	Total slurry volume in tank
W_p	Mass of hydrogen peroxide
WTP	Waste Treatment Plant
WTPSP	Waste Treatment Plant Support Project
Y	Yield number
x_p	Weight fraction of H_2O_2 in solution
ZOI	Zone of influence

Notation

α	Average retained gas-volume fraction (m^3 gas/m^3 bubbly slurry)
α_{MAX}	Maximum gas volume fraction during cyclic operation
α_{MIN}	Minimum gas volume fraction during cyclic operation
α_0	Initial gas-volume fraction prior to a gas-release test
α_{ss}	Gas holdup (m^3 gas/m^3 bubbly slurry)
$\dot{\gamma}$	Shear rate or strain rate
ΔH	Change in tank waste level during PJM discharge
ΔL	Level change in pulse tube during discharge
ΔL_A	Actual measured level change in pulse tube
κ	Bingham plastic consistency (mPa-s)

μ	viscosity
ρ	Density
ρ_{ps}	Density of hydrogen peroxide solution
τ	Fluid shear stress
τ_R	Gas release time constant
τ_s	Shear strength
τ_y	Bingham yield stress

Contents

Figures

Tables

1.0 Introduction

Pulse jet mixer (PJM) technology was selected for implementation in the Hanford Waste Treatment Plant (WTP). However, the understanding required to apply this technology to mobilize the non-Newtonian slurries that will be processed through these tanks was not mature. Consequently, an experimental testing effort was undertaken to investigate PJM performance in several scaled versions of WTP vessels and to develop mixing system configurations that met WTP requirements. This effort evolved into a large, multifaceted test program involving many different test facilities. Elements of the test program included theoretical analysis, development and characterization of simulants, development of instrumentation and measurement techniques, hundreds of tests at various scales in numerous test stands, and data analysis and application.

The objectives of this report are to provide an overview of the PJM Test Program, including the approaches and methods used, and a summary of the key technical results that formed the technical basis of the final mixing system configurations to be used in the WTP.

1.1 Background

The Hanford Site contains 177 single- and double-shell tanks holding radioactive waste. The U.S. Department of Energy (DOE) Office of River Protection's WTP is being designed and built to pretreat and then vitrify a large portion of these wastes. The WTP will consist of three primary facilities (Figure 1.1): 1) pretreatment, 2) low-activity waste (LAW) vitrification, and 3) high-level waste (HLW) vitrification. The pretreatment facility receives waste feed from the Hanford tank farms and separates it into 1) a high-volume, low-activity, liquid process stream stripped of most solids and radioisotopes and 2) a much smaller-volume HLW slurry containing most of the solids and most of the radioactivity. In the pretreatment facility, solids and radioisotopes are removed from the waste by precipitation, filtration, and ion exchange processes to produce the LAW stream. The slurry of filtered solids is blended with the ^{137}Cs ion exchange eluate to produce the HLW stream. The HLW and LAW vitrification facilities convert these process streams into glass, which is poured directly into stainless steel canisters.

1.1.1 Mixing Requirements for Non-Newtonian Slurries

The process streams significant to this report are those containing relatively high concentrations of solids expected in the ultrafiltration feed processing (UFP) vessels and the HLW lag storage (LS) and blend vessels located in the Pretreatment facility. These concentrated waste slurries are expected to exhibit non-Newtonian rheology, which can be represented by a simple Bingham plastic model. With this model the slurries are characterized by yield stress and a consistency factor. The presence of yield stress means that a certain amount of excess shear must be applied to maintain material motion. Many slurries also develop gel-like properties when they are at rest for a period of time. These behave like very weak solids, a behavior that is characterized by shear strength that is typically greater than yield stress. When an applied force exceeds the shear strength the gel structure fails, and the slurry acts like a fluid and begins to flow.

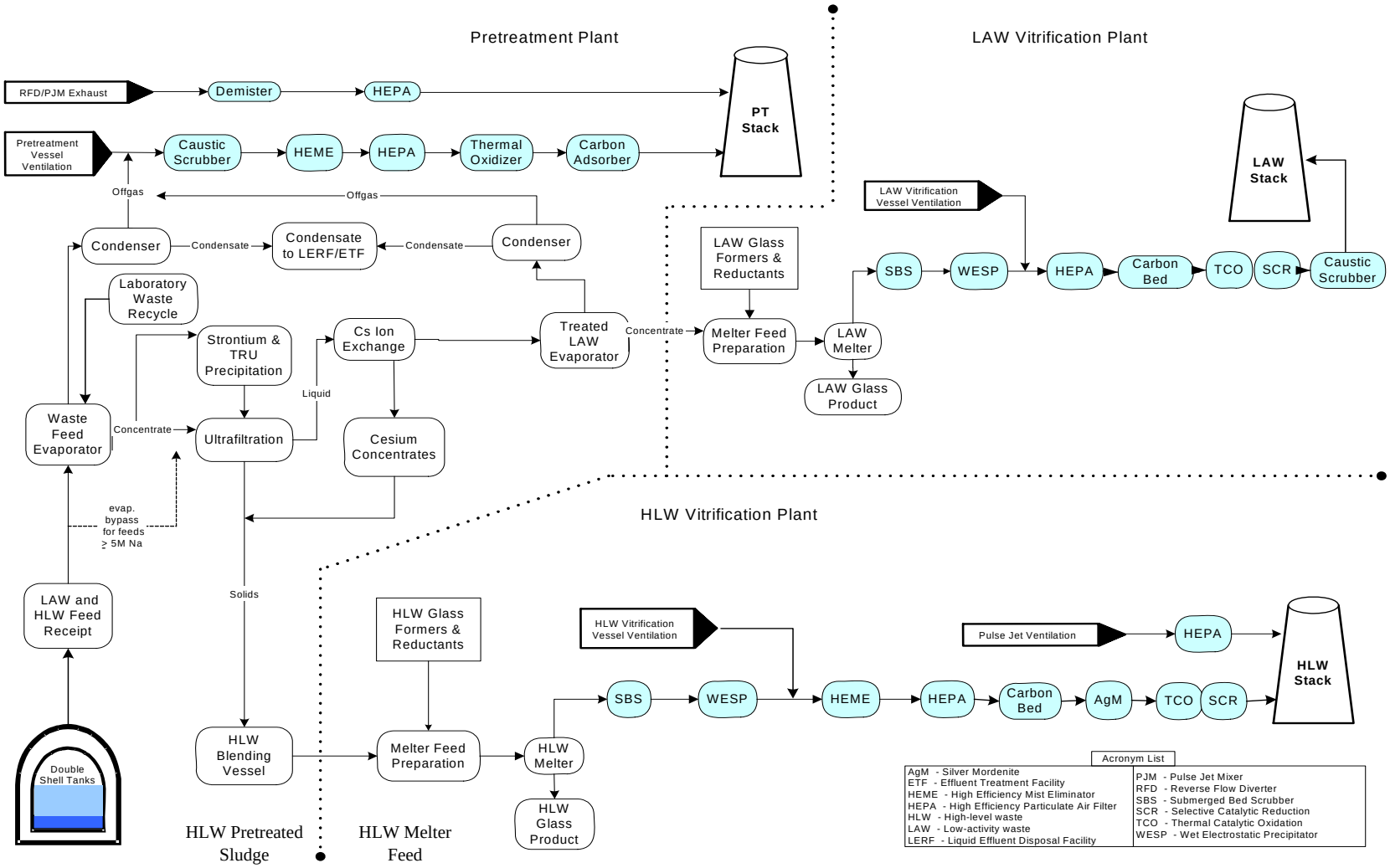

Figure 1.1. WTP Basic Process Flow Sheet

One of the primary concerns with non-Newtonian slurries is their propensity to retain flammable gases. Radioactive waste generates hydrogen and other gases by the processes of radiolysis and thermolysis. Hydrogen is the primary flammable gas of concern. Other gases generated in significant quantities include (but are not limited to) ammonia, methane, carbon dioxide, nitrogen, nitrous oxide, and oxygen. These gases will generally bubble out of slurries with low concentrations of solids. However, concentrated slurries with a significant yield stress or shear strength will trap gas bubbles in situ and can allow buildup of 20 to 40% total retained gas in a stagnant state (Gauglitz et al. 1996). A sudden release of this gas could form a flammable gas mixture in the headspace of the tank and/or the plant ventilation system. Thus the mixing system must be able to adequately shear the waste contents to allow the gas to be released more gradually in a safe and controlled manner.

The tank contents must be mixed adequately for several reasons beyond ensuring controlled releases of flammable gases, including maintaining a reasonable degree of homogeneity in process vessels to ensure representative samples, limiting solids settling and stratification, improving heat transfer, and mixing in various process solutions that are typically added to the top of the vessel contents. Examples of process solutions include water, caustic, and nitric acid eluent from cesium ion exchange. All of these solutions are less dense than the concentrated slurries, so vigorous mixing is needed at the surface to overcome buoyancy.

Based on an assessment of the plant flow sheet and rheological data from actual tank wastes, seven tanks were projected to be used for non-Newtonian slurries: two UFP vessels, two HLW LS vessels, a HLW blend tank, and two HLW CRVs. The LS vessels and the blend tank are very similar in size and geometry and are generally treated the same for testing purposes. The CRVs have been removed from the plant design and are mentioned here only for completeness. Three scaled prototype vessels represent the plant vessels, as outlined in Table 1.1.

Table 1.1. Relationship of WPT Vessels to Test Vessels

Scaled Prototype Nomenclature	WTP Vessel Identification
Lag Storage (LS)	HLW Lag Storage: HLP-VSL-00027A/B HLW Blend: HLP-VSL-00028
Ultra Filtration Process (UFP) Vessel	UFP-VSL-00002A/B
Concentrate Receipt Vessel (CRV)	HCP-VSL-00001/00002

1.1.2 Pulse Jet Mixer Technology Applied to Non-Newtonian Slurries

PJM technology was planned for mixing most vessels in the WTP. This technology had been selected for use in so-called “black cell” regions of the WTP where maintenance capability will not be available for the operating life of the WTP. PJM technology was selected for use in these regions because it has no moving mechanical parts that require maintenance.

PJM mixing technology involves a pulse tube coupled with a jet nozzle. One end of the tube is immersed in the tank while periodic pressure, vacuum, and venting are supplied to the opposite end. Changing the applied pressure creates three operating modes for the pulse tube: 1) the drive mode, when pressure is applied to discharge the contents of the PJM tube through the nozzle at high velocity; 2) the

vent mode, when the pressure is vented to the atmosphere and the pulse tube and tank approach the same fill level; and 3) the refill mode, when vacuum is applied to refill the pulse tube. The PJM system uses these operating modes to produce a sequence of drive cycles that provide mixing in the vessel. PJM operating parameters—number of PJMs, applied pressure, nozzle diameter, nozzle exit velocity, and drive time—along with the rheological properties of the fluid being mixed contribute to the effectiveness of mixing within the vessel.

PJM technology had been used successfully in the past for mixing Newtonian fluids in radioactive environments. However, the technology had not been applied to non-Newtonian slurries, so an adequate supporting technical basis was not available. The field of Newtonian fluid mixing is mature and supported by significant theoretical and practical knowledge for designing mixing systems. These systems can be mechanical (impellers or agitators) or hydrodynamic (steady or pulse fluid jets). For non-Newtonian fluids, the majority of mixing experience is associated with mechanical agitators. The subject of jet mixing in non-Newtonian fluids is a relatively new and developing field, with some theoretical analysis and applied research being pursued in industry and academia. Nonsteady jet mixing in non-Newtonian fluids is essentially a new topic of study. However, some of the concepts and approaches associated with mechanical mixing of non-Newtonian fluids are applicable to the nonsteady jet mixing processes associated with PJMs.

One essential phenomenon observed in mixing of non-Newtonian fluids is the formation of a cavern in the mixing zone, as illustrated in Figure 1.2. A cavern is an enclosed region near the mixing jet that is highly agitated and turbulent during portions of the mixing cycle. The cavern is surrounded by material that is essentially stationary, and the transition between the two regions can be very abrupt. The cavern forms because the fluid velocity in the jet decreases with distance from the nozzle. At some point, fluid velocities are so low that the resulting flow-induced fluid stresses are no longer able to overcome the shear strength of the non-Newtonian material. Hence, a stable force balance occurs and flow ceases at the boundary of the cavern. As the jet discharge increases, fluid velocities increase and cavern volume grows. As the strength of the non-Newtonian material increases, the cavern becomes smaller.

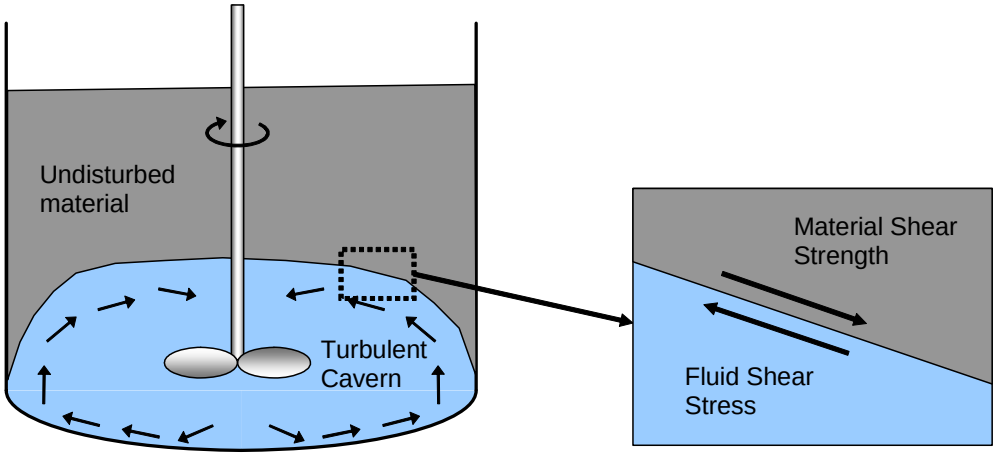

Figure 1.2. Illustrating Cavern Formation in Non-Newtonian Waste

The primary mixing requirement for the PJM systems in the WTP vessels containing non-Newtonian slurries was eliminating the cavern altogether because effective gas release, blending, and solids suspension all depend on complete fluid motion everywhere in the vessel. Eliminating the cavern required an adequate understanding of the performance of PJMs in non-Newtonian slurries as well as the various factors affecting performance (e.g., number of PJMs, nozzle diameter, and discharge velocity).

1.1.3 The Need for an Experimental Test Program

Given the limited knowledge of how PJMs perform in non-Newtonian slurries, early efforts to rate the mixing system designs used computational approaches. Computational fluid dynamics (CFD) was used with some success to model mixing in Newtonian fluids, but applying it to PJM mixing in WTP vessels was very difficult. Major challenges included modeling yield stress materials, defining minimum velocities that accurately delineate between moving and stationary regions, and modeling turbulent and laminar regions resulting from unsteady-state PJM operation. These challenges needed to be resolved before CFD could model mixing behavior accurately. Thus, pursuing a CFD approach for non-Newtonian slurries involved the significant risk of developing new computational models, benchmark testing, and protracted analyses.

To reduce this risk, a less analytical, more empirical strategy was developed that included testing at various scales. On the basis of recommendations from an assembled PJM Task Team, which included representatives from WTP Research and Technology (R&T), WTP Engineering, Bechtel Research and Development (R&D), fluidics contractor AEA Technology, and mixing consultants, it was agreed to shift the design validation approach to testing non-Newtonian fluid-filled vessels. This was seen as more efficient in terms of cost, schedule, and assurance of closure of the technical issues.

1.2 The WTP Non-Newtonian PJM Test Program

Phase I of the test program was established in June 2003. The PJM Task Team developed an integrated strategy for scaled testing to demonstrate mixing in WTP vessels containing non-Newtonian slurries.[(a)] The scaled PJM system tests were intended to provide information on the operating parameters critical for uniform movement (total mobilization) of these non-Newtonian slurries. The WTP project also funded work addressing the behavior of flammable gas in the non-Newtonian slurries. This involved determining hydrogen generation rate source terms and evaluating gas transport characteristics during PJM operation. Gas transport testing investigated gas retention and release (GR&R) characteristics within non-Newtonian slurries during mixing operations to 1) support development of PJM mixing systems, 2) understand these characteristics within the selected mixing system, and 3) allow development of normal operation and post-design basis event (DBE) mixing strategies. Phase I employed a scaled testing strategy that incorporated simulant development, scaling tests, and scaled prototype testing.

The initial scaled tests in October 2003 demonstrated that the baseline pulse jet designs did not mix the non-Newtonian slurries to the extent necessary to meet WTP requirements. In November 2003,

(a) Smith GL, H Abodishish, P Meyer, and A Bronner. June 17, 2003. *Action Plan: WTP Pulse Jet Mixing and Hydrogen Release for Process Vessels Containing non-Newtonian Slurries*. 24590-WTP-PL-RT-04-0002, Bechtel National Inc., Richland, Washington.

Phase I of the PJM program developed an alternative “PJM-only” configuration that mixed the vessels containing non-Newtonian slurries in accordance with WTP requirements. In December 2003, Phase I scaled GR&R testing demonstrated that the WTP could provide safe gas control with these configurations. In the same time frame, the hydrogen generation rate source testing was completed using actual waste samples from "expected worst-case" tanks, and a better correlation was developed to predict hydrogen generation for use by the WTP Project.

While the alternative PJM configuration was acceptable, implementation of the PJM-only mixing systems severely impacted the WTP facility designs due to increased numbers of PJMs, additional piping, and the significantly increased air consumption needed to operate the systems. Accordingly, the PJM Task Team was directed to develop PJM hybrid mixing systems to minimize the impact to overall project cost and schedule. Phase II of the PJM program investigated alternative configurations to assess the effects of slurry rheology changes, reduced tank volume, PJM jet velocity and nozzle size, sparging, and recirculation pump operation. Additional testing of Phase II PJM hybrid mixing systems demonstrated that the modified configurations mixed non-Newtonian slurries in accordance with WTP requirements. GR&R testing demonstrated that the selected PJM hybrid configurations provided safe gas control in accordance with WTP requirements.

While the testing performed in Phase II addressed most of the issues associated with management and scale-up of mixing and flammable gas retention and release, some WTP engineering issues required additional testing, including the size of backup important-to-safety (ITS) air compressors and diesel generators, the removal of recirculation pumps from the LS and blend vessels, and the need for redundant infrastructure for operating the PJMs. Hence a confirmatory demonstration of a large, correctly scaled hybrid mixing system was determined to be necessary. This demonstration was to address specific operation scenarios such as normal operations, post-DBE operations, and near-term accident response (NTAR) operations.

This large-scale demonstration became Phase III of the test program. Testing was performed in a half-scale vessel representing the plant LS and blend vessels. Phase III of the test program was completed by applying the test results to the plant-scale LS and blend vessels. This was necessary because the design-basis gas generation rates for the plant were somewhat different than those required by the testing approach. The results from the Phase III testing on scaled LS and blend vessels were also extended to the plant-scale UFP vessels.

The WTP non-Newtonian Test Program was a highly accelerated, integrated effort. As test data became available, the ramifications to the plant design were assessed by the WTP in terms of impact on cost and schedule. Hence, the test program evolved to respond in a timely manner to engineering requirements. The list below chronicles the key decisions and milestones that dictated the direction of the testing efforts.

4/03 WTP recognized that CFD is inadequate to predict mixing behavior in non-Newtonian vessels and identified need for test program.

4/03 Scaled testing strategy developed.

6/03 Scaled testing program approved by WTP.

- Simulant selection activities began at Battelle – Pacific Northwest Division (PNWD).
- Design and procure activities for ¼-scale prototypic vessels (CRV, UFP, LS) began.

8/03 Transparent and opaque simulants selected.
9/03 Phase I proof-of-scaling tests began in 4PJM vessels.
9/03 Began testing ¼-scale prototypes.
10/03 Demonstrated baseline PJM designs fail.
- Investigation of alternative PJM geometries began.

10/03 GR&R work authorized.
11/03 Final PJM-only mixing options identified.
12/03 Final PJM-only mixing configuration recommended.
1/04 Engineering analysis demonstrated design not acceptable from cost perspective.
- Decision made to pursue PJM hybrid mixing systems.
- Hybrid options selected (PJM, sparge, recirculation pumps).

2/04 Hybrid mixing configuration testing completed.
2/04 Single sparge tube ZOI testing initiated.
2/04 PJM nozzle angles selected for testing distributed PJMs.
3/04 Final hybrid system configuration option 1 recommended (PJMs, sparge tubes, recirculation pumps).
- Intermittent sparge operation suggested (Option 2 allows for elimination of recirculation pumps).

3/04 Cluster PJM configuration selected over distributed PJMs
3/04 Hydrogen generation rate calculated by WTP Project.
4/04 Engineering decided pumps in LS vessel not feasible; decision made to pursue Option 2 design.
5/04 Multiple sparge tube testing begins to support Option 2.
6/04 Multiple sparge tube data show effective gas release, supporting Option 2.
6/04 Project directed to pursue ½-scale testing (HSLS) for confirmation and final demonstration.
7/04 CRV eliminated from plant design.
9/04 Decision made to operate PJMs at ½-stroke to avoid control difficulties.
9/04 HSLS testing began.
12/04 HSLS testing completed.
3/05 Bubble column tests with antifoaming agent.
6/05 Completed reporting.

1.3 Technical Overview of the Non-Newtonian PJM Test Program

Small-scale testing is a common approach used successfully in the many varied fields of applied fluid dynamics. The approach is successful because system performance usually depends on certain non-dimensional groupings of physical parameters and, if these parameter groupings can be preserved at different geometric scales (i.e., large and small), the essential behavior of the system will be the same at both. This principle is referred to as similarity in the theory of fluid dynamics engineering. In complex fluid dynamic problems there can be many nondimensional parameter groups; however, the essential behavior of the phenomenon is often dominated by only a few key groups. In this situation, small-scale testing can produce results that are very close to large-scale behavior. The non-Newtonian PJM Test Program used the following scaled testing approach:

- ***Simulant Development***. Develop simulants that are physically similar to actual non-Newtonian waste expected in the WTP. The key parameters are density, yield stress, shear strength, consistency, and particle morphology.

- ***Develop Scaling Laws***. Determine important nondimensional parameters governing mixing and GR&R in non-Newtonian slurries. From these, determine how to design and operate reduced-scale mixing systems so that the results accurately simulate full-scale mixing.
- ***Validate Scaling Laws***. Perform mixing and GR&R tests at multiple physical scales. Compare results nondimensionally to validate the scaling laws.
- ***Prototypic Testing at Reduced Scale***. Perform tests of key WTP vessels with PJM configurations at reduced scale to evaluate PJM mixing performance. Modify systems as needed to achieve acceptable performance.

As the program evolved into hybrid mixing systems using both PJMs and air sparging, the scaled testing approach was modified somewhat. The geometric scale-up of sparge operation is highly nonlinear and introduces a number of complexities. Hence a new approach was employed, using scaled PJM test results combined with large-scale sparge results.

The key components of the non-Newtonian PJM Test Program are shown in Figure 1.3. The program essentially evolved into three phases. Phase I was the initial program to perform scaled testing of PJM systems. Phase IA addressed mixing in non-Newtonian slurries and involved simulant development, testing to validate the scaling approach, and finally tests in scaled prototypic WTP vessels. Phase IB directly paralleled the mixing work, but the focus was on GR&R behavior. Phase II of the program involved PJM hybrid mixing systems. Much of the same equipment and approaches were used in this phase; however, the addition of sparging required modifications to the scaled testing approach because sparge mixing does not scale easily. Instead, nearly full-scale sparge testing was undertaken. In the final phase of the test program, ½-scale tests were performed to demonstrate various operational scenarios that involved intermittent operation. The following sections summarize the technical approach used in each of key aspects of the test approach.

1.3.1 Simulant Development

To assess mixing performance and GR&R behavior in the test vessels, extensive use was made of two clay simulants, one Laponite-based and the other a kaolin/bentonite clay simulant. The Laponite-based simulant is a synthetic clay that is transparent in an aqueous slurry. This simulant was particularly useful for the initial testing because it allowed direct visual observation of mixing and GR&R behavior. The kaolin/bentonite clay is opaque, but it is a closer match to the rheology and particle morphology of the particulate waste slurries. Both simulants are inexpensive, nonhazardous, and representative of pertinent physical and rheological properties of actual waste. The technical basis for the development and selection of these simulants is provided in Poloski et al. (2004a).

Oxygen gas generated by the decomposition of hydrogen peroxide was selected to simulate in situ generation of hydrogen and other gases for testing GR&R behavior. A further advantage of kaolin/ bentonite clay is that it provided the catalytic surfaces required for hydrogen peroxide decomposition. The technical basis for the development of the gas generation method is provided in Russell et al. (2005).

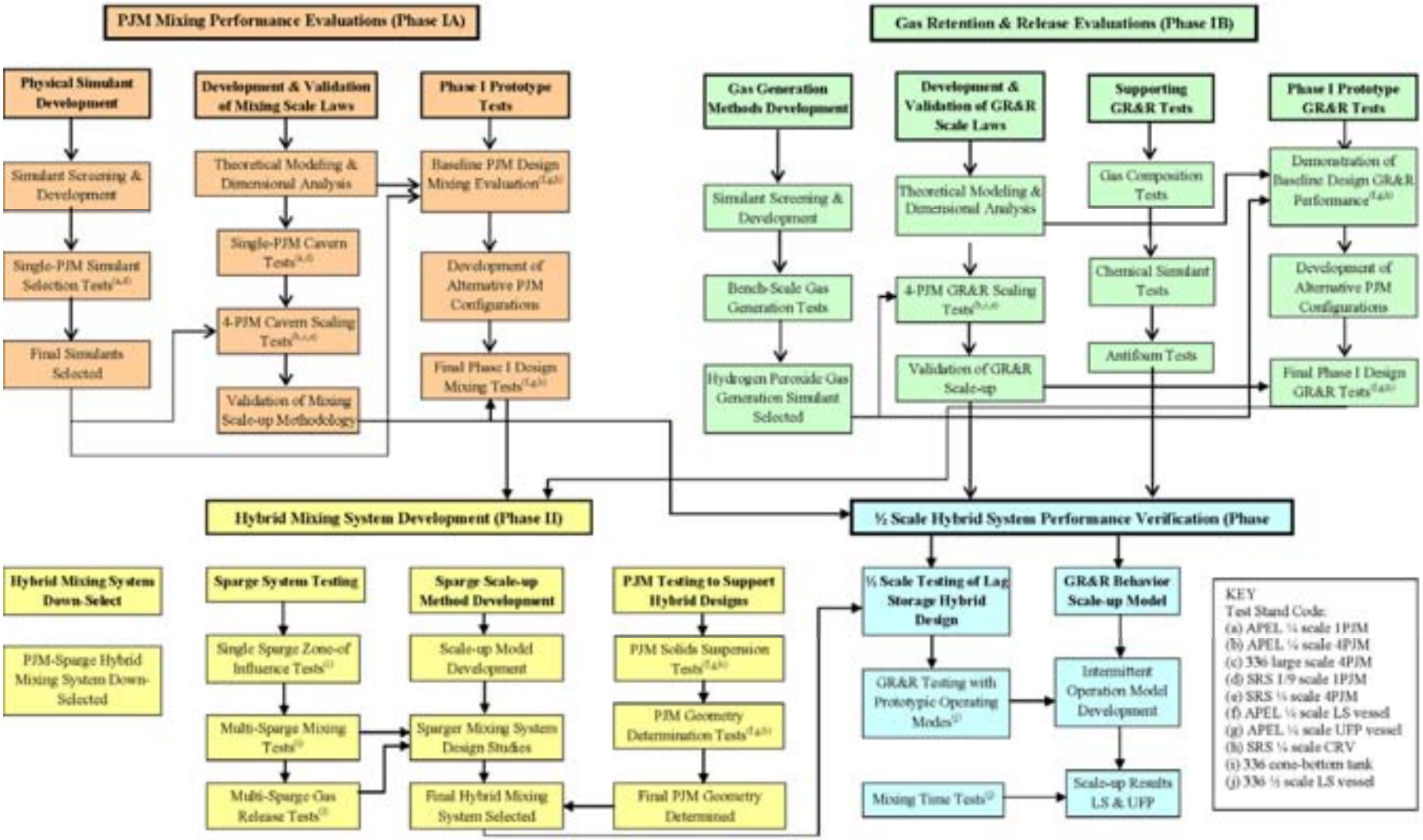

Figure 1.3. The Non-Newtonian PJM Test Program

1.3.2 Development and Validation of a Scaling Methodology

The technical basis for scale-up of nonsteady mixing induced by PJMs is based on theoretical modeling, dimensional analysis, and mixing tests. Theoretical modeling developed a physically based model that predicted the height of a mixing cavern resulting from pulse jets in non-Newtonian fluids. Dimensional analysis identified the important dimensionless parameters and guided the experimental design. Mixing tests conducted at three physical scales proved that testing at a reduced scale was adequate for assessing mixing performance. These scales included large-scale (nearly full-scale) tests at the 336 Building, ~¼-scale tests at the Applied Process Engineering Laboratory (APEL), and small-scale (~1/9) tests at Savannah River National Laboratory (SRNL) (formerly Savannah River Technology Center) (Wilson et al. 2004). Each of these geometrically similar vessels had a mixing system consisting of four geometrically similar PJMs. Mixing results were compared to demonstrate that testing at a reduced scale is a conservative way to predict full-scale mixing performance in WTP vessels (Bamberger et al. 2005).

In a similar fashion, theoretical analysis and scaling tests were also performed on mixing systems with GR&R. Results were again compared at the three physical scales to demonstrate scale-up laws for GR&R behavior (Russell et al. 2005).

1.3.3 Scaled Prototype Testing at Reduced Scale

Another component of the scaled test strategy was to test prototypic vessels at reduced scale. The seven vessels designed to contain and mix non-Newtonian simulants are adequately represented by a subset of three: the UFP vessel, the LS vessel, and the CRV. Models at approximately ¼ scale were fabricated that maintained the essential prototypic features, including vessel and PJM geometry, number of PJMs, operational parameters, and major vessel internals. These reduced-scale prototypic vessels allow for performance assessment of the baseline design, obtaining information on key operating parameters, and identifying PJM configurations with improved performance. The initial phase of prototypic vessel tests to assess mixing focused on the use of PJMs only and is reported in Bates et al. (2004) and Guerrero and Eberl (2004a). The second phase of testing evaluated various PJM/hybrid mixing designs that are reported in Johnson et al. (2005) and Guerrero and Eberl (2004a). The results of GR&R tests are reported in Russell et al. (2005) and Guerrero and Eberl (2004b).

1.3.4 Hybrid Mixing System Development

As the program evolved into hybrid mixing systems using both PJMs and air sparging, the scaled testing approach developed in Phase I of the program required modification. The rising sparge bubbles and the associated fluid interaction of the surrounding slurry exhibit nonlinear scaled behavior, and a test program required to develop nonlinear sparge mixing scale laws was impractical. Therefore, a strategy was developed that applied small-scale PJM mixing results in the lower region of the vessels (the region mixed by PJMs) and nearly full-scale sparge mixing results to the upper region (the region primarily mixed by the rising sparge bubbles).

Because basic data were lacking on the mixing performance of air sparge systems in non-Newtonian slurries, it was necessary to generate these data. Several nearly full-scale tests were conducted in a large-

scale vessel with single and multiple sparge-tube systems to characterize the mixing and gas release performance of air-sparged systems in simulants with non-Newtonian rheology. The tests performed on single sparge-tube systems provided an understanding of the basic characteristics of a sparge-induced mixing zone. From these results, a conservative approach was determined for specifying arrays of sparge tubes required to mix the upper region of plant scale vessels. Tests with a multiple sparge tube system addressed the GR&R characteristics of sparge mixing. The large-scale sparge tests are reported in Poloski et al. (2005).

1.3.5 Large-Scale Demonstration of Operational Modes

This phase of the test strategy was essentially a confirmatory demonstration of a large, correctly scaled hybrid mixing system. A scale factor of ½ was considered large enough to render any potential scaling issues negligible. The test represented the plant LS and blend vessels. The primary testing objective was to demonstrate successful cyclic operation that reestablished full mixing and released accumulated gas each time full mixing resumed. Tests included normal operations with continuous PJM operation with intermittent sparging, post-DBE operations with intermittent operation of both PJMs and spargers, and an NTAR scenario with intermittent sparging. The main challenge in planning these tests was simulating uniform continuous gas generation with oxygen generated by hydrogen peroxide decomposition. The challenge was met by injecting the hydrogen peroxide at a higher rate during mixing periods and shortening the idle portions of the cycle to accommodate its relatively rapid decomposition. Mixing tests using a chloride ion tracer were also performed with continuous sparging and continuous operation of both PJMs and spargers to determine blend and mixing times and quantify the volume of unmixed slurry during sparger-only operation.

A simple gas inventory model was developed as a vehicle to apply the established scaling laws to the cyclic mixing tests and to scale the results up to full-scale LS and blend vessels. The scale-up process employed a Monte Carlo simulation to correctly include variability in the test data, measurement uncertainty, and uncertainty in the scale-up process itself. The scale-up methodology was also extended to the plant UFP vessel based on ¼-scale test data.

1.4 Report Scope

This report summarizes the major approaches, techniques, and testing efforts used to support the PJM non-Newtonian Test Program. Section 2 presents the quality requirements of the work. Section 3 presents the important theoretical considerations and models developed to guide the design and operation of scaled tests. Simulant development activities that supported the test program are summarized in Section 4, and the various test stands, measurement methods, and instrumentation are discussed in Section 5. Section 6 presents test results that were used to validate the scaled testing approach; the results of the Phase I scaled prototype performance evaluations are summarized in Section 7. Section 8 contains an overview of the results of the Phase II hybrid mixing systems development testing. Section 9 summarizes the Phase III ½-scale confirmatory tests, while final scale-up of these results is presented in Section 10. Cited references are listed in Section 11.

While the work summarized in this report captures the major activities supporting the PJM non-Newtonian Test Program, the report is by no means comprehensive. Several additional activities were

performed in support of the program that were not included in this report for the sake of brevity or because they didn't play a direct role in developing the final mixing systems. These activities are mentioned here only for completeness.

Bubble column tests with various simulants were carried out to support GR&R scale-up. Results of these tests are found in Russell et al. (2005), as are testing and analysis of mass transfer rates for dissolved gases in clay slurry. Measurements of aerosols generated from sparge operation are reported in Poloski et al. (2005). Surface tension measurements for clay and chemical simulants that were made to support the understanding of aerosol phenomena as well as the potential for foaming are presented in Poloski et al. (2005) as well. Various rheology modifiers were evaluated to reduce simulant yield stress. Results of these studies are presented in Stone (2005). Finally, bench-scale measurements of gas holdup and release characteristics were made at Florida International University. Results of these tests can be found in Sundar (2004).

2.0 Quality Requirements

The Battelle – Pacific Northwest Division (PNWD) Quality Assurance Program is based on the requirements defined in the U.S. Department of Energy (DOE) Order 414.1A, Quality Assurance, and 10 CFR 830, Energy/Nuclear Safety Management, Subpart A, Quality Assurance Requirements (a.k.a. the Quality Rule). PNWD has chosen to implement the requirements of DOE Order 414.1A and 10 CFR 830 Subpart A by integrating them into the Laboratory's management systems and daily operating processes. The procedures needed to implement the requirements are documented through PNWD's Standards-Based Management System.

PNWD implements the Waste Treatment Plant (WTP) quality requirements by performing work in accordance with the PNWD WTP Support Project quality assurance project plan (QAPjP) approved by the WTP Quality Assurance organization. This work was performed to the quality requirements of NQA-1-1989 Part I, Basic and Supplementary Requirements, NQA-2a-1990, Part 2.7 and DOE/RW-0333P, Rev. 13, Quality Assurance Requirements and Description. These quality requirements are implemented through PNWD's WTP Support Project (WTPSP) Quality Assurance Requirements and Description Manual. The analytical requirements are implemented through WTPSP's Statement of Work (WTPSP-SOW-005) with the Radiochemical Processing Laboratory Analytical Service Operations.

Experiments that were not method-specific were performed in accordance with PNWD procedures QA-RPP-WTP-1101, "Scientific Investigations," and QA-RPP-WTP-1201, "Calibration Control System," ensuring that sufficient data were taken with properly calibrated measuring and test equipment to obtain quality results.

Reportable measurements of distance were made using standard commercially available equipment (e.g., tape measure, scale) and required no traceable calibration requirements. All other test equipment used to generate reportable data was calibrated according to PNWD's WTPSP Quality Assurance program. The DASYLab software used to acquire data from the sensors was verified and validated by PNWD WTPSP staff prior to use, and BNI conducted an acceptance surveillance of the verification and validation activities with no problems noted.

PNWD addresses internal verification and validation activities by conducting an independent technical review of the final data report in accordance with PNWD procedure QA-RPP-WTP-604. This review verifies that the reported results are traceable, that inferences and conclusions are soundly based, and that the reported work satisfies the Test Plan objectives. This review procedure is part of PNWD's WTPSP Quality Assurance Requirements and Description Manual.

3.0 Supporting Theory

This section summarizes the important theoretical bases of the WTP non-Newtonian Scaled Test Program. It provides an overview of the theory and technical approach to scaled testing of PJM mixing systems, GR&R behavior, and PJM-sparge hybrid mixing system testing. Many of the results presented here are based on in-depth analyses that are documented in other reports. The primary sources are Bamberger (2005), Russell et al. (2005), Poloski et al. (2005), Wilson et al. (2004), and Bontha et al. (2005).

3.1 Introduction

Analyzing mixing in non-Newtonian slurries is much more challenging than analyzing Newtonian fluids. In Newtonian fluids, the fluid stress is directly proportional to the fluid strain, and viscosity is generally constant. Examples of Newtonian fluids are water, oils, solvents, and, in some cases, slurries. Non-Newtonian fluids are a broad class encompassing all fluids whose rheology deviates from Newtonian. Many of the Hanford waste slurries to be received and processed in the WTP exhibit non-Newtonian behavior. In particular, when stationary, they can develop gel-like properties where they behave like very weak solids. When an applied force exceeds their shear strength, they act like a fluid and begin to flow. And when they flow they can still exhibit an additional nonviscous stress referred to as yield stress.

The field of Newtonian fluid mixing is mature and supported by a broad theoretical and practical knowledge base for designing mixing systems. These systems can be mechanical (impellers or agitators) or hydrodynamic (steady or pulse fluid jets). For non-Newtonian fluids, the majority of mixing experience is associated with mechanical agitators. The subject of jet mixing in non-Newtonian fluids is a relatively new and developing field, with some theoretical analysis and applied research being pursued in industry and academia. Nonsteady jet mixing in non-Newtonian fluids is essentially a new topic of study. Although in its infancy, non-Newtonian fluid jet mixing can derive a great deal of understanding and guidance from the more mature fields of jet mixing in Newtonian fluids and mechanical mixing in non-Newtonian fluids.

Gas retention and release behavior in non-Newtonian slurries is also complex; there is little first-principle or practical information available. However, mass balance models combined with bubble rise modeling has proved to be an excellent basis for understanding many of the essential phenomena.

Like jet mixing, the understanding of air sparge mixing of non-Newtonian slurries is in its infancy. Spargers have been used extensively to mix and suspend solids in Newtonian fluids, and design rules are available to guide the number of spargers and air flow rates required. No such general rules exist for air sparging in non-Newtonian slurries. Therefore, it was necessary to develop from first principles an elemental theory to help guide the design of scaled test approaches as well interpret and apply test results to plant-scale mixing systems.

3.2 Theory of Pulse Jet Mixing in Non-Newtonian Fluids

3.2.1 Non-Newtonian Rheology and Cavern Formation

One essential phenomenon observed in mechanical mixing of non-Newtonian fluids is the formation of a cavern, as illustrated in Figure 3.1. A cavern is essentially a bounded region near the impeller that is highly agitated and turbulent surrounded by material that is essentially stationary. The transition between the two regions can be very abrupt. The cavern forms because fluid motion created by the impeller decreases with distance from the impeller. At some point, fluid velocities are so low that the resulting fluid stresses are no longer able to overcome the shear strength of the non-Newtonian material, and a stable force equilibrium occurs (illustrated in Figure 3.1). As the impeller speed increases, fluid velocities increase and the cavern grows. As the strength of the non-Newtonian material increases, the cavern becomes smaller at a given impeller speed. A successful mixing system design involves placing and operating agitators so there are no regions of stationary material in the mixing vessel.

Caverns have also been observed to form when using steady jets. Early testing at PNWD also confirmed that caverns form when fluid is agitated using steady jets created by PJMs (Enderlin et al. 2003). This result is to be expected given the similarity between jet mixing and mechanical agitation (both create fluid motion). However, in the absence of established design guidelines for PJM operation in non-Newtonian fluids, a test program was required to establish design criteria for PJM systems that ensure the entire vessel contents are mobilized and no caverns are present.

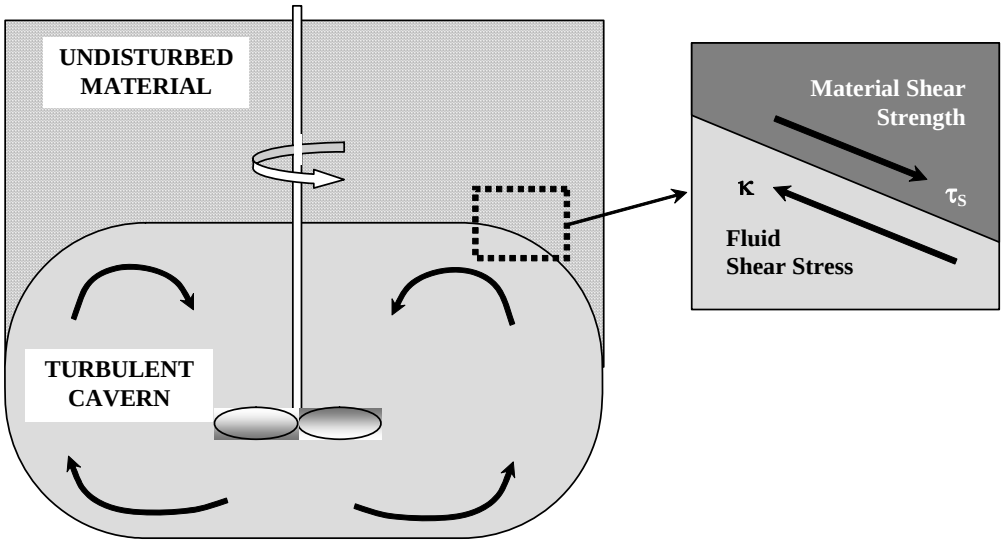

Figure 3.1. Illustration of Cavern Formation During Mechanical Mixing in Non-Newtonian Material

Cavern formation is highly dependent on the rheological properties of the slurry. Tests with actual waste samples suggest the waste is best represented by the Bingham plastic rheological model illustrated by the rheogram shown in Figure 3.2. The rheogram is obtained with a rheometer, which measures the shear stress as a function of rate of strain for laminar flow. The model is characterized by yield stress, τ_y, which is the shear stress extrapolated to zero strain rate, and consistency, κ, the slope of the linear region. The bounding best-fit parameters of actual waste slurry are τ_y = 30 Pa and κ = 30 cP.

While the laminar flow rheogram is useful, it does not adequately describe all the relevant rheology for the cavern formation problem. Before it is disturbed, actual waste slurry will possess shear strength, τ_s. Thus, the actual waste appears to be thixotropic, i.e., the shear stress can decrease while experiencing a strain rate. Specifically, we expect the shear stress of a fluid undisturbed for some time to exhibit one characteristic value, shear strength, which then decreases asymptotically over time during strain to a smaller value, yield stress. This is illustrated by the point on the rheogram at zero strain rate in Figure 3.2, as well as in Figure 3.3 in the region entitled "applied shear." If the fluid remains unstrained for some time, the shear stress extrapolated to zero strain rate will return from the yield stress to the shear strength. This is illustrated in the region entitled "re-gel period" in Figure 3.3. Apparently, the time to decrease from the shear strength to the yield stress is fast enough and the time to return from the yield stress to the shear strength long enough that effectively the fluid behavior divides into one region where strain events are repeated quickly enough that the zero-strain shear stress remains at the yield strength, and another region in which the fluid rarely experiences strain and the zero-strain shear stress remains at the shear strength.

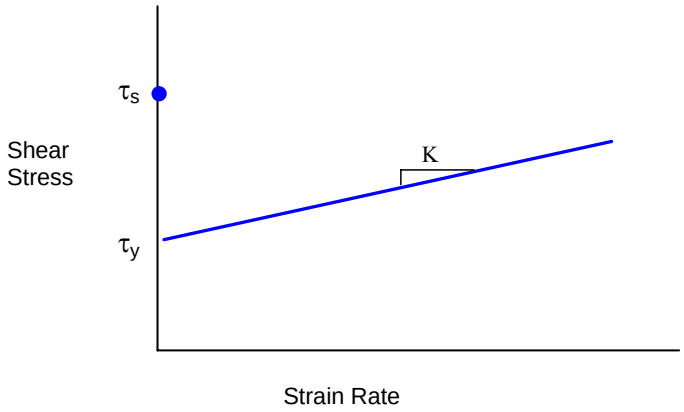

Figure 3.2. Bingham Plastic Rheological Model. Also shown is shear strength of undisturbed slurry.

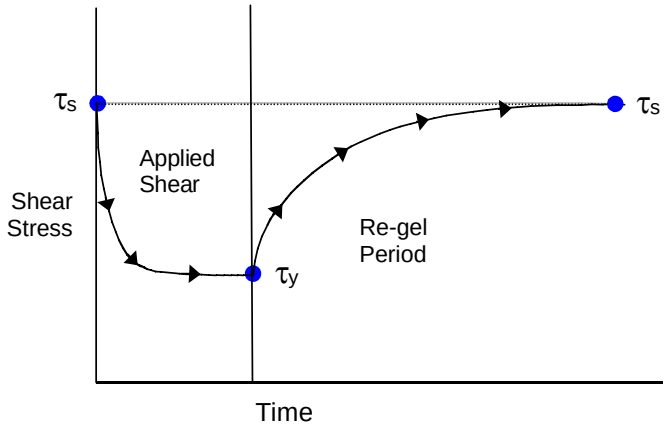

Figure 3.3. Illustration of Time-Dependent Behavior of Non-Newtonian Slurry

The shear strength will generally be larger than the yield stress. The ratio of shear strength to yield stress is a useful characterization parameter for a particulate slurry. There is no general relationship between shear strength and yield stress, and the ratio τ_s/τ_y can range from approximately one to many orders of magnitude.

Another limitation of the Bingham plastic model is that turbulent conditions exist inside the cavern. The behavior of Bingham plastic fluids in turbulent flow is not well understood. The yield stress may not be present (or significant) for turbulent flow of a particulate slurry. Rather, the behavior is more Newtonian, with the Newtonian viscosity (μ) approximately equal to Bingham consistency (κ). However, the Bingham yield stress may be important in the boundary layer at the cavern interface. As the velocity slows at the interface, it will at some point relaminarize. Under these conditions, the laminar Bingham rheology will apply. This boundary layer region is believed to be quite thin, and the effects of the yield stress are therefore minor. However, the topic of turbulent to laminar transition in a non-Newtonian slurry is not well understood generally, and it is possible that the presence of yield stress in the boundary layer could affect the extent of the cavern. Overall, the shear strength, τ_s, yield stress, τ_y, and the consistency, κ, are thought to be the most important rheological parameters governing cavern formation in a non-Newtonian particulate-laden slurry.

3.2.2 Principles of PJM Operation

PJM mixing technology involves a pulse tube coupled with a jet nozzle. One end of the tube is immersed in the tank while periodic pressure, vacuum, and venting are supplied to the opposite end. There are three operating modes for the pulse tube: 1) the drive mode, when pressure is applied to discharge the contents of the PJM tube through the nozzle at high velocity; 2) the vent mode, when the pressure is vented to the atmosphere and the pulse tube and tank approach the same fill level; and 3) the refill mode, when vacuum is applied to refill the pulse tube. The PJM system uses these operating modes to produce a sequence of drive cycles that provide mixing in the vessel. PJM operating parameters—applied pressure, nozzle exit velocity, nozzle diameter, and drive time—along with the rheological properties of the fluid being mixed contribute to the effectiveness of mixing within the vessel.

A typical PJM system configuration in a vessel is shown schematically in Figure 3.4.[(a)] The tank has diameter D_T, volume V_T, and operating level H. There are N PJMs in the tank, each with pulse tube diameter D_{PT} and volume V_{PT}. Each PJM has a conical nozzle with diameter d_0. Typically, the total volume of the pulse tubes, N V_{PT}, is approximately 10 to 15% of the operating volume of the vessel. During the drive phase, the tube is pressurized and a volume of slurry is discharged. The level change in the tube during discharge is ΔL with a corresponding increase in waste level ΔH, which is about 8 to 12% of the operating level, H.

(a) The PJM configuration used for this analysis is somewhat simplified. Vessels and PJMs are assumed to be cylindrical, and other vessel internals are neglected.

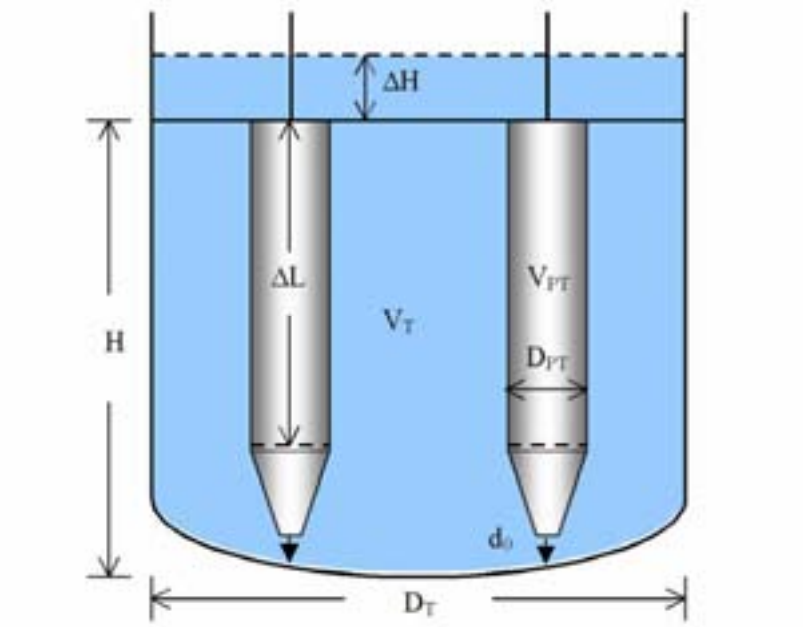

Figure 3.4. Illustration of a Typical PJM System in a WTP Vessel

The discharge velocity during the drive phase is constrained by the drive pressure and the geometry of the pulse tube. The nominal velocity, u_0, is given by

$$u_0 = \frac{D_{PT}^2}{d_0^2}\frac{\Delta L}{t_D} \tag{3.1}$$

where t_D is drive time. The drive pressure, p_D, required to produce the discharge velocity is given by

$$p_D = p_e + \frac{C_L}{2}\rho u_0^2 \tag{3.2}$$

where p_e is the pressure head at the nozzle exit, C_L is the nozzle loss coefficient, and ρ is the slurry density.

Immediately after the drive phase, a vent is opened and excess pressure allowed to vent to atmosphere. During the suction phase, vacuum is applied to the pulse tube, which fills due to a combination of applied vacuum and difference in hydrostatic head between the fluid level and the level in the tube. Vent and suction times are given by t_V and t_S, respectively; total cycle time for PJM operation is given by

$$t_C = t_D + t_V + t_S \tag{3.3}$$

The average drive velocity is averaged both spatially and temporally. Spatially, the velocity varies over the cross section of the nozzle. Temporally, the velocity varies due to inertial effects. Figure 3.5 illustrates the temporal variation of velocity during one PJM cycle. At the beginning of the drive phase,

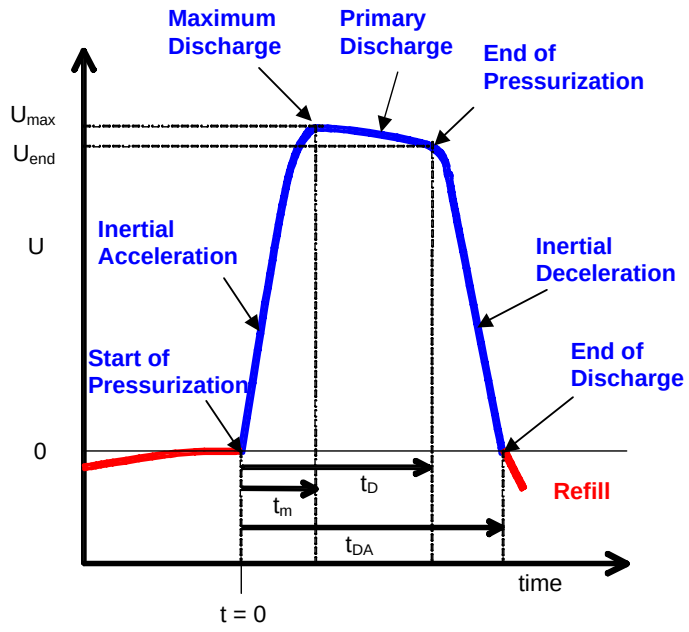

Figure 3.5. Illustration of Temporal Variation of Velocity During PJM Discharge

the fluid inside the PJM is stationary and must be accelerated. When the drive phase is over, some fluid continues to discharge due to the inertia of the moving column of fluid. The inertial effects depend on the physical size of the system. Hence, the actual velocity varies over the operating cycle. For comparing PJM operation at different scales, various average velocities can be considered. The peak average velocity is given by

$$u_P = \frac{1}{t_D - t_m}\int_{t_m}^{t_D} u\,dt \tag{3.4}$$

where u is instantaneous velocity and t_m is the time of maximum discharge. Average velocity is given by

$$u_a = \frac{D_{PT}^2}{d_0^2}\frac{\Delta L_A}{t_{DA}} \tag{3.5}$$

where ΔL_A and t_{DA} are the actual measured level change and drive times in the pulse tube. In general, it was found that the peak average velocity correlated scaled test data somewhat better than the average velocity (Section 6).

3.2.3 A Model for Cavern Formation

This section summarizes a theoretical derivation for the position of the cavern resulting from the action of a downward-oriented pulse jet. This theory was developed to provide an understanding of the important parameters affecting cavern formation as well as an insight into scaling issues. The full theory is presented in Bamberger et al. (2005).

Figure 3.6 shows a single PJM system in a vessel with non-Newtonian slurry. As a starting point, the model assumes the jet is steady. The discharging jet impinges on the tank bottom, then moves up the side wall and turns inward. The model assumes that the flow inside the cavern is fully turbulent and approximately Newtonian. The jet is assumed to behave like well-understood turbulent jets whose velocity decays in inverse proportion to the distance traveled, z. The fluid stress at the cavern interface, z_C, is characterized by a friction coefficient. A force balance at the interface equates the fluid stress to the shear strength of the unyielded material. This approach results in an expression for the cavern height, H_C, given by

$$\frac{H_C}{D_T} = a\frac{d_0}{D_T}Re_\tau^{1/2} - \frac{1}{2} \tag{3.6}$$

Eq. (3.6) demonstrates the dependence of cavern height on the yield Reynolds number, Re_τ. The yield Reynolds number is essentially the ratio of jet dynamic pressure to material shear strength and is given by

$$Re_\tau = \frac{\rho u_0^2}{\tau_s} \tag{3.7}$$

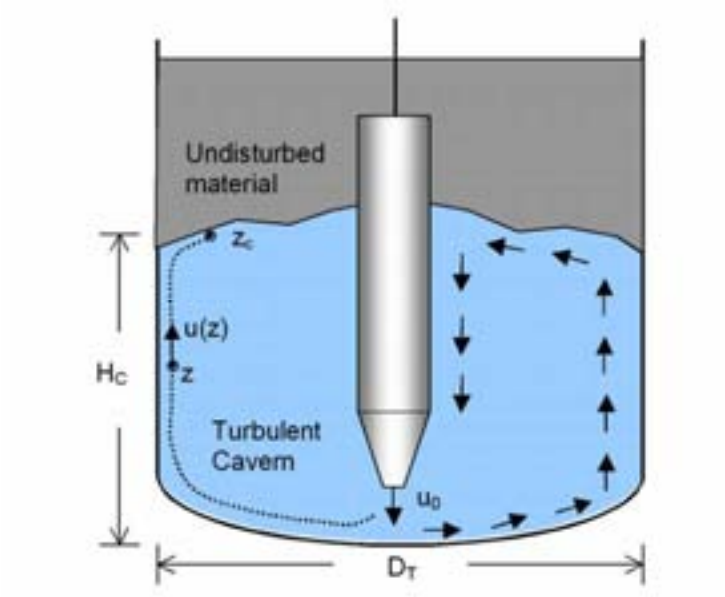

Figure 3.6. A Single Steady Jet in a Vessel with Non-Newtonian Slurry

Figure 3.7 compares the cavern height predicted by Eq. (3.6) and the results of a cavern formation experiment with a steady jet (Enderlin et al. 2003). The simulant used was Laponite[(a)] with a shear strength of 44 Pa and a density of ρ = 1,000 kg/m^3. There is good agreement between the data and the theoretical result when the value of the constant, a, in Eq. (3.6) is 1.67.

(a) Laponite simulant is discussed in detail in Section 4 of this report.

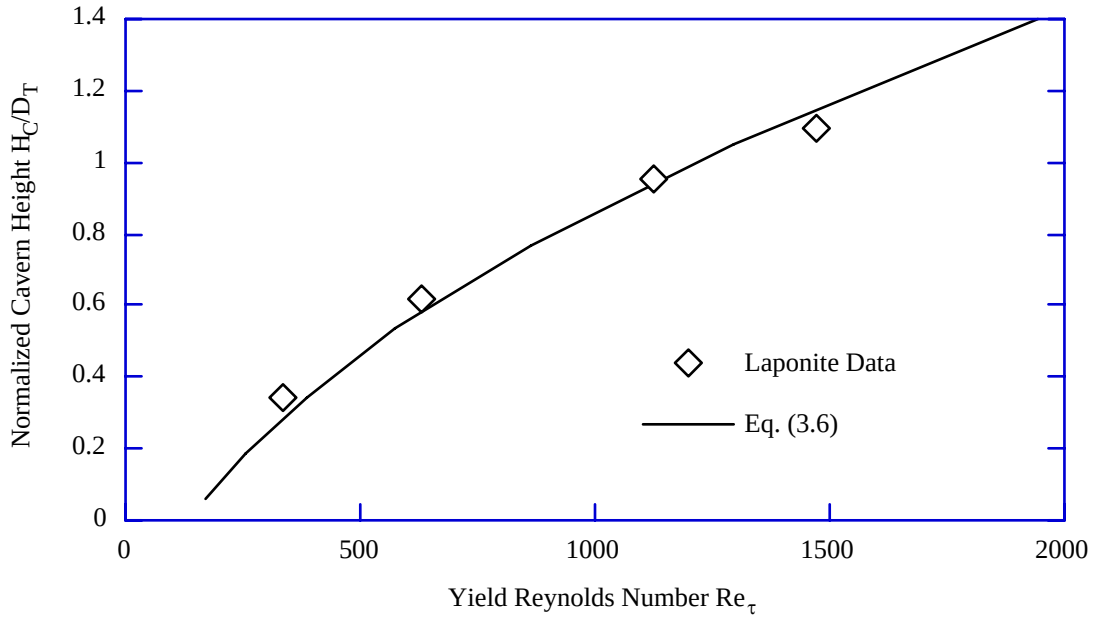

Figure 3.7. Theoretical Prediction of Cavern Height for a Steady Jet Compared with Laponite Data. Test conditions correspond to τ_s = 44 Pa, d_0 = 0.875 in., D_T = 34 in., ρ = 1000 kg/m^3 with velocities ranging from u_0 = 12 – 27 ft/sec.

To account for nonsteady effects associated with pulse jet operation, the theory was modified by introducing the flow establishment time, t_{SS}. Any real jet has a finite time required to establish steady-state flow conditions. The magnitude of the nonsteady effect depends upon the ratio of pulse jet drive time to flow establishment time and can be shown to be related to the pulse tube discharge volume, nozzle diameter, and yield Reynolds number by

$$\frac{t_D}{t_{ss}} \sim \frac{V_P}{d_0^3 \, Re_\tau} \tag{3.8}$$

where V_P is the volume of fluid that is discharged during a pulse.

When the drive time is short relative to the flow establishment time, nonsteady effects dominate. If the drive time is large compared with flow establishment time, the flow behaves essentially like a steady jet. The resulting expression for cavern height after inclusion of nonsteady jet effects is given by

$$\frac{H_C}{D_T} = b \frac{d_0}{D_T} Re_\tau^{1/2} \left(1 - \exp(-c \frac{V_P}{d_0^3 \, Re_\tau}) \right)^{1/2} - \frac{1}{2} \tag{3.9}$$

where b and c are constants. Figure 3.8 compares the cavern height predicted by Eq. (3.9) and results of cavern formation experiments with a single pulse jet. Tests were conducted with a 1-inch nozzle using Laponite with a 31-Pa shear strength and a 2-inch nozzle using Laponite with a 44-Pa shear strength. The pulse volume, V_P, was 1,090 in.^{3} for the 1-inch nozzle test and 1,960 in.^{3} for the 2-inch nozzle test. Excellent agreement was seen between data and theoretical results with the value of b = 1.67 and c = 1.4. Steady jet data are also shown in Figure 3.8 for comparison.

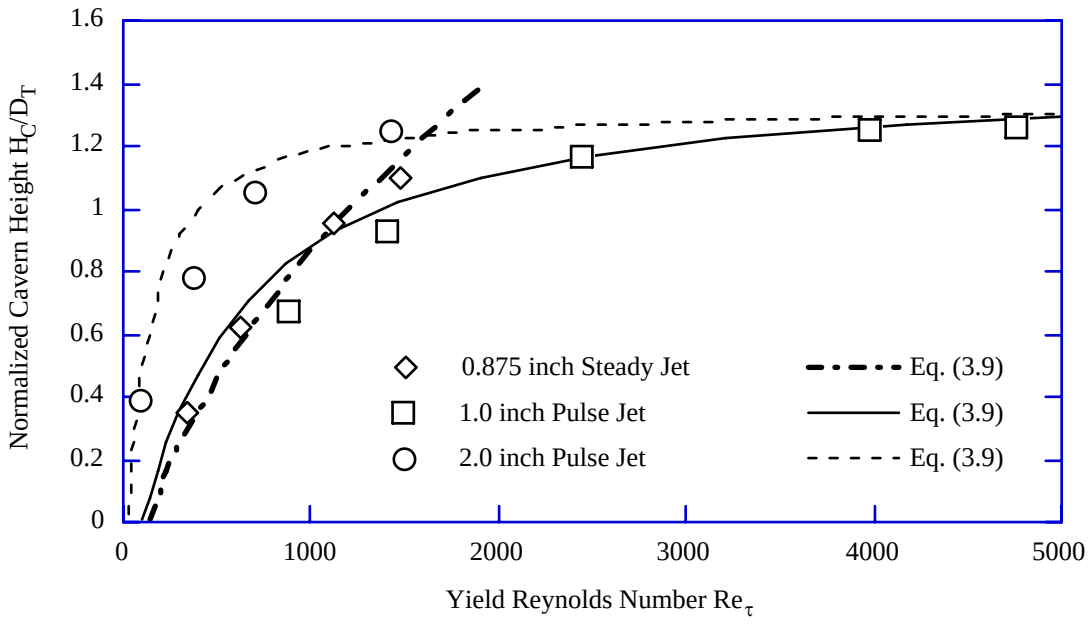

Figure 3.8. Theoretical Prediction of Cavern Height for Single Pulse Jet Compared with Laponite Data. The yield Reynolds number is based on average PJM velocity. Steady jet data are shown for comparison [where pulse volume is taken as infinite in Eq. (3.9) to recover the steady jet result].

The results presented in Figure 3.8 show that the ability of a pulse jet to erode a cavern diminishes significantly if the relative pulse time is short. According to Eq. (3.9) the relative pulse time diminishes with the inverse square of the velocity, providing less time to establish steady flow in the cavern and producing a cavern height less than that of the steady jet.

The model for cavern height was also extended to include viscous effects. The friction coefficient and jet decay constants are known to depend on the viscous jet Reynolds number given by

$$Re_0 = \frac{\rho u_0 d_0}{\mu} \tag{3.10}$$

For a Bingham plastic, the consistency, κ, can be used instead of the viscosity, μ, in Eq. (3.10). Generally, jet Reynolds number effects will be small if flow is highly turbulent. As flow becomes less turbulent and even laminar, jet Reynolds number effects can be significant.

The theoretical cavern height modeling provided mathematical expressions useful for understanding cavern formation from PJM operation. Like any model, assumptions and limitations were implicit in its derivation. However, even with the limitations, the model suggests various nondimensional parameters that are important. A more sophisticated modeling exercise would likely produce the same parameters.

3.2.4 Multiple PJM Systems

The model for cavern height applies to a single PJM centered in a cylindrical flat-bottomed vessel. WTP vessels are cylindrical and have elliptical bottoms and multiple PJMs. Typically, six or eight PJMs are arranged symmetrically. The PJMs can operate in or out of phase. A multi-PJM vessel configuration is illustrated in Figure 3.9.

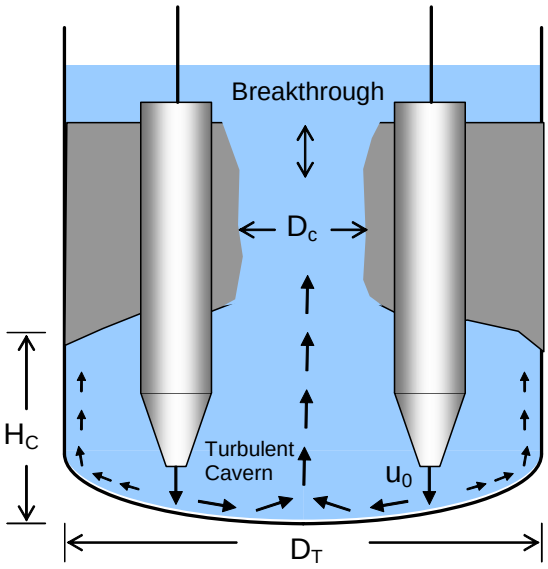

Figure 3.9. Illustration of Potential for Cavern Breakthrough due to Central Upwelling

One difference between single- and multi-PJM mixing systems is a strong central upwelling flow. While the jets impinge on the elliptical bottom, a significant fraction of the flow moves radially inward and then turns up at the center of the tank. The central upwelling can potentially lead to breakthrough at the surface, leaving an annulus of stationary slurry shown by the dark gray area in Figure 3.9.

The functional dependence of physical parameters illustrated by the single PJM theory should apply to the multi-PJM configuration. The primary difference is that the effective nozzle diameter is given by

$$d_{0e} = c\sqrt{N}d_0 \tag{3.11}$$

where N is the number of PJMs and c is a constant determined by geometry.

Because the primary flow is upward, it is likely that the cavern interface will be dominated by the normal stress of the jet as opposed to the shear stress. Because normal fluid stress is always larger than fluid shear stress, cavern height should be greater than Eq. (3.9) suggests, and breakthrough should occur more readily. Once breakthrough has occurred, the basic model for cavern height will likely fail to predict subsequent cavern behavior because increases in jet velocity may increase the diameter of the breakthrough region, D_c. The dominant flow at this point may be more like confined flow than a jet. It may not be necessary to directly mobilize all of the material once breakthrough has occurred because some of the fluid brought to the surface during discharge may stay there during the refill stage of the PJM

cycle. For mass continuity to be satisfied, this implies that the unmobilized annulus of material must move downward during refill. After sufficient cycles, this annulus will be completely mobilized. If the annulus is able to adhere to the vessel wall, the above-mentioned phenomena will not apply, and the annulus will remain unmixed.

The strong central upwelling created by downward-oriented multiple PJMs in vessels with dished bottoms results in a poor distribution of mixing energy within the slurry. The cause of this is the negative jet impingement angle relative to the vessel floor. This situation can, in principle, be greatly improved by changing the jet impingement angle. By angling the PJM nozzles slightly radially outward so the angle of impingement relative to the curved vessel bottom is normal or slightly positive, a larger fraction of the mixing jet will penetrate up the vessel walls. This should produce flatter caverns more closely resembling those created by a single centered PJM.

3.3 Theory of Gas Retention and Release

This section provides the theoretical framework for analyzing GR&R behavior in PJM slurry systems. The theory is predicated on a model of gas bubble migration in well-mixed non-Newtonian slurry. The model addresses normal mixing operations in which a steady-state retained gas fraction (gas holdup) is attained and released upon restart of the mixing system after a quiescent period. Several important parameters are identified in the model development. These parameters help identify the important factors contributing to GR&R behavior, as well guiding the design and scale up of GR&R mixing tests.

3.3.1 Bubble Migration in Well-Mixed Slurry

A simple, well-mixed slurry bubble migration model explains the basic elements of gas retention and release associated with PJM operation in non-Newtonian slurries. Though a PJM system (except for air spargers and recirculation pumps) is actually intermittently mixed due to the cyclic nature of PJM operation, we assume that gas-release rates and the rate of change of gas content represent appropriate averages over space and time such that the well-mixed model is applicable to the pulse system.

Gas is generated continuously within the waste slurry. Gas molecules are generated in solution in the liquid phase, but the solution quickly supersaturates, bubbles nucleate, and existing bubbles grow. The GR&R model considers only this gas as it exists in bubbles. The large sparger air bubbles are not included in this analysis unless they provide mixing. The gas generation rate, g_v, is the volume of gas in the form of bubbles generated per unit volume of gas-free slurry per unit time referenced to the vessel headspace pressure and the gas bubble (i.e., slurry) temperature. The retained gas fraction, α, is defined as the average gas volume fraction existing as bubbles in the slurry. The gas holdup is the gas volume fraction retained at steady state during normal operation and continuous gas generation, α_{ss}.

The model begins by assuming that the vessel is cylindrical and the gas well mixed on a mole basis throughout the vessel contents. Further, it assumes that the pressure and temperature of the gas are average values. The gas is assumed to exist as bubbles that rise and break at the surface. The molar gas generation rate is assumed to be uniform. Applying mass conservation results in the following differential equation:

$$\frac{d\alpha}{dt} + \frac{\alpha U_R}{H} - g_v = 0 \tag{3.12}$$

where U_R is the average bubble rise velocity at the surface, g_v is the volumetric gas generation rate, and H is the height of the slurry. Eq. (3.12) has the general solution:

$$\alpha(t) = \alpha_0 \exp(-\frac{U_R}{H}t) + g_v \frac{H}{U_R}(1 - \exp(-\frac{U_R}{H}t)) \tag{3.13}$$

where α_0 is the initial gas fraction at t = 0. The time dependence of the gas fraction α is completely characterized by the time constant, $\tau_R = H/U_R$. The bubble rise velocity, U_R, cannot be calculated or measured directly but can be derived from experimental data as described in Section 3.3.3.

3.3.2 Gas Retention in Gelled Slurry

When the mixing system is not operating, small bubbles are held in place by the strength of the gelled slurry, and the bubble rise velocity is zero. Solving Eq. (3.13) for $U_R = 0$ gives

$$\alpha(t) = \alpha_0 + g_v t \tag{3.14}$$

Hence, when the mixing system is not operating, gas accumulates at a rate given directly by the in situ volumetric generation rate, g_v.

3.3.3 Gas Holdup

As previously defined, gas holdup is the gas volume fraction retained at steady state during normal operation and continuous gas generation. From Eq. (3.13), the holdup at long times, α_{ss}, is given by

$$\alpha_{ss} = g_v \frac{H}{U_R} = g_v \tau_R \tag{3.15}$$

Hence, for a well-mixed slurry with rising bubbles, the steady-state holdup increases with increasing generation rate and slurry depth and decreases with increasing bubble rise velocity. While the molar flammable gas inventory within the slurry is the primary concern, the retained gas volume is most readily quantified. Eq. (3.15) provides a way to determine the bubble rise velocity from holdup test data. And because bubbles are expected to be roughly the same size and rise at roughly the same speed, Eq. (3.15) implies that the gas generation rate must vary inversely with the test scale to achieve the same holdup.

The bubble rise velocity in Eq. (3.15) is expected to be a function of the gas bubble diameter and the non-Newtonian slurry density and rheology (expressed by yield stress, τ_y, and consistency, κ). Because bubbles can rise only when the slurry is mobile, the effective bubble rise velocity should also vary with the extent and intensity of slurry mobilization produced by the mixing system.[(a)] Important parameters

(a) Mixing in this context refers to the hydraulic mobilization or fluidization of a non-Newtonian slurry, not necessarily to homogenization.

affecting mobilization effectiveness could include the ratio of PJM drive time to total cycle time (t_D/t_C), the number of PJMs, the PJM nozzle diameter, nozzle velocity, tank diameter, and the gas release process during a restart of the mixing system.

Consider a gelled slurry with initial retained gas fraction α_0. If the slurry mobilization process and gas release are relatively fast, i.e., the time constant $\tau_R = H/U_R$ is small, gas generation can be neglected, and the transient gas fraction is found by setting $g_v = 0$ in Eq. (3.13):

$$\alpha(t) = \alpha_0 \exp(-\frac{U_R}{H}t) = \alpha_0 \exp(-\frac{t}{\tau_R}) \tag{3.16}$$

The total volumetric gas-release rate is given by

$$R_v(t) = R_0 e^{-t/\tau_R} \tag{3.17}$$

where $R_0 = \alpha_0 U_R A$ is the release rate at t = 0, where A is the slurry surface area. As noted above, $\tau_R = H/U_R$ is the time constant for the release. The total release volume, V_R, can be found by integrating Eq. (3.17) from t = 0 to ∞, which results in

$$V_R = R_0 \tau_R \tag{3.18}$$

3.4 Theory of Air Sparge Mixing

Air spargers have been used extensively in industry for mixing Newtonian fluids where moderate fluid circulation is required. They have also been used in applications requiring solids suspension. The primary advantage of air-sparge mixing systems over mechanical mixing techniques is their intrinsic simplicity; there are no moving parts or complex components. They are also reasonably efficient to operate and, in principle, have a long operational life.

3.4.1 Sparge Mixing in Newtonian Fluids

Air spargers provide mixing that is driven entirely by buoyant forces due to the density difference between sparged air and the test fluid. Air bubbles formed at the exit of the sparge tube rise due to the buoyant force, entraining some of the surrounding fluid into their wake and lifting it upward. The sparge bubbles expand and accelerate as they rise in the decreasing hydrostatic pressure and entrain even more fluid. Rising bubbles also break up by various mechanisms, so the average size of the rising bubbles remains roughly constant. Because there is a net transport of fluid upward in the vicinity of the sparge bubbles, mass continuity requires that an equal amount of fluid move downward. This produces recirculation cells that mix the region near the sparge zone.

The size and structure of the recirculation zones, the fluid velocities, and the level of turbulence in the mixing region depend on the air flow rate through the sparge tube, the submergence of the sparge tube, and the rheological characteristics of the fluid. The sparge tube nozzle diameter has only a weak effect because the emerging sparge bubbles tend to coalesce and form larger bubbles.

Sparge mixing systems typically employ multiple sparge tube arrays to achieve adequate mixing over the entire vessel. Air sparge mixing systems involving sparge tube arrays typically are characterized in terms of superficial velocity, U_s, given by

$$U_s = Q_T / A \tag{3.19}$$

where Q_T is the total air flow rate and A is the surface area of the vessel. The total air flow rate is related to the flow rate in a single sparger, Q_s, by

$$Q_T = N_s Q_s \tag{3.20}$$

where N_s is the number of sparge tubes.

Superficial velocities in the range of 0.5 to 1 ft/sec are typical for industrial mixing applications in Newtonian fluids. There is some latitude in how the number of sparge tubes is specified. For the same superficial velocity, fewer sparge tubes can be used if sparge flow rate per tube is increased. Conversely, more sparge tubes can be used with a lower flow rate per sparge tube.

3.4.2 Sparge Mixing in Non-Newtonian Fluids

The mechanics of air sparger systems have been investigated primarily for aqueous-based Newtonian fluids. Potentially significant differences in mixing performance could be anticipated in non-Newtonian fluids. An inverse cavern-type phenomenon could likely produce a stagnant unmixed “sparger heel” near the base of the sparge tube and limit the radial extent of the mixing zone. Additionally, non-Newtonian rheology likely affects initial sparge bubble formation as well as the mechanics of bubble breakup and fluid entrainment.

A limited number of studies have been performed with air sparging in non-Newtonian fluids. Tilton et al. (1982) describe the fluid mechanics of air sparging systems in non-Newtonian fluids as having two primary flow regions. In the first region, fluid flows with the bubbles as they rise. This is referred to as the “region of bubbles” (ROB). Outside the ROB, the fluid flow is reversed and is, on average, opposite the direction of bubble rise. This region is referred to as the “zone of influence” (ZOI). Farther outside the ZOI is a region of fluid that is unaffected by the spargers. Tilton et al. describe the fluid flow regime in the ROB region as typically turbulent, while the ZOI region is laminar. The fluid outside of the ZOI region is quiescent. Each of these regions is separated by boundary layers that form the transition between the various regions and flow regimes. These concepts are illustrated in Figure 3.10.

3.4.3 PJM-Sparge Hybrid Mixing Systems

PJM mixing systems are effective for producing an active mixing region in the vicinity of the pulse tube nozzles. Extending the mixing cavern to include the entire vessel contents requires very high nozzle velocities (and the associated large amounts of air and power) or more PJMs in the vessel. Another option is to use air sparge systems in conjunction with PJMs.

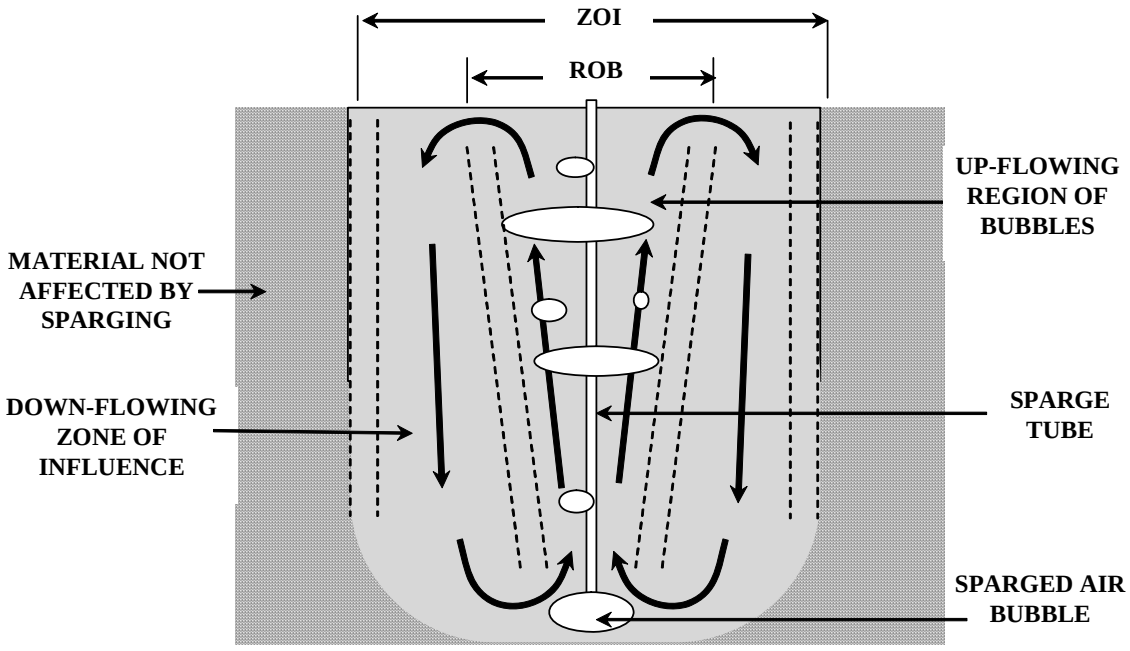

Figure 3.10. Illustration of Sparger Mixing Zone Concepts in Non-Newtonian Fluids

Downward-discharging PJMs are most effective at mixing the lower region of the vessel. Spargers, on the other hand, produce mixing regions that expand with elevation. Thus the combination of PJMs and air spargers results in a hybrid mixing system that combines the inherent strengths of both approaches.

The PJM/sparger hybrid mixing system concept uses PJM technology to mix the lower portion of the vessel and air sparging to mix the upper region. If the sparge tubes are submerged in the PJM mixing cavern, material will move between the lower and upper regions. In this manner, the entire contents of the vessel should exhibit turbulent mixing. Figure 3.11 is an illustration of this mixing concept.

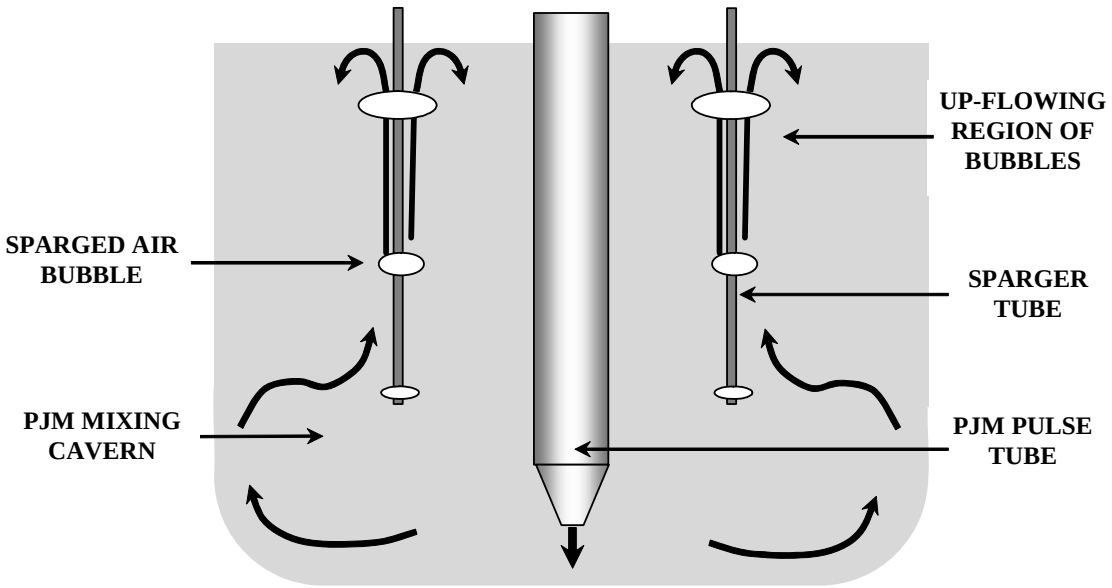

Figure 3.11. Illustration of Hybrid PJM/Sparger Mixing Concept

3.5 Important Parameters and Nondimensional Groups

This section summarizes the important physical parameters and nondimensional groups that govern mixing and GR&R behavior in PJM mixing systems. Identification of the most important nondimensional groups is necessary to develop a scaled test strategy that preserves the essential physical behavior of the mixing system.

3.5.1 Important Physical Parameters

The following list summarizes waste properties and system parameters relevant to PJM mixing and GR&R phenomena.

Slurry properties-

- τ_y Bingham plastic yield stress (Pa)
- κ Bingham plastic consistency (mPa-s)
- τ_s Slurry shear strength
- ρ Gas-free slurry density (kg/m^3); assumes well-mixed slurry with no settling.

Physical parameters-

- H Slurry fill level in the tank (m)
- D Nominal tank diameter (m)
- N Number of PJMs
- d_0 PJM nozzle diameter (m)
- U_0 PJM nozzle velocity (average or peak-average over the drive cycle)
- t_D, t_C PJM drive time (s) and total cycle time (s)
- p Average in situ pressure at H/2 (Pa)
- T Slurry and gas-bubble temperature (K)
- V_s Gas-free or initial slurry volume (m^3)

Gas and bubble properties-

- α Average retained gas-volume fraction (m^3 gas/m^3 bubbly slurry)
- α_{ss} Gas holdup (m^3 gas/m^3 bubbly slurry)
- g_v Specific volumetric gas-generation rate at the average in situ hydrostatic pressure and gas-bubble (slurry) temperature (m^3 gas/m^3 gas-free slurry/s)
- R_v Volumetric gas release rate from the slurry at the headspace pressure (m^3 gas/s)
- R_0 Initial (maximum) volumetric gas release rate from the slurry (m^3 gas/s)
- v_{bH} Average bubble volume at the slurry surface (m^3).

Sparge system properties-

Q_T Total sparge tube air flow rate (m^3/s or cfm)

N_s Number of sparge tubes

U_s Sparge air superficial velocity (m/s).

3.5.2 Important Nondimensional Groups

The physical parameters identified in the previous section can be used to form nondimensional groups that dictate how scaled tests should be designed and operated to provide meaningful results. Some of these appear naturally in the mathematical models by virtue of the physical laws involved. Others can be identified by dimensional analysis. This section summarizes the most important nondimensional parameters believed to influence PJM mixing and GR&R behavior. A thorough development of nondimensional groups is given in Bamberger et al. (2005) and Russell et al. (2005).

The following nondimensional groups relate directly to PJM mixing. Many of them also have an indirect effect on GR&R behavior because the rheological state of the slurry depends on the degree of mixing.

Yield Reynolds number: $$\mathrm{Re}_\tau = \frac{\rho u_0^2}{\tau}$$

The yield Reynolds number is the ratio of dynamic stress to relevant slurry shear stress, which directly affects the size of the mixing cavern. The shear stress used in the yield Reynolds number can be either the shear strength or the Bingham yield stress, depending on which is considered to better characterize a non-Newtonian simulant.

Jet Reynolds number: $$\mathrm{Re}_0 = \frac{\rho u_0 d_0}{\kappa}$$

The jet Reynolds number is the ratio of dynamic stress to viscous stress. It affects the degree of turbulence in the mixed region as well as transitional flow regimes associated with nonsteady mixing. It also affects the stress at the cavern (hence cavern height) and the thickness of boundary layers at the vessel wall.

Strouhal number: $$S_0 = \frac{t_D u_0}{d_0}$$

The Strouhal number is the ratio of pulse time to jet flow time scale. It affects the degree to which the jet approaches steady behavior. In the limit of steady jet flows, the Strouhal number becomes infinite, and the effects of pulsation are no longer present. For small Strouhal numbers, the mixing behavior is highly dominated by pulsation effects.

Other parameter groups are sometimes used in the literature that are a combination of the yield Reynolds number and jet Reynolds number. For example,

Yield number: $$Y = \frac{\tau_s d_0}{\kappa u_0} = \mathrm{Re}_0 / \mathrm{Re}_\tau$$

Hedstrom number: $$He = \frac{\rho \tau_s d_0^2}{\kappa^2} = Re_0^2 / Re_\tau$$

The following nondimensional parameters are uniquely associated with GR&R phenomena. Of particular importance is the bubble rise time, the time constant of the gas release process in the well-mixed slurry bubble migration model:

$$\tau_R = \frac{H}{U_R}$$

Some relevant nondimensional parameter groups for the physical system follow.

Gas-holdup number: $$N_\alpha = \frac{g_v H}{U_R} = g_v \tau_R$$

The gas-holdup number represents the ratio of gas generated to gas leaving by virtue of bubble rise. It is actually equal to the theoretical holdup predicted by the bubble migration theory.

Gas-release number: $$N_R = \frac{t_C U_R}{H} = \frac{t_C}{\tau_R}$$

The ratio of PJM cycle time, t_C, or any relevant system time to bubble rise time is defined as the gas release number. It directly affects gas release rates and other transients.

Nondimensional groups associated with sparge mixing can also be formed. However, given the fact that individual sparge mixing zones will be determined from large scale tests, there is no need to consider nondimensional parameters. The method used for scale-up of reduced scale hybrid mixing systems is two-dimensional in nature and is discussed in Section 3.6.3.

One important parameter governing sparge mixing performance is the superficial velocity, U_s, defined by Eq. (3.19) and rewritten here:

Superficial velocity: $$U_s = Q_T / A$$

The other important parameter is the number of sparge tubes per unit area, or number density:

Sparge number density $$n_s = N_s / A .$$

3.6 Scaling Laws

The nondimensional groups presented in the previous section should be preserved when tests are performed at different scales. How tests are designed and operated is therefore subject to certain constraints. Additionally, if certain nondimensional parameters cannot be preserved at reduced scale, the effects of this must be understood to interpret the test results.

3.6.1 Geometric Scaling Approach

The non-Newtonian test program used geometric scaling in which the geometric scale factor is defined by $s = L_L / L_S$, where L_L is any characteristic linear dimension of the large-scale system (such as tank diameter, nozzle diameter, and waste level). At small scale, every linear dimension, L_S, is reduced or scaled by s (i.e., $d_{0_S} = d_{0_L} / s$, $D_{T_S} = D_{T_L} / s$, $H_S = H_L / s$). Thus, the ideal small-scale test is an exact geometric miniature of the large system, with all areas scaled according to $A_S = A_L / s^2$ and all volumes scaled according to $V_S = V_L / s^3$.

Scale factors up to about 10 are considered acceptable in typical fluid mixing tests; that is, much of the important physics can be captured at small scale. For the non-Newtonian test program, the design of scaled prototypic vessels was limited to conservative scale factors in the range of 4 to 5 due to the immaturity of the technology and the importance of the outcome.

When testing at small scale, one must determine how to scale velocity (i.e., PJM drive velocity, u_0). One choice is to scale velocity by the scale factor. This is problematic, however, because it tends to reduce the Reynolds number by $1/s^2$ and introduce further difficulties with the scaling of time. A better choice is to keep jet velocity constant at both scales ($u_{0_S} = u_{0_L}$).

For steady jet mixing, time does not come into play. However, PJM operation is a periodic process, so the scaling of time must be addressed. If velocity is held constant and geometry scaled, it follows that all imposed time scales must be reduced at small scale. Similarly, to keep the jet discharge velocity the same while scaling pulse volume geometrically, pulse time will be reduced by the scale factor according to $t_{DS} = t_{DL} / s$. Hence the PJM drive time, refill time, and cycle time are all reduced by s at small scale.

3.6.2 Scaling Nondimensional Groups

In general, for a given non-Newtonian PJM mixing test, the nondimensional mixing and GR&R characteristics should depend on all of the important nondimensional groups. The ideal small-scale test is one in which the all of the nondimensional groups are the same as those at full scale. Hence, the extent to which the nondimensional parameters scale determines the success of the small-scale test approach. To this end, we consider how each nondimensional parameter scales with the geometric scale factor, s.

Yield Reynolds number: $\mathrm{Re}_{\tau S} = \mathrm{Re}_{\tau L}$

The yield Reynolds number will be the same at both scales as long as the simulant used has the same shear strength, τ_S, and density, ρ.

Jet Reynolds number: $\mathrm{Re}_{0s} = \frac{1}{s}\mathrm{Re}_{0L}$

The jet Reynolds number at small scale is reduced by the geometric scale factor. For highly turbulent conditions, this should introduce only minor differences in test results because the Reynolds numbers in both tests are quite large. For moderate turbulence or transitional flow, the effect will be larger. In

general, mixing effectiveness will be diminished at lower jet Reynolds numbers; hence the loss of net effect on mixing performance will be conservative, with small-scale tests producing a reduced quality of mixing compared with full-scale performance. The jet Reynolds number can be matched at small scale by reducing the consistency or viscosity by the scale factor; however, this is difficult because it would require changing the consistency of the simulant while keeping the yield stress unchanged.

Strouhal number: $S_{0S} = S_{0L}$

The Strouhal number will be the same at both scales, implying all nonsteady effects will be adequately captured in small-scale tests.

Gas-holdup number: $N_{\alpha S} = N_{\alpha L}$

The gas-holdup number at small scale would be reduced by the scale factor for the same gas generation rate. However, the gas generation rate should be increased by the scale factor in the small scale tests so that the gas holdup, and therefore the gas holdup number, is the same.

Gas-release number: $N_{RS} = N_{RL}$

The gas release number is preserved at small scale. However, because the bubble rise velocity is approximately constant and the simulant depth is reduced at small scale, the gas release time constant is also decreased by the scale factor at small scale:

$$\tau_{RS} = \tau_{RL}/s$$

3.6.3 Scaling Methodology for Air-Sparge Mixing

The design approach for air sparge systems is as follows. First, the ZOI for a single sparge tube with nearly full-scale submergence is determined as a function of air flow rate. The ZOI (or some fraction of it to allow for overlap of mixing zones) is used as the distance between sparge tubes for multiple sparge tube arrays. This distance, together with the diameter of the vessel, determines the total number of sparge tubes. The scaling methodology for testing air sparge systems in reduced-scale tests involves maintaining the same superficial velocity and sparge number density as the full-scale design. Results of this scaling approach should be somewhat conservative because full-scale vessels have a greater sparge submergence, hence more effective mixing from a given sparge mixing zone.

This sparge scaling methodology is also applied to PJM-sparge hybrid mixing systems. The air sparge plumes are affected by PJM operation only during the drive phase, which is a fraction of the total cycle time. Hence, most of the time the sparge plumes behave like they would without PJMs present. The interaction during the drive phase will tend to displace sparge bubbles somewhat and possibly broaden the effective ZOI. The lower PJM mixing zone is assumed to scale according to the principles outlined in Section 3.6.2. The presence of sparge bubbles will likely enhance mixing in this region. Thus, the scaling methodology for the hybrid systems is the linear combination of the scaling methodologies for the PJM and sparge mixing, respectively. No credit is taken for any interaction effects.

4.0 Rheology and Simulant Selection

This section contains a summary of the pertinent waste physical properties and an overview of the simulant development and selection process. Ideally, testing would be conducted with actual waste, but this was not possible due to the high cost and safety issues associated with working with large amounts of actual waste slurries. Accordingly, a transparent Laponite-based simulant and an opaque kaolin/bentonite clay were selected as appropriate simulants to model the properties of the actual waste slurry. This section describes the process used to select these materials.

The rheology measurements and parameters relevant to the PJM program are discussed in Section 4.1. The relevant physical properties were determined with relatively small amounts of actual wastes for several samples, as is discussed in Section 4.2. These results form the basis for the selection of a rheology model and values for the model parameters. Several potential simulants were identified and subjected to a screening process, as discussed in Section 4.3. This resulted in a small subset of simulants that were further evaluated and developed for application to the PJM mixing program discussed in Sections 4.4 and 4.5. Section 4.6 describes how simulant use was extended to assess GR&R behavior.

4.1 Rheological Background

Rheograms, or plots of shear stress versus shear rate, are typically used to characterize non-Newtonian fluids, as shown in Figure 4.1. Waste slurries with low concentrations of solids are typically Newtonian in nature, while the more concentrated slurries of interest to the PJM program exhibit non-Newtonian characteristics.

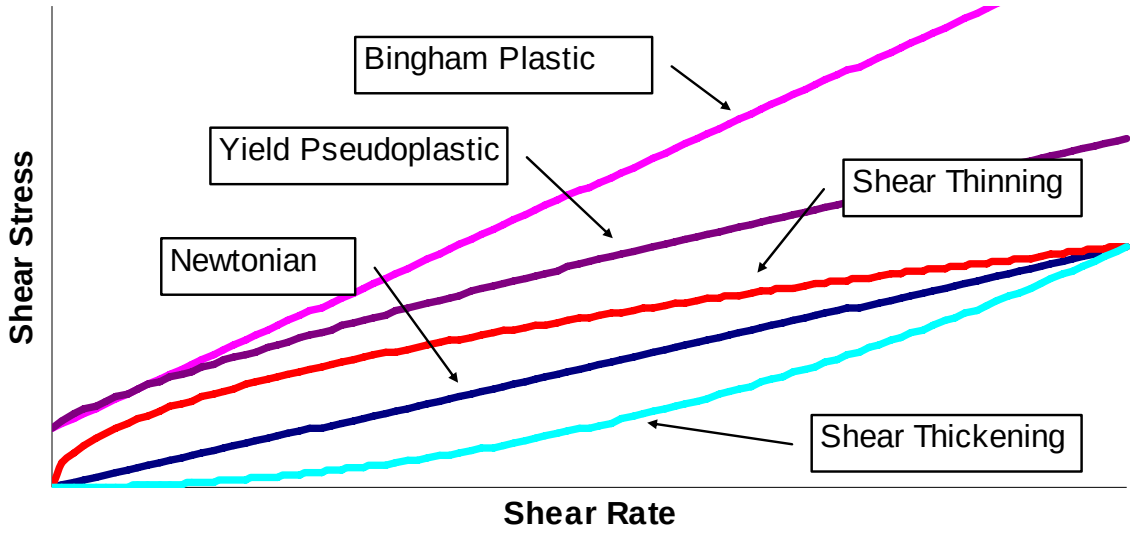

Figure 4.1. Rheograms of Various Fluid Types

Steffe (1996) explains that many methods have been developed to evaluate yield stress. These methods produce varying results based on the rheological techniques and assumptions used in the evaluation. To explain these variations, the concept of static and dynamic yield stress is introduced. The idea behind static and dynamic yield stress can be explained by assuming that there are two structures that present yield stress-exhibiting fluids. One structure is insensitive to shear rate and defines the dynamic yield stress associated with a flow curve. However, a second, weak structure is also present that forms while the fluid is at rest. This structure is sensitive to shear rate and breaks down as the fluid is sheared. Combined, these two stresses define the static yield stress value (Figure 4.2).

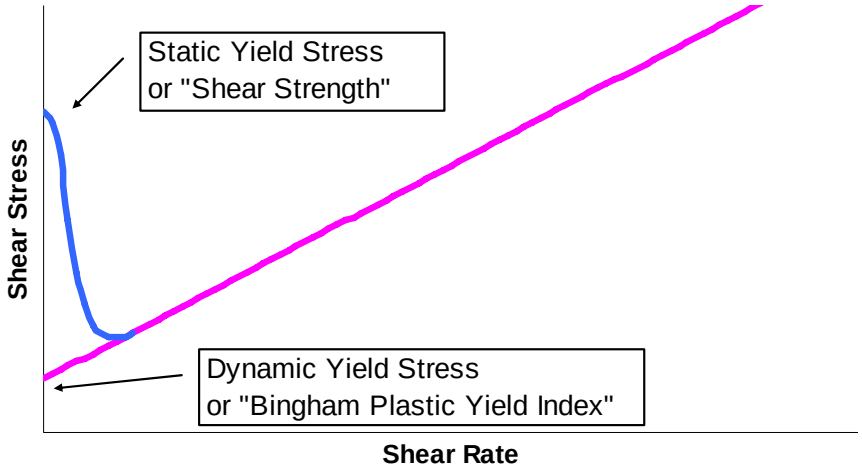

Figure 4.2. Rheogram Illustrating the Concept of Dynamic and Static Yield Stress

The use of static and dynamic yield stress values varies with application. For instance, the dynamic yield stress value extrapolated from a rheogram should be used when performing laminar pipeline head-loss calculations or assessing dynamic mixing behavior in WTP vessels. The static yield stress should be used for process restart applications where the second structure could form while the fluid is at rest. In general, there is no established relationship between the two parameters. Because static yield stress is a cumulative function of resting time, the value is always greater than or equal to the dynamic value.

A common method of measuring the static shear strength of a fluid is a device called a shear vane. A WTP procedure for measuring the static yield stress of a fluid was provided by Smith and Prindiville (2002). The WTP adopted convention is to refer to the static yield stress as “shear strength.” The dynamic yield stress obtained from a rheogram is referred to as the yield stress.

The non-Newtonian rheological behavior indicated on a rheogram for actual waste slurries may be represented by a number of models, including the Ostwald, Bingham plastic, Hershel-Bulkley, and Casson models. Because the concentrated slurries of interest to the PJM program exhibit yield stress, the Newtonian and Ostwald models are not appropriate; they do not contain a yield stress term. The Hershel-Bulkley model is a nonlinear, three-parameter model, and the Casson is a nonlinear, two-parameter model. The Bingham plastic is a linear equation, as defined in Eq. (4.1):

$$\tau = \tau_y + \kappa\dot{\gamma} \tag{4.1}$$

where τ_y is the Bingham yield stress, κ is Bingham consistency, and $\dot{\gamma}$ is shear rate. In the limit of the Bingham yield stress going to zero, the Bingham consistency is equivalent to the Newtonian viscosity.

The rheological parameters may be a function of the previous shear history of the fluid. This is referred to as thixotropy or rheopexy and appears as a time-dependent response to shear. When subjected to a fixed shear rate, thixotropic fluids decrease in viscosity over time, while rheopectic fluids increase in viscosity over time. Often thixotropy is seen as a large initial viscosity loss followed by further, more gradual loss. Once shear is removed, thixotropic fluids may recover their viscosity over a period of time.

4.2 Target Physical Properties and Rheological Model Selection

As part of the WTP design effort, samples of actual Hanford tank waste were processed through laboratory-scale unit operations. At various stages of processing, the samples were characterized for several rheological and physical properties. The physical and rheological properties from several tanks processed to the HLW pretreated sludge stage were compiled in Poloski et al. (2004), where the measurements were compared with unit operations to be performed in the WTP in order to develop a set of bounding rheological and physical properties. The WTP selected upper-bound Bingham plastic a consistency of 30 cP and a yield stress of 30 Pa. This upper bound is shown along with actual rheograms in Figure 4.3. The AZ-102 20 wt% Bingham and Power Law curve fits are also shown.

Each HLW pretreated waste rheogram shown in Figure 4.3 fits well with the Bingham plastic, Ostwald, or Herschel-Bulkley rheological models. However, the actual measurements were limited to relatively low shear rates. Actual waste processing involves shear rates that exceed this range. Taking the limit of apparent viscosity as shear rate approaches infinity reveals that the Herschel-Bulkley and Ostwald equations trend toward zero apparent viscosity, while the apparent viscosity of the Bingham plastic tends toward the consistency value. Consequently, the Ostwald and Herschel-Bulkley equations likely underpredict flow resistance when extrapolating to higher shear rates. Due to the increased shear

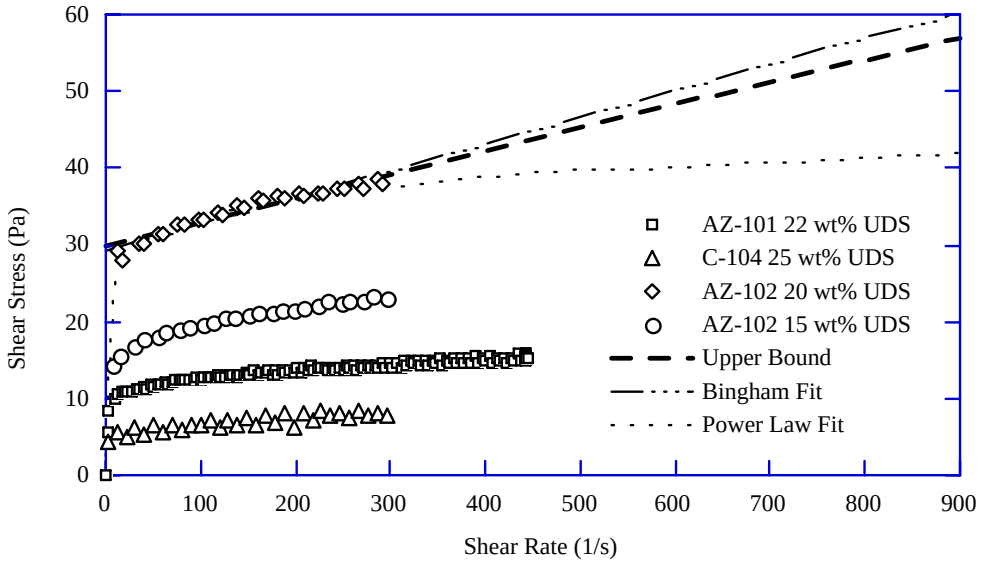

Figure 4.3. Rheograms of Laboratory-Scale HLW Pretreated Sludge Samples

thinning of the HLW pretreated sludge (i.e., the curvature shown in the rheograms), the Bingham plastic model provides a conservative bound when extrapolating to higher shear rates. It also simplifies the development of scaling relationships. On this basis, the Bingham plastic model was selected over the Ostwald and Herschel-Bulkley equations for characterizing WTP process streams.

Shear strength measurements were obtained during characterization of AZ-101 HLW pretreated sludge (Poloski et al. 2004) using the vane technique. A 22-wt% undissolved solids pretreated HLW sludge sample was stirred and allowed to sit undisturbed for various periods of time (referred to as gel time) between measurements. This allowed investigation into how sludge shear strength rebuilds after being sheared.

Speers et al. (1987) described this rebuild behavior for several drilling mud slurries with a first-order rate model (Eq. 4.2). The model appears to be a good fit to the shear-strength data shown in Figure 4.4. The best-fit parameters are shown below. The initial shear strength parameter (16.8 Pa) should agree roughly with the measured rheological Bingham yield stress (11.4 Pa). Taking the ratio of shear strength to yield stress, the y-axis of Figure 4.4 can be nondimensionalized. The plot indicates that shear strength begins rebuilding immediately and continues to increase while it remains unsheared. A steady-state shear-strength-to-yield-stress ratio of approximately 2.7 was established after about 18 hours of gel time. The steady-state condition was defined by a threshold point where the model (Eq. 4.2) predicted 99% of the steady-state growth:

$$\tau_s = A(1-e^{-Bt})+C \qquad (4.2)$$

where

τ_s	=	shear strength (Pa)	see Figure 4.4
t	=	gel time (hr)	0 to 120 hr
A	=	initial (t = 0 hr) shear strength (Pa)	16.8 Pa
B	=	time constant (hr^{-1})	0.262 hr^{-}
C	=	difference between initial and steady-state shear strength (Pa)	14.2 Pa.

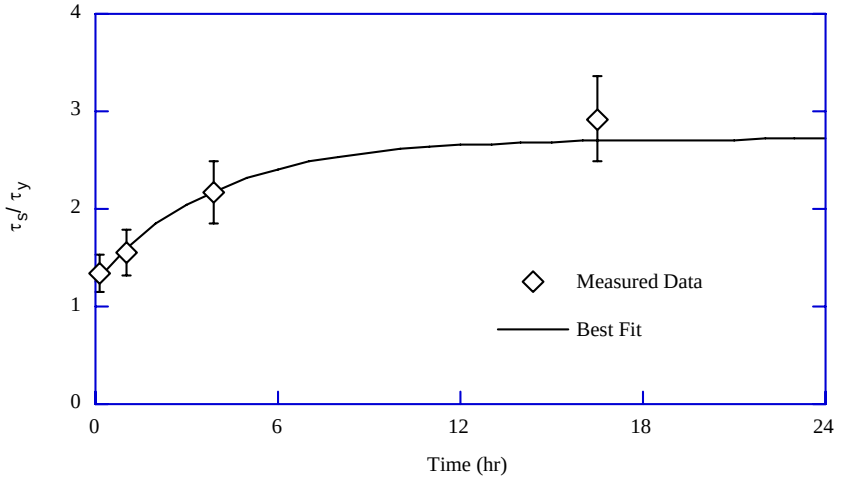

Figure 4.4. Ratio of Shear Strength to Yield Stress as a Function of Gel Time for HLW Pretreated Sludge

Shear strength is a function of many variables, including the packing efficiency of the solid particles, particle shape, particle size distribution, density of the solids particles, pH, viscosity of suspending medium, ionic strength of suspending medium, and density of suspending medium. Therefore, the shear strength behavior of a particular slurry is expected to be similar to that of a slurry with similar particles and suspending medium. Given the absence of shear strength data for other HLW pretreated sludges, the HLW pretreated sludge was assumed to consist of similar solid particles and suspending medium. Accordingly, the shear strength of a HLW pretreated sludge sample was estimated by measuring the yield stress of the sample and using the nondimensional correlation shown in Figure 4.4. Applying this concept to the hypothetical bounding-condition HLW sample with yield stress of 30 Pa, a steady-state shear strength of approximately 2.7×30 Pa = 80 Pa was estimated. The 80-Pa shear strength was a single data point extrapolated for HLW pretreated sludge based on best engineering judgment. Actual shear strength values for HLW pretreated sludge from other waste tanks may exceed the 80 Pa value. Our objective was to develop a simulant that matched the target rheological parameters shown in Table 4.1.

Table 4.1. Significant Simulant Properties for PJM Performance and Goal Values

Property	Target Values
Density	1.2 g/mL
Bingham Consistency	30 cP
Bingham Yield Stress	30 Pa
Shear Strength	30–80 Pa

4.3 Simulant Screening Process

A transparent simulant and an opaque simulant were developed for the PJM program. The transparent simulant was very useful for assessing cavern formation and allowing the visualization of flow patterns in the mixing vessels. An opaque particulate simulant was necessary to better represent the rheological and GR&R behavior of the actual waste. The initial development of the simulant to assess cavern formation and mixing behavior required the following criteria to be considered:

- Rheological properties: The simulant needed to be a reasonable match to the Bingham plastic parameters of consistency and yield stress as well as shear strength.
- Thixotropy: Cavern formation in PJM vessels often required several hours to reach steady state. During this time, the simulant was exposed to shear forces. If the simulant was thixotropic, the Bingham yield stress and consistency would vary during the test and could have affected the cavern height in an unknown manner. If a simulant developed shear strength, the material was considered thixotropic, and a trade-off existed between thixotropy and shear strength of the simulant. The ideal transparent simulant possessed shear strength that, once exceeded, would instantaneously exhibit constant rheological parameters. Therefore, it was desirable for the material to develop constant flow behavior quickly during the test and to have little thixotropic behavior.
- Safety: Because much of the testing occurred in relatively open vessels with amounts ranging from 100 to 10,000 gallons, the simulant formulation needed to be nonhazardous.

- Ease of preparation and disposal: Significant amounts of simulants were prepared and required subsequent disposal, so it was important from a cost standpoint that both activities be easy and inexpensive.
- Expense: Given the significant quantities of simulant that were needed, it was important that inexpensive materials be used.
- Stability: Testing occurred over several months, so it was essential that the simulant have constant rheological properties over time. During each test the simulant was exposed to shear forces that had the potential to degrade the simulant and change the rheology. The possibility of continued hydration and biological growth (e.g., bacteria and algae) was also considered.

A literature search revealed two classes of materials that appeared to meet these requirements. For transparent simulants, rheological modifiers for the food and cosmetic industry were determined to be promising candidates. Examples included Laponite (a synthetic clay), Xanthan gum, Carbomers, polyacrylates, Traganth gum, cellulosic materials, and several other polymeric materials. For opaque simulants, drilling fluids and various mineral slurries were a good choice. Poloski et al. (2004a) contains a complete listing and description of the candidate simulants considered in the screening process.

After the initial screening of transparent simulants, three materials were selected (Laponite, Carbopol, and Rhodicare, a form of Xanthan gum) and carried forward for development and evaluation in a single-tube PJM test stand, as described in Section 4.4. Kaolin/bentonite clay was selected as the opaque simulant, as described in Section 4.5.

4.4 Transparent Simulant Evaluation and Selection

Laponite is a synthetic smectite clay mineral consisting of nanoscale crystals in the form of platelets. Laponite makes a transparent solution when dispersed in water due to its small particle size. Carbopol is a cross-linked acrylic polymer that forms translucent to transparent suspensions of hydrated spheres of the polymer in water. Xanthan gum is a microbial polymer, a polysaccharide consisting of thousands of glucose units. Rhodicare T was selected as a satisfactory grade of Xanthan gum based on the manufacturer's claim of good transparency and development of shear strength.

Important mixing parameters were explored with every simulant, and each one displayed unique mixing properties and presented different complexities for modeling the resultant behavior. The Laponite was thixotropic and not viscous enough to be ideal with regard to the viscous Reynolds number. The Carbopol was not thixotropic but also did not have real shear strength. Additionally, the Carbopol degrades irreversibly under prolonged exposure to high shear. The Xanthan gum modeled the target rheology most accurately based on rheograms, but the bacterial growth in the Rhodicare meant the material could not be reused, and that presented a handling and disposal issue.

Formulations were developed for the three simulants that approximately met the target shear strength of 30 Pa (Table 4.2). Because Carbopol does not have shear strength, the Casson yield stress was used. A comparison with the HLW pretreated sludge upper bounding target (see Section 4.2) of 30 Pa Bingham yield stress and 30 cP Bingham consistency is shown in Figure 4.5. It is apparent that at the concentration tested the Laponite was not viscous enough for a good flow curve match to the WTP upper bound; the

Table 4.2. Significant Transparent Simulant Properties for PJM Performance and Target Values

Simulant	Concentration (wt%)	Bingham Consistency (cP)	Bingham Yield Stress (Pa)	Shear Strength (Pa)
Laponite	1.92	10	0	30
Carbopol	0.134	100	33	13–19 (Casson model yield)
Xanthan Gum	2.08	40	35	37

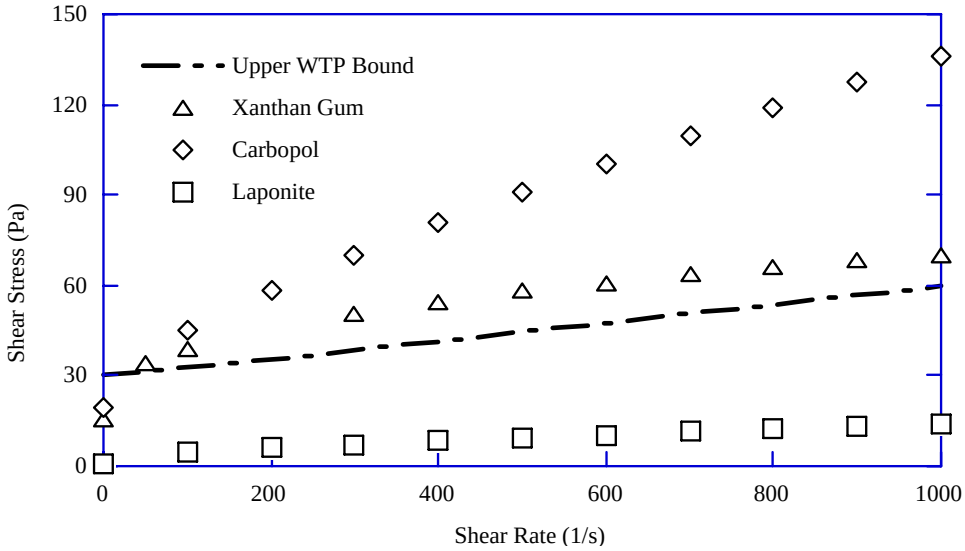

Figure 4.5. Comparison of Transparent Simulant Flow Curves to the WTP HLW Pretreated Sludge Upper Rheological Bound at Ambient Temperature

Xanthan gum is a relatively good fit but the Carbopol is much too viscous. Laponite formulations at higher concentrations were later developed with shear strength ranging from 80 to 120 Pa and yield stress in the 10-Pa range.

The simulants were further evaluated in a series of cavern tests in a single PJM test stand (described in Section 5.1.2). A chemical, rheological, and physical simulant representing pretreated waste slurry from Tank AZ-102 was also tested. The AZ-102 is the best available simulant for representing actual waste slurry behavior. The results of these tests were used in conjunction with the PJM scaling relationships to evaluate the simulants for PJM testing.

When the relevant PJM operating parameters were compiled and the nondimensional cavern height and yield Reynolds number calculated, the plotted variables followed the relationship described in Eq. (3.9). Because the tests were performed in the same PJM vessel, the constants in Eq. (3.9) were identical for different simulants. This suggests that, if all the significant properties were captured by Eq. (3.9), the data would follow the same nondimensional correlation regardless of simulant. PJM scaling results from several tests are shown in Figure 4.6. In addition to those described above, other Laponite, Carbopol, and Xanthan gum solutions were prepared with different rheological properties by varying the concentrations. PJM tests were performed on these simulants and the results are shown in the figure.

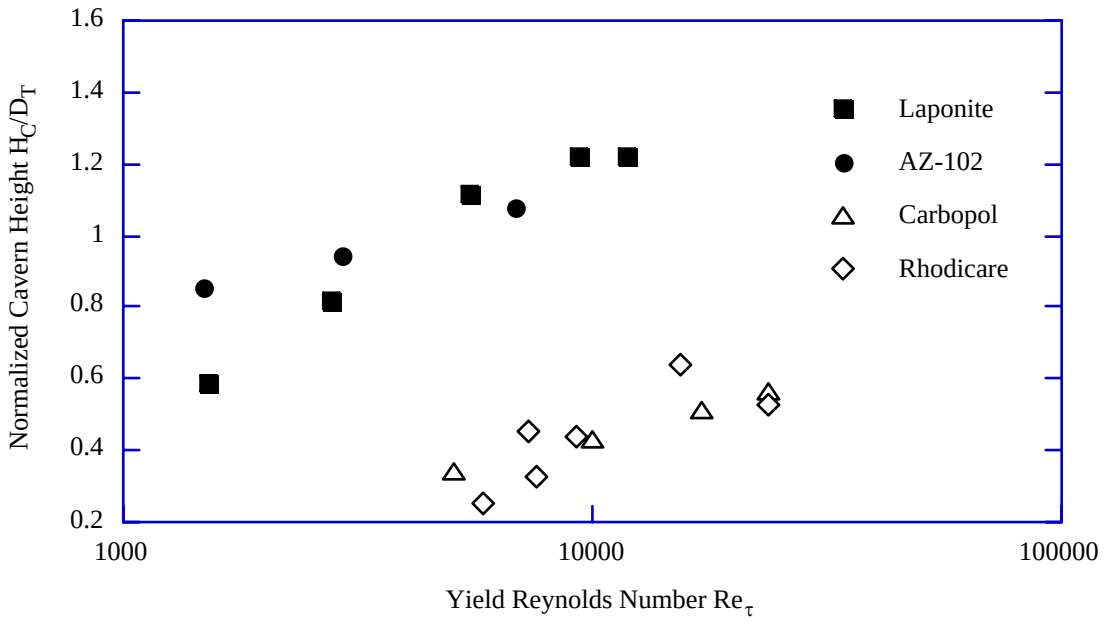

Figure 4.6. Nondimensional PJM Scaling Correlation for Several Simulants and Operating Conditions

Contrary to expectations that a single correlation would be observed in Figure 4.6, two non-dimensional correlations were observed, one for Laponite and the AZ-102 simulant and another for Carbopol and Xanthan gum. From these correlations, it can be seen that the performance (i.e., cavern height) of the Laponite simulant far exceeds that of Carbopol and Xanthan gum.

The difference is hypothesized to be the viscoelasticity of the simulants. Polymer-based materials are known to have significant viscoelastic properties because the polymer chain compresses and stretches with shear rather than moving with the bulk fluid. Conversely, particulate slurries may rearrange in packing structure, but individual particles do not significantly compress and stretch like polymer-based systems. Therefore, particulate slurries typically possess significantly lower levels of viscoelasticity than polymer-based systems.

Based on these results, the Laponite simulant was selected as the transparent simulant for the initial testing of the scaled prototypes and for demonstrating the PJM mixing scaling laws in the 4PJM scaled test stands. Laponite was used primarily to represent the gelled-state conditions upon restart from idle periods. As such, shear strength was considered the most important parameter. For low-strength Laponite (30 Pa shear strength) that has been fully sheared, yield stress is essentially zero, and the material behaves like a Newtonian fluid. For higher-strength Laponite (80 to 120 Pa), the yield stress was typically in the 10-Pa range. The Laponite used had a density slightly greater than water, a shear strength that ranged from 30 to 120 Pa, and a consistency ranging from 10 to 20 cP.

4.5 Opaque Simulant Selection

Clay suspensions are used widely in industry and commonly exhibit a shear-thinning pseudoplastic flow. Brownian motion, van der Waals forces, and electrostatic forces determine the interactions between

clay particles. The main mode of particle interaction is flocculation, or formation of agglomerates. The agglomerates organize themselves into a three-dimensional structure or coagulated suspension that resists flow. When shear is placed on the structure, it breaks down and the suspension flows. As shear increases agglomerate size decreases, resulting in diminishing viscosity—characteristic of a pseudoplastic fluid. In this manner, interaction between the agglomerates contributes to energy dissipation during viscous flow.

A simulant developed by Rassat et al. (2003) for Hanford tank retrieval studies was a mixture of 80% kaolin (EPK Feldspar Pulverized) and 20% bentonite (WYO-Ben Big Horn CH-200) powder mixed to various solids concentrations in water. This recipe produced a simulant with Bingham plastic properties near the target 30-Pa yield stress and 30-cP consistency. The simulant also developed shear strength at rest that was typically 1.5 to 2 times the yield stress. The typical density was about 1200 kg/m^3. The rheological properties of the kaolin-bentonite clay simulant were characterized extensively for solids loadings in the 20 to 30 wt% range (Poloski et al. 2004a), as shown in Figure 4.7. This clay simulant was used extensively in the PJM program. Significant applications included the final all-in tests for Phase I scaled prototype work, all of the Phase II scaled prototype tests, demonstration of the PJM scaling laws, single and multiple sparge tube testing, and half-scale LS (HSLS) testing.

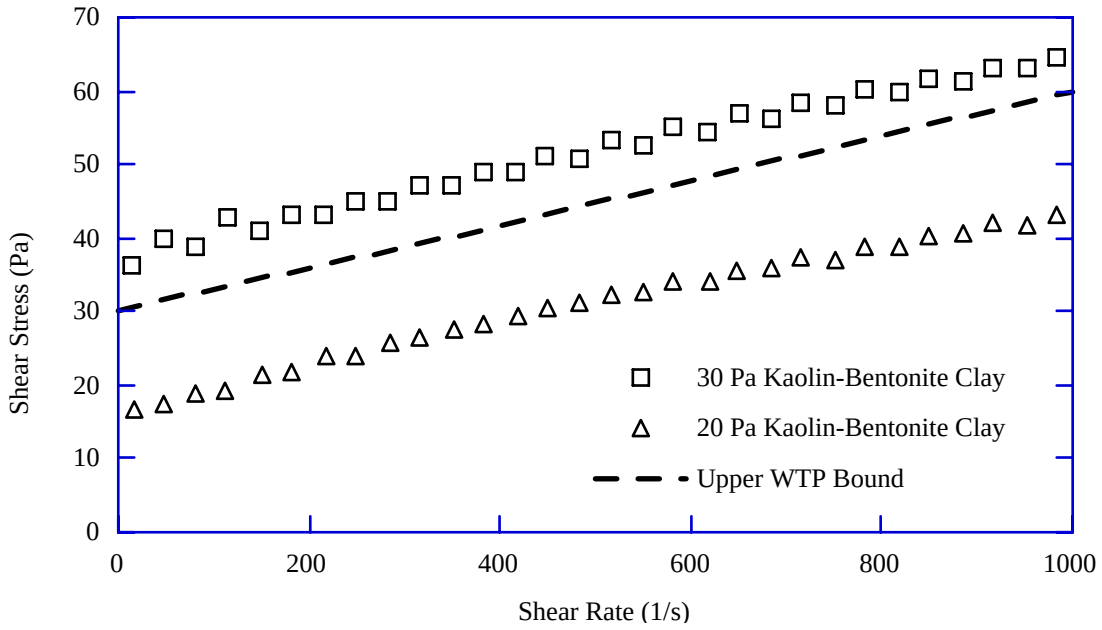

Figure 4.7. Kaolin-Bentonite Simulant Flow Curves Compared with WTP HLW Pretreated Sludge Upper Rheological Bound

4.6 Simulant Use in GR&R Testing

Shortly after the simulants were developed for assessing mixing in PJM systems, their use was extended to the testing and evaluation of GR&R behavior. In this testing (Russell et al. 2005) the decomposition of hydrogen peroxide was used to generate gas bubbles that simulate gas generation in actual waste slurries via radiolysis and thermolysis.

The initial assessment involved a number of bench-scale gas generation tests with both simulants. These tests were designed to assess the rates of decomposition with and without the addition of catalysts. The catalysts evaluated for the kaolin/bentonite clay were iron and manganese dioxide. The manganese dioxide produced a significantly greater effect than the iron oxide and was chosen for extensive testing. The catalysts considered for Laponite included copper and iron powders, nitrate salts of copper and iron, and 50 wt% sodium hydroxide. Except for the iron powder and the sodium hydroxide, all of the catalysts produced a noticeable effect. The copper nitrate trihydrate was selected for bench-scale tests because of its efficacy in relatively low concentrations and the ease of distribution in the simulant.

The bench-scale testing with Laponite involved copper nitrate catalyst concentrations that varied from 0 to 100 ppm copper nitrate. As expected, higher concentrations of catalyst resulted in an increased rate of decomposition. Measurement of the rheology indicated that the catalyst also increased the shear strength and the yield stress but had little effect on the consistency factor. Only a few GR&R tests were conducted in the PJM test stands with Laponite.

The bench-scale testing with the clay involved manganese dioxide concentrations that ranged from 0 to 500 ppm. As expected, higher concentrations of catalyst resulted in an increased rate of decomposition. It was also found that smaller particle sizes with more surface area increased the decomposition rate. Shear strength measurements indicated that as the gas fraction increased the shear strength decreased. Most of the GR&R tests were conducted in the PJM test stands with the clay simulant. In general, the addition of a catalyst was not needed to obtain useful decomposition rates.

Regardless of the simulant, using hydrogen peroxide decomposition to simulate uniform, constant gas generation in plant waste slurries presents challenges. Hydrogen peroxide has a relatively high decomposition rate and must be mixed uniformly in the simulant to produce a uniform gas generation rate. However, hydrogen peroxide can be placed into, and the resulting retained gas released from, only those regions that participate in mixing. Methods to deal with these challenges for intermittently mixed systems are discussed in conjunction with HSLS testing in Section 9.

5.0 Test Stands, Instrumentation, and Methods

This section contains a summary description of the test stands, instrumentation, and the measurement methods used in the PJM program. Section 5.1 contains an overview and description of the various test stands. Section 5.2 summarizes the types of tests performed and the methods used to obtain data.

5.1 Test Stands and Instrumentation

The information in this section comprises an overview of the test stands and instrumentation used in the PJM program, as well as some of the details pertinent to the testing.

5.1.1 Test Stand Overview

Several different test vessels were used with a number of internal configurations. The relative size of the full-scale vessels is compared to the test vessels in Figure 5.1 and a summary of the applications is presented in Table 5.1. The initial PJM testing was conducted with the APEL single-PJM test stand to demonstrate the formation of mixing caverns and to develop and select simulants for further testing. Three scaled vessels containing four PJMs each were used to demonstrate the mixing and GR&R scaling rules for PJMs in non-Newtonian fluids. Three scaled prototypes representing three types of plant vessels (LS/blend vessels, UFP vessels, CRVs) were used to investigate the performance of a large number of PJM configurations, air sparging, and steady jets generated by recirculation pumps. The large-scale 336

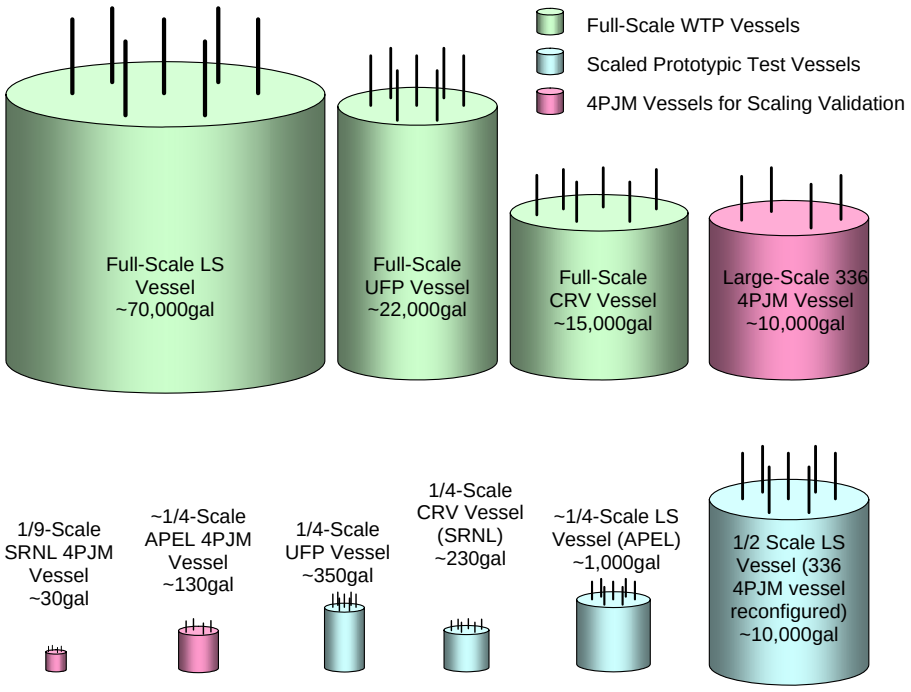

Figure 5.1. Relative Size of Full-Scale Vessels Compared with the Test Vessels. Volumes shown are nominal batch volumes; actual vessel volumes are somewhat larger.

Table 5.1. Summary of PJM Test Vessels and Applications

Vessel	Internals	Description	Approximate volume, gallons	Scale	Purpose
APEL single PJM	1 PJM	Single pulse tube in a clear acrylic vessel	250	NA	Select and develop simulant; demonstrate PJM cavern formation.
4 PJM Scaled Vessels					
336 supernatant tank	4 PJM	Four pulse tubes in a stainless steel vessel	10000	1	Demonstrate scaling approach for PJM mixing and GR&R in WTP vessels containing non-Newtonian slurries. Also overblow tests in 336 super-natant tank.
APEL 4 PJM	4 PJM	Four pulse tubes in a clear acrylic vessel	250	1/4-scale version of the 336 4PJM supernatant tank	
SRNL 4 PJM	4 PJM	Four pulse tubes in a clear acrylic vessel	30	1/9 scale version of the 336 4PJM supernatant tank	
Scaled prototypes					
UFP scaled prototype	Variable PJMs, spargers, recirculation pump	Scaled prototype vessel representing the UFP vessel	350	1/4.94 scaled version of the full-scale UFP vessel	Assess performance of a variety of vessel internal configurations, including the number of PJMs, size and angle of PJM nozzles, drive velocity, sparging and recirculation pumps.
LS scaled prototype	Variable PJMs, spargers, recirculation pumps	Scaled prototype vessel representing the LS and blend vessels	1000	1/4.29 scaled version of the full-scale LS vessel	
CRV scaled prototype	Variable PJMs, spargers, recirculation pump	Scaled prototype vessel representing the CRV	230	1/4-scaled version of the full-scale CRV	
Half-scale LS vessel and cone-bottom tank (CBT)					
Half-scale LS vessel	8 PJMs in a cluster configuration (7 around 1), 7 spargers	Half-scale version of the LS vessel	10000	1/2-scale version of the full-scale LS vessel	Assess GR&R and mixing in the LS vessel with WTP operational cycles.
Cone bottom tank (CBT)	spargers	Variable number of spargers (1-9) in a tank with a cone shaped bottom	10000	NA	Develop sparger design guidelines for mixing; provide data on gas release and aerosol entrainment.

vessel was reconfigured to a half-scale replica of the LS vessel for assessing GR&R and mixing behavior during specific WTP operational cycles. A large cone-bottom tank (CBT) was used to investigate the performance of single and multiple sparge tube arrays.

Some additional details on each test stand are given in the following sections, but all PJM test stands have the same basic components. The PJM assemblies were suspended in a dish-bottomed tank. Each pulse tube consisted of a cylindrical section (which made up most of its length), a rounded shoulder (header) at the top with riser piping for connecting to air and/or vacuum supplies, and a 60° cone section at the bottom with a nozzle at the tip (either as a truncated cone or as a piece of pipe attached to the tip of the cone). Flexible hoses connected to the top of the riser piping to provide air pressure, vacuum, and venting capabilities for each PJM. Test stands may have separate riser pipes in the vessel for sample collection, air sparging, and recirculation of the simulant.

Operation of the PJMs includes a fill or suction phase, a drive or discharge phase, and a vent phase. During the fill phase, an applied vacuum draws fluid up into the PJM from the vessel. During the drive phase, the PJM is pressurized to expel fluid through the nozzle at high velocity to induce mixing in the vessel. The vent phase occurs after the drive phase and consists of allowing the pulse tube pressure to equilibrate with atmospheric pressure. The total time for a complete fill-drive cycle ranges from seven seconds (SRNL 4PJM) to two minutes (336 HSLS) following the geometric scale of the vessel. The drive time was generally on the order of one-fourth of the total pulse-cycle time.

The PJM nozzle exit velocity was a test-specific parameter obtained by manually manipulating the durations of the suction and discharge phases, the supply pressure, and the amount of vacuum. PJM drive-cycle nomenclature and nozzle velocity calculation methods were described in Section 3.1.

In addition to PJMs, the scaled prototype systems were equipped with recirculation pumps and air spargers that were used in various combinations in some tests to enhance mixing and gas release. Recirculation was performed with centrifugal recirculation pumps controlled manually using variable frequency drives. In some cases, a pneumatic diaphragm pump was also used in line with the centrifugal pumps to avoid pump cavitation. The diaphragm pump flow rate was regulated by manually adjusting the air supply pressure to the pump. Air spargers consisted of small-diameter stainless steel tubes with an open end submerged in the simulant. Air was expelled through the sparging tubes, creating large bubbles that agitated the simulant as they rose to the surface.

All test stands were monitored and controlled with PC-based data acquisition and control systems (DACS). The data acquisition functions were the primary means of recording experimental conditions. Manual recording on data sheets and test instructions supplemented and backed up the data recorded by the DACS. The control function was used to operate the PJMs.

The PJMs in the 336 supernatant tank (HSLS and 4PJM) were operated with plant-type jet pump pairs (JPPs) using compressed air and controlled by a prototypical control system. This was typically operated in the timer mode to keep PJM cycle times constant. For the scaled prototypes and the ¼ and $^1/_9$-scale 4PJM test stands, a compressor/vacuum/receiver-tank system supplied the pressurized air and vacuum through a control manifold and solenoid-actuated valves to operate the PJMs. The functionality of the plant PJM control system was mimicked by a DACS array of solenoid valves controlling compressed air and vacuum supply sources.

Each PJM pulse tube was instrumented with a capacitance level probe for monitoring the simulant level in the pulse tube. Additionally, each pulse tube contained a pressure transducer to monitor air pressure. The capacitance level probes were generally used to monitor the stroke length in the pulse tube, but in some cases the output was suitable for determining the PJM drive velocity by applying a mass balance to the simulant level in the pulse tube. In most cases the PJM drive velocity was determined using the pulse tube pressure and applying Bernoulli's equation with the form drag taken into account (Bontha et al. 2005).

Spargers were typically instrumented with an air flow meter, a pressure gauge or transducer, and a thermocouple for measuring the air temperature. The actual air flow rates were calculated using data from these instruments (Poloski et al. 2005).

5.1.2 APEL Single PJM Test Stand

Initial tests were conducted in a clear acrylic vessel at the Applied Process Engineering Laboratory (APEL) with a single pulse tube for evaluation of transparent simulants (Section 4.4) and for demonstrating the basic principles of cavern formation and measurement (Section 3.2). In these tests, the cavern height was determined by visual observation for various PJM nozzle velocities. An opaque chemical and physical simulant representing pretreated waste from Tank AZ-102 was also tested. For this test, the cavern height was visually assessed by adding dye to the cavern and observing the color on the walls of the vessel.

The vessel had an inside diameter of 3 ft and was 7 ft high, with a clear acrylic plastic bottom of a 2:1 elliptical shape. A single 10-inch-ID, 4-ft-long clear acrylic pulse tube with a 60^{o} cone at the bottom was situated in the center of the vessel.

Figure 5.2 is a photograph of the test stand. To the right of the vessel is the compressor (background, with large horizontal tank) and vacuum receiver tank (smaller horizontal tank). The exhaust line is supported from the top of the scaffold structure, and the tank drain line is in the foreground. Additional information on this test stand may be found in Johnson et al. (2003).

5.1.3 Test Stands for Demonstrating Scaling of PJM Mixing

Mixing tests were performed in geometrically similar vessels equipped with 4PJM arrays at three different scales to validate the scaling laws to be used when conducting scaled prototype tests. The largest of these was the large-tank 336 Building test facility. Experiments were conducted using geometrically scaled test stands at ¼ scale at APEL and at 1/9 scale at SRNL under similar conditions to develop test data to support a methodology for predicting large-scale behavior from the small-scale test results. Tests were conducted on two non-Newtonian simulants, Laponite (transparent) and a kaolin-bentonite clay mixture (an opaque HLW simulant).

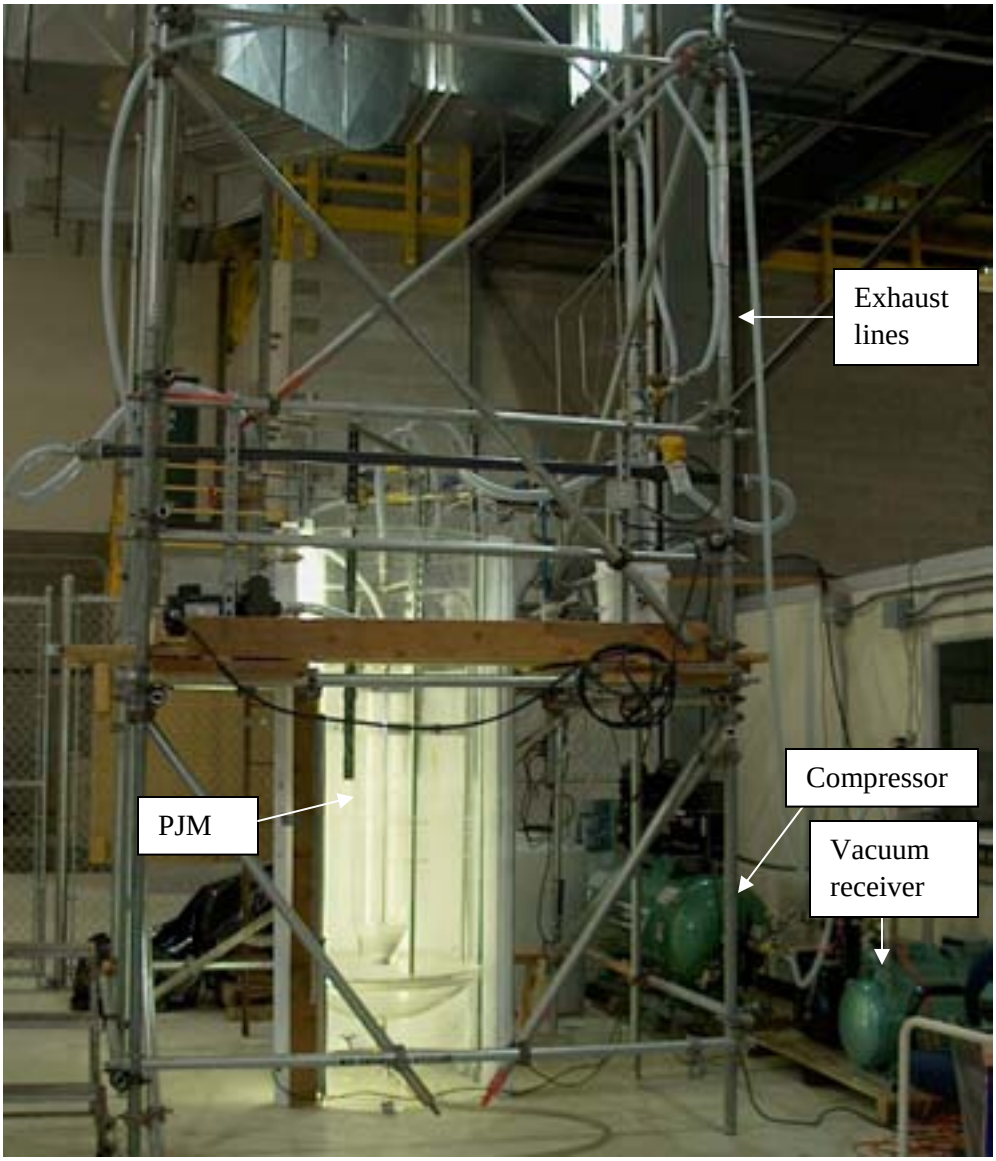

Figure 5.2. APEL Single PJM Test Stand

5.1.3.1 336 Large-Scale 4PJM Test Stand

The large-tank test stand (also referred to as the "supernatant tank") shown in Figure 5.3 is a vertically oriented cylinder 12.75 ft in diameter and 14.9 ft deep with a 2:1 elliptical bottom, making a working volume of about 10,000 gallons. Transfer lines (not shown) at the top and bottom of the tank allow adding or removing materials during loading or disposal operations. The supernatant tank was positioned on three load cells that were used to determine the weight of the tank and its contents.

The PJM system installed in the large tank consisted of four cylindrical pulse tubes, each 10 ft long and 2 ft in diameter. The bottom end was a 60º cone truncated to a 4-inch nozzle opening. The overall height of the pulse tube, shown in Figure 5.4, was approximately 12 ft. Detailed descriptions of this test stand may be found in Bontha et al. (2003) and Bamberger et al. (2005).

Figure 5.3. Photograph of Large-Tank Test Stand (Supernatant Tank)

Figure 5.4. A Pulse Tube Before Installation in the Large-Tank Test System. The pulse tubes were connected to 2-inch pipe couplings that enabled insertion of level gauges and attachment of the air/vacuum lines required for PJM operation.

5.1.3.2 APEL 1/4-Scale 4PJM Test Stand

The APEL 4PJM test stand was a geometrically scaled version of the large-scale 4PJM test stand in the 336 test facility. Its scale factor relative to the large-scale 4PJM test stand was 4.53. It consisted of four PJMs constructed of a 5-inch (5.29-inch ID) schedule 10 stainless steel pipe tapered to a custom-built nozzle of 0.88-inch ID. The cylindrical section of the PJMs was 48 inches long. The height was intentionally set longer than the PJMs in the 336 test facility to enable testing at higher H/D_T ratios than were possible at the large scale. The schematic in Figure 5.5 shows the placement of the four pulse tubes in the transparent acrylic tank. The vessel was the same tank that was used in the single-PJM testing. Additional descriptions of the test stand may be found in Bamberger et al. (2005).

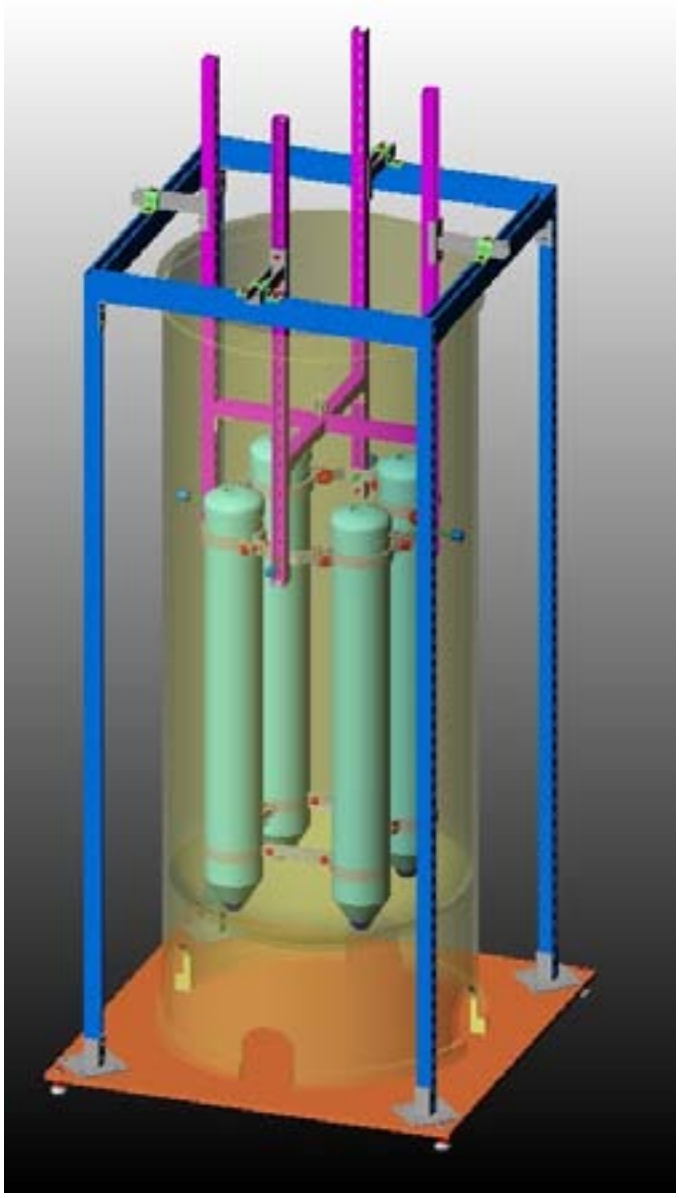

Figure 5.5. Schematic of APEL 4PJM Pulse Tube Square Array in the Tank with Supporting Structure

5.1.3.3 SRNL 1/9-Scale 4PJM Test Stand

The SRNL 4PJM test stand (Wilson et al. 2004) shown in Figure 5.6 was also a linearly scaled version of the 4PJM setup in the 336 test facility. This test vessel was a clear cylindrical shell with a stainless steel 2:1 elliptical head. The vessel's average ID was 17.25 inches, and it had a working volume of about 30 gallons. Four PJMs fabricated from 2.5 NPS, schedule 10S stainless steel pipe had average ID of 2.63 inches. The 60-degree nose cone on the outlet of the PJM had a nominal nozzle diameter of 0.45 inch; the nozzle centerline elevation was 1 inch above the vessel head.

Figure 5.6. Photograph of the SRNL 4PJM Test Stand

5.1.4 Scaled Prototype Vessels

Three scaled prototype vessels representing plant vessels were tested, as outlined in Table 5.2. The actual plant LS and blend vessels are not exactly the same size and geometry but were judged similar enough that a single LS prototype was a suitable representation for both vessel types.

Table 5.2. Relationship of WPT Vessels to Test Vessels

Scaled Prototype Nomenclature	WTP Vessel Identification
Lag Storage (LS)	HLW LS: HLP-VSL-00027A/B HLW Blend: HLP-VSL-00028
Ultrafiltration Feed Process (UFP) Vessel	UFP-VSL-00002A/B
Concentrate Receipt Vessel (CRV)	HCP-VSL-00001/00002

These test stands were used to investigate mixing and GR&R behavior with a wide variety of PJM configurations often combined with air sparging and steady jets generated by recirculation pumps. PJM configurations investigated included the number and size of pulse tubes plus pulse tube nozzle size, angle, height above the vessel bottom and configuration. Various configurations of sparge tubes and air flow rates were investigated, typically in conjunction with PJM operation. The steady jet configurations evaluated included both the number (1–4) and geometry of the nozzles. Detailed descriptions of the test stands may be found in Bates et al. (2004), Johnson et al. (2005), and Guerrero and Eberl (2004a, b).

All vessels were clear acrylic with steel dished bottoms inserted into the tank or bolted to the bottom. The dish bottoms had the same shape as the plant scale vessels. The clear acrylic tanks allowed visual observation of the mixing zones and flow patterns when using the transparent Laponite simulant. When using opaque clay simulant, visual observations were limited to the surface and wall, aided by the use of dyes. Various PJM configurations were investigated using a set of pulse tubes that could be bolted together in a variety of configurations. As shown in Figure 5.7, the PJM assemblies were removed from the tanks for reconfiguration and then lifted back into the tanks using a crane. Different PJM nozzle types and geometries were investigated using combinations of commercially available steel and PVC pipe as well as custom fabricated parts.

The 168-inch-diameter, full-scale UFP vessel was represented by a 34-inch-ID acrylic vessel outfitted with a scaled array of internals and PJMs. The scaling factor for the vessel and internals was 168/34 = 4.94. The 300-inch-diameter, full-scale LS vessel was represented by a 70-inch-ID acrylic vessel

Figure 5.7. LS Scaled Prototype Vessel with PJM Configuration Lifted into Test Vessel (left) and UFP Scaled Prototype Vessel with PJM Configuration Removed for Reconfiguration (right)

outfitted with a scaled array of PJMs and vessel internals (Figure 5.8). The scaling factor for the vessel was 300/70 = 4.29. The PJM cycle time was inversely proportional to the scaling factor. The 168-inch-diameter full-scale CRV tank was represented by a 40-inch-ID vessel with a scale factor of about 4.2, pictured in Figure 5.9.

For tests that involved air sparging, the sparging system layout and air flow rates were determined using the ZOI performance guidelines developed in Poloski et al. (2005). Air sparging was provided by an array of steel tubes suspended from above with the number of sparge tubes ranging from 1 to 8, depending on the test stand and the operating mode under investigation. The outlets of the tubes were placed near the bottom of the vessels to maximize the volume mixed by the spargers. The sparger air flow rates were measured with in-line rotometers for each sparge tube. The actual air flow rates (acfm) as well as the flow rates at standard conditions (scfm) were determined by correcting the rotometer readings for pressure, temperature, and pressure head due to simulant depth. Two flow rates were generally used, a low rate representing idle mode and a higher one representing the mixing mode. The idle mode prevents plugging of the sparge tubes when they are not being used for mixing.

The effectiveness of steady jets for mixing was investigated in the scaled prototypes using a recirculation system. The simulant was recirculated using two centrifugal pumps placed in parallel and connected in series with a diaphragm pump that served to eliminate cavitation in the centrifugal pumps. The centrifugal pumps fed a manifold that could supply flow to as many as four separate discharge lines. Several nozzle configurations and geometries were investigated using combinations of commercially available steel and PVC pipe fittings. A single intake line was located near the bottom of the vessels. The flow rate and density of the slurry from the recirculation pump was measured using a 3-inch MicroMotion Coriolis mass flow meter.

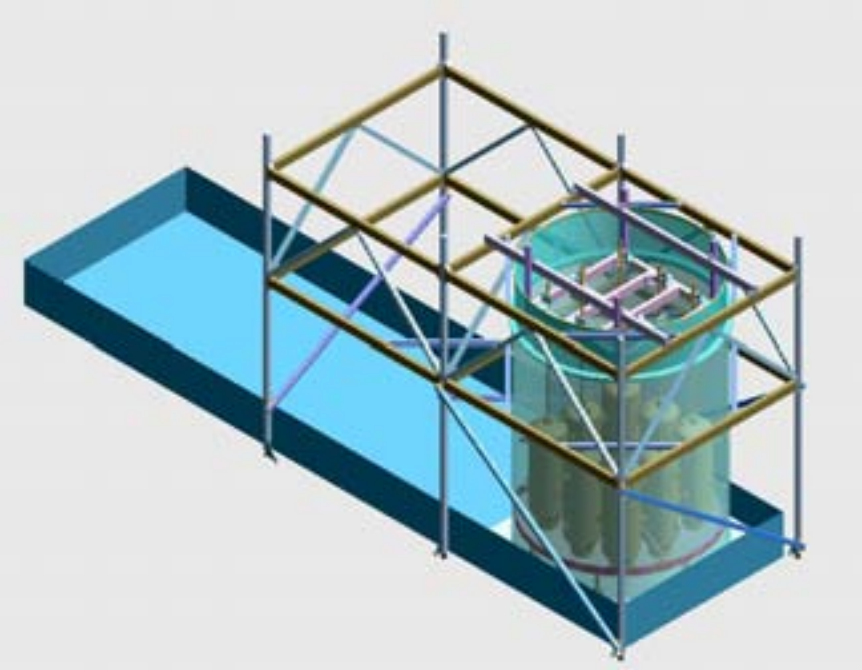

Figure 5.8. LS Vessel Scaled Prototype Typical Assembly Shown with PJM Support Structure and Secondary Containment

Figure 5.9. Scaled CRV Test Stand (baseline PJM configuration installed)

The pump flow rates were scaled approximately by the inverse square of the geometric scale factor. For the UFP vessel the flow rate was scaled by 4.94^2 (24.4), and the pumps were operated at a target flow rate of 90 ±5 gpm. For the LS vessel the flow rate was scaled by 4.29^2 (18), and the pumps were operated at a target flow rate of 120 ± 5 gpm. The velocity of the simulant exiting the discharge nozzles was set at 30 or 40 ft/sec by varying the nozzle diameter.

5.1.5 Cone-Bottom Tank in the 336 Facility

The test program required a large vessel test platform to develop design guidelines for air sparging of non-Newtonian slurries. While the specific geometry of the vessel was not important, sufficient depth and wall clearance were required to evaluate sparge mixing behavior. A large CBT in the 336 facility was selected and configured with single and multiple sparge tube arrays. Tests included various measurements to define the shape and size of the surface and subsurface ZOI: an ultrasonic probe to determine the subsurface shape of the ROB, velocity measurements at various locations in the ZOI,

simulant recirculation times in the ROB and ZOI using dye and tracer, aerosol generation at various sparge rates, and gas retention and release behavior. All sparging work in the CBT was conducted using the opaque kaolin/bentonite clay simulant.

The experimental apparatus consisted of a large-scale combined cylindrical and CBT with either a single or multiple sparge tube array (Poloski et al. 2005). The upper, cylindrical portion of the tank was 96 inches high with an ID of 152 inches. The cone-shaped section extends a further 70 inches, tapering to a diameter of 12 inches at the tank bottom. The overall tank height was 166 inches. The typical working volume of the tank was about 10,000 gallons. Figure 5.10 is a photograph of the tank.

Figure 5.10. Overall View of the CBT

Three-quarter-inch Schedule-40 pipe was used for each of the sparge tubes for all tests, both single and multiple sparge tube configurations (Figure 5.11). Each tube was immersed in the simulant to a known depth, and air was forced through the tube, exiting at the nozzle at the lower end. Although Figure 5.11 shows the sparge tubes 6 inches from the bottom of the vessel, this distance was changed as needed by moving the tubes up or down on the support structure. A dedicated rotameter, pressure gauge, and thermocouple were used to measure volumetric air flow rate, pressure, and temperature for each tube.

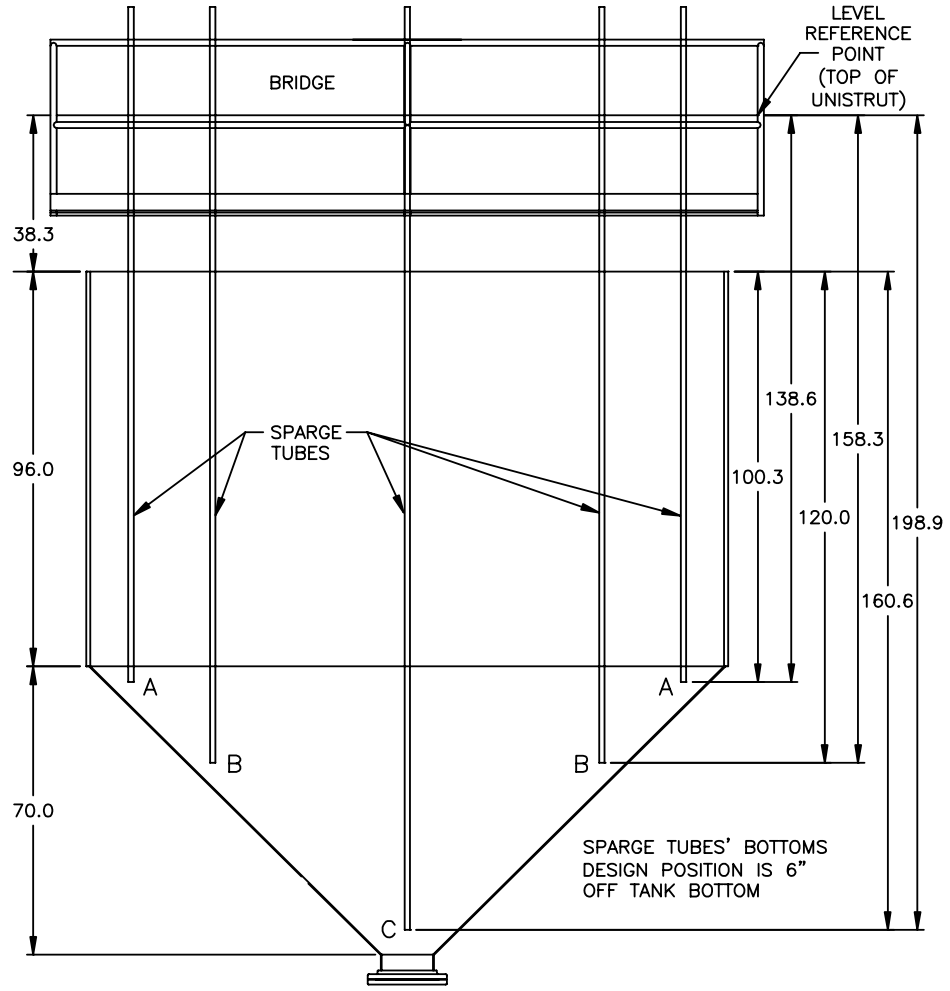

Figure 5.11. Plan View of the Multiple Sparge Tube Test Stand

5.1.6 Half-Scale Lag Storage

The HSLS confirmatory holdup and mixing tests were conducted in one of the large tanks available in the high bay of PNWD's 336 test facility. The tank was equipped with 1) PJM/sparger assemblies, 2) auxiliary systems for providing air to the test equipment and for injecting hydrogen peroxide and chloride tracer, and 3) instruments to monitor gas holdup and release behavior and to evaluate the mixing effectiveness of the PJMs and sparger assembly. The vessel was equipped with several injection lines for injecting the hydrogen peroxide (to simulate gas generation) and chloride tracer (to evaluate mixing times and effectiveness of mixing). This test stand was used to conduct a series of mixing and GR&R tests to demonstrate WTP operational scenarios (Bontha et al. 2005).

This test stand was a half-scale replica of the full-scale plant design. The PJM assembly consisted of eight pulse tubes in a cluster configuration (7 around 1), as shown in Figure 5.12. A shroud was placed

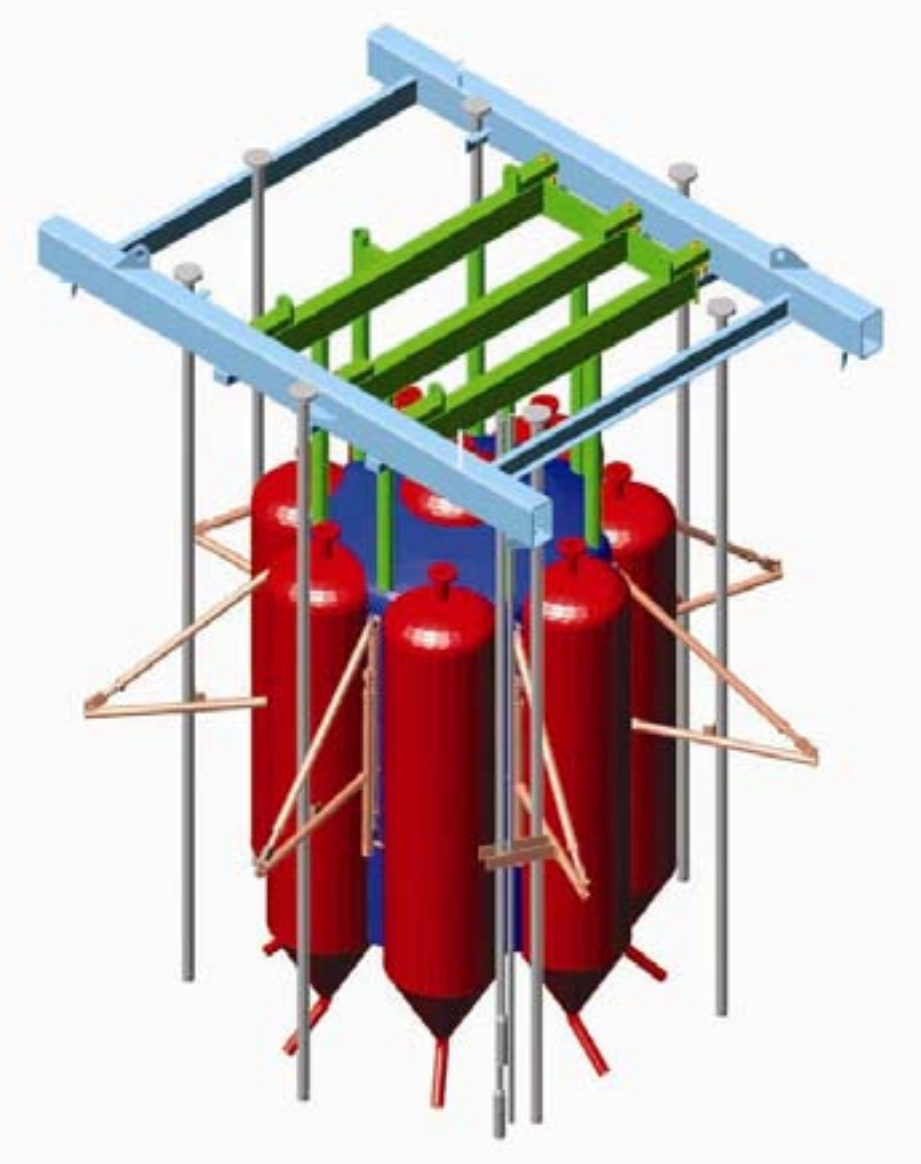

Figure 5.12. PJM and Sparger Assembly for the HSLS Test Stand

around the perimeter of the PJMs to prevent the slurry from entering the area between the PJMs. Seven sparge tubes were placed in the annulus around the PJM cluster. The spargers were arranged according to the performance guidelines developed in the sparging work (Poloski et al 2005). The actual plant design includes more spargers because the tank surface area is larger.

The PJM operation was controlled using a prototypic system provided by BNI. Although the WTP controller has the ability to operate the PJMs in the plant prototypic mode, it was only used to operate the PJMs in a fixed timer mode. In this mode, the drive, vent, vacuum, and delay times were prespecified, and the controller action was switched from one phase to another at the appropriate time. The timer mode for the controller function was used primarily to keep the cycle times constant. This enabled comparisons among tests with different gas generation rates. The suction and discharge of the simulant to and from the pulse tubes was regulated by eight JPPs mounted on two skids at ground level beside the tank.

The air flow to the spargers was regulated through a manifold located on the mezzanine adjacent to the HSLS tank. The manifold consisted of two lines for regulating the air flow under normal (main) operation and idle (reduced flow) operation. Switching was performed manually using ball valves in the headers of the two flow loops. Flow meters are present on the primary and idle flow lines for each sparger, along with pressure gauges and temperature sensors at the inlet and outlet of the flow meters to enable conversion of the air flow rates from actual (acfm) to standard temperature and pressure (scfm).

5.2 Measurement Methods and Conduct of Tests

This section contains a discussion of the types of tests that were performed and the measurement methods used in the tests.

5.2.1 Cavern and Breakthrough Scaling Tests

Experiments to characterize the development and size of a cavern generated by PJMs were conducted at three scales with the 4PJM test stands using well-characterized simulant with approximately matching rheological properties. The results from these experiments were used to demonstrate the scaling laws for mixing with PJMs and to establish the technical basis for performing scaled tests of PJM systems in non-Newtonian slurries (Bamberger et al. 2005). Important controlled variables in the experiments included the stroke length, nozzle velocity, simulant height-to-diameter ratio (H/D), and simulant properties.

Experiments were conducted using both Laponite and kaolin-bentonite clay simulants. In a Laponite test, the simulant was well mixed and then allowed to sit undisturbed for at least 18 hours to develop constant shear strength. Mixing with the PJMs would than be initiated and the growth of the cavern monitored until a steady-state size was reached. In a clay test where shear strength was not an important variable, the simulant was well mixed and the test started.

Several techniques were used to measure the cavern size. These ranged from simple visual observations, where the cavern height was measured using a tape measure fixed to the side of the mixing vessel, to the use of video cameras in camera wells in the 336 4PJM mixing vessel. The 336 vessel was made of stainless steel and thus was opaque, whereas the APEL and SRNL vessels were transparent.

Brilliant blue dye was added to the mixing cavern of some of the Laponite tests to more clearly delineate the cavern. This was done by adding a concentrated dye solution into the bottom portion of the tank. Dye improved the contrast between the mixing and nonmixing portions of the fluid. After each individual test, the tank contents were homogenized by vigorously pulsing the jets. Additional dye or a different color dye could be used to produce good contrast between mixing and nonmixing regions. The dye approach to marking the cavern was also used with the kaolin-bentonite simulant with some success.

Cavern tests were designed to evaluate the size of the mobilized region of a cylindrical tank with an elliptical tank bottom and symmetrically spaced PJMs. Breakthrough occurs when the cavern reaches the fluid surface. Because the tank surface level goes up and down during PJM operation, the measurements were made at full PJM discharge when the surface level was at its maximum. Breakthrough was monitored by visually observing the surface.

5.2.2 Mixing Effectiveness and Time to Mix (dye, tracer, PIT tags, poly beads)

Several methods were developed and implemented for assessing the effectiveness of the various mixing configurations and the time to mix. These methods involved the addition of various colored dyes, chemical tracers (sodium chloride), passive integrated transponder (PIT) tags, and polymeric beads. The spatial and temporal distribution of these materials was monitored to assess the effectiveness of the mixing configurations. The monitoring techniques included grab and core sampling followed by chemical analysis, in situ monitoring with ion selective electrodes (ISEs), and antennas for detecting the PIT tags. Each of these methods is discussed separately below.

5.2.2.1 Chemical Tracers for Assessing Mixing

One of the most widely used methods was the chemical tracer method employing either colored dyes or sodium chloride. The development of these methods for the PJM program is discussed in Poloski et al. (2004b). In a typical experiment, these materials would be added to one or more of the pulse tubes and injected under the surface of the simulant or added to the top of the simulant. Before the experiment started, baseline samples were obtained. Additional samples were obtained during the experiment. At the end of the experiment, the simulant was homogenized and final samples taken. The concentration of the colored dyes was determined with an ultraviolet-visible (UV-vis) spectrometer, and the concentration of the chloride ion was determined by ion chromatography (IC). ISEs were used in some cased for in situ monitoring of chloride concentration. Unfortunately, quantitative measurements with this method were hampered by instrument drift. The resulting concentration data were analyzed by various methods to determine the extent of mixing and the time to mix.

Based on literature reviews, several dyes were chosen for preliminary evaluation, including bromocreosol purple, Congo red, ethyl orange, methyl orange, malachite green, and fluorescein. Absorbance curves were developed in both water and Laponite. Brilliant blue and ethyl orange were recommended for use in Laponite based on the linearity and reproducibility of the Beer's law results.

Because kaolin and bentonite clays are minerals prominent in hydrogeological investigations, previous research on tracers in hydrology experiments was used to shorten tracer developmental efforts. A review of tracers for vadose zone hydrology is given by Flury and Wai (2003). The discussion of these tracers involved ease of quantification, stability, interactions with other species, and toxicology. The authors recommend optical dyes and concluded that Brilliant blue, which has been well investigated, is the best for use in vadose zone hydrology. The authors also noted that tracer dyes can be used in conjunction with other common inorganic ion tracers such as chloride and bromide.

The tracer method was applied to both the Laponite and the kaolin-bentonite clay with varying degrees of success. The colored dyes were preferred with Laponite because of its transparency, and the dye concentration can be determined directly in the sample with the UV-vis method. The kaolin-bentonite clay is opaque, and samples required separation of the interstitial liquid from the clay particles with centrifugation. An additional difficulty was that some of the dye was absorbed by the clay. This required that isotherms giving the relationship between the concentration of the dye in the liquid and the solid be developed. This was a time-consuming process that added uncertainty to the final results. A further disadvantage is that the time required for the dye to reach equilibrium between the clay and the water phases ranged from 24 to 48 hours. Because chloride is an anion, it is not absorbed by the clay and

determination of isotherms is not necessary. The only significant disadvantage to using chloride is that the salt addition increased the rheological properties of the clay. By limiting the change in tracer concentration to about 20 ppm, the effect on the simulant properties was minimized while allowing good accuracy in the sample analysis. For these reasons, sodium chloride became the preferred tracer for mixing tests using kaolin-bentonite clay. In some cases both tracers were used simultaneously.

The extent of mixing was characterized by both the fraction mixed and a mixing ratio. The fraction mixed offers the advantage that it is intuitively easy to understand. Unfortunately, the equation defining the fraction mixed often leads to inconsistent results. For example, when the sample concentration is less than the final sample concentration the fraction mixed is greater than 1, which is not realistic. When the sample concentrations are equal to the initial test concentration, the fraction mixed approaches infinity. Therefore, a mixing ratio was defined that is essentially a normalized concentration ratio. When the sample tracer concentration is equal to the initial test concentration, the mixing ratio is unity and indicates no mixing where the sample was taken. When the sample tracer concentration is equal to the final test concentration, the mixing ratio is zero and indicates good mixing. Lastly, when the sample tracer concentration is higher than the final test concentration, the mixing ratio is negative, indicating incomplete mixing. This corresponds to a situation in which the sample location is within the mixing cavern, and the fraction mixed calculation may be performed. From this information, the interpretation of the mixing-ratio data is summarized by Table 5.3.

Table 5.3. Mixing-Ratio Data Interpretation

Mixing-Ratio Value	Description
~1	Tracer concentration near initial test concentration; tracer has not reached sample location.
~0 to 1	Tracer concentration between initial and final tracer test concentration; tracer has begun to reach sample location, or slow laminar mixing is occurring with large concentration gradients.
~0	Tracer concentration is near final tracer test concentration; vessel is nearly homogenous.
< ~0	Tracer concentration is above final tracer test concentration; sample location is within the mixing cavern. Fraction mixed values can be calculated.

All of the results contained sampling and analytical uncertainty that was characterized in an error analysis. Probability scores were calculated for the results, and probability scores were assigned. The probability scores represented the probability that the actual mean value of the mixing ratio was between +0.1 and –0.1). Probability scores greater than 68% were considered high confidence that the vessel contents were well mixed, while values < 68% were considered lower confidence.

In time-to-mix studies conducted in the HSLS vessel, the mixing time was defined as the time required for the chloride ion concentration to reach and remain between 95 and 105% of the final equilibrium value. The approach used for determining the mixing time involved computing the root-mean-square (RMS) probability log variance (also referred to as the log variance) of the tracer (chloride ion) concentration as measured by IC using the analysis outlined in Edward et al. (2004). There are two main advantages to using the log variance approach as opposed to estimating the time to mix from the

concentration data. First, it is easier to pick the time to mix from the log variance data, and second, the log variance approach weights all of the data toward the locations showing the largest concentration deviation to ensure that all regions of interest are fully mixed. Details of this method and the results can be found in Bontha et al. (2005).

5.2.2.2 Passive Integrated Transponder (PIT) Tags

PIT tags were used in several applications, including determination of the subsurface ZOI in single sparger tests in the CBT and determination of cavern size and extent of mixing (large-tank 4PJM and scaled prototypes). This novel application of PIT tags provided a relatively noninvasive method for assessing fluid motion that did not require sampling.

PIT tags are small identification tags (Figure 5.13) that comprise integrated circuits with an antenna that is encapsulated in glass. The term passive refers to the fact that there is no battery on the tag; it is powered by activating a handheld or stationary transceiver/reader that generates an electromagnetic signal. When activated by the reader, the tag transmits a unique digital code back to the reader, where the code is displayed and/or stored. The tag only transmits its unique code when the tag is present in the transceiver's electromagnetic activation field. The penetration depth of the signal ranged up to 9 inches, making this method particularly useful with the clay simulant.

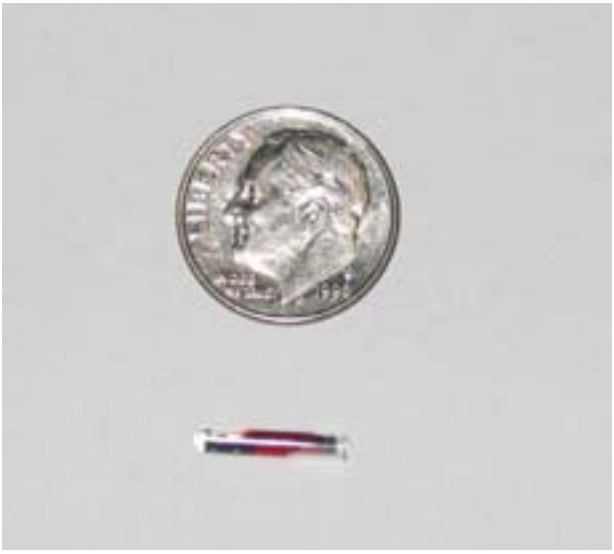

Figure 5.13. Photograph of a PIT Tag

Before a test started the tags were placed on the surface of the simulant, in a pulse tube, or under the simulant surface. The tags were most often used with the opaque clay simulant. The PIT tag transceiver/readers were either placed around the outside surface of the vessel or in PVC tubes inserted into the simulant. Information on the extent of mixing could be obtained by analyzing the spatial and temporal data obtained from the recorders. Movement of the simulant was determined by identifying individual PIT tags during multiple antenna passes. The results of tests using the PIT tags may be found in Bates et al. (2004), Bamberger et al. (2005), and Poloski et al. (2005).

5.2.2.3 Polymeric Beads

Neutrally buoyant lexan beads approximately 1 mm in diameter were used in a few tests to determine cavern height and extent of mixing. In these tests, thousands of the lexan beads were inserted into each of the pulse tubes and were dispersed throughout the simulant when the PJMs were started. After several hours the PJMs were turned off, and core samples were obtained in several locations. The cores were frozen in a walk-in freezer and then cut into sections. The number of beads in each section was counted after the sections were melted. A statistical analysis was conducted on the results to determine the cavern size and assess the homogeneity of the mixed simulant. This technique was applied in the UFP scaled prototype (Bates et al. 2004) and the large-tank 4PJM test stand (Bamberger et al. 2005). While the technique was applied successfully, it was not pursued extensively due to practical experimental difficulties. The size of the beads limited the number that could be used in a given test and thus the accuracy and resolution of the method. This also limited the number of applications to 1 or 2 for a given batch of simulant. Recovery of the beads was difficult and time-consuming, and disposal of the simulant was then required. The beads also interfered with the operation of the simulant transfer pumps.

5.2.2.4 Sampling Methods

Sampling methods included grab samples with a bottle on a rod or through installed sample lines (referred to as tube samples) and core samples. The grab and tube samples were easier to obtain and were typically obtained during the course of a test. Core samples were usually taken after the mixing tests were completed, although in some cases pre- and post-test cores were obtained to provide a baseline. While the core samples were more difficult to obtain and analyze, they provided a complete profile of the mixing behavior in a vertical section of the test vessel.

The simplest and most flexible grab sampling method was using a bottle on a rod. In this method a sealed container was inserted into a known location in the simulant and the top was removed, allowing the simulant to fill the container. This method allowed samples to be obtained from most locations in the tank. One disadvantage of this method was that the insertion of the sample bottle and rod disturbed the simulant and concentration profiles. The tube sample method involved using installed sample lines. This method was used extensively in the scaled prototype test stands. The viscous nature of the simulants required that a vacuum be applied to the sample bottle to draw the sample through the sample line.

Core sampling consisted of inserting a hollow polyvinyl chloride (PVC) pipe into the mixed slurry simulant using a technique called vibracoring, which is commonly used by geologists to sample unconsolidated sediments under water. In this method a concrete vibrator is used to vibrate the pipe into the simulant. For relatively small diameters (<1 inch) the pipe was allowed to sit undisturbed for about 30 minutes so the simulant could develop yield strength. The pipe could then be capped and withdrawn without losing the simulant. In some cases a larger pipe-in-pipe arrangement was used, and dry ice was added to the annulus to freeze the core in situ. The larger pipe was needed for cores longer than a few feet when core shortening (compaction of the sample caused by wall friction) and loss of sample were a concern. After the cores were obtained they were taken to a walk-in freezer to be completely frozen. The frozen cores were sectioned and melted, and samples were submitted for the appropriate analyses. Additional discussion of the sampling methods may be found in Bates et al. (2004), Johnson et al. (2005), and Bamberger et al. (2005).

5.2.3 Velocity Measurements (upwell and profiling)

An ultrasonic Doppler velocity probe mounted on a mast was used to measure the upwell velocity in the 4PJM scaling tests and later to obtain velocity profiles in the LS and UFP scaled prototypes with the final PJM/hybrid mixing configurations. The velocity probe read liquid movement along its longitudinal axis by correlating a detected Doppler shift of reflections from an outgoing 1-MHz ultrasonic pulse train. The probe measured fluid velocities along its longitudinal axis only (i.e., moving directly toward or away from the probe face). The upwell velocities from the 4PJM test stands were used to demonstrate PJM scaling laws (Bamberger et al. 2005). The velocity profiles from the LS and UFP scaled prototypes (Johnson et al. 2005) provided information for heat transfer calculations for the plant vessels. The velocity probe was also used to estimate the cavern boundary with the PJMs (and recirculation pump for the UFP vessel) operating at plant prototypic conditions (Johnson et al. 2005, Guerrero and Eberl 2004a).

5.2.4 Solids Suspension and Mixing Tests

Several solids suspension tests were carried out in the scaled prototype test stands. These tests were performed with water by placing a small concentration (0.4 to 0.5 wt%) of 4-mm glass beads in the bottom of the tank and increasing the PJM nozzle velocity incrementally until the solids were observed to lift off the bottom. Due to the intermittent operation of the PJMs, the solids would be lifted and then settle to the bottom of the vessel between pulses. Solids lift-off was declared if at any point during the drive phase of the PJM cycle all the beads were lifted off the tank bottom.

Solids mixing tests were conducted in the CRV prototype to determine the uniformity of solids distribution in the vessel and thus verify the adequacy of mixing in the CRV to meet the plant specification for solids uniformity. In these tests, the kaolin-bentonite clay simulant (yield stress of 6 and 30 Pa) was used with 0.6–0.7 wt% 4-mm glass beads. The vessel contents were mixed for a specified time. After mixing was halted, several 250-mL grab samples were obtained from the upper and lower portions of the vessel. Samples were also obtained from the heel with the RFD sampler system.

5.2.5 Sparging

Several methods were used to characterize the surface and subsurface flow patterns with single and multiple sparge tube arrays in the CBT. These tests were conducted to determine the size and shape of the surface and subsurface ROB and ZOI, the resulting fluid velocities and recirculation times, and the time to establish a steady-state flow pattern as well as to assess aerosol generation (Poloski et al. 2005).

Most of the work to characterize the flow patterns was conducted with a single sparge tube in the large CBT in the 336 facility. Data on surface and subsurface flow patterns were obtained for air flow rates that ranged from 5 to 40 acfm, where acfm is the actual air flow rate at the bottom of the sparge tube in cubic feet per minute. The multiple sparge tube array was used to provide data on gas retention and release and aerosol entrainment. All test results from the CBT were obtained using the kaolin-bentonite clay simulant.

5.2.5.1 Surface ROB and ZOI

The initial experiments were directed at determining the surface ZOI and ROB using buoyant flow followers (ping pong balls) placed on the surface near the sparge tube. The surface tracers moved readily outward because of the induced secondary flow and stopped at the boundary where radial flow ceases and axial flow downward dominates.

The ZOI and ROB were measured with a laser reference system coupled with video imaging software. This technique involved placing two laser points 6 inches apart on the surface of the simulant. The surface of the simulant was video recorded. The laser reference marks were used by the video analysis software to provide a reference of distance on the recorded video. The frames from the video images were then analyzed to determine the number of pixels between various features in the frame. By knowing the number of pixels and the actual distance between the laser reference points, the actual distance between two features on the frame was determined.

5.2.5.2 Ultrasonic Velocity Probe Measurements

An ultrasonic velocity probe was used to obtain the following:

- Subsurface ZOI vertical boundary profile at steady state. In this test the velocity probe was repositioned at a prescribed depth relative to the sparge tube until a velocity within the zero range and a velocity outside the zero range had been measured within 3 inches (laterally) of each other.
- Time to reach the steady-state subsurface ZOI: For these tests, the ultrasonic velocity probe (UVP) sensor was positioned at both 67 and 95% (approximately) of the expected ZOI steady-state boundary radius. Two-thirds of the ZOI steady-state boundary radius is a key design parameter where the ZOI of one sparge tube meets the ROB boundary of the next one (shown in Figure 6.17). Based on the surface ROB and ZOI measurements and predictions of subsurface flow behavior, that intersection was thought to occur at approximately two-thirds of the ZOI steady boundary radius. (Further discussion can be found in Poloski et al. 2005.) The measurement position at approximately 95% of the ZOI steady-state boundary radius was chosen to ensure that non-zero-range velocities would be detected. To conduct this test, the velocity probe would be positioned and the sparger turned on at the specified air flow rate. Velocities were measured until a steady-state value was reached, typically after about 15 minutes.
- ZOI velocity profiles below the liquid surface. In these tests the velocity probe was positioned at various vertical and radial positions. Measurements were typically taken at 6 inch increments from the ZOI boundary to within about one-third of the ZOI radius.
- The location of the ZOI boundary below the sparger nozzle. In these tests the UVP was positioned beneath the sparge tube and slowly raised until a positive average velocity outside of the zero range was measured.

5.2.5.3 ZOI Subsurface Measurements Using PIT tags

In these tests the PIT tags described in subsection 5.2.2.2 were used with three custom-made antennas. Approximately 6000 tags were placed in the simulant by randomly spreading them on the surface. They were vigorously mixed into the simulant by manually moving a portable sparger tube

around the perimeter of the tank while simultaneously sparging using the test sparge tube. Pit tags were located using three custom-made antennas, each 4 cm in diameter and 25.5 cm long and specially designed to operate inside a PVC pipe. The antennas had a detection range of approximately 8 to 10 cm. These antenna wells were placed at various locations within the simulant to determine whether tags were moving within the reception range of the antennas. Antennas were moved up and down inside the antenna wells by a specialized system that relayed the depth of the antenna within the pipe.

5.2.5.4 ROB Subsurface Measurements Using an Ultrasonic Probe

The size and shape of the submerged ROB at various air-flow rates were characterized using an ultrasonic probe. Ultrasonic amplitude measurements were used to identify submerged regions containing a large fraction of bubbles. Ultrasound in the frequency range 0.5 to 10 MHz is able to penetrate dense slurries and opaque fluids. When ultrasound passes through a simulant, the signal strength is reduced by the interaction of the ultrasound with the particles (or bubbles) in the simulant.

To characterize the submerged ROB, the sensor was suspended in the simulant with the transducer faces parallel to the vertical axis so that the fluid could rise between the transducers without depositing on the transducer face. The sensor was mounted on a mast so the mast would not affect the measurements. For each measurement, the sensor was positioned in the simulant at the desired location using a traversing table. The horizontal x and y positions of the mast were determined from the position of the table. The vertical position of the sensor was determined using a reference mark on the mast. The sparger air flow was then turned on and adjusted to the desired flow rate at the nozzle. The presence of a sparge bubble (ROB) was indicated by severe attenuation of the signal.

5.2.5.5 ROB and ZOI Recirculation Time

The simulant circulation time as a function of air-flow rate was measured using a combination of chemical (ion concentration) and dye tracer detection. The dye tracer was injected in the ROB near the bottom of the sparge tube, and a video recording detected the arrival of the dye at the surface and its movement to the ZOI outer boundary. The chemical tracer was placed just below the surface at two-thirds ZOI, and the detectors were positioned to determine the time of travel from the surface to the sparger nozzle. Two subsurface chloride ISEs were placed in the tank; the movement of the tracer was monitored by observing the voltage output from the ISE.

5.2.5.6 Aerosol Generation

This test was conducted in the CBT, which was shrouded with a plastic tarp to evaluate the mass of aerosol emitted into the tank headspace under various sparging conditions. A size-fractioned point sampling technique was used to collect the aerosol. This technique used size-selective samplers to collect aerosol particles in the headspace above the tank at three size classifications: total suspended particulates (TSP), PM10, and PM2.5. TSP are any particles suspended in the air, PM10 includes all particles less than 10 μm in aerodynamic diameter, and PM2.5 includes all particles less than 2.5 μm in aerodynamic diameter. This technique uses impaction plates to remove all particles larger than the desired particle size before they are collected on the sample filter. The filters were weighed before and after sample collection to determine the aerosol mass collected. A mass concentration measurement for each size classification

was then determined. Nominally, target air flow rates were ⅓, 1, and 7/5 times the baseline sparging flow rate of 200 ft^3 per minute. The kaolin-bentonite clay simulant was used in these tests.

5.2.6 Gas Retention and Release

Gas retention and release tests were conducted to obtain data for demonstrating the GR&R scale-up theory and the WTP operational cycles. The work generally used the kaolin-bentonite clay simulant, although some tests were conducted with Laponite. Oxygen was generated in situ by the decomposition of hydrogen peroxide that was mixed into the simulant. The use of hydrogen and other gases expected in the WTP was precluded by safety concerns and the lack of a method for generating the gases in situ.

Two types of tests were conducted to demonstrate the GR&R scale-up theory: gas release and gas holdup (Russell et al. 2005). Gas release tests were conducted by injecting a specified mass of 30 wt% H_2O_2 over a short period (10 to 20 minutes) with full mixing. After 10 to 30 minutes of additional mixing, the system was shut down to allow the H_2O_2 to decompose and gas bubbles to be retained in the quiescent simulant. As the peroxide decomposed the oxygen was trapped by the simulant, resulting in a rise in simulant level. After the simulant level reached a steady-state value, indicating the decomposition of peroxide was complete, the specified mixing system (PJMs, spargers, recirculation pumps) was started to release the gas. The volume of gas released was calculated from the simulant level drop.

In gas holdup tests, the H_2O_2 solution was added to the simulant at a fixed rate over several hours to generate O_2 gas continuously while the simulant was mixed in the vessel using the specified mixing system. Injection of the hydrogen peroxide continued until a steady-state level was achieved in the test vessel. In all GR&R tests, the retained gas volume was determined by monitoring the simulant level and comparing it with the level corresponding to no retained gas.

Proposed WTP operational cycles were demonstrated in the HSLS vessel in the 336 building (Bontha et al. 2005). Although a small number of gas release and holdup tests were conducted, most of the tests involved intermittent operation of the mixing systems. While gases will be generated continuously in the WTP vessels, the addition of peroxide in these tests had to be intermittent, corresponding to the times when the mixing systems were on. This was necessary to avoid the buildup of hydrogen peroxide at the injection ports during periods without mixing. As with the GR&R tests, the retained gas volume was determined by monitoring the simulant level.

Several methods were used for measuring the simulant level. In the LS and UFP scaled prototypes and the SRNL and APEL 4PJM test stands, heights were measured on a scale affixed to the outer wall of the tank at an arbitrary vertical location; for the 336 4PJM test stand, heights were measured as distance down from the top of the tank rim. Primary among the tank simulant surface level sensors was an ultrasonic-type sensor stationed a fixed distance above the simulant surface. The ultrasonic sensor projects ultrasonic waves in a cone shape (8 degrees from vertical) from the face of the sensor, requiring attention to sensor placement to avoid obstructions. Some tests also used a micropower impulse radar (guided wave radar) sensor to measure the tank simulant surface level. This waveguide level sensor consists of dual solid rods that sense immersion in fluid based on the time of flight between sending a microwave pulse and receiving the reflected signal. A third level sensor used in some tests was a radio frequency (RF) admittance sensor rod like those used within the PJMs. The method used in the HSLS

tests used four laser level sensors placed in different quadrants of the tank. In most of the tests, additional manual measurements were recorded using tape measures or rulers fixed in the tank.

5.2.7 Gas Holdup in a Bubble Column

Hydrogen gas was not used in the GR&R tests because of the experimental difficulties associated with generating H_2 in situ in relatively large quantities and the potential safety issues. Therefore, bench-scale tests were completed to compare the relative gas holdup of O_2, H_2, and other gases in various simulants. These results were used as input to a model for predicting gas retention and release behavior in selected WTP vessels.

The gas-holdup apparatus consisted of a 6-in diameter, 6 ft tall, Perspex column that was filled with 15 to 20 L of simulant. Gas was introduced into a diffuser at the column base through a rotameter and pressure transducer. Hydrostatic pressure within the column was measured by mounting two pressure transducers through the column wall at different heights. The pressure transducers and thermocouples located in the fume hood and column were configured into a data acquisition system.

A statistically designed test matrix was constructed to determine the gas holdup in water, kaolin-bentonite clay, and simulated AZ-101/102 HLW matrixes with H_2, Ar, O_2, and air at up to five different flow rates. The matrixes were adjusted with sodium nitrate and an antifoaming agent (AFA), product Q2-3183A, manufactured by Dow Corning. The gas flow rate was reduced incrementally, allowing15 minutes for achieving steady state between each reduction. It was found that increasing the flow rate incrementally gave rise to anomalous results, possibly because the slurry was insufficiently sheared. Additional details may be found in Russell et al. (2005).

5.2.8 Mass Transfer Demonstration with Air Sparging

Proof-of-concept tests were conducted to demonstrate gas-stripping mass transfer in non-Newtonian simulants (Russell et al. 2005). Bench-scale experiments conducted in a bubble column demonstrated the stripping of O_2 from O_2-saturated kaolin-bentonite clay and simulated AZ-101/102 HLW resulting from air sparging at different flow rates, and the results were used to calculate mass-transfer coefficients. A similar proof-of-concept gas-stripping test was conducted with clay simulant in the UFP model vessel.

In these experiments, the simulant was first saturated with oxygen by the addition of hydrogen peroxide, which decomposed to water and oxygen. Sparging was provided by the addition of air near the bottom of the simulants. The concentration of dissolved oxygen was monitored with a dissolved oxygen probe. Three slurries (dilute kaolin-bentonite clay, concentrated kaolin-bentonite clay, and pretreated AZ-101 HLW simulant) were tested in the bubble column, each at air sparge flow rates of 13.9, 32, and 54.4 L/min corrected to standard temperature and pressure.

5.2.9 PJM Overblow Testing in the 336 Supernatant Tank

The objective of these tests was to measure hydro-acoustic pressures resulting from PJM overblows and to provide BNI with data to assess whether PJM overblows could contribute to structural damage of a PJM mixing tank or its internal components and equipment. Overblows occur when the PJM drive air

pressure is applied for a sufficient period to purge the pulse tube of liquid so that air exits the PJM nozzles. This causes a sudden expansion of pressurized air in the pulse tubes as it discharges through the PJM nozzle. Continual discharge of air from the PJM nozzle is similar to sparging and was not assessed in these tests.

Testing was performed on February 27, 2004 in the 336 Building in the supernatant tank configured with four PJMs (Bontha 2003) using kaolin/bentonite clay simulant. Hydrophones (underwater microphones) sensed acoustic pressure generated by PJM overblows. The majority of hydrophone measurements were made in horizontal planes at tank elevations of 1.1 ft (the plane of the nozzle discharge) and 5.1 ft relative to the bottom center interior of the tank. Typical peak pressures ranged from a few to several thousand Pascals. The largest acoustic pressure of 13 kPa was measured for a PJM drive pressure of 500 kPa near the PJM nozzle.

The large fluid disturbance of PJM overblows was also used in many gas retention and release tests to assist mixing. Overblows helped to ensure the most uniform distribution of hydrogen peroxide in the simulant prior to gas release tests and were used to degas the simulant after tests were completed.

6.0 Experimental Validation of Scale-up

An important component of non-Newtonian PJM test program technical strategy was to validate that the mixing and GR&R behavior observed in reduced-scale tests was applicable to plant-scale vessels. Confidence in the small-scale prototype tests results was needed to apply the results to plant-scale vessels. This was accomplished by testing in geometrically similar 4PJM mixing systems at three different scales: large, ~one-quarter, and ~one-ninth scale. The data were compared nondimensionally using the scaling parameters developed in Section 3 to demonstrate the validity of testing prototypic PJM mixing systems at reduced scale.

The relationship of these three scales is shown in Figure 6.1. WTP vessels generally differ from the 4PJM mixing systems in height, diameter, number of PJMs, and operating conditions. However, the vessels have all the essential features of the plant vessels, and thus the scaling methodology demonstrated by the 4PJM systems is the same for reduced-scale vessels.

As the program evolved into hybrid mixing systems using both PJMs and air sparging, the scaled testing approach was modified. The geometric scale-up of sparge operation is highly nonlinear and introduces a number of complexities; therefore, testing geometrically scaled sparge systems in vessels of different sizes was not pursued. Instead, mixing behavior resulting from a single, nearly full-scale sparge tube was investigated. From these data, a methodology for specifying multiple sparge tube arrays in plant-scale vessels was developed.

This section summarizes of the tests performed to validate the scaling methodology. Mixing tests performed in 4PJM vessels are documented in Bamberger et al. (2005) and Wilson et al. (2004) and are summarized in Section 6.1 of this report. Gas retention and release tests performed in 4PJM vessels are documented in Russell et al. (2005) and summarized in Section 6.2. Sparge array scale-up data obtained from single sparge tube tests are documented in Poloski et al. (2005) and summarized in Section 6.3.

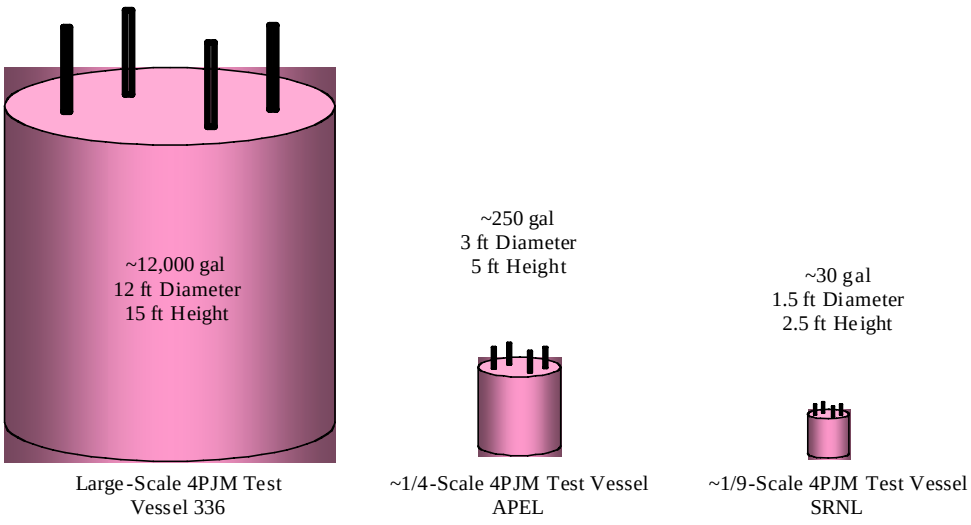

Figure 6.1. Relative Size of 4PJM Mixing System Vessels Used for Validation of Scaling Approach

6.1 PJM Scaling Tests

Tests were performed with Laponite and a kaolin-bentonite clay simulant, and PJM systems were operated according to the scaling rules discussed in Section 3. For this work, mixing is defined as fluid mobilization within the cavern (Figure 6.2). No attempt was made to quantify the degree of turbulence within the cavern. Generally, PJM velocities varied over a range that provided useful data. Given the geometric similarity (specifically that of the pulse tubes), PJM drive time was reduced by the scale factor "s" for a given velocity. Given the nondimensional nature of the scaling approach, the simulant rheological properties or PJM velocities did not need to be identical in the various test stands. However, the properties were similar, and velocities were maintained within useful and prototypic ranges.

Generally, the rheology and PJM velocities used during the testing were close to prototypic. However, in some cases higher-strength rheologies and velocities were used to fully exercise the range of experimental conditions for a given test. In spite of this, the yield Reynolds numbers were generally maintained within the prototypic range expected in the WTP. Three types of data were analyzed to make nondimensional comparisons:

- Cavern height measurements with Laponite at three vessel scales (s = 1, s = 4.5, and s = 8.9)
- Breakthrough velocity measurements with Laponite and kaolin-bentonite clay at three vessel scales (s = 1, s = 4.5, and s = 8.9)
- Upwell velocity measurements in kaolin-bentonite clay at two vessel scales (s = 1 and s = 4.5).

Time-to-mix experiments were conducted using Laponite and kaolin-bentonite clay simulants at three scales. When the data were compared, significant differences in experimental conditions, measurement approaches, and a limited test matrix were noted. Thus data from these tests did not contribute to the scaling analysis.

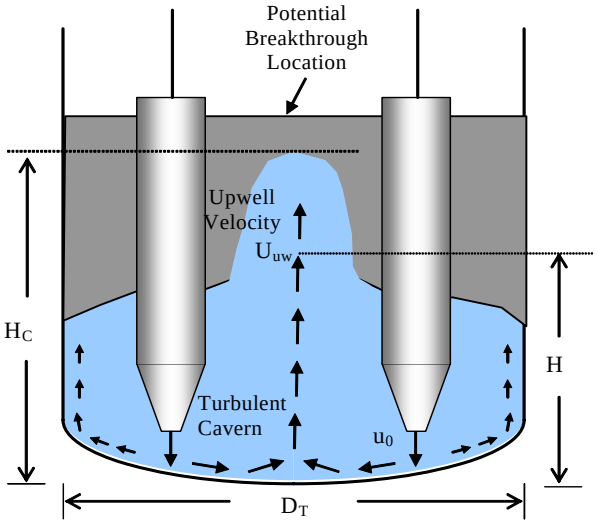

Figure 6.2. Features of Central Cavern for Collecting Data in 4PJM Vessels

The range of test conditions was selected to provide enough variation to establish a wide range of comparable data and to span full-scale plant operating conditions where possible. The approximate range of test conditions, including dimensional and nondimensional parameters, is listed in Table 6.1.

Table 6.1. Range of Conditions Tested in 4PJM Experiments Compared with Full-Scale WTP Bounding Conditions

Parameter	Symbol	Units	WTP Bounding	Test Range
Average PJM drive velocity	u_a	m/s	9	3.0–10.2
Peak average PJM drive velocity	u_p	m/s	12	3.3–12.2
PJM drive time	t_D	s	15–60	2–20
Nominal vessel batch volume	V_T	gal	12,000–70,000	30–12,000
PJM nozzle diameter	d_0	cm	10	1–10
Slurry density	ρ	kg/m^3	1300	1000–1200
Slurry consistency	κ	cP	30	10–27
Slurry yield stress	τ_y	Pa	30	18–46
Slurry shear strength	τ_s	Pa	75 (est.)	30–125
Yield Reynolds number (based on u_p)	Re_τ		6,200	120–4,900
Jet Reynolds number (based on u_p)	Re_0		52,000	5,500–52,000
Strouhal number (based on u_p)	S_0		1800–7200	900–2400

6.1.1 Cavern Height Measurements in Laponite

Cavern heights (H_C) were measured using Laponite in the 336 (large scale), APEL, and SRNL 4PJM test vessels. Simulant shear strength (τ_s) and PJM velocity (u_p and u_a) were the two primary test variables. The primary independent test variable is the yield Reynolds number (Re_τ), and the nondimensional cavern height is the resulting parameter. Yield Reynolds numbers were calculated with both peak average (u_p) and average (u_a) PJM velocities. The majority of the tests were performed with a nondimensional simulant fill level of approximately $H/D_T = 0.9$; however, some higher fill levels were considered. These tests were conducted to examine the effect of artificially high caverns and premature surface breakthrough resulting from Laponite bulk fracture at smaller vessel scales.

Nondimensional cavern heights in Laponite are shown plotted versus yield Reynolds number (Re_τ) in Figures 6.3 and 6.4. Linear regressions of the data are also shown on the plot to aid in scale comparison. In Figure 6.3, the yield Reynolds number is calculated using peak average PJM velocity (u_p), and only cases with $H/D_T = 0.9$ are shown. Data for the three scale vessels are plotted separately. In addition, several breakthrough points are included. The data show that nondimensional cavern height increases with increasing yield Reynolds number. While some scatter exists, the linear regression curves demonstrate that cavern heights are generally largest in the 336 vessel and decrease in the smaller vessels. Figure 6.4 includes data from higher fill levels. This was done because of the observation that Laponite often failed in discrete chunks. At small scale, as the cavern approaches the surface, a fracture could result in a higher cavern and potentially premature breakthrough. From Figure 6.4 it appears that this was in fact the case because the breakthrough points for the APEL and SRNL tests are shifted considerably to higher yield Reynolds numbers.

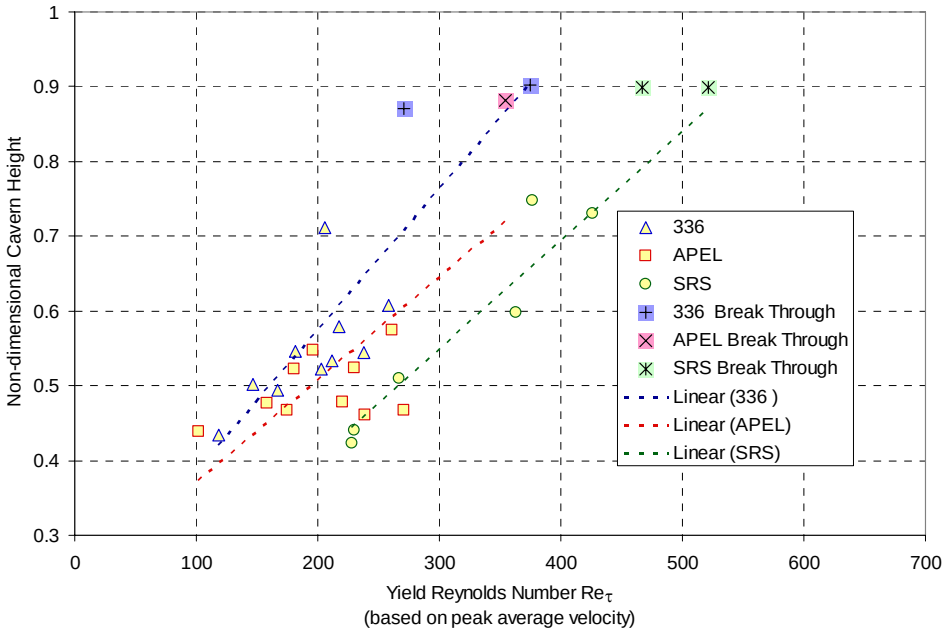

Figure 6.3. Nondimensional Cavern Height (H_C/D_T) Versus Yield Reynolds Number for Laponite. The yield Reynolds number is based on peak average PJM velocity; data are limited to the nondimensional fill level of $H/D_T = 0.9$.

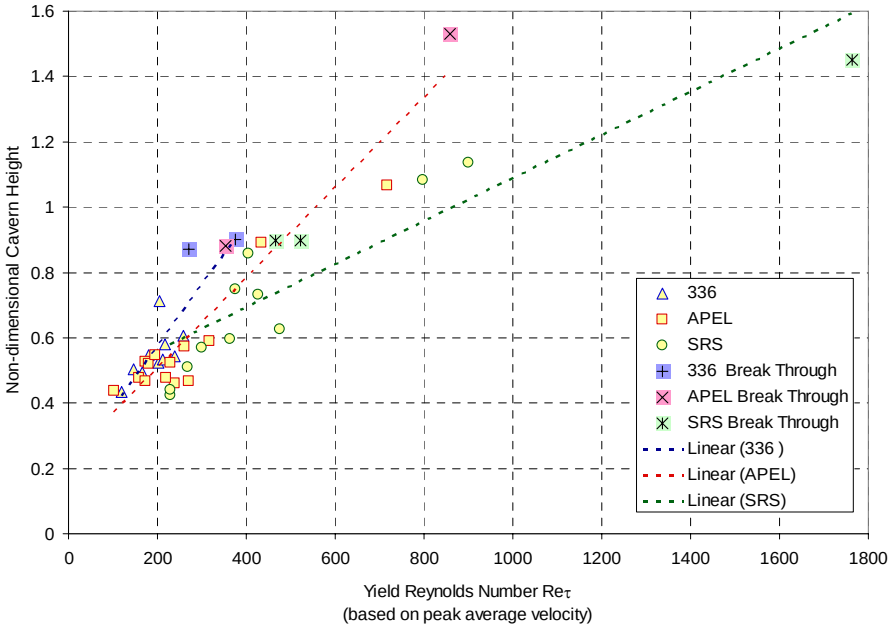

Figure 6.4. Nondimensional Cavern Height (H_C/D_T) Versus Yield Reynolds Number for Laponite. The yield Reynolds number is based on peak average PJM velocity; the data for higher nondimensional fill levels are included.

The general trend that nondimensional cavern heights become larger with increasing vessel scale supports the anticipated result that jet Reynolds number effects will produce higher caverns in larger vessels. These effects are examined in detail when considering breakthrough data in the next section.

6.1.2 Surface Breakthrough Measurements in Clay and Laponite Simulants

Surface breakthrough velocities were measured using Laponite and kaolin-bentonite clay simulants in the 336, APEL, and SRNL 4PJM test vessels. In these tests, PJM velocities were increased until the central upwell caused the cavern to reach the surface. The specific velocity at which breakthrough occurs can be compared nondimensionally to examine the scaling relationship between the various vessel scales.

Simulant shear strength (for Laponite) or yield stress (for clay) are the primary test variables for measuring the required PJM breakthrough velocity. The tests were performed with a nondimensional simulant fill level of approximately $H/D_T = 0.9$ for all tests. For Laponite the density is nearly a constant 1000 kg/m^3; for kaolin-bentonite clay it is approximately 1200 kg/m^3. The jet Reynolds number (Re_0) and yield Reynolds number (Re_τ), are calculated using the measured breakthrough velocities. The yield Reynolds number uses the shear strength for Laponite and the yield stress for clay.

Yield Reynolds numbers at breakthrough for clay and Laponite are plotted versus vessel scale factor in Figure 6.5. When peak average velocities (u_P) are used, the data clearly suggest that large vessels require a lower yield Reynolds number for breakthrough. The same trend is seen when the average PJM velocity (u_a) is used to correlate the data, only here it could be argued that no real difference is seen between the large-scale 336 vessel (s = 1) and the APEL vessel (s = 4.53). Yield Reynolds numbers for breakthrough are significantly larger for clay than for Laponite. Part of this difference is attributed to the fact that shear strength in clay is about 50% higher than yield stress. However, a factor of ~5 would be required to explain the difference. This suggests that clay exhibits non-Newtonian effects on the flow structure, not just on the flow boundary, as is believed for Laponite. Hence, larger yield Reynolds numbers are required for breakthrough in clay than in Laponite at the same conditions.

In Figure 6.6, the yield Reynolds number (Re_τ) is plotted versus jet Reynolds number (Re_0). While there is some scatter in the data, these correlations suggest that the yield Reynolds number required for breakthrough is reduced as the jet Reynolds number is increased. In physical terms this implies, for equal simulant rheology, that breakthrough velocities will be smaller at larger test scales.

6.1.3 Upwell Velocity Measurements in Clay Simulant at Two Physical Scales

Velocities in the central upwell of the cavern were measured using clay simulant in the 336 and APEL test vessels. In these tests, the upwell velocity was measured at various elevations for a given PJM velocity. This allows a direct comparison of actual velocities in the two vessels.

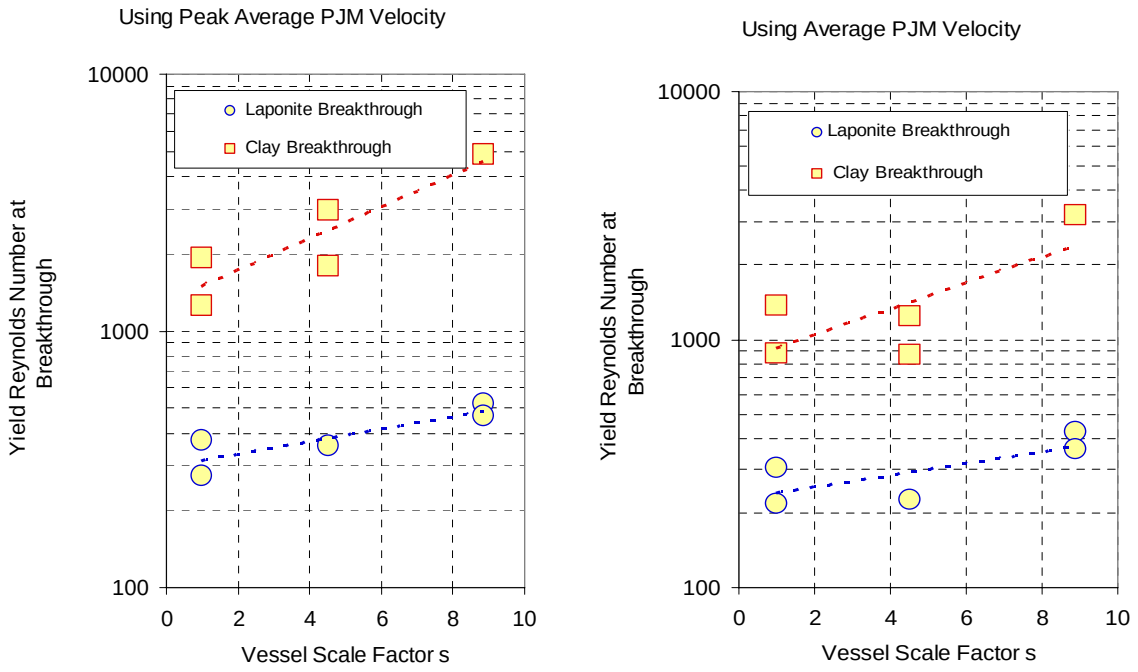

Figure 6.5. Yield Reynolds Number (Re_τ) at Breakthrough Versus Vessel Scale Factor for Breakthrough Tests in Clay and Laponite

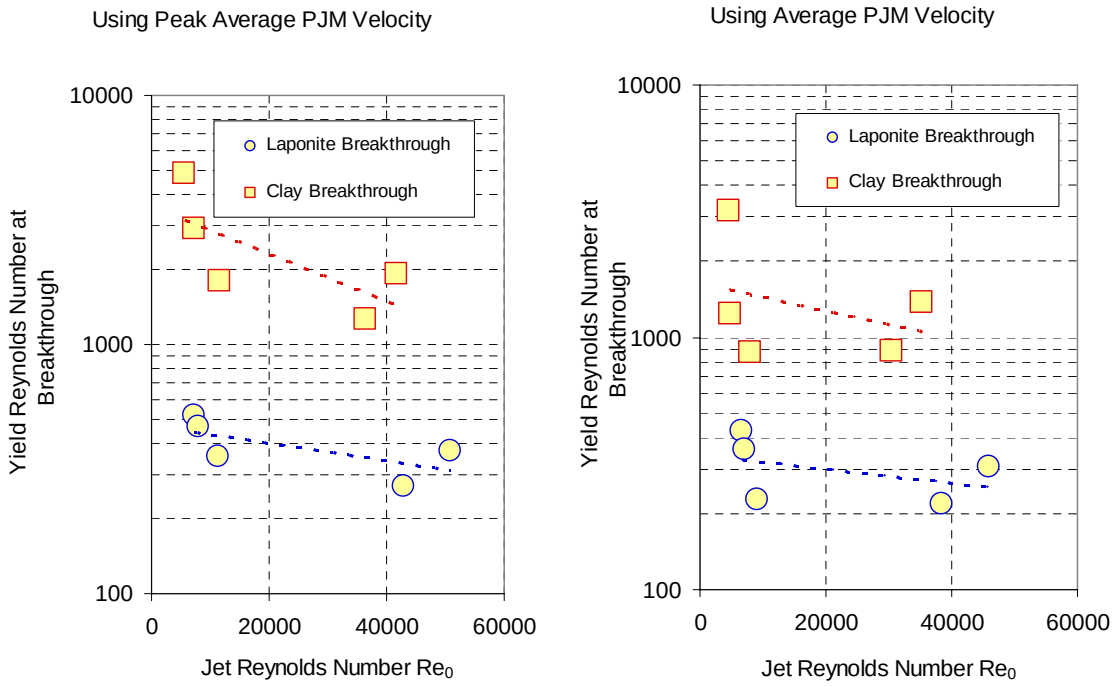

Figure 6.6. Yield Reynolds Number (Re_τ) at Breakthrough Versus Jet Reynolds Number (Re_0) for Breakthrough Tests in Clay and Laponite

Clay rheology, PJM velocity, and vertical elevation are the primary test variables, with upwell velocity a measured dependent variable. The tests were performed with a nondimensional simulant fill level of approximately $H/D_T = 0.9$. When the PJMs were operating, upwell velocities oscillated between low and high values as the pulse formed, stabilized, and then diminished. The maximum velocity for each PJM drive was determined, and the average over many cycles was calculated. Jet Reynolds and yield Reynolds numbers were calculated using both peak average and average PJM velocities. The elevation of the measured upwell velocity is nondimensionalized by the vessel diameter, and upwell velocity is nondimensionalized by peak average or average PJM velocity.

Figure 6.7 explores the effect of jet Reynolds number on upwell velocity. It is not clear, however, that the velocities from the 336 facility bound the APEL velocities. In fact, several of the 336 data points are clearly lower than the APEL velocities at the same vertical elevation, a trend that appears inconsistent with jet Reynolds number scaling. In Figure 6.8, the normalized upwell velocities are correlated with yield Reynolds number. These data indicate a general trend that upwell velocity increases with increasing yield Reynolds number. Also, the APEL data generally fall below the 336 data (or at least the apparent trend of the 336 data). The dominant parameter affecting upwell velocity appears to be the yield Reynolds number; jet Reynolds number effects are secondary. Careful examination of Figure 6.8 shows clearly that the upwell velocities measured in APEL are equal to or less than those measured in 336.

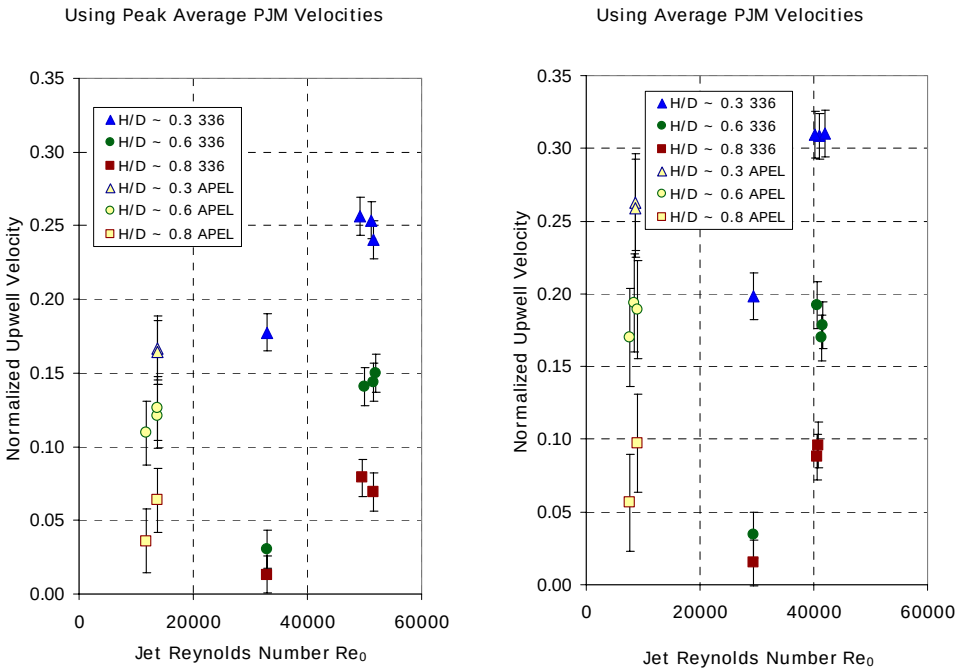

Figure 6.7. Normalized Upwell Velocity Versus Jet Reynolds Number in Clay Compared at Two Vessel Scales; upwell velocity (u_{uw}) normalized by peak average PJM velocity (u_p) (left) and average PJM velocity (u_a) (right)

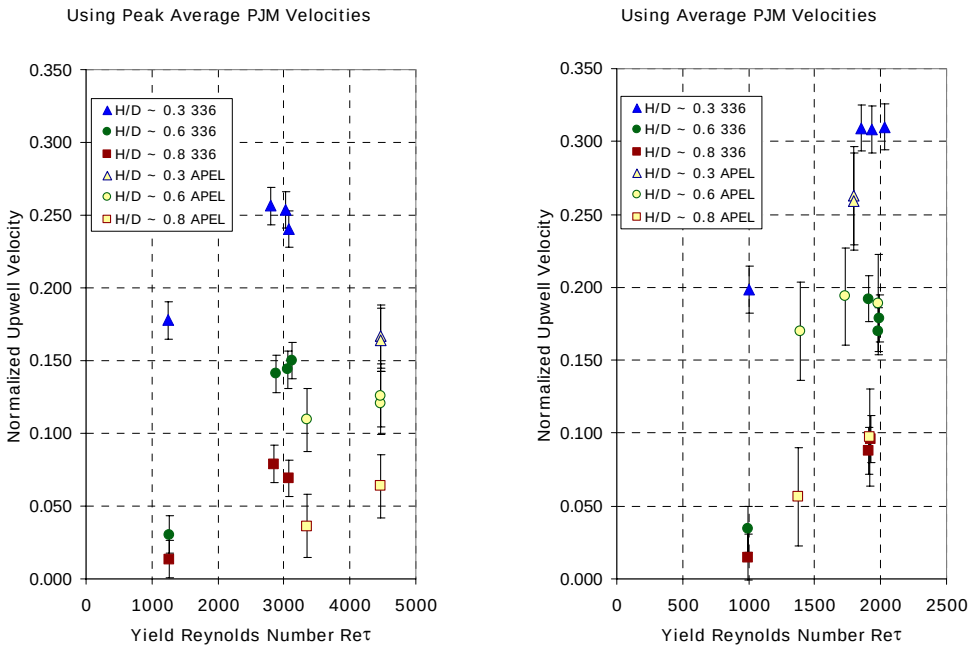

Figure 6.8. Normalized Upwell Velocity Versus Yield Reynolds Number in Clay Compared at Two Vessel Scales; upwell velocity (u_{uw}) normalized by peak average PJM velocity (u_p) (left) and average PJM velocity (u_a) (right)

6.1.4 Summary of Test Results

Normalized cavern heights in Laponite were found to be an increasing function of the yield Reynolds number. Although significant scatter exists in the data, cavern heights were generally found to decrease at smaller scales. This behavior is consistent with the reduction in jet Reynolds number associated with smaller test scales. Surface breakthrough velocity tests performed in both clay and Laponite also showed that the yield Reynolds number associated with surface breakthrough increased with the test scale factor. Upwell velocity measurements indicated that normalized velocities generally decreased with yield Reynolds number. While it was difficult to conclusively observe jet Reynolds number effects, the data suggest that upwell velocities are a weak, decreasing function of jet Reynolds number. The role of Strouhal number was not explicitly examined in the tests. However, at equivalent operating conditions, the Strouhal number was constant at the different test scales and thus not affected by test scale factor.

The scaling theory and experimental test results obtained from these tests demonstrate that the mixing performance of PJM systems in non-Newtonian slurries can be conservatively assessed at reduced scale for the following reasons:

- The three most important nondimensional parameter groups are the Strouhal number, the yield Reynolds number, and the jet Reynolds number. If these parameters are preserved at reduced scale, the essential behavior of the mixing phenomena will be the same as at full scale.
- The Strouhal number, which takes into account nonsteady PJM operation, is the same at reduced and full scale when the PJM cycling is reduced by the geometric scale factor.

- The yield Reynolds number, which determines cavern formation due to non-Newtonian fluid behavior, is the same at reduced and full scale when rheology and PJM velocities are the same at both scales.
- The jet Reynolds number, which determines the flow regime (laminar or turbulent), the degree of turbulence, and the magnitude of mixing velocities, will be decreased by the geometric scale factor at reduced scale when rheology and PJM velocities are the same at both scales. This is conservative because full-scale mixing will always occur at higher jet Reynolds number and thus have a higher degree of turbulence.

The actual mixing results (e.g., cavern heights or breakthrough velocities) obtained from the 4PJM scaling tests are not to be directly applied to full-scale WTP vessels. Rather, the results were obtained to prove that PJM mixing systems for WTP vessels can be adequately assessed at reduced scale. If prototypic systems are tested at reduced scale according to the scaling principles outlined in Section 3.6, PJM geometries and operational scenarios that meet plant mixing requirements can be determined with confidence.

6.2 Gas Retention and Release Scaling Tests

This section demonstrates the scaling laws for gas holdup and release in the three scaled 4PJM systems using kaolin/bentonite clay. Tests were also conducted using Laponite. The 12.75-ft-diameter 336 4PJM system is the largest, followed by the APEL and SRNL systems at 1:4.5 scale and 1:9 scale, respectively. Scaling for gas holdup is covered in Section 6.3.1 and gas release in Section 6.3.2. Section 6.3.2 summarizes the findings.

6.2.1 Gas Holdup Tests

The holdup scaling law derived from the well-mixed bubble migration model and expressed by Eq. (3.15) states that the holdup at steady state is equal to the volumetric gas generation rate multiplied by the gas release time constant, $\tau_R = H/U_R$, where U_R is the bubble rise velocity at the surface and H is the slurry depth. This means that, because the bubble rise velocity is roughly constant, the gas generation rate in a small-scale system should be increased by the scale factor to achieve the same holdup.

Figure 6.9 compares results of the 12-16-03 test in the 336 facility, the 12-15-03 test in APEL, and the 12-13-03 experiment at SRNL. For equal holdup, the APEL and SRNL tests should have 4.5 and 9 times the gas generation rates of the 336 test, respectively. Because the APEL and SRNL tests used only 2.6 times the gas generation rate of the 336 test, their holdup should be less, especially since the SRNL clay simulant also had less than half the yield stress of the stiff clay used in the larger-scale tests. The higher 3.7 vol% holdup in the 336 test bears this out, as the scaling law implies.[(a)] Figure 6.10 compares the results of more closely scaled tests that used a similar simulant rheology. The gas generation rates, at least between 336 and APEL, were in the correct proportion according to the length scale. As a result, the holdups are in the same range though the approach to steady state occurred at different rates.

(a) The APEL test showed an unexpected and unexplained increase in holdup starting shortly before hydrogen peroxide injection was shut off, though the PJMs continued to operate.

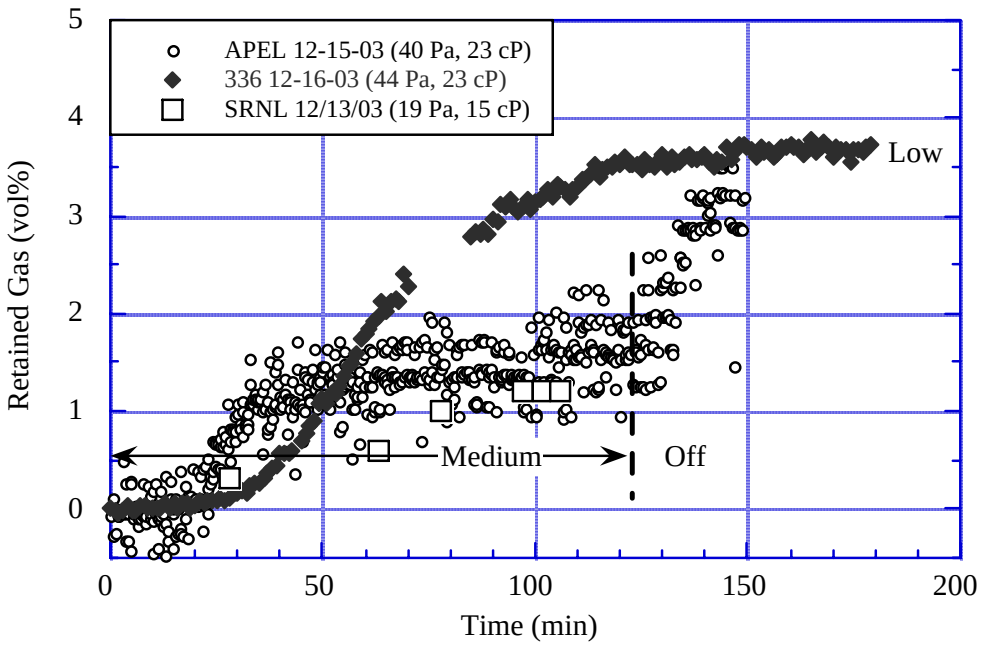

Figure 6.9. APEL (12-15-03), 336 (12-16-03) and SRNL (12-13-03) 4PJM Holdup Test Results

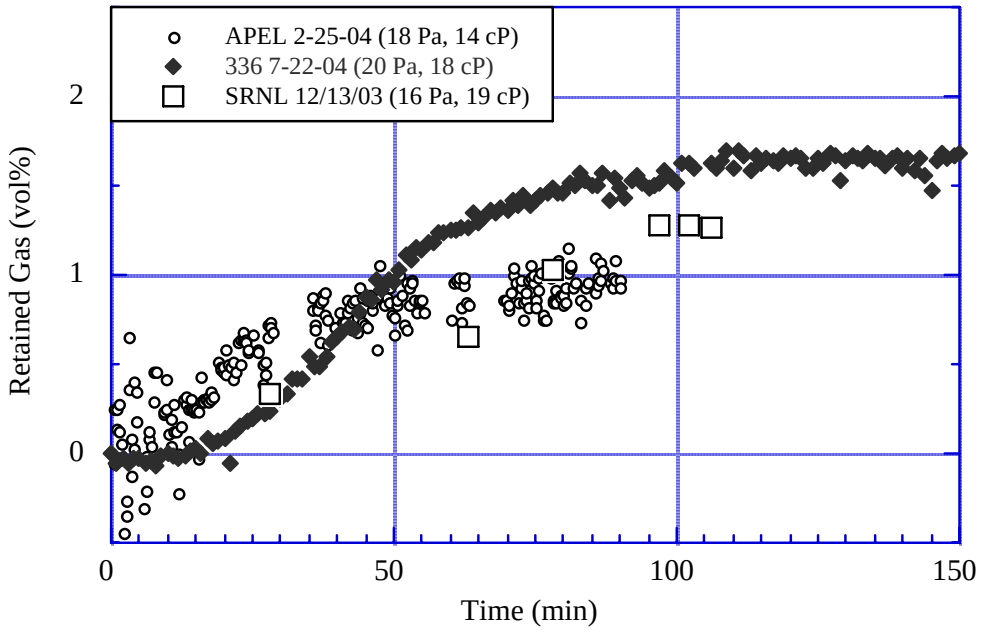

Figure 6.10. APEL (2-25-04), 336 (7-22-04) and SRNL (12-13-03) 4PJM Holdup Test Results

6.2.2 Gas Release Tests

The time dependence of the gas fraction, α, during gas release is also characterized by the time constant, $\tau_R = H/U_R$. Because the bubble rise velocity is roughly constant in all well-mixed systems with similar slurry rheology, gas release rates should be lower in larger systems in inverse proportion to the scale factor. However, for intermittent mixing in PJM systems, the time can be computed as the product of the number of PJM cycles and cycle time. Thus, measured in PJM cycles, the effective time constant is $\tau_N = H/(U_R t_C) = \tau_R/t_C$, which is approximately invariant with scale if the PJM cycle time is reduced by the scale factor, that is, if t_C is proportional to the H/U_R at the various scales. In that case, gas release tests at different scales should plot on the same curve of gas fraction versus PJM cycle number.

Figure 6.11 plots gas fraction versus the number of PJM cycles for gas release tests at each of the three scales. Test conditions were equivalent except that the SRNL test started with a higher gas fraction and the simulant yield stress was considerably lower (16 Pa versus 40–44 Pa). The results of all three tests are similar, but the APEL test showed a slower release rate in the latter stages. Figure 6.12 presents the results of three tests with similar simulant rheology, though the 336 test had a much lower initial gas fraction. This time the 336 and APEL tests compare more closely during the initial release, while the 336 test results show very slow releases in the later stages.

Additional verification of the GR&R scaling laws can be obtained by comparing the predictions of a model based on the same well-mixed bubble migration theory. The model outlined in Section 10 for scale-up predictions of plant scale behavior was used to assess whether latent gas generation might have affected the gas release test results for the hybrid LS and UFP prototype tests (Russell et al. 2005). Figure 6.13 shows the measured and predicted gas volume fractions along with the hydrogen peroxide

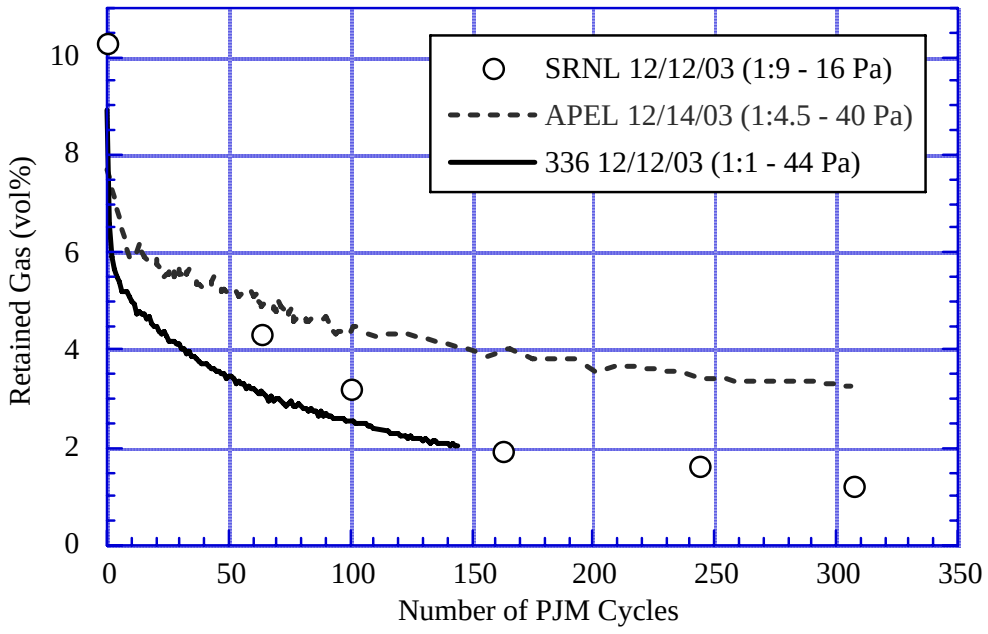

Figure 6.11. Scaled 4PJM Gas Release Test Comparison

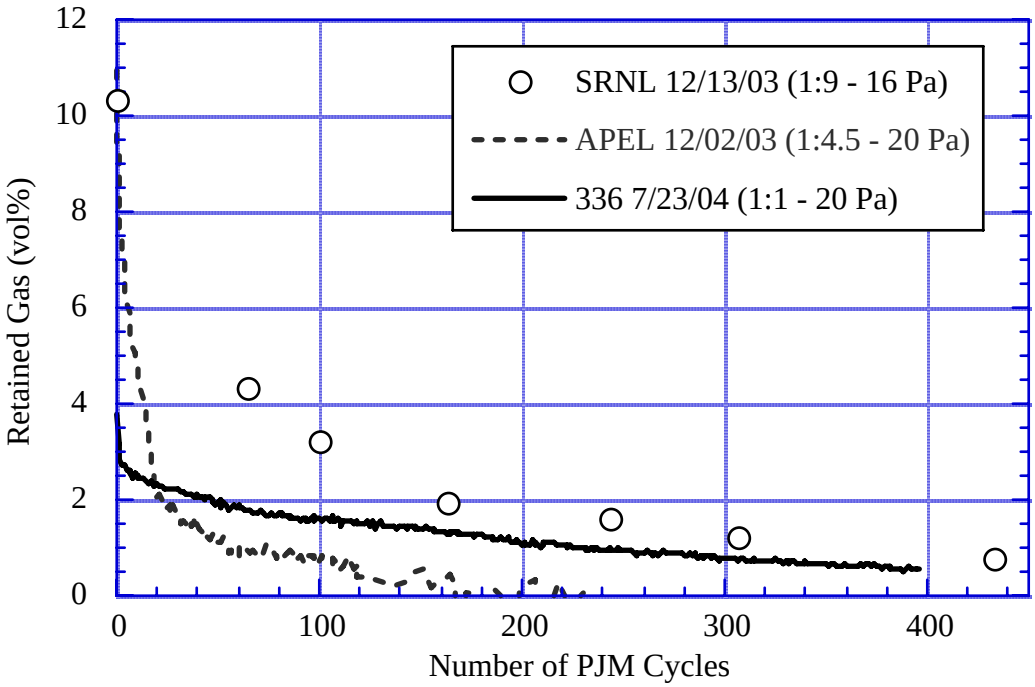

Figure 6.12. Scaled 4PJM Gas Release Tests with Similar Rheology

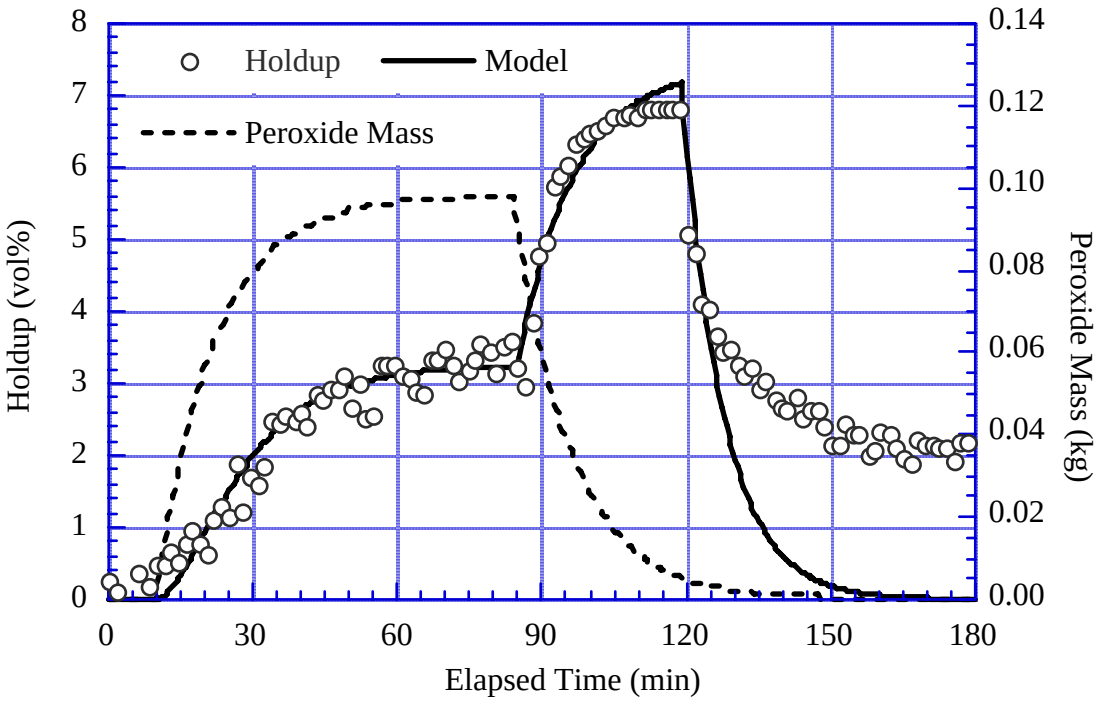

Figure 6.13. Gas Retention and Release Model Results: UFP Sequence 5

mass for combined gas holdup/release test of UFP sequence 5. The gas release rate was set to zero during the gas accumulation period leading up to the release test, when the mixing system was not operating. The rate constants for GR&R were determined from an error minimization on only the holdup test portion but applied to the entire test. The results show that the gas release model with constants fit to the gas holdup test also follows the gas accumulation period and the initial part of the gas release quite well. However, as observed in the 4PJM scaling comparison, the actual gas release at later times is generally much slower than predicted, apparently following a longer time constant.

6.2.3 Summary

While uncertainty fluctuations in the gas volume fraction during holdup tests makes comparison difficult, the holdup scaling law of Eq. (3.15) is qualitatively verified by test results from the three 4PJM systems. The results of scaled release tests are more difficult to interpret and less conclusive because of the tendency for a much lower release rate in the later stages of the process in some tests.

Perhaps most relevant is the observation that the simple conservation equations with a single gas release coefficient predicted gas volume fractions that match the data during both retention and initial gas release periods. This result supports the gas bubble migration model derived in Section 3 as the fundamental description of the gas retention and release process. However, as observed in the 4PJM gas release tests, the relatively abrupt departure of the predicted and measured gas volume fractions after the initial release show that additional effects come into play as the gassy simulant is remobilized after the gas accumulation period.

Evidence suggests that the slow, steady release of gas after the initial rapid release may be the result of a persistent region of less-than-fully mobilized simulant slowly eroding away. Apparently, the first few PJM cycles may release gas rapidly from a fully mobilized cavern in the lower part of the tank, leaving most or all of the retained gas above it. This unreleased gas may create a buoyant cap on top of the now heavier degassed cavern that slows further mobilization. The slow-releasing region is not a permanent, unmobilized heel; it is simply mobilized slower, apparently by a different process.

6.3 Sparge Array Scale-up Data

The scaling methodology for air sparge systems required obtaining basic data on the mixing characteristics of a single, large-scale sparge tube. This involved determining the mixing ZOI as a function of air flow rate in a non-Newtonian simulant. This information was then used to develop guidelines for specifying sparge tube spacing and air flow rates for multiple sparge tube systems. These guidelines applied to both plant-scale designs and reduced-scale tests. In this way, the sparge mixing performance in reduced-scale tests will be similar to that in plant-scale vessels. This scaling approach is conservative because full scale vessels will have a greater sparge submergence and thus more effective mixing from a given sparge mixing zone.

This section summarizes experimental data obtained from single-sparger ZOI tests. The results are then analyzed and the air flow sparge array guidelines recapped. A complete description of the tests and methods are presented in Poloski et al. (2005).

6.3.1 Single Sparge Tube ZOI Tests

Testing was performed in the CBT in the 336 facility. This vessel had enough depth and wall clearance to evaluate sparge mixing behavior. Tests included various measurements to define the shape and size of the surface and subsurface ZOI. An ultrasonic probe was used to determine the subsurface shape of the central ROB. Velocity measurements were made at various locations in the ZOI, and simulant recirculation times in the ROB and ZOI were obtained. All tests were performed using the opaque kaolin/bentonite clay simulant.

The leading edge of the ZOI was measured by placing buoyant flow followers, or "surface tracers" (ping pong balls or tracer dye), on the surface near the sparge tube. The surface tracers moved radially outward because of the induced secondary flow and stopped at the boundary where radial flow ceases and axial flow downward dominates. The ZOI and ROB were measured with a laser reference system coupled with video imaging software.

Tests were performed with airflow rates ranging from about 2 to 60 acfm. The sparge tube submergence ranged from 66 to 118 inches. Surface ZOI data are shown in Figure 6.14. The data indicate that the ROB and ZOI diameters are a weak function of submergence depth, which suggests that these regions have a nearly cylindrical submerged vertical profile. Because the full-scale sparger systems will be submerged deeper than in these experiments, and because the ZOI and ROB diameters will increase slightly with submergence depth, using these data was concluded to be conservative, meaning that one doesn't want to overestimate the ZOI and hence underdesign the sparging system.

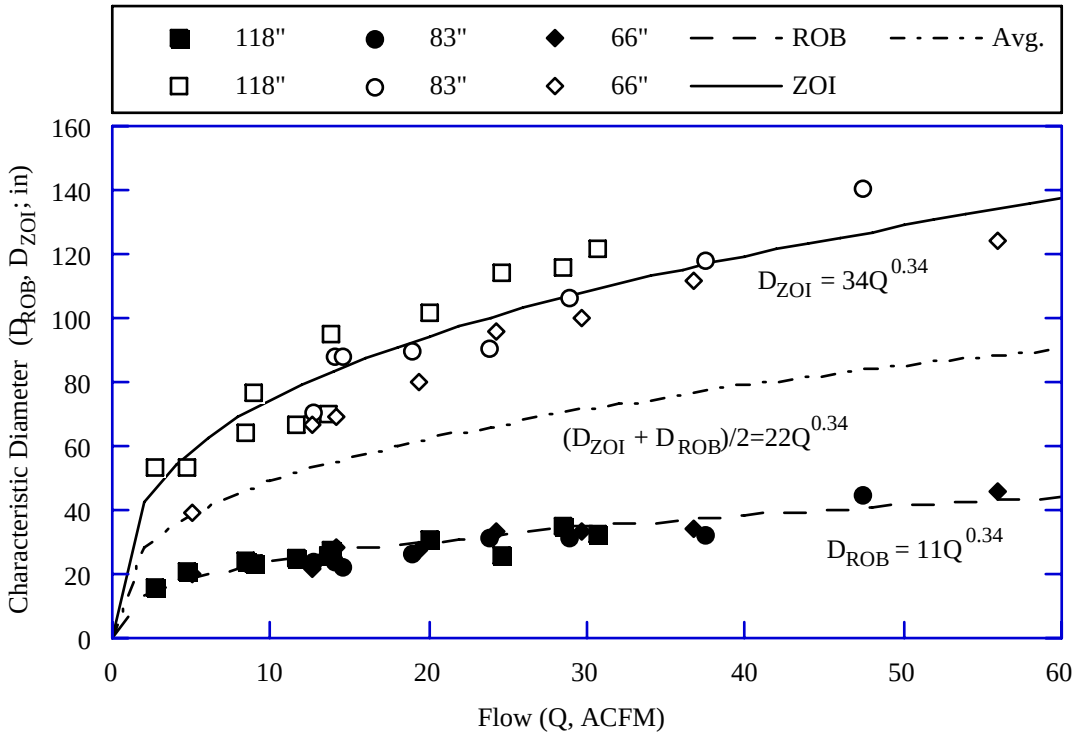

Figure 6.14. ZOI and ROB Diameters at Various Air Flow Rates

The data in Figure 6.14 indicate that both the ROB and the ZOI are increasing functions of flow rate. A power law correlation of the ROB and ZOI diameters to the actual volumetric air flow rate at the sparge nozzle gives

$$D_{ROB} = 11Q_S^{0.34} \tag{6.1}$$

$$D_{ZOI} = 34Q_S^{0.34} \tag{6.2}$$

where D_{ROB} is the ROB diameter (in.), D_{ZOI} is the ZOI diameter (in.), and Q_S is the actual volumetric flow rate of the air at the sparge tube nozzle (ft^3/min).

Figure 6.15 shows the results of the ZOI subsurface boundary measurements using the UVP. Surface ZOI boundary data are based on the surface tracer tests data shown in Figure 6.14. Note that the liquid surface, tank walls, and sparge tube are shown, including the position of the sparger nozzle. The ZOI boundary position with respect to the sloping portion of the tank wall appears to be consistent with the slope of the wall, suggesting there may have been a wall effect. The uncertainty in the vertical and lateral position of the UVP sensor was estimated to be ± 2 inches and about ± 4 inches, respectively.

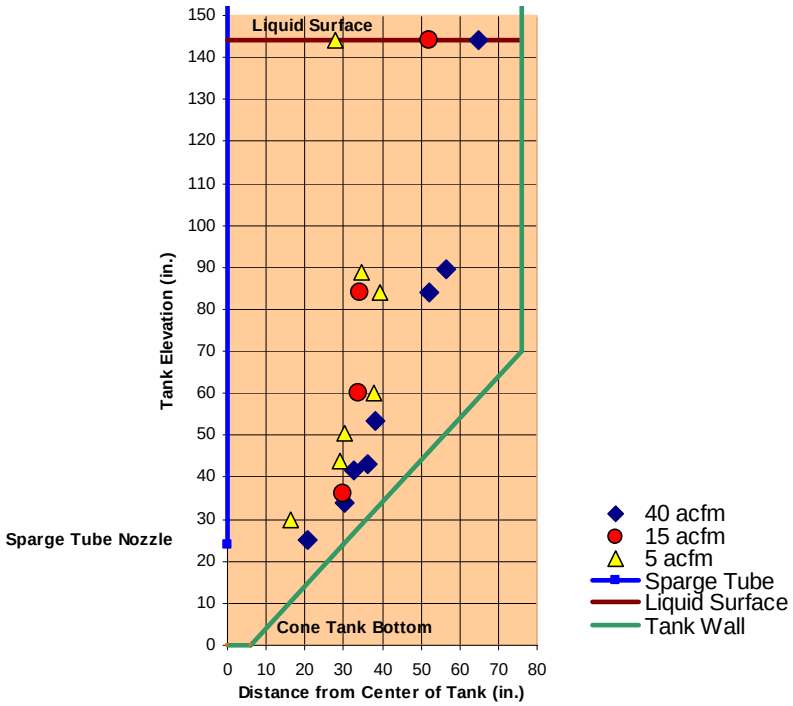

Figure 6.15. Subsurface ZOI Boundary Measurement Data for all Test Runs

Figure 6.16 shows a second-order polynomial fit of the data for 40 acfm. Confidence boundaries of 95% are shown. Additional data obtained for the depth of ZOI below the sparger nozzle suggest that the polynomial fit shown is adequate for vertical positions greater than 10 inches off the tank bottom. A more complex correlation that describes the complete ZOI boundary, including the region of sparge heel, was also developed and is reported in Poloski et al. (2005).

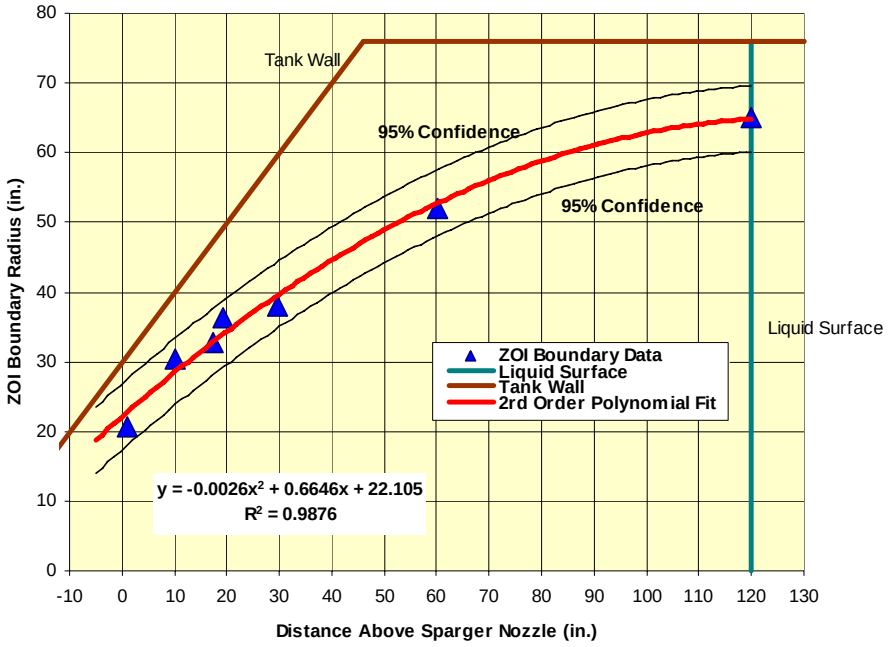

Figure 6.16. Subsurface ZOI Boundary Measured Data for 40 acfm, Including Polynomial Curve Fit

6.3.2 Sparge Array Guidelines

The single sparge tube performance data shown in Figures 6.14 and 6.15 provided the basis for specifying multiple sparge tube arrays for PJM-hybrid mixing systems. Adequate mixing is ensured if sparge tubes are arranged so there is sufficient overlap of the mixing regions. One conservative approach is to configure the sparge tubes so that the ZOI from one sparge tube meets the ROB from an adjacent sparge tube, as shown in Figure 6.17. Mathematically, this implies the sparge tube spacing D_S is given by

$$D_S = (D_{ROB} + D_{ZOI})/2 \tag{6.3}$$

With this spacing, it follows from Eq. (6.1) and (6.2) that

$$D_S \approx \frac{2}{3} D_{ZOI} \tag{6.4}$$

Combining Eq. (6.4) with (6.1) gives the required sparge tube spacing in terms of the airflow rate:

$$D_S \approx 22 Q_S^{0.34} \tag{6.5}$$

Equation (6.5), (3.19), and (3.20) form the basis for specifying the number of sparge tubes, N_S, and total airflow requirement, $N_S Q_S$, for a given vessel. As a general rule, there is a trade-off between the number of sparge tubes and total air requirement. For constant superficial velocity, as the number of sparge tubes is reduced the air flow rate per sparge tube is increased such that the total airflow requirement is increased. Conversely, the total air flow can be reduced by increasing the number of spargers.

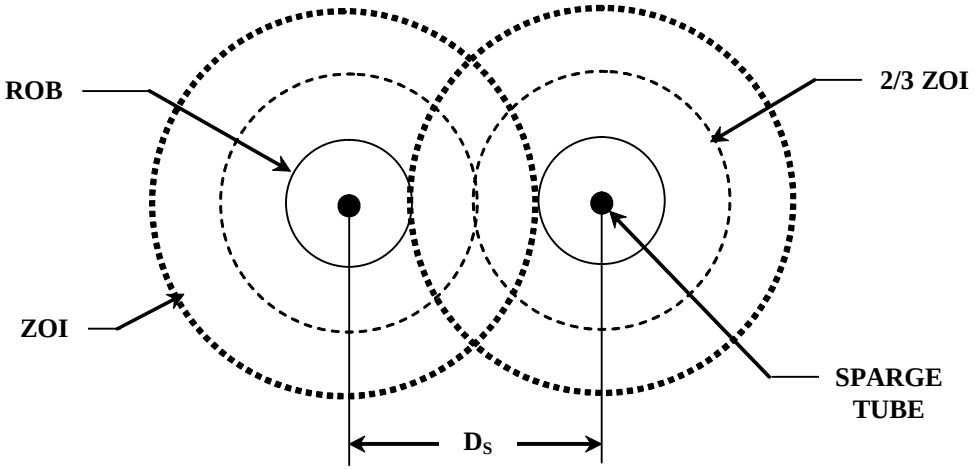

Figure 6.17. Adjacent ZOI and ROB Interaction Option

This relationship between the number of sparge tubes and total air requirement provided WTP project engineers a means to specify sparge tube spacing so that the air requirements were within acceptable limits while adequate mixing was ensured.

7.0 PJM Mixing Performance Evaluations (Phase I)

This section contains a summary of the PJM mixing performance evaluations conducted in Phase I with the scaled prototypes. The first tests were conducted to assess the baseline design, as discussed in Section 7.1. When these tests indicated that the baseline did not adequately mix the tanks, an extensive set of optimization tests was conducted to evaluate different PJM configurations and design variables. The significant findings from this evaluation are presented in Section 7.2. Based on the results from the optimization tests and considering WTP requirements, a final PJM-only configuration was selected for verification testing (referred to as "all-in" tests), as discussed in Section 7.3. Most of the initial experiments were conducted using Laponite, while the all-in tests were conducted with kaolin-bentonite clay.

7.1 Evaluation of Baseline PJM Design

The initial mixing tests evaluated the baseline designs for LS, UFP, and the CRV. These tests were conducted with Laponite. The extent of mobilization was evaluated by visual observation, as defined in Figure 7.1. In reporting the mobilization state, "a+" or "a–" was often used to denote the relative degree of mixing within a given state, with + indicating more mixing and – indicating less. Achieving a type IV mixing state was required for a successful configuration. In conducting the tests, the Laponite was added, fully sheared and then allowed to sit undisturbed for at least 18 hours to develop adequate shear strength,

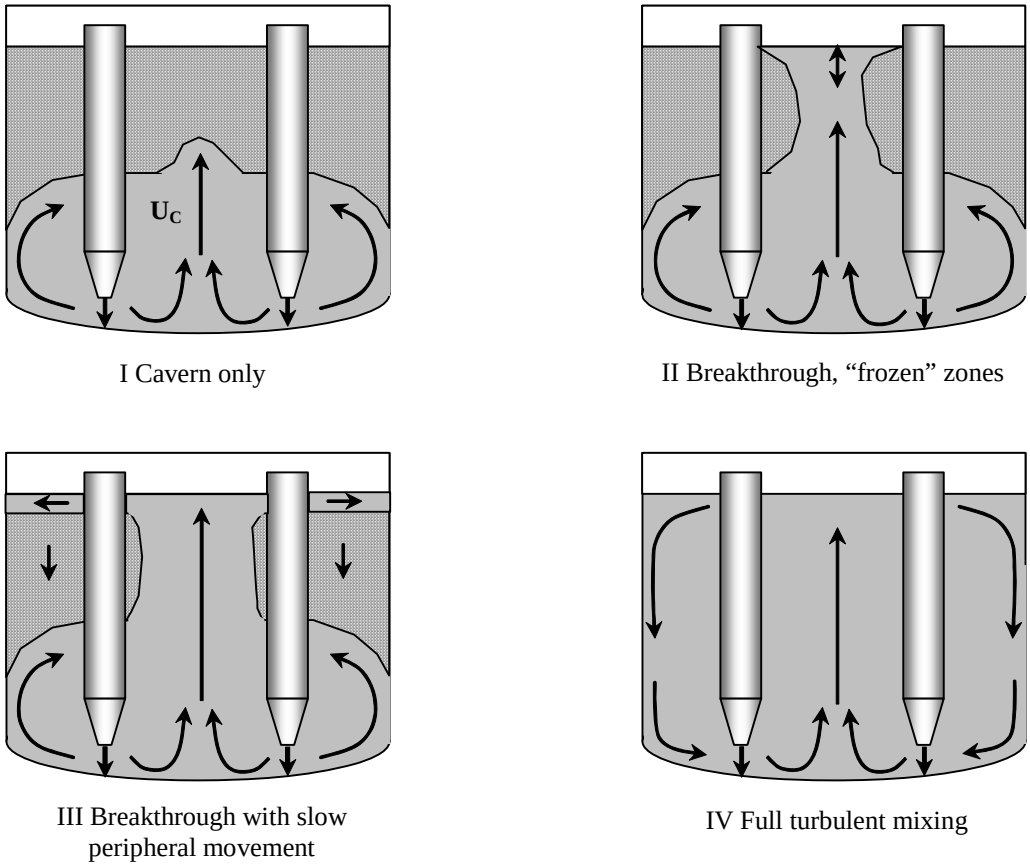

Figure 7.1. Definition of PJM Mobilization States

according to test matrix parameters. The tests were generally conducted at the target H/D, which was 1.06 for the LS vessel, 1.84 for the UFP, and about 1 for the CRV. The mixing test continued until a steady-state mixing zone was observed, which typically required 1 to 2 hours.

Figures 7.2 and 7.3 are schematics of the baseline design for the LS vessel. The design features eight pulse tubes in a roughly square array in the tank. Each pulse tube had nozzles oriented straight down at the dished bottom. During the drive phase, the flow was primarily radially inward, then upward to form a

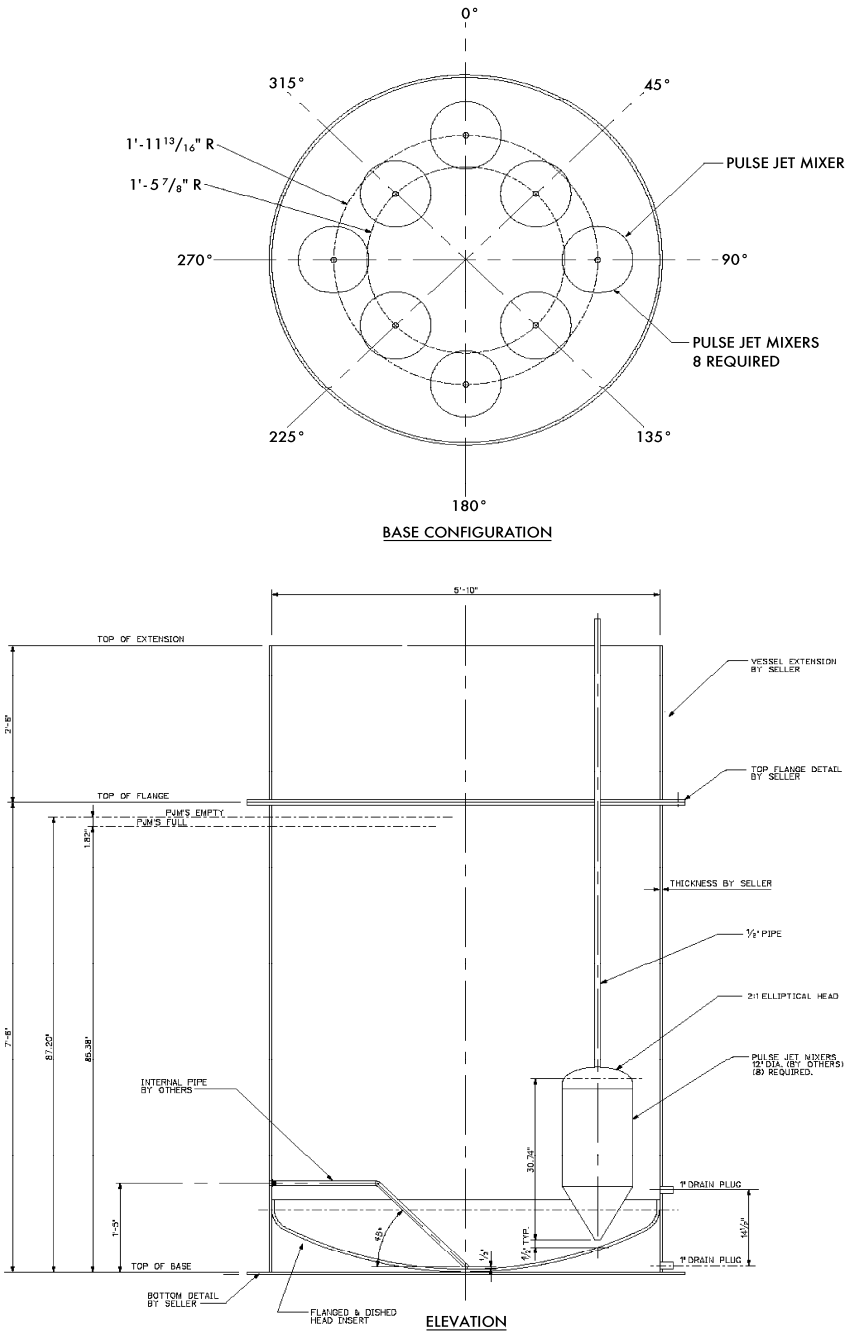

Figure 7.2. Schematic of LS Vessel with Baseline PJMs

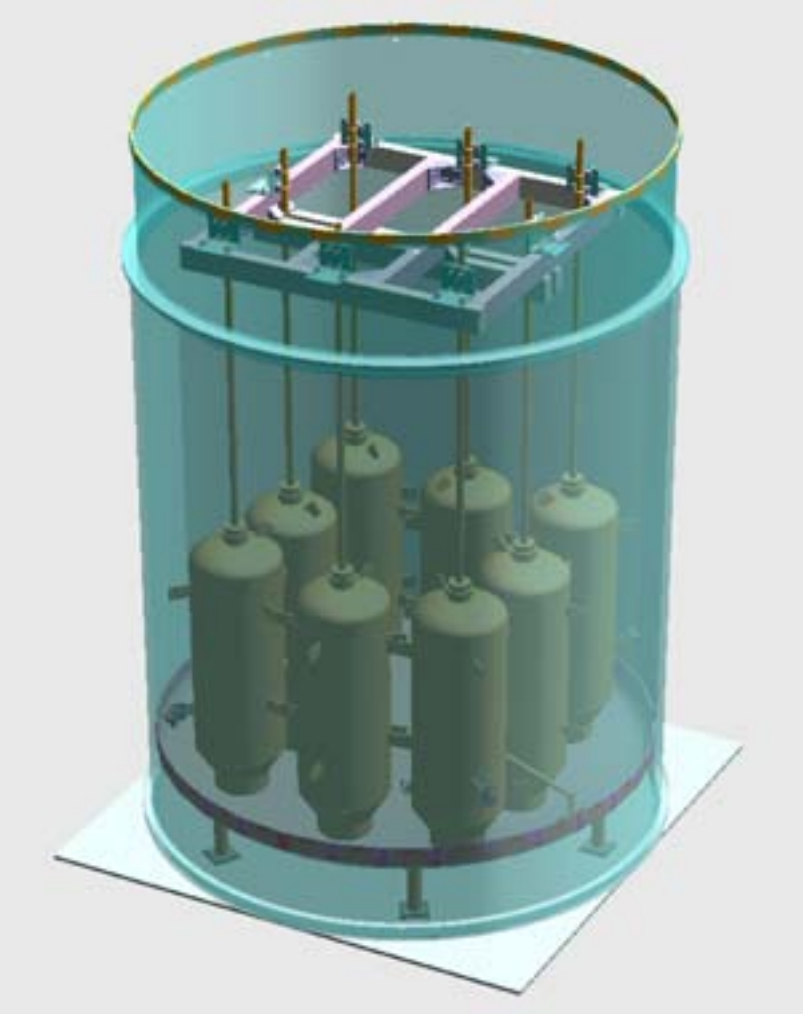

Figure 7.3. LS Vessel Depiction Showing Baseline PJMs

central upwell. The system was designed to operate at a peak average nozzle velocity of 8 m/s. Tests with this configuration used Laponite with a shear strength that ranged from 67 to 80 Pa and a simulant H/D of 1.06 at a nominal peak average nozzle velocity of 8 m/s. The extent of mobilization ranged from Type I to Type III, which meant that the tank was not fully mixed. Increasing the nozzle velocity to 12 m/s resulted in Type II mixing. Increasing the nozzle diameter from 0.93 to 2.065 inches resulted in Type III mixing at a nozzle velocity of 8 m/s and Type III+++ mixing at a nozzle velocity of 10.8 m/s.

Figure 7.4 is a schematic of the UFP vessel with the baseline PJMs (outer ring) and the optional upper PJMs. The baseline design used six pulse tubes in a ring configuration. Each pulse tube had nozzles at the bottom pointing straight down at the dished bottom. During the drive phase the flow was directed down and then turned by the tank bottom to form a central upwell. The system was designed to operate at a peak average nozzle velocity of 8 m/s. The orange PJMs represent an alternative configuration that was tested during the optimization phase. Several tests were conducted with this configuration, using Laponite with shear strength that ranged from 76 to 119 Pa and simulant H/D of ~1.84. Mobilization states of Type I and II were obtained with nozzle velocities ranging from 8-17 m/s. The poor mixing was due in part to the high H/D.

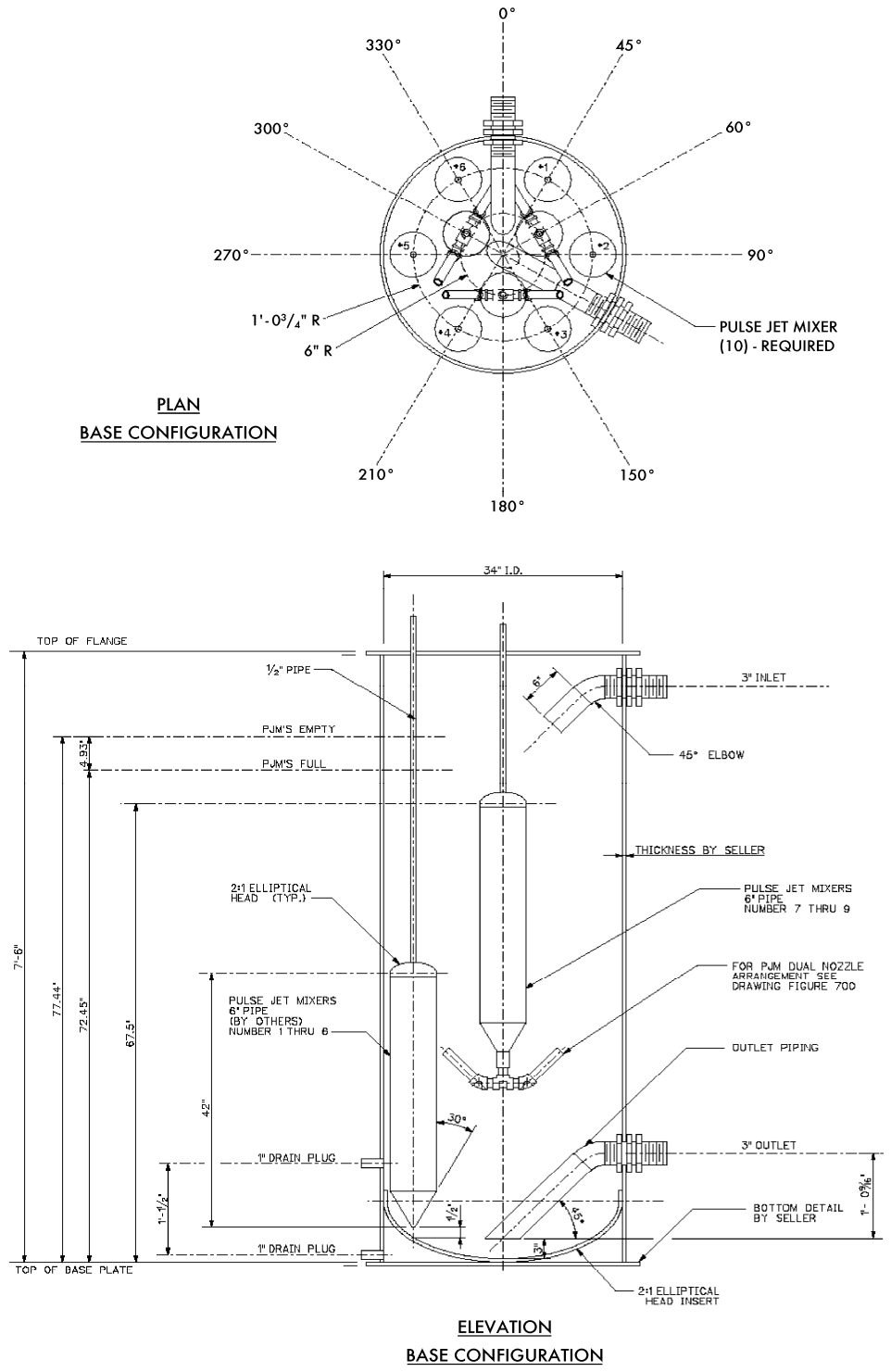

Figure 7.4. UFP Vessel Showing Baseline (outer ring) and Optional Upper PJMs

The baseline CRV design is shown in Figure 7.5, featuring six PJMs in an outer ring, four large charge vessels (for operating the RFD transfer pump system), and two small charge vessels (for operating the RFD sampling system). During the drive phase the flow was directed downward from the six PJMs, then turned by the tank bottom to form a central upwell. Also shown in Figure 7.5 are two additional

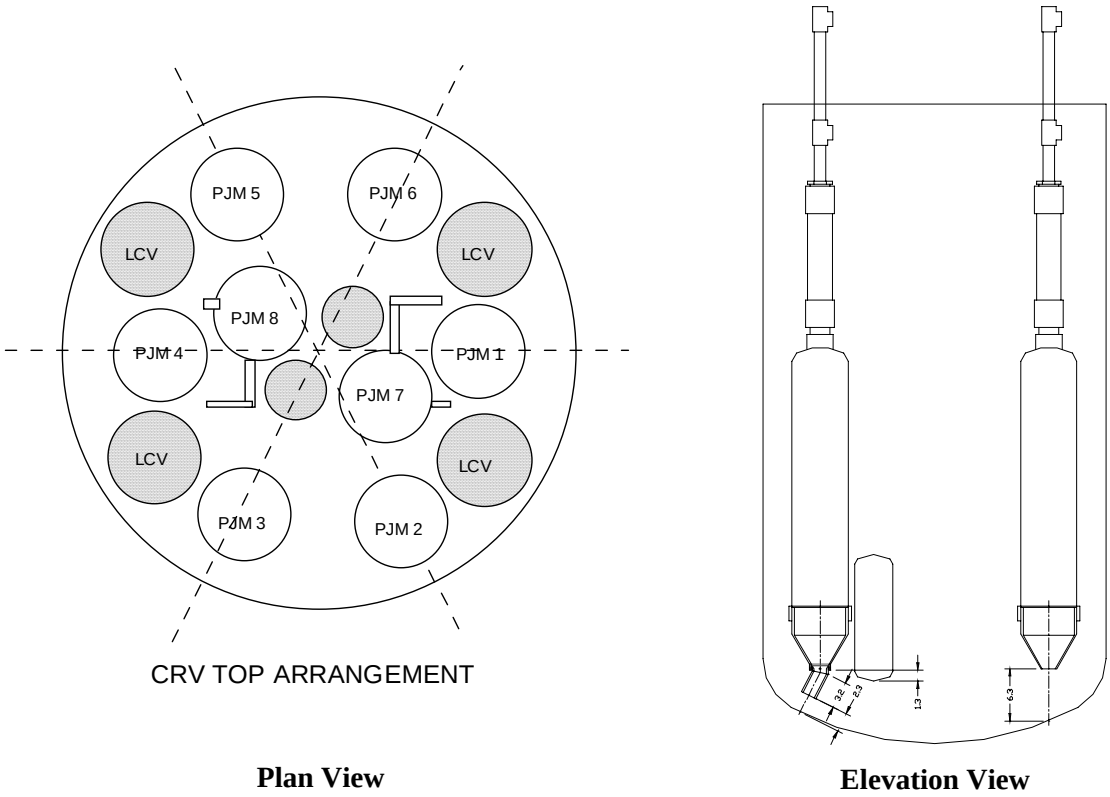

Figure 7.5. Baseline CRV PJMs Plan and Elevation Views (dimensions in elevation view are in inches)

rams-head PJMs that were used during optimization testing. Six tests were conducted with Laponite with shear strength ranging from 36 to 86 Pa. The nozzle velocity ranged from 4.9 to 11.8 m/s. The best mobilization was Type III, observed at a nozzle velocity of 11.8 m/s and Laponite shear strength of 36 Pa.

7.2 Evaluation of PJM Design Variables

The initial tests with the baseline PJM configurations showed that these designs did not provide adequate mixing (Type IV) of the Laponite simulant. Subsequently, over 100 additional tests were conducted in the LS, UFP and CRV scaled prototypes to evaluate alternative PJM configurations and design variables. The results of these tests can be found in Bates et al. (2004) and Guerrero and Eberl (2004a). A list of the design variables evaluated along with a summary of the findings is provided below.

- **Larger pulse tubes:** Increasing the pulse tube diameter, thereby increasing the volume per tube by as much as 80%, was found to improve mixing but also increased air supply requirements.
- **Increased nozzle velocity:** Increasing the nozzle velocity up to 17 m/s improved mixing over the baseline 8 m/s, though the drive time decreased. While greater nozzle velocity may have been more effective, 12 m/s was the maximum velocity achievable with WTP air supply pressure and JPP designs.

- **Larger-diameter pulse tube nozzles:** Increasing the pulse tube nozzle diameter by a factor of 1.5 to 2.2 (cross-sectional area increased by a factor of 2.25 to 4.9) improved mixing but also increased the air supply requirements.
- **More pulse tubes in different configurations:** The number of pulse tubes was increased from eight to 12 in the LS vessel, from six to nine in the UFP vessel, and from six to eight in the CRV. The additional pulse tubes were placed at a higher level in a central cluster in an effort to mix the upper region of the tank. The lower level pulse tubes formed a large-diameter ring. This arrangement was found to increase mixing in some regions, but the additional pulse tubes tended to block the flow of the central upwell from the lower pulse tubes. The larger number pulse tubes increased the air supply requirements.
- **Nozzle geometry:** Downward-firing PJMs in dish-bottom tanks are not an optimal configuration. The presence of a strong central upwell in these configurations results in poor mixing in the outer annulus and excess mixing in the center. Angling the nozzles outward (up to 135^{o} relative to straight down) so they had normal or nearly normal impingement with the vessel bottom improved mixing by spreading the jet momentum more uniformly between the central and annular areas.
- **Multiple nozzles:** Up to four nozzles per pulse tube were tested. This promoted regional mixing, with slightly upward-pointing nozzles being most effective. However, these nozzles were thought to be prone to abrasive wear by the waste slurries and were somewhat more difficult to fabricate.
- **Asychronous operations:** Various firing patterns were investigated, including the alternate firing of PJMs in their respective half of the vessel and sequential firing of the lower and then the upper PJMs in configurations with pulse tubes on two levels. None of the asynchronous firing patterns were found to be effective.
- **Recirculation pump:** A recirculation pump, which is part of the UFP system for providing feed to the cross-flow filters, was tested to supplement the PJM mixing and found to be effective.
- **Cluster configuration:** This configuration, consisting of several PJMs arranged in a central cluster, approximated a single, large, centrally located PJM. This configuration generally produced a uniform cavern in the vessels that achieved Type I mixing in the LS scaled prototype and Type IV mixing in the CRV. This configuration was unsuitable for use in the UFP because of the relatively large H/D (1.8). Nevertheless, for reasons discussed in Section 8, the cluster configuration was found to be ideal when combined with sparging and/or recirculation pumps.

7.3 Final PJM Configurations and Results

Based on the results of the optimization studies, the WTP Program selected final configurations for verification testing using Laponite and/or kaolin-bentonite clay. These configurations, referred to as "all-in," are described in this section, along with a brief summary of the results.

The LS all-in configuration selected in Phase I is pictured in Figure 7.6. This design featured 12 PJMs; eight lower PJMs in a ring, and four central PJMs in the upper portion of the tank. The eight lower PJMs had alternating large-diameter (2.065 inches) nozzles, with one set pointing straight down and the

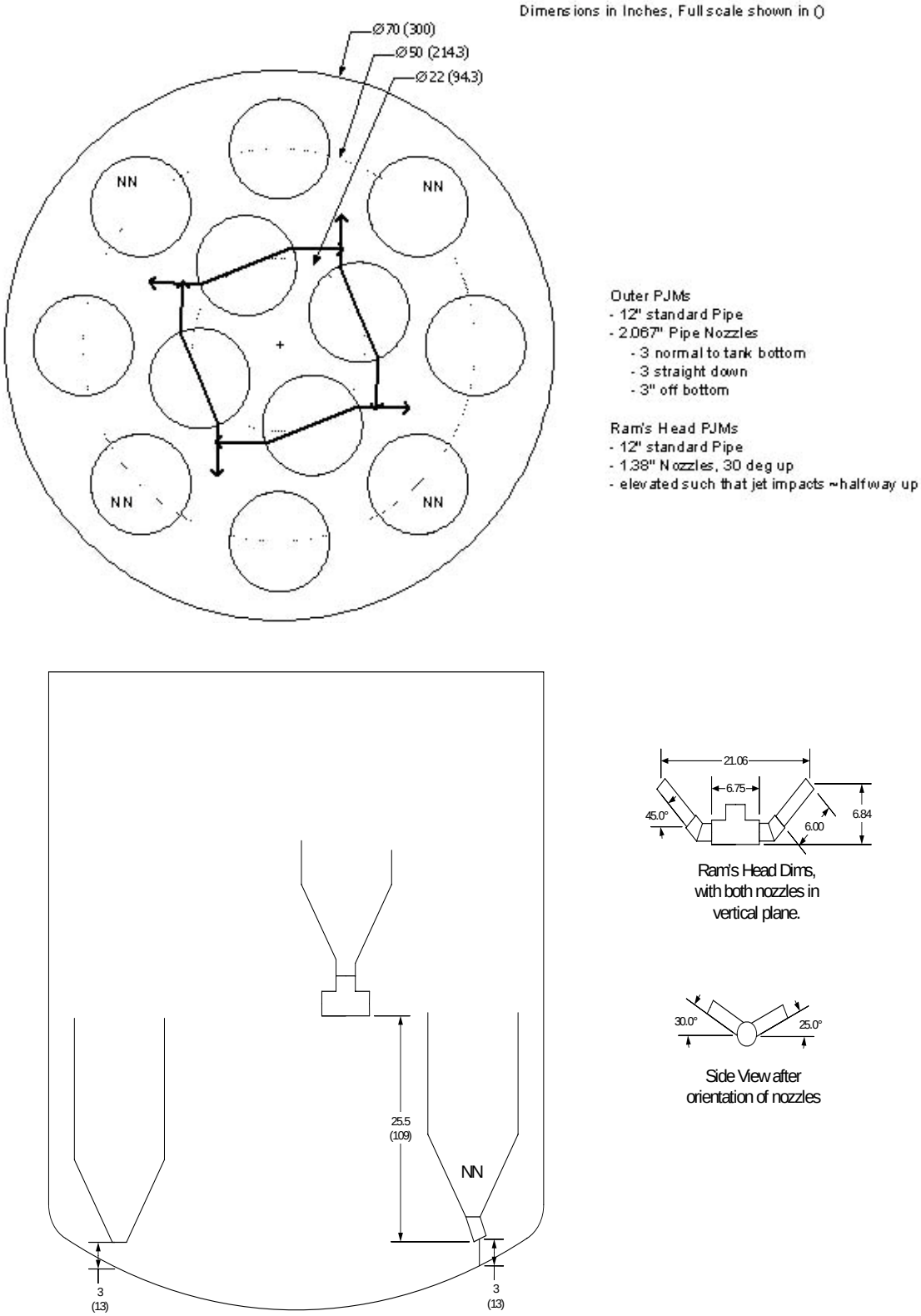

Figure 7.6. LS All-in Configuration

other set angled outward pointing toward the vessel floor. A photograph of the nozzles on the four upper PJMs is shown in Figure 7.7. These dual nozzles were directed outward and up toward the gaps in the lower PJMs. An initial test using Laponite with this configuration resulted in a Type IV- mixing mode. A subsequent test with kaolin-bentonite clay using the dye method indicated nearly complete mixing with ~96% mixed.

The UFP all-in configuration is shown in Figure 7.8. This design consisted of four lower pulse tubes in a ring plus two upper pulse tubes in the center, each the same size as the baseline PJMs. The nozzle diameter of the four lower pulse tubes was increased from 0.81 to 1.21 inches, increasing the cross-sectional area of the nozzles by a factor of 2.2. The diameter of the dual nozzles on the upper pulse tubes was 0.82 inch, which provided the same total flow area as the single nozzle on the lower pulse tubes. The dual nozzles were oriented outward and slightly up to ensure mixing behind the upper portion of the lower pulse tubes and to mix the upper portion of the vessel (Figure 7.9). The lower nozzles were oriented vertically down.

The tests were conducted with Laponite with shear strength that ranged from 65 to 80 Pa and nozzle velocities ranging from 8 to 12 m/s. Type III mixing was achieved at a nozzle velocity of 8 m/s and Type IV at 12 m/s. Tests were also conducted with kaolin-bentonite clay with a yield stress of 24 Pa and a consistency of 27 cP at nozzle velocities of 8 and 12 m/s. Visual observation and the results of a dye test indicated that the UFP vessel was well mixed at the end of the two-hour test. A second test was conducted using beads and core sampling as well as PIT tags. The results were statistically analyzed and showed acceptable homogeneity.

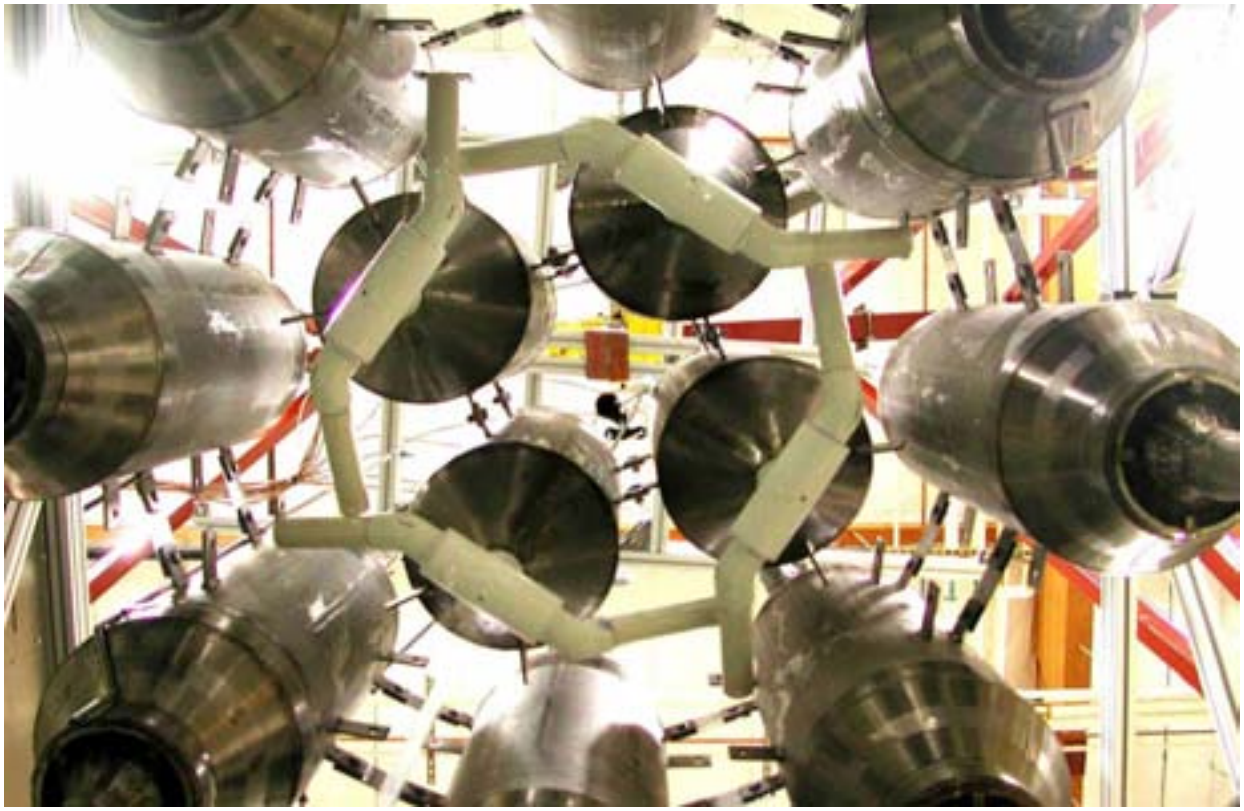

Figure 7.7. LS All-in Nozzle Configuration (from below)

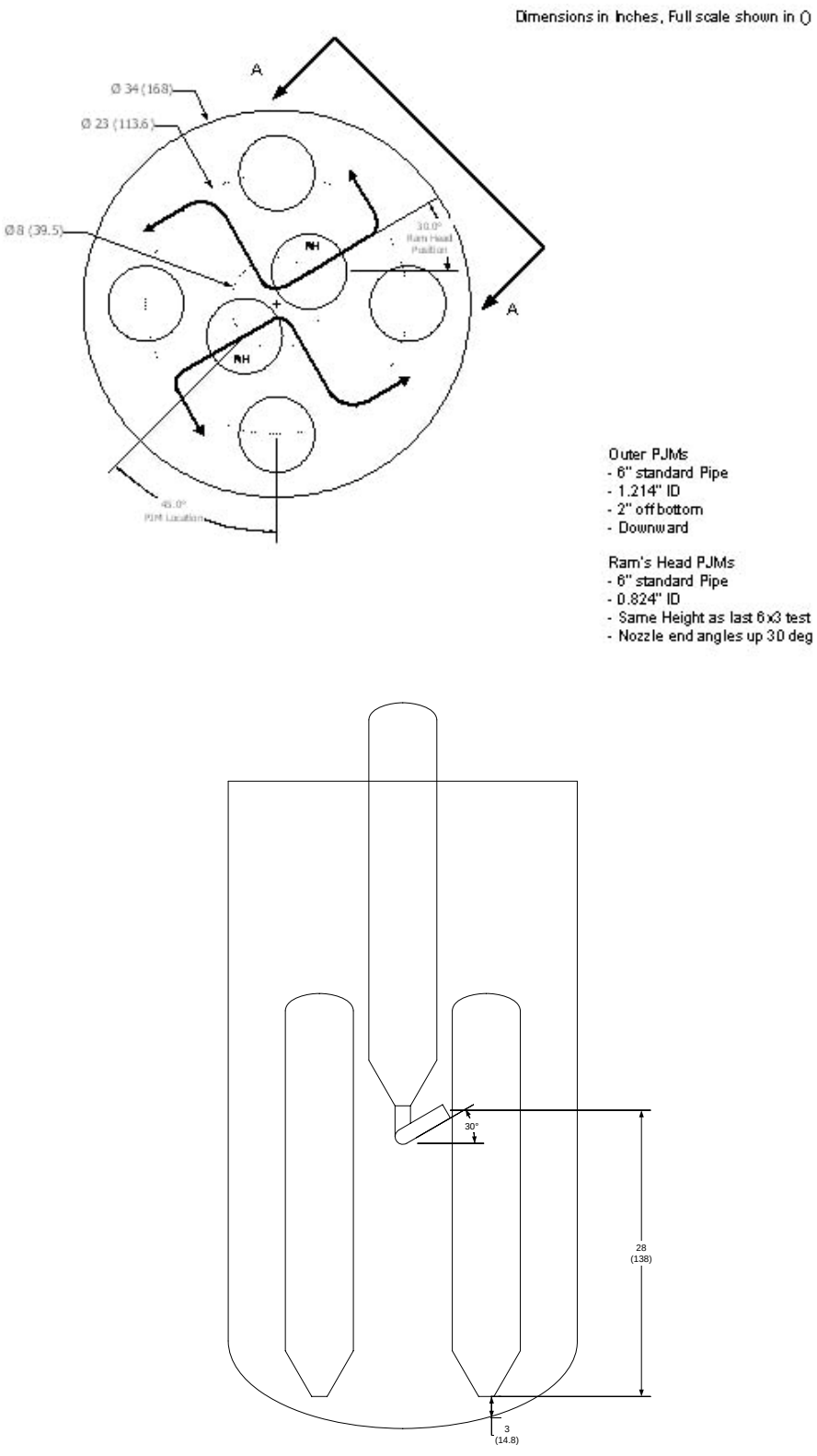

Figure 7.8. UFP All-in PJM Configuration

Figure 7.9. UFP Rams-Head Discharge Nozzles for the All-in Configuration

The CRV All-in configuration is shown in Figure 7.10. It consisted of six pulse tubes in a central cluster (five around one). The pulse tube diameter was increased from 6 to 8 inches, increasing the total volume about 80%. The nozzle diameter was increased from 1 inch to 1.5 inches, increasing the nozzle cross-sectional area by a factor of 2.25. The nozzle on the center tube pointed straight down, while the nozzles on the outer pulse tubes were angled outward at 45^{o}. The tests were conducted with Laponite with shear strength of 70 Pa and nozzle velocities ranging from 8 to 12 m/s. Essentially complete mixing was achieved, with 95% Type IV mixing and 5% Type III mixing.

7.4 Summary of Phase I Testing and Rationale for Phase II

The final all-in tests demonstrated that PJM-only designs could provide acceptable mixing in the LS, UFP, and CRV vessels. However, a WTP engineering evaluation of the impacts of the necessary design changes projected unacceptable cost increases and schedule delays. The main factors contributing to this were the need for additional piping and instrumentation, a large increase in the infrastructure necessary to supply additional air to the larger and more numerous PJMs, and the resulting increase in load on the off-gas system.

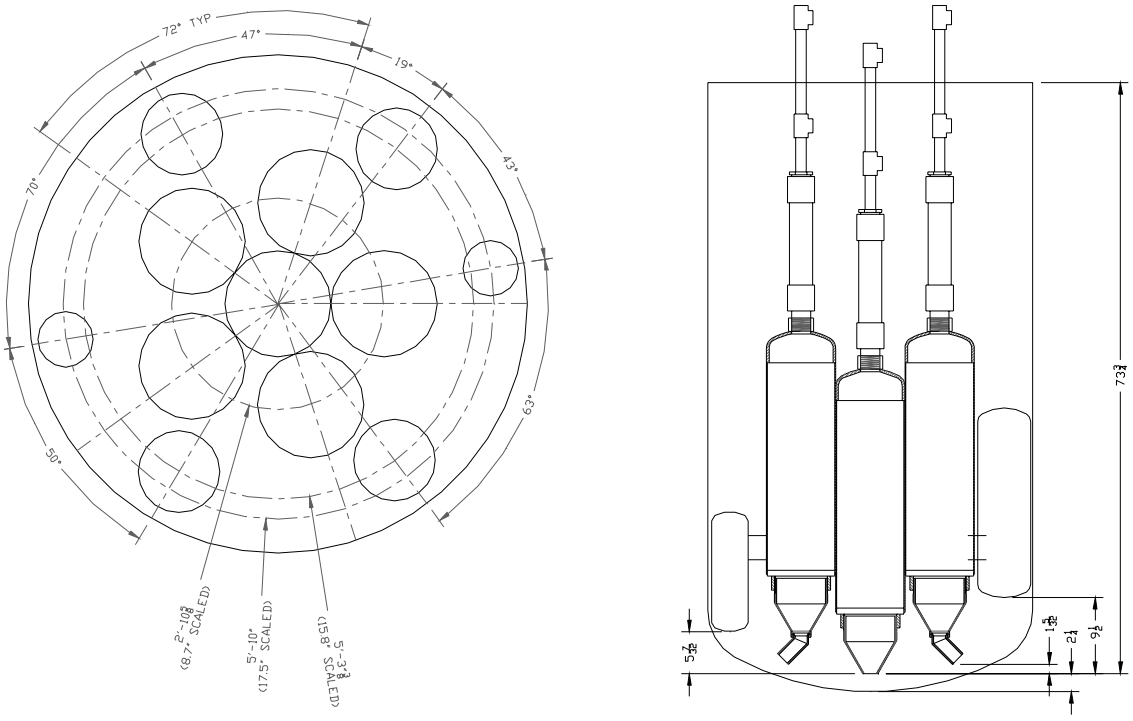

Plan View **Elevation View**

Figure 7.10. CRV Cluster Configuration All-in Test (dimensions in elevation view are in inches)

Several alternatives and supplements to PJMs were evaluated by the WTP project, and the decision was made to investigate the use of air sparging and/or recirculation pumps in conjunction with PJMs for mixing the non-Newtonian vessels. While the PJM configurations, geometry, and nozzle velocity remained viable design variables, it was necessary to stay within the capability of the plant infrastructure to supply air and handle the off-gas stream. This eliminated the design variables of more or larger pulse tubes and larger nozzles. The PJM/hybrid system performance evaluation (Phase II) is discussed in Section 8.

8.0 PJM/Hybrid System Performance Evaluations (Phase II)

This section summarizes the PJM/hybrid system performance evaluations (Phase II) for the UFP, LS, and CRV scaled test stands. Section 8.1 discusses the selection of the PJM/hybrid mixing system approach, and Section 8.2 presents the evaluation of the selected PJM/hybrid mixing systems. The results of this evaluation provided the final PJM/hybrid mixing system configurations, which are presented in Section 8.3 along with a summary of the final testing results. Section 8.4 contains a summary of the Phase II scaled prototype evaluation and discusses the release of retained gas in a large-scale multiple sparge tube array.

8.1 Hybrid Mixing System Selection

While it became apparent that a PJM only mixing system for the vessels with non-Newtonian slurries would have an unacceptable impact on the WTP cost and schedule, a wide ranging evaluation of alternatives was completed by the WTP. As a result of this evaluation, the decision was made to evaluate PJM/hybrid mixing systems. In this evaluation the PJM design was limited to the original baseline design in terms of pulse tube and nozzle size. A hybrid jet pump pair (JPP) was designed to provide the additional airflow capacity to enable operation of the PJMs at a peak average nozzle velocity of 12 m/s. The supplemental mixing methods included air sparging in the LS, UFP, and CRV and steady jets generated by recirculation pumps in the LS and UFP vessels. Other options evaluated included reducing the operating level in the LS, sparging using the PJMs, and using controlled PJM overblow.

A number of detailed requirements were developed by the project for the PJM/hybrid systems to guide their development, testing and evaluation. These included the following:

- Slurry rheology: Bingham plastic with a yield stress ranging from 5-30 Pa.
- Complete mixing of the tank contents (no stagnant regions) with turbulent conditions in the majority of the volume. Adequate suspension of the waste particulates.
- Limited retained gas inventory during normal operations.
- Controlled release of retained gas after a DBE or non-mixing period.
- Enhanced vessel heat transfer characteristics (greater convection at vessel walls).
- Minimum cost and schedule impact to the WTP.
- Minimum air requirements for both the air supply and the vessel ventilation systems.
- Minimum aerosol carry-over into the ventilation system.
- Minimum vessel penetrations.
- Simplified fabrication.
- Mature technology approaches preferred over emerging technologies.
- Minimum overall risk to the project.

The general approach for the PJM/hybrid concept was to use the PJMs to mix the lower portion of the vessel contents and the supplemental methods (air sparging and recirculation) to mix the upper portion. The PJMs were generally arranged in a central cluster configuration, with perimeter tubes equally spaced around a central pulse tube. The nozzle on the center pulse tube pointed straight down to ensure mixing in the bottom center of the vessel. The nozzles on the perimeter pulse tubes were oriented radially out from the center of the tank at angles (from vertical down) ranging from about 15^o to 135^o (i.e., pointing up). For tests with sparging, the sparging system layout and air flow rates were determined using the ZOI sparging performance guidelines developed in Poloski et al. (2005) and discussed in Sections 5.4 and 6.3. Recirculation pumps were added to the LS and UFP test stands to provide supplemental mixing with steady jets. Typically, these jet nozzles were oriented at the upper region of the vessels.

8.2 Evaluation of PJM/Hybrid Mixing System Alternatives

Mixing tests using dye and chloride tracer as well as GR&R tests with hydrogen peroxide were conducted in the scaled prototypes, which were outfitted with hybrid systems containing PJMs, recirculation pumps, and spargers. The simulant was kaolin-bentonite clay, generally with rheology at the upper bound (yield stress ~30Pa). More than 125 mixing tests were conducted in the LS, UFP, and CRV scaled prototypes. The PJM overblow alternative was evaluated in the large 4PJM test stand in the 336 facility.

8.2.1 Examples of Hybrid Mixing System Test Results

Figure 8.1 plots the volume percent mixed versus a yield Reynolds number correlation parameter[(a)] for some of the tests conducted with the UFP scaled test stand. Similar results for the LS scaled test stand are shown in Figure 8.2 (Johnson et al. 2005). The data show that, with PJMs only, an increase in the yield Reynolds number generally increases the percent mixed. This reflects the increase in PJM cavern size with increasing PJM nozzle velocity or decreasing yield stress suggested by Eq. (3.9). It is also obvious that PJMs alone are not sufficient to completely mix the tank given the constraints on nozzle velocity. The addition of sparging and/or recirculation generally results in complete mixing. When spargers are operating, modest changes in PJM velocity or rheology (yield Reynolds number) have a negligible effect on mixing. Similar observations can be made for the LS scaled test stand.

Four GR&R test sequences were conducted in the LS and UFP vessels. Tests were conducted with PJMs and spargers or PJMs and recirculation pumps for supplemental mixing. The results from one test sequence are shown in Figure 8.3 compared with a gas and hydrogen peroxide inventory model (see Section 10). This test was conducted in the LS vessel with recirculation pumps. The initial part of the curve shows the holdup portion of the test where peroxide is added steadily to the tank with mixing. Two rates of hydrogen peroxide injection were used, and gas holdup approached steady state for each one (Figure 8.3). Peroxide addition and mixing were then halted, allowing the gas inventory to increase. When mixing was turned on, the retained gas was removed rapidly. Similar results were obtained in the LS with PJMs and spargers and in the UFP with PJMs + recirculation pumps and PJMs + spargers (Russell et al. 2005). Results of GR&R tests in the CRV can be found in Guerrero and Eberl (2004b). These tests demonstrated that flammable gas inventories could be managed using PJM/hybrid mixing configurations.

(a) This correlation parameter follows the form of Eq. (3.9) but was modified to include the number of PJMs, N.

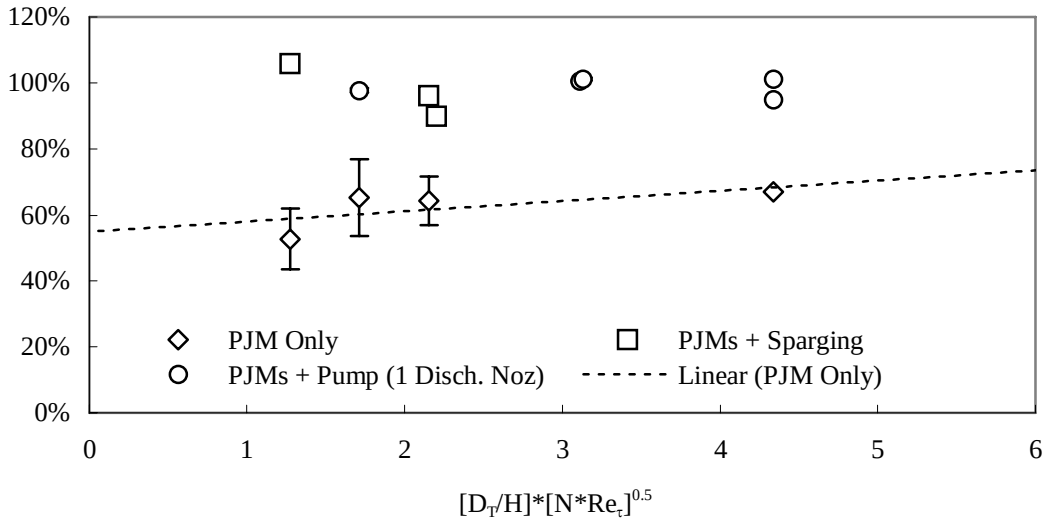

Figure 8.1. Percent Mixed Versus Yield Reynolds Number for UFP Scaled Test Stand During Operating Conditions

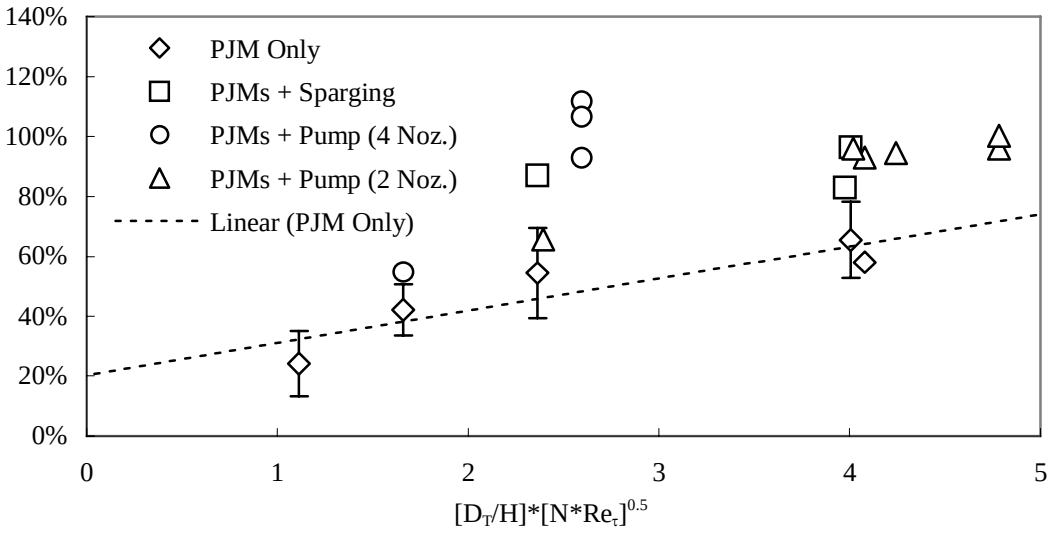

Figure 8.2. Percent Mixed Versus Yield Reynolds Number for LS Scaled Test Stand During Operating Conditions

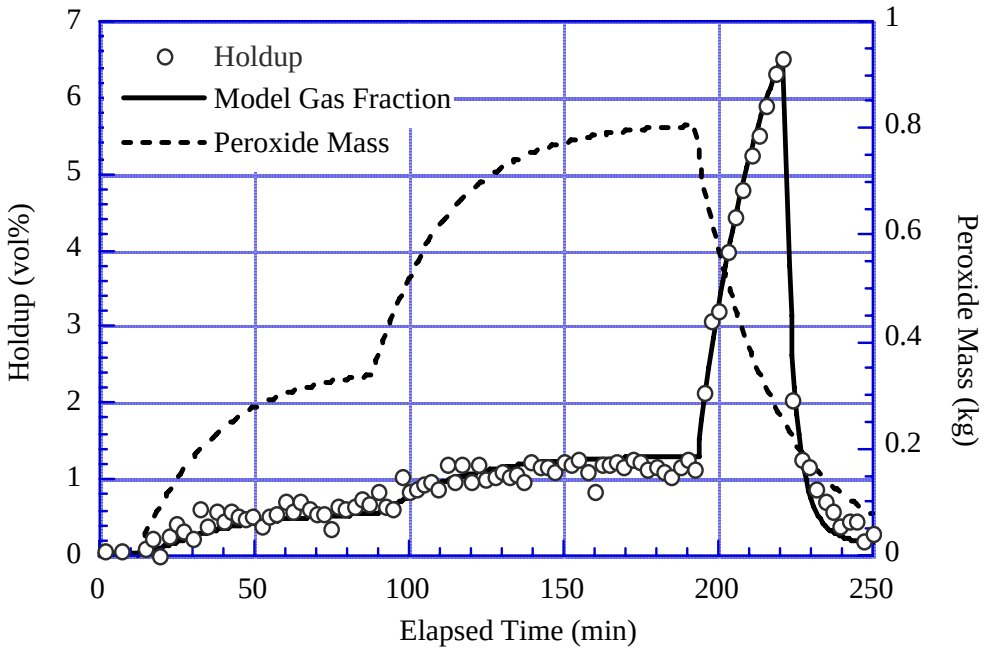

Figure 8.3. GR&R Test in LS Scaled Prototype with PJMs and Supplemental Mixing Provided by Recirculation Pump. Hydrogen peroxide added at two mass flow rates; approach to steady-state holdup for each can be seen as can the sharp increase in holdup when PJMs stopped and decrease as operation resumed.

8.2.2 Evaluation of Hybrid Mixing System Design Variables

Based on the results from the mixing and GR&R tests, the effect of the major design variables on mixing performance could be evaluated. A summary of those evaluations is presented in this section.

PJM placement and configurations. All PJM configurations investigated in Phase II were of the central cluster type. The two main variations were a tightly compact arrangement with minimal space between the pulse tubes and an expanded cluster that provided more space between the pulse tubes. One of the disadvantages of the cluster configuration is that the slurry in the small spaces between the pulse tubes is difficult to mix. This problem was solved by placing a shroud around the central cluster to exclude material from the spaces between pulse tubes. The expanded cluster was an attempt to create more space and enhance mixing between pulse tubes. Because a shroud was not required, fabrication costs were reduced. However, tracer testing showed that, while the expanded cluster allowed slightly better mixing between the tubes, the mixing in the rest of the vessel was not as good. The characteristics of cluster configurations are shown in Table 8.1. The cluster configuration with a shroud was selected by the WTP Project and implemented in a final configuration for testing, as discussed in Section 8.3.

Table 8.1. Comparison of PJM Cluster and Expanded Cluster Characteristics

Cluster Characteristics	Expanded Cluster Characteristics
Well-defined scaleable turbulent cavern	Mixing cavern shape sensitive to PJM nozzle angle
Higher measured mixing volumes	
Compact arrangement was well suited for combination with sparging or recirculation pumps	Placement better suited for PJM overblow mixing
Approximately 4 to 5% of the vessel operating volume was lost due to the shroud	No loss of operating volume
Higher fabrication cost	Standard PJM support design, lower fabrication cost

PJM nozzle geometry. The nozzle angle relative to vertical was the primary nozzle-related variable evaluated. Nozzle angles ranging from 15^o to 135^o were tested. Perimeter nozzle angles of 45^o were selected for the cluster PJM configuration. This angle provided reasonable off-bottom suspension of the solids and a well-mixed cavern in the lower portion of the tank. Upward-pointing nozzles were not as effective at off-bottom suspension but created a larger cavern. Because sparging was included in all final PJM/hybrid mixing designs, upward-pointing PJM nozzles were not needed.

Recirculation pumps in UFP and LS. Recirculation pumps were evaluated for use in the LS and UFP vessels in combination with PJMs. Recirculation outlet nozzle geometries considered in the UFP included a single nozzle pointing straight down and three nozzles pointing up at a 30^o angle to mix the upper regions of the tank. Nozzle geometries considered in the LS vessel included a single nozzle directed at the bottom of the tank, and two or four nozzles pointing up to mix the upper regions of the tank. In general, the combination of PJMs and recirculation pumps was demonstrated to mix both the UFP and the LS vessels. It was found that more nozzles resulted in more rapid and complete mixing. A recirculation pump with a single downward-pointing nozzle was selected for the UFP, in part because it minimized tank penetrations, and was viewed as more robust from an erosion standpoint.

Sparging. Several PJM configurations were tested in combination with sparging. The general conclusion from these tests was that sparging + PJMs in a number of configurations could provide adequate mixing in the UFP and LS vessels and the CRV. The requirements for effective mixing with sparging were found to be 1) cavern sufficiently large and well-mixed, as generated by the PJMs; 2) spargers submerged in the PJM cavern to allow exchange of material between mixing zones; and 3) sparger spacing and flow rate sufficient to adequately mix the upper zone of the vessel.

PJM Sparging/Overblow. Using a PJM overblow to mix the vessels was evaluated in the large-scale 4PJM test vessel containing the kaolin-bentonite clay simulant. In these tests one of the four pulse tubes was subjected to overblow by setting the Prescon controller parameters to overblow. Four Prescon drive pressures were used: 200, 300, 450, and 500 kPa. At each drive pressure, the drive time was incremented until a drive time was achieved that resulted in a very small (initialization of) overblow. Subsequently, 1.5 seconds were added to the drive time to initiate a significant, consistent period of overblow. During these tests, two hydrophones were used to record the pressure pulses. These data were subsequently used in structural analyses.

Visual observation indicated vigorous mixing as well as generation of a large amount of aerosol. While quantitative mixing tests were not conducted, PJM overblows were routinely used as a tool to quickly homogenize the tank contents before and after tests. Because of concerns over the potential impact on the vessel supporting infrastructure and the apparently large amount of aerosol generated, the PJM overblow approach was abandoned. The results of these initial evaluations led to two approaches for mixing the non-Newtonian vessels. These options were configured in the scaled prototypes, and final mixing tests were conducted, as discussed in Section 8.3.

- Option 1: Use PJMs and recirculation pumps for normal operations in the UFP and LS vessels. In case of recirculation pump failure, activate full sparging. With this option, spargers would operate in idle mode during normal operations.

- Option 2: Use PJMs plus intermittent sparging for normal operations. Intermittent sparge cycling constrained by limited air supply capacity.

8.3 Final Hybrid Design Configurations

This section describes the final hybrid designs that were tested and some of the significant test results. The configurations are similar to the plant design but do not necessarily reflect the final plant design configuration.[(a)] The tests included mixing tests with tracers, solids suspension tests to assess off-bottom suspension capability, solids uniformity tests (in the CRV), and velocity mapping to provide information for heat transfer. The mixing tests evaluated the extent of mixing and the time to mix using dye and sodium chloride tracers with the kaolin-bentonite clay simulant. Solids suspension tests were conducted using glass beads in water, and solids uniformity tests were conducted with glass beads and kaolin-bentonite clay simulant in the CRV. Velocity mapping was conducted with an ultrasonic velocity probe using the kaolin-bentonite clay simulant. The information generated in these tests was used to support the final design decisions. Details on the configurations, test methods, and results can be found in Johnson et al. (2005) for the UFP and LS vessels and Guerrero (2004a) for the CRV.

8.3.1 LS Final Test Configuration

The final PJM test configuration for the LS scaled test stand (scale factor = 4.29) was the cluster (7+1) with a Plexiglas/foam shroud enclosing the PJMs, eight spargers, and a recirculation system (Figures 8.4 and 8.5). The nozzles on the perimeter PJMs angled radially out toward the tank wall at 45º, while the center nozzle pointed straight down. The eight spargers were equally distributed around the tank circumference, as indicated in Figure 8.5. The recirculation system used two discharge lines and one suction line located under the PJM cluster and slightly off center. The discharge nozzles were complicated assemblies that were directed slightly up and toward the annular region between the PJM cluster and the vessel wall. The nozzles were sized to provide a nozzle exit velocity of 40 ft/sec at the target flow rate of 120 gpm.

(a) The test configurations include minor geometric differences from the proposed plant design due to the use of commercially available pipe, the number and size of the sparge tubes, and the LS recirculation pump, which is not included in the plant design. The CRV was removed from the plant design.

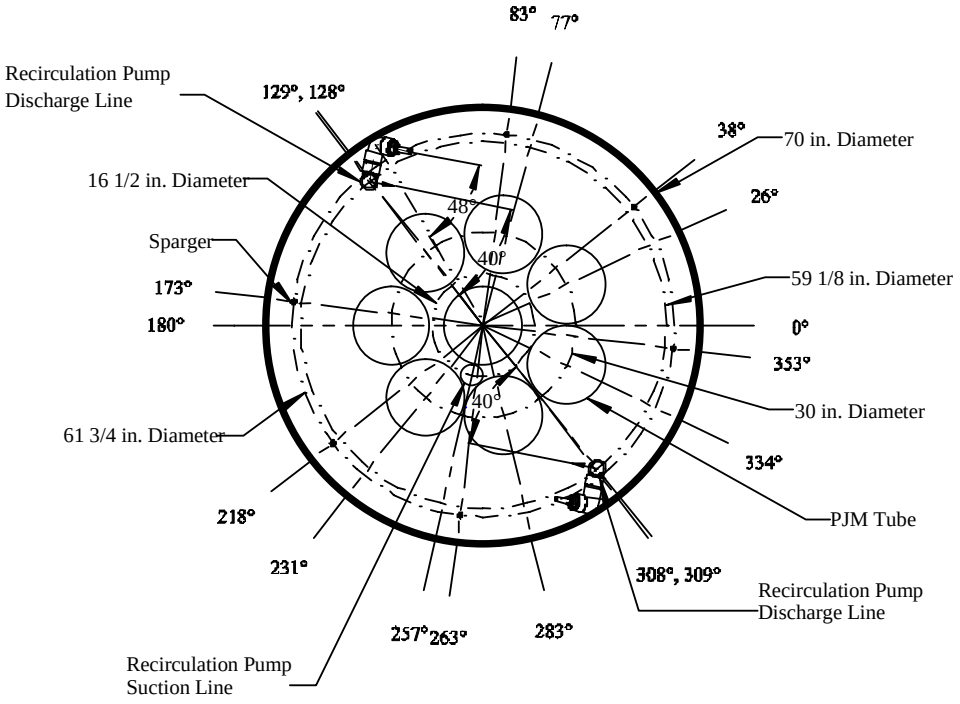

Figure 8.4. Top View of Cluster Final Test Configuration in LS Scaled Test Stand Showing Nominal Locations of PJMs, Spargers, and Recirculation System Components

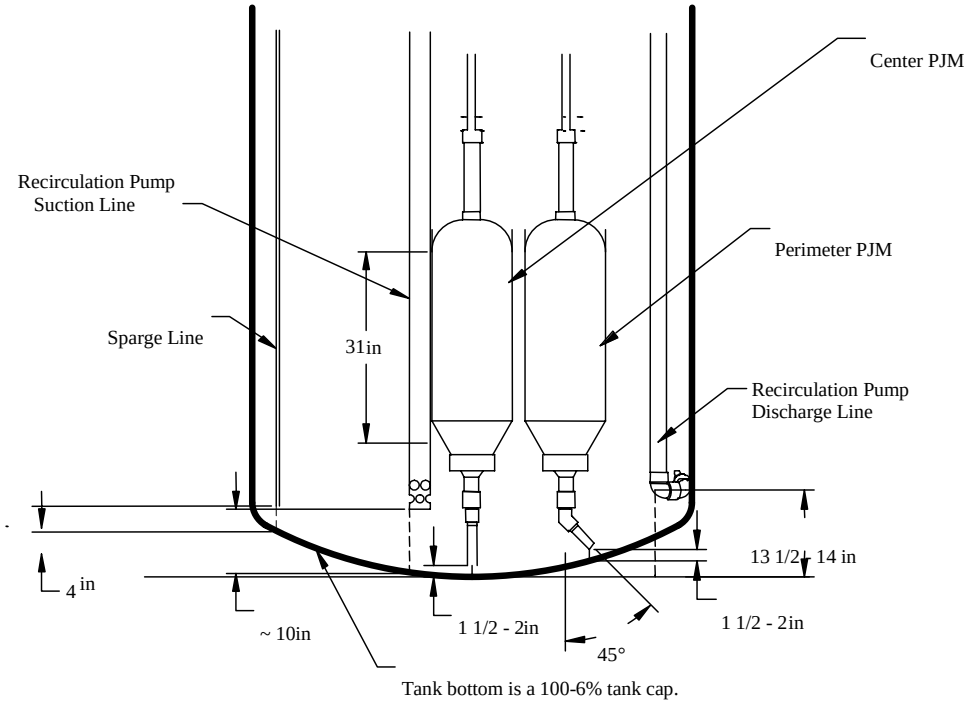

Figure 8.5. Plan View of Expanded Cluster Final Test Configuration in LS Scaled Test Stand Showing Nominal Elevations of PJMs, Spargers, and Recirculation System Components

8.3.1.1 Mixing tests

The test conditions, percent mixed, and mixing ratio results for the LS scaled test stand are summarized in Table 8.2. All tests were performed with kaolin/bentonite clay simulant. For tests using a recirculation pump, the flow rates were scaled approximately by the inverse square of the geometric scale factor ($4.29^2 = 18.0$) and are based on the average flow rate measured over the duration of a run. The sparger air flow rates are actual flow rates (acfm) at the bottom of the sparge tube outlet. The relatively low air flow rates for sequences 26 and 28 represent the spargers in an idle mode, in which the air is supplied primarily to prevent the simulant from plugging the sparge tubes.

The fraction mixed and mixing ratio data presented in Table 8.2 are based on the final sampling tube array results obtained during the tracer mixing tests. With only PJMs operating the vessel was not fully mixed, but the 58% fraction mixed indicates a substantial cavern. With supplemental mixing (pumps and spargers) the fraction mixed was >93%, indicating that the tank was well mixed but not homogeneous. With PJMs + spargers (no pump) operating, the tank was not completely mixed at the end of the test, indicating that a longer mixing time was needed to approach homogeneity.

Core samples of the simulant were taken at several occasions before, during, and after the tests. The average mixing ratio and the probability score for each core sample segment and associated error were calculated and are shown in Table 8.3. With the exception of core 2 from LS tests 27 and 28, every core sample mixing ratio yielded a range of values containing zero mixing ratio within the given error. The average value of core 2 from LS tests 27 and 28 is relatively close to zero but of lower confidence, as indicated by the probability scores. These results indicate that the tank contents were reasonably well mixed but not completely homogenized.

To assess tracer uniformity as a function of depth, the mixing ratio depth profile for each core segment is shown in Figures 8.6 and 8.7. In general, the data indicate the tracer concentrations fluctuating close to a fraction mixed value of unity for all core samples. This behavior is characteristic of a fully mobilized system in the process of complete homogenization. Because these results do not indicate any stagnant regions, the variation in data indicates that there are regions where mixing occurs at a slower rate.

Table 8.2. Test Conditions/Fraction Mixed/Mixing Ratio Results from Tube Samples for Final LS Test Configuration

Seq. (a)	Run	Test Mode	H/D	Yield Stress (Pa)	Peak Avg Noz. Vel. (m/s)	Sparger Flow Rate (per sparge tube)	Pump Flow Rate (gpm)	Fraction Mixed[a]	Mixing Ratio (b)				Mixing Ratio Probability Score [c]	
									Dye	Error	Chloride	Error	Dye	Chloride
26	1	PJMs only	0.74	32	12.2	--	--	0.58	-0.16	0.14	Inc	--	12%	Inc
26	2	PJMs + pump + spargers	0.74	32	12.2	0.9 acfm	118	0.93	Inc	--	-0.07	0.22	Inc	59%
27	1	PJMs + spargers	0.74	33	12.3	2.2 acfm	--	0.83	Inc	--	-0.21	0.25	Inc	15%
28	1	PJMs + pump + spargers	0.74	34	12.3	0.16 acfm (4.5 L/m)	119	0.96	-0.01	0.28	-0.04	0.24	60%	62%

(a) Seq = sequence (test identifier); run # identifies different conditions within a run.
(b) A mixing ratio of zero indicates homogeneity; Inc = inconclusive results; N/M = not measured.
(c) Mixing ratio probability score indicates confidence that tank was well mixed.

Table 8.3. Mixing Ratio Values and Probability Scores from Chloride IC Data for Core Samples Taken During Testing of the Final LS Configurations

Test	Core 1	Core 2	Core 3
LS-T26	-0.01 ± 0.05	-0.02 ± 0.05	nm[a]
LS-T27	-0.05 ± 0.05	-0.14 ± 0.06	-0.01 ± 0.05
LS-T28	0.00 ± 0.05	-0.08 ± 0.06	nm
Probability Scores			
LS-T26	94%	92%	nm
LS-T27	82%	26%	94%
LS-T28	94%	62%	nm

(a) nm = not measured

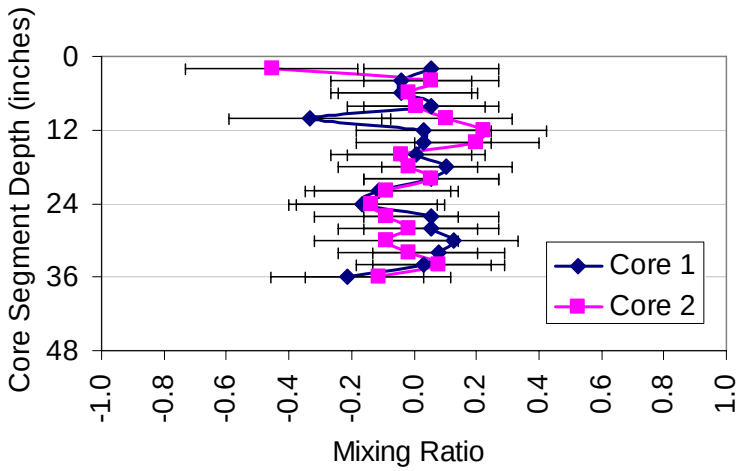

Figure 8.6. Mixing Ratio Results from LS Test Sequence 26 Core Samples with Chloride Tracer

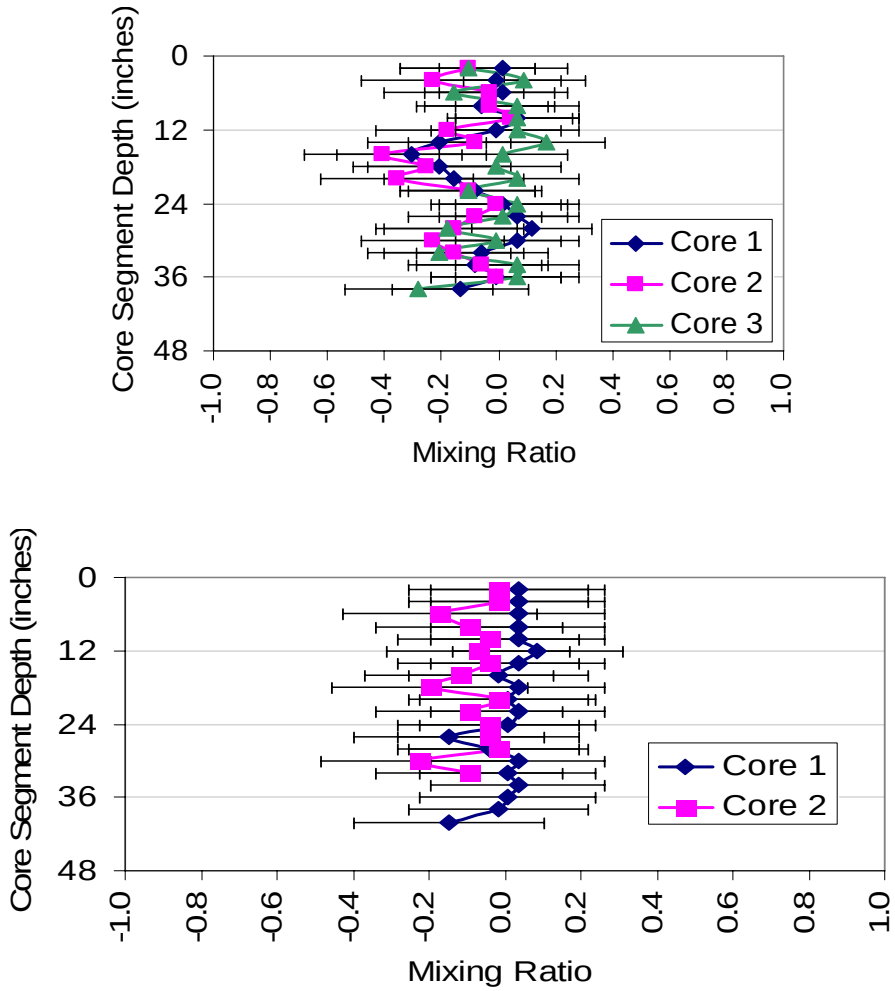

Figure 8.7. Mixing Ratios from Sequences 27 (top) and 28 (bottom) Core Samples with Chloride Tracer

8.3.1.2 Solids suspension tests

Solids lift tests were conducted with PJMs in the cluster and expanded cluster configurations with different nozzle angles on the perimeter PJMs. The solids lift tests were performed by placing a small concentration (0.5 wt%) of 4-mm glass beads in the bottom of the tank and increasing the nozzle velocity in increments until the solids were observed to lift off the bottom. The solids lift velocities in Table 8.4 are the minimum nozzle velocity required to lift all of the solids off the vessel bottom at any moment during the PJM drive phase. These lift velocities are not representative of plant conditions. A scale-up methodology for determining the required lift velocity in plant vessels is presented in Johnson et al. (2005).

Table 8.4. Summary of LS Solids Lift Tests

UFP PJM Configuration	Perimeter Nozzle Angle from Vertical (degrees)	Solids Lift Velocity: Peak Average Nozzle Velocity (m/s)
Cluster (7 around 1)	45	8.7[(a)]
Expanded cluster (7 around 1)	23	10.4[(a)]
(a) Measured lift velocities must be scaled to plant conditions.		

8.3.1.3 Velocity mapping results

Velocity mapping was carried out in the LS vessel using a mast-mounted ultrasonic Doppler velocity probe. All testing was done at a peak average nozzle velocity of 12 m/s using the kaolin-bentonite clay simulant with a target yield stress of 30–36 Pa at an aspect ratio (H/D) of 0.74. In these tests cavern height was determined by finding the point where a maximum velocity of 80 mm/s was obtained for a majority (>50%) of PJM cycles in a sample train (typically >10 cycles).

The average cavern height was found to be 23.5 inches (H/D = 0.34) and 19.4 inches (H/D = 0.28) with PJMs only, depending on velocity probe orientation. Cavern heights are smaller than those determined with tracer tests because of the velocity cutoff of 80 mm/s used to determine cavern boundary. Center tank bottom average velocities varied from about 600 to 1250 mm/s and were probably greater than this since the detector was saturated at this point. Additional discussion of the velocity measurement method and the results can be found in Johnson et al. (2005).

8.3.2 UFP Final Test Configuration

The final PJM test configuration for the UFP scaled test stand was the cluster (5+1) configuration with a Plexiglas shroud enclosing the PJMs, three spargers, and a recirculation system using a single discharge and suction line (Figures 8.8 and 8.9). The nozzle on the center PJM pointed straight down to mix the region directly under the cluster. The nozzles on the outer PJMs were angled toward the vessel wall at 45^{o} and directed flow up the wall to form a cavern. The three spargers used in the final configuration were equally spaced around the tank centerline. The orientation was chosen to place one sparger tube on the opposite side of the tank from the recirculation pump discharge line. The intake line for the recirculation pump was under the PJM cluster, and the discharge line extended from the top of the vessel and connected to a nozzle pointing straight down on the opposite side of the tank from the recirculation pump suction line. The discharge nozzle had an exit velocity of about 30 ft/sec at the target flow rate of 90 gpm.

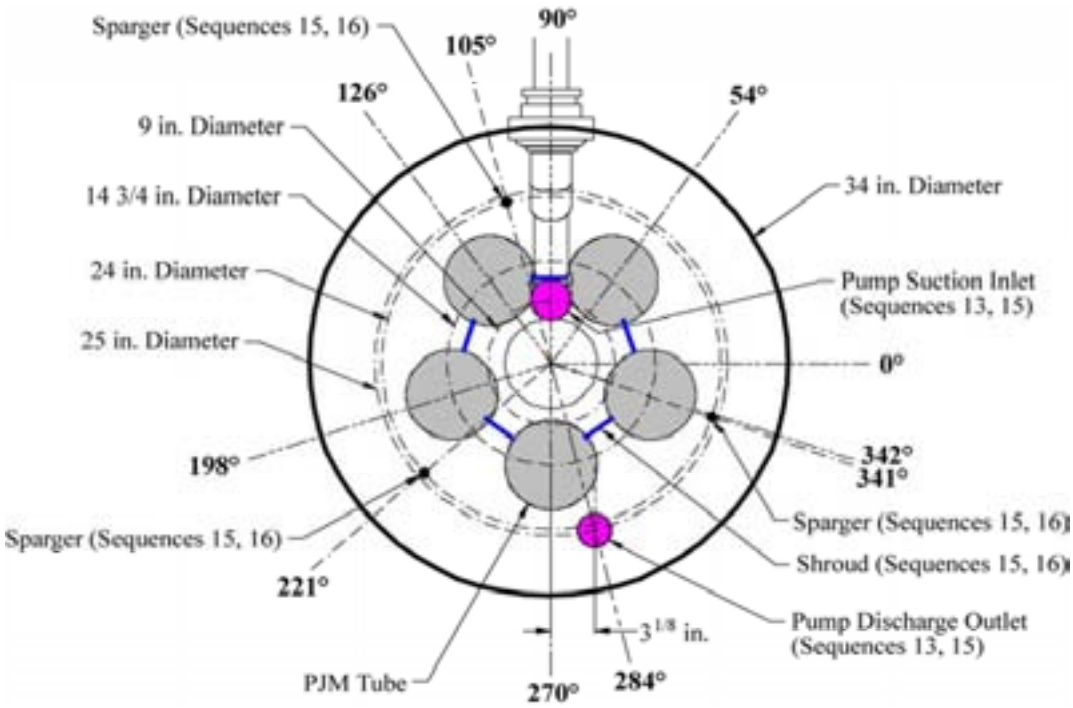

Figure 8.8. Top View of Cluster (5+1) Final Test Configuration in UFP Scaled Test Stand Showing Nominal Locations of PJMs, Spargers, Recirculation System Components

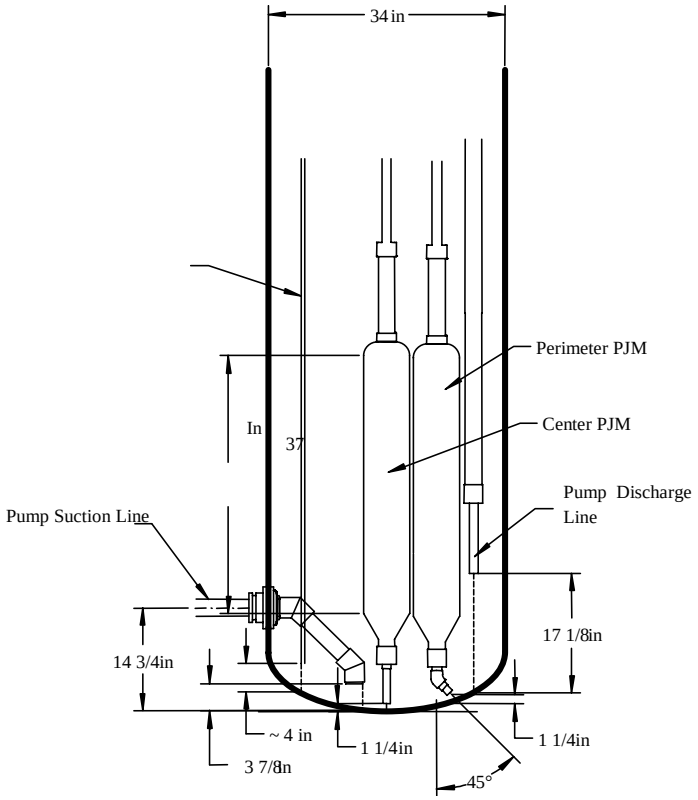

Figure 8.9. Plan View of Cluster Final Test Configuration in UFP Scaled Test Stand Showing Nominal Locations of PJMs, Spargers, and Recirculation System Components

8.3.2.1 Mixing tests

The test conditions, percent mixed, and mixing ratio results for the UFP scaled test stand are summarized in Table 8.5. All tests were performed with kaolin/bentonite clay simulant. For tests using a recirculation pump, the pump flow rates were scaled approximately by the inverse square of the geometric scale factor ($4.94^2 = 24.4$) and are based on the average flow rate measured over the duration of a run. The sparger air flow rates are actual flow rates (acfm) at the bottom of the sparge tube outlet. The relatively low air flow rate for sequence 15 run 2 represents the spargers in idle mode, in which the air is supplied primarily to prevent the simulant from plugging the sparge tubes.

The fraction mixed and mixing ratio data presented in Table 8.5 are based on the final sampling tube array results obtained during the tracer mixing tests. With only PJMs operating the vessel was not fully mixed, but the 67% fraction mixed indicates a substantial cavern. With supplemental mixing (pumps/spargers) the fraction mixed was >90%, indicating that the tank was well mixed but not homogeneous.

The average mixing ratio and the probability score for each core sample segment and associated error are shown in Table 8.6. The mixing ratio and associated error for UFP-T15 creates a range of values that includes zero. This is not the case for UFP-T16. The probability scores for UFP-T15 and UFP-T16 are reasonably high, indicating good confidence that the tank contents were reasonably well mixed but not completely homogenous.

To assess the tracer uniformity as a function of depth, the mixing-ratio depth profile for the core segments is shown in Figures 8.10 and 8.11. In general, the data indicate that the tracer concentrations fluctuate close to a mixing ratio of zero (fraction mixed of 1) for all core samples. This behavior is characteristic of a fully mobilized system that is in the process of complete homogenization. Because these tracer results do not indicate the presence of stagnant regions, the variation in the data indicates that there are regions of the tank where the mixing process occurs at a slower rate.

Core samples from UFP test 16 show a pattern of slightly decreased tracer concentration in the midsection of each core. Increased tracer concentration is present at the top and bottom of each core. This test consists of PJMs operating with spargers and is consistent with a two-zone mixing model. This situation may occur if the sparging system is creating a relatively large circulation cell, where the tracer injected in the pulse tubes is brought to the surface by the sparger system and then forced back to the bottom along the tank walls. Because of the location of tracer injection, increased tracer concentration would be present along the top, sides, and bottom of the tank.

With PJMs and full flow sparging, samples taken every 15 minutes after the start of the test showed that the tank was well mixed after the first 15 minutes. Mixing times generally increase with the scale factor, so the time to mix in the full-scale vessel can be estimated as being less than 15 minutes multiplied by the geometric scale factor of 4.94. This provides an estimate of the time to mix in the full scale vessel of <75 minutes. A time to mix for operation with the PJMs and the recirculation pump (sequence 15) is not possible because run 1 (PJMs only) did not result in a mixed vessel and run 2 did not start with an unmixed simulant.

Table 8.5. Test Conditions and Fraction Mixed Results from Grab Samples for Final Test Configuration of UFP Test Stand

Seq.[a]	Run	Test Mode	H/D	Yield Stress (Pa)	Peak Avg. Noz. Vel. (m/s)	Sparger Flow Rate (per sparge tube)	Pump Flow Rate (gpm)	Fraction Mixed	Mixing Ratio[b]				Mixing Ratio Probability Score[c]	
									Dye	Error	Chloride	Error	Dye	Chloride
15	1	PJM Only	1.4	29	11.9	--	--	0.67	Inc	--	Inc	--	Inc	Inc
15	2	PJM + Pump + Spargers	1.4	29	11.6	0.08 acfm (2.3 L/m)	84	0.95	0.01	0.11	-0.1	0.26	67%	62%
16	1	PJM + Spargers	1.4	34	11.3	2.1 acfm	--	0.90	N/M	--	0.04	0.05	N/M	86%

(a) Seq = sequence (test identifier); run # identifies different conditions within a run.
(b) A mixing ratio of zero indicates homogeneity; Inc = inconclusive results; N/M = not measured.
(c) Mixing ratio probability score indicates confidence that tank was well mixed.

Table 8.6. Average Mixing Ratio Values and Probability Scores from Chloride IC Data for Core Samples Taken During Phase II Scaled Test Platform Tests

Test	Core 1	Core 2
UFP-T15	0.03 ± 0.06	-0.01 ± 0.06
UFP-T16	0.05 ± 0.02	0.06 ± 0.02
Probability Score[a]		
UFP-T15	85%	88%
UFP-T16	99%	96%

(a) Probability that the mixing ratio lies between -0.1 and 0.1.

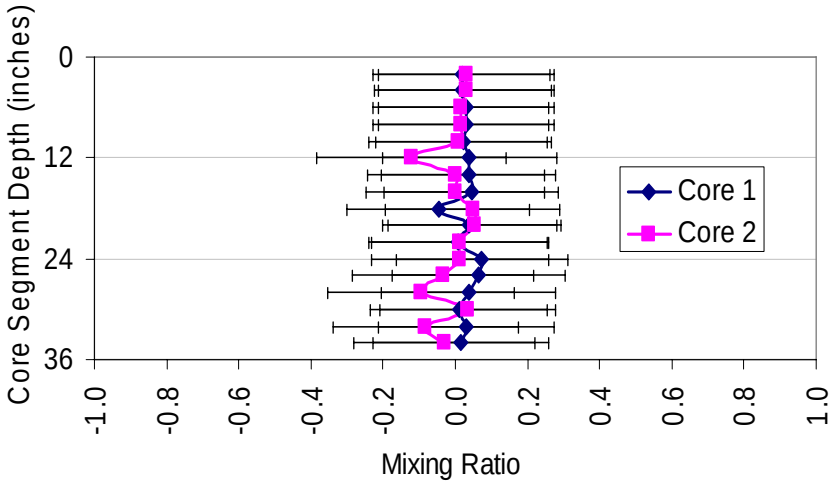

Figure 8.10. Mixing-Ratio Results from UFP Test Sequence 15 Core Samples Using Chloride Tracer

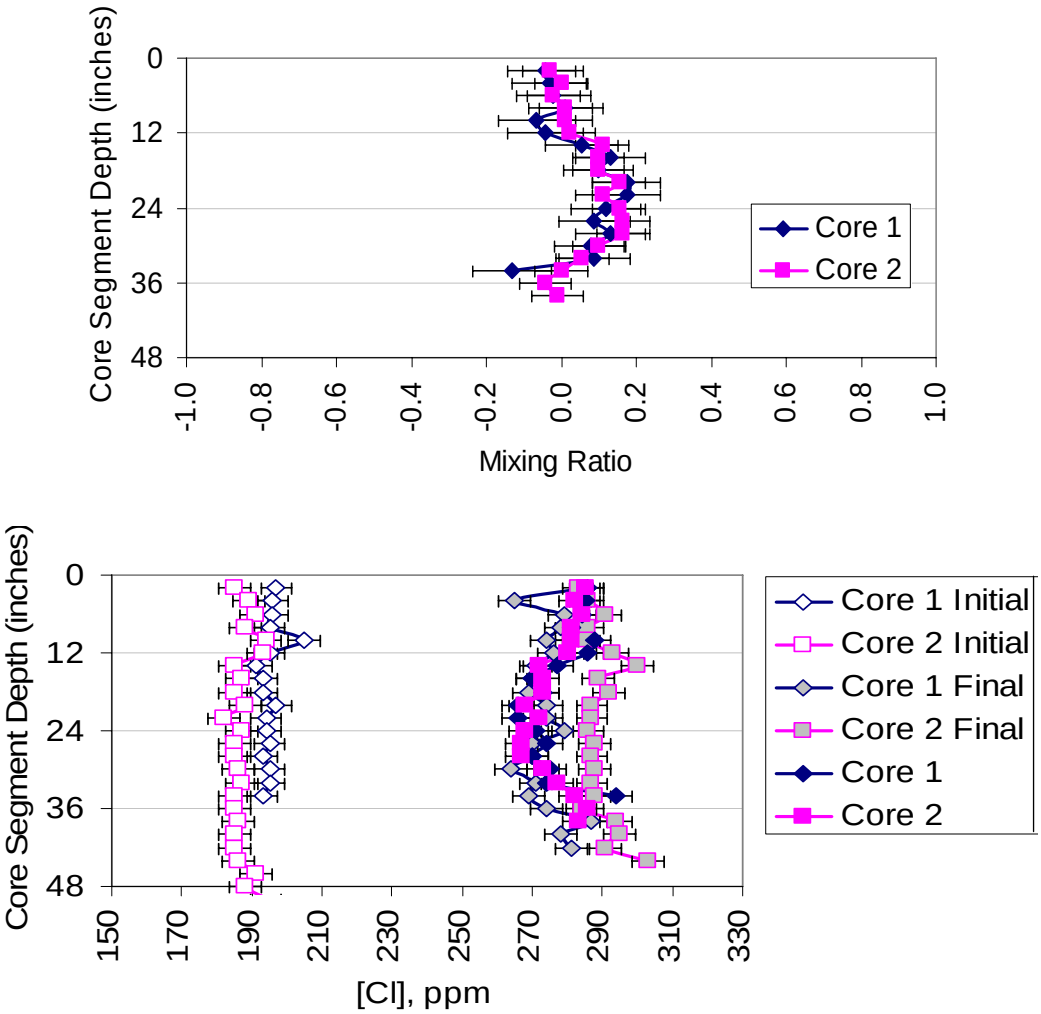

Figure 8.11. Mixing-Ratio Results from UFP Test Sequence 16 Core Samples Using Chloride Tracer (top) and Chloride Concentration as a Function of Depth (bottom)

8.3.2.2 Solids suspension tests

Solids lift tests were conducted with PJMs in the cluster and expanded cluster configurations with different nozzle angles on the perimeter PJMs. The solids lift tests were performed by placing a small concentration (0.4 wt%) of 4-mm glass beads in the bottom of the tank and increasing the nozzle velocity in increments until the beads were observed to lift off the bottom. The solids lift velocities in Table 8.7 are the minimum required to lift all of the solids off the vessel bottom at any moment during the PJM drive phase. These lift velocities are not representative of plant conditions. A scale-up methodology for determining the required lift velocity in plant vessels is presented in Johnson et al. (2005).

Table 8.7. Summary of UFP Solids Lift Tests

UFP PJM Configuration	Perimeter Nozzle Angle from Vertical (degrees)	Solids Lift Velocity: Peak Average Nozzle Velocity[(a)] (m/s)
Cluster (5 around 1)	45	7.1
Cluster (5 around 1)	60	7.4
Expanded cluster (5 around 1)	45	7.5
Expanded cluster (5 around 1)	30	7.2
(a) Measured lift velocities must be scaled to plant conditions.		

8.3.2.3 Velocity mapping results

Velocity mapping was carried out in the UFP vessel using a mast-mounted ultrasonic Doppler velocity probe. All testing was done at a peak average nozzle velocity of 12 m/s using kaolin-bentonite clay simulant with target yield stress ranging from 30–36 Pa at an aspect ratio (H/D) of 1.4. The test matrix for the UFP test stand included a recirculation pump (90 gpm target flow rate). In these tests the cavern height was determined by finding the location at which a maximum velocity of 80 mm/s was obtained for a majority (>50%) of PJM cycles in a sample train (typically >10 cycles).

The average cavern height was found to be 16.4 inches (H/D = 0.49) with PJMs only and 18 inches (H/D = 0.53) for PJMs plus the recirculation pump. Vertical velocities at the tank wall showed sharp delimitation with elevation, often changing tens of centimeters per second over a 1-inch elevation change. While velocity mapping did not indicate a big increase in cavern height, the recirculation pump provided full mobilization (shown in tracer mixing tests) of the simulant, which was not achieved using only PJMs. Cavern heights are smaller than those determined in tracer tests because of the velocity cutoff of 80 mm/s used to determine the cavern boundary. Additional discussion of the velocity measurement method and the results may be found in Johnson et al. (2005).

8.3.3 CRV Final Test Configuration

The final PJM configuration was the cluster (5 around 1) with charge vessels positioned at the vessel wall along radial centerlines between PJMs (Figure 8.12). This ensured a nearly symmetrical flow distribution. Two PJM configurations were selected for final verification. Configuration A comprised five 45° and one center 1-inch nozzles pointing downward plus five spargers operating with air flow rates of 3 scfm. The 8-inch PJMs operated at a stroke length consistent with the delivered volume of a 6-inch

Figure 8.12. Final CRV Test Configuration; 8-inch Diameter Cluster PJM and Charge Vessel Assembly (1.5-inch-diameter nozzles installed)

PJM. Configuration B was PJM only, comprising two 45° downward-pointing 1.5-inch nozzles, three 135° upward-pointing 1.5-inch nozzles, one center downward-pointing 1.5-inch nozzle, and no spargers.

8.3.3.1 Mixing tests

Several tests were conducted with the CRV final configuration (Table 8.8). The dye and UVP probe methods were used to determine cavern height or mixed volume. In test group D several nozzle sizes, directions, number of spargers, and total air flow rates were investigated. In test group E the final configurations were evaluated. Table 8.8 contains the conditions and results for the configurations that resulted in a completely mixed vessel as determined by the dye or UVP probe method. In some cases the percent mixed volume could not be calculated by the dye method because sample absorbance was less than the final homogenized value. This suggests that the 45 minutes of mixing allotted for each mixing condition was insufficient to fully distribute the dye inside the cavern. Also, UVP measurements indicate a region of low flow around the sampling vessels near the bottom of the tank.

Table 8.8. Selected Percent Volume Mixed for Final CRV Configurations

Test Group	Test Sequence	Nozzle Config.	Nozzle Diameter (in.)	Measured Nozzle Velocity (m/s)	No. of Spargers @ scfm total	Measured Yield Stress (Pa)	UVP Cavern Ht. (in. dn/up) Nozzle	% Tank Volume Mixed (UVP)	Tank Vol. Mixed, Dye (%)
D	1d	Down	1	12.32	(5) 7.6	11.4	26	100%	76%
D	4d	Down	1.5	13.7	(5) 7.6	32.6	40	100%	100%
D	5d	Down	1.5	13.77	(5) 7.6	31.2	34	100%	96%
D	6d	Up/Down	1	12	(5) 9.5	28.2	31/40	100%	^ 90%
D	7d	Down	1.25	7.5	(5) 9.5	32.4	34	100%	100%
E	1e	Down	1	12.76	(5) 9.56	30	40	98	100
E	3e	Up/Down	1	11.4	(5) 9.56	32.8	40/40	100%	*
E	7A	Up/Down	1.5	12.27	N/A	27.7	40/40	100%	100%

8.3.3.2 Solids suspension and uniformity tests

Solids lift tests were conducted with PJMs in the cluster configuration with different nozzle angles on the perimeter PJMs. The solids lift tests were performed by placing a small concentration (0.4 wt%) of 5-mm glass beads in the bottom of the tank and increasing the PJM nozzle velocity in increments until the beads were observed to lift off the bottom. The solids lift velocities in Table 8.9 are the minimum nozzle velocity required to lift all of the solids off the vessel bottom at any moment during the PJM drive phase.

Table 8.9. Summary of CRV Solids Lift Tests

CRV PJM Configuration	Perimeter Nozzle Angle from Vertical (degrees)	Solids Lift Velocity: Peak Average Nozzle Velocity (m/s)
Cluster (5 around 1)	45	4.1
Cluster (5 around 1)	2@ 45, 3 @135	4.9

Solids uniformity tests were conducted to verify the adequacy of mixing in the CRV to meet the plant specification. In these tests, kaolin-bentonite clay simulant (yield stress of 6 and 30 Pa) was used with 0.6 to 0.7 wt% 4-mm glass beads. After mixing was halted, several grab samples were obtained at random locations from the upper and lower portions of the vessel. Samples were also obtained from the heel with the RFD sampler system. Statistical tests were performed to compare the glass bead sample concentrations from the three locations.

For the 6- and 30-Pa tests with Configuration A (PJMs + sparging), no significant statistical difference in glass bead concentrations was found between the upper and lower regions of the vessel. A small but statistically significant difference was found between the heel samples and the rest of the vessel.

For the 6-Pa test with configuration B (PJMs only), the maximum deviation from the experimental true mean was 1.5%. For the 30 Pa test with Configuration B, a high standard deviation was measured for the heel pump samples and the deviation from the experimental true mean was 31.3%. If this is discounted as experimental error, the maximum deviation for the 30-Pa test would still be 4.8%.

8.3.3.3 Velocity probe results

In these tests, the 1-inch down nozzle configuration was used with several kaolin/bentonite solutions with yield stresses from 10 to 30 Pa. The objective was to provide a correlation of cavern height as a function of nozzle velocity and yield stress. The original intent was to use different tank levels (40, 30, 20, and 15 inches) to observe the nozzle velocity at breakthrough and determine the cavern height. However, the UVP probe was used and only the 40- and 30-inch tank levels were tested. For some conditions, the cavern was also detected by slowly lowering the tank level with the PJMs operating to determine the point of breakthrough.

The cavern height data were correlated as a function of yield Reynolds number. The data plotted are shown in Figure 8.13, including data obtained with other nozzles. The data for the 1.25- and 1.5-inch nozzles are higher than for the 1-inch nozzles, indicating a dependence on nozzle size. This is consistent with the trends indicated by Eq. (3.9).

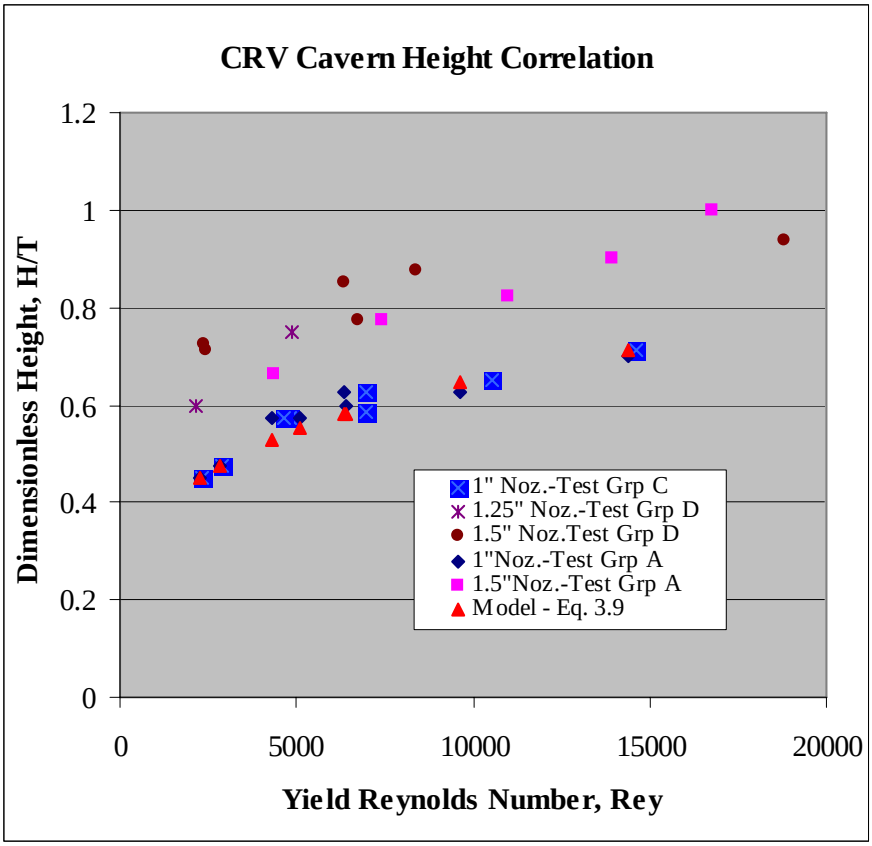

Figure 8.13. Cavern Height Versus Yield Reynolds Number for CRV Tank, Downward Nozzle Configuration

8.3.3.4 Comparison of test results of final CRV configurations

Two PJM configurations were selected for final verification. Configuration A consisted of five 45° downward nozzles and one center downward 1-inch nozzle and five spargers with 3 scfm each. The 8-inch PJMs operated with delivered volume simulating a 6-inch PJM. Configuration B (PJMs only) consisted of two 45° downward nozzles, three 135° upward nozzles, one center downward 1.5-inch nozzle and no spargers. The UVP probe and dye method both indicated 100% mixing for both configurations. Configuration A was selected because the air requirements for the 1.5-inch nozzles and 8-inch PJMs translated to a new development effort for a larger JPP than is currently available.

Solids uniformity tests were then performed with Configuration A, which determined that the upper and lower regions of the vessel had no significant statistical difference in glass bead tracer concentrations, but the heel (pump) samples had a small but significant statistical difference in the upper and lower regions. A comparison of the tracer concentrations in the three regions with respect to a true mean was not available. The technique could have been improved with homogenization of the tank after PJM/ sparger mixing to obtain an experimental true mean, and grab samples could be taken from the heel and retested; however, there was no opportunity to do so. Configuration A was thought to be a viable design.

Because the sparger air requirements for Configuration A were deemed excessive for the plant, Configuration B (PJM only) was tested for solids mixing final verification. The off-bottom velocity tests required a higher nozzle velocity to clear the glass beads from the vessel bottom than Configuration A. This was due to the unsymmetrical flow distribution of the downward-facing nozzles because the outer nozzles and the center nozzle were essentially in- line. The upward facing nozzles were also not arranged symmetrically. The results of the solids mixing test at 30 Pa showed a maximum probable deviation (excluding experimental error) of 4.77% for the sampled means from an experimental true mean. It was thought that given more time and adjustments of the PJM arrangements this deviation could be reduced.

8.4 Conclusion of Phase II Testing

The tests discussed in Section 8.3 demonstrate that using PJMs along with recirculation pumps or air sparging provide acceptable performance. However, an evaluation by the WTP Project indicated that it was not feasible to use a recirculation pump in the LS vessel. This left only air sparging as the supplemental mixing method, and it was determined that full-time sparging would exceed the allowable air capacity. This difficulty was solved by intermittent sparging. One issue associated with intermittent sparging was releasing retained gas after a quiescent period. This issue was addressed by conducting multiple sparge tube gas release tests in the CBT (Poloski et al. 2005). In these tests, hydrogen peroxide was used to generate in situ gas in a kaolin-bentonite clay simulant. The gas was released using the multiple sparge tube array. The sparge tube placement and air flow rates for the sparge tube array were based on the design guidelines presented in Poloski et al. (2005). A rapid gas release rate required the full sparger flow rate. Figure 8.14 compares a full air flow (206 acfm) test on 6/15/04 with a one-third-flow test (68 acfm) on 6/11/04. The initial gas-volume fractions were of similar magnitude (2.1 and 2.6 vol% including sparger holdup), and simulant rheology was essentially the same in both tests. The full-flow results clearly show essentially all the retained gas being released in about 5 minutes. The one-third-flow test releases much more slowly and, even accounting for 0.5 vol% sparger holdup, about 1 vol% gas remains after 20 minutes. The motivation for the one-third-flow test is that, had this been successful, sparging could have operated continuously at the lower rate and met the air supply requirements.

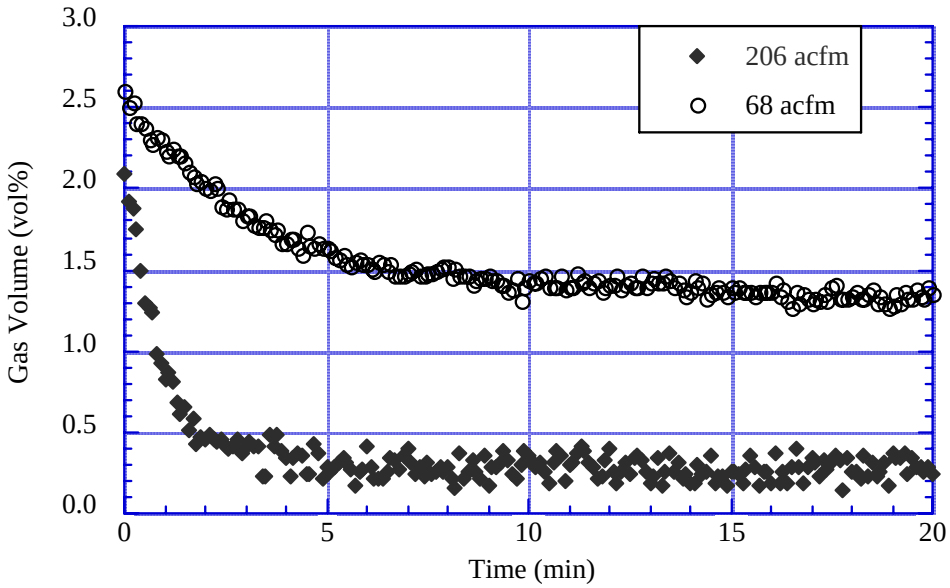

Figure 8.14. Effect of Sparger Air Flow (CBT 6/15 and 6/11)

Several more gas release tests conducted in the CBT confirmed that retained gas could be removed quickly using air sparging. Some remaining design and operational issues were addressed in a HSLS demonstration (Phase III). The results of this demonstration are presented in Section 9.

9.0 Half-Scale Confirmatory Testing (Phase 3)

While the testing summarized in Sections 7 and 8 addressed most of the issues associated with management and scale-up of mixing and flammable gas retention and release, some WTP engineering issues required additional testing. These issues included the need to define the size of backup ITS (important to safety) air compressors and diesel generators, the decision on removal of recirculation pumps from the LS and blend vessels, and the need for redundant infrastructure for operating the PJMs. A confirmatory demonstration of a large, correctly scaled hybrid mixing system was also required. These needs were addressed in a half-scale test representing the plant LS and blend vessels.

9.1 Introduction

The primary testing objective was to demonstrate successful cyclic operation by repeatable re-establishment of full mixing and release of accumulated gas (i.e., no gradual, long-term gas buildup) each time full mixing resumed. The three plant operating cycles to be demonstrated are as follows:[(a)]

- Normal Operations. Demonstrate intermittent sparging with continuous PJM operation during the normal operating cycle (continuous PJM operation with 1 hour at full sparge and 2 hours at idle sparge). This test confirmed that the duration of full mixing was adequate and that recirculation mixing pumps were not necessary.
- Post-DBE Operation. Demonstrate intermittent PJM and sparger operation for the post-design basis event (post-DBE) operating cycle (2 hours at full sparge with PJM operation and 12 hours at idle sparge without PJMs). This test confirmed the post-DBE mixing duration and frequency and helped define the size of backup ITS air compressors and diesel generators.
- Near-Term Accident Response. Demonstrate intermittent sparging for the NTAR loss-of-PJM operating scenario (2 hours at full sparge and 12 hours at idle sparge). This test also assessed the need for redundant equipment to support PJM operation.

Several additional tests bearing on NTAR issues were performed in the HSLS vessel and other facilities. Because slurry inside the pulse tubes will develop a yield stress during the 100 hours that PJMs are idle, the PJMs may be difficult to restart. PJM restart tests with clay and Laponite mixtures of yield stress over 600 Pa were performed at SRNL to allay this concern. Spargers alone without PJM operation do not mix the entire slurry volume. Accumulation of the gas generated in this heel volume over the 100-hour NTAR period might create a flammability hazard. The unmixed heel volume was measured in sparger-only HSLS mixing tests using salt tracer and confirmed by direct geometric calculation to be less than 40% of the total slurry volume as described in Section 9.3.

The rest of this section describes the strategy employed to demonstrate the three cyclic operating modes and summarizes the results of testing in the HSLS vessel.

(a) Cycle times given here are for the WTP. The scaled times are half those listed for the half-scale test described in Section.9.2.1.

9.2 HSLS Test Approach

A half-scale replica of the LS vessel constructed in the 336 Building "supernatant tank" was chosen as the test bed. The tank was equipped with PJMs and sparger arrays representative of the LS vessel, auxiliary systems to provide air to the test equipment and to inject hydrogen peroxide and tracer, and instrumentation and DACS to monitor the gas volume fraction, evaluate mixing, and operate the system. Details of the test system are described in Section 5.1.6. Similar to most of the previous testing, a kaolin/bentonite simulant was used. Oxygen was generated in situ by decomposition of hydrogen peroxide that was mixed into the simulant. A sodium chloride tracer was used to monitor the progress and extent of mixing.

The HSLS test program used the same geometric scaling approach as the scaled testing supporting the PJM non-Newtonian tests performed at PNWD and SRNL. The scaled testing approach is described in Section 3 and summarized as follows:

- All linear dimensions are reduced by the scale factor, which is the ratio of plant scale to test scale (i.e., reduced by a factor of 1/2 in this half-scale test). These include vessel diameter, fill level, PJM nozzle diameter, etc.
- PJM discharge velocities are the same at both reduced and full scale.
- Except where necessary to meet experimental objectives, all imposed times are reduced by the scale factor. These include PJM drive time, intermittent sparge times, etc.

9.2.1 Strategy for Intermittent Mixing

For tests performed in this manner, the fluid mixing results and gas release rates (i.e., exponential decay of gas content following restart of mixing) follow the linear scale factor(s) directly. However, the steady-state gas holdup is proportional to both the scale factor and the in situ volumetric gas generation rate (g_v). This means that the same gas generation rate will produce half the gas holdup in a half-scale test that it produced at full scale. Conversely, to achieve an equal gas holdup requires twice the gas generation at half-scale as at full scale.

An example illustrating the scaling principle for the normal operations mixing scenario is shown in Figure 9.1. Mixing system operation at both full-scale (continuous PJMs with 1 hour full sparge and 2 hours idle sparge) and half-scale (continuous PJMs with ½ hour full sparge and 1 hour idle sparge) is indicated by the horizontal bars in the figure. If the in situ gas generation rate is doubled in the half-scale test, gas will accumulate twice as rapidly during the idle sparge period, but, because the accumulation occurs over half the time, it will achieve approximately the same peak retained gas fraction (indicated by α_{max} in Figure 9.1). In addition, after full sparge operation resumes, gas will be released at twice the rate of the half-scale test. However, because the release occurs over half the total time, the minimum gas fraction (indicated by α_{min} in Figure 9.1) is approximately the same for the half-scale test.

Following this same strategy, the half-scale post-DBE cycle in the test was 1 hour of full sparging with PJMs operating at half-stroke followed by 6 hours of idle sparging only with double the full-scale gas generation rate. The half-scale NTAR tests also doubled the gas generation rate with 1 hour of full sparging and 6 hours of idle sparging. This produced the same minimum and maximum gas volume

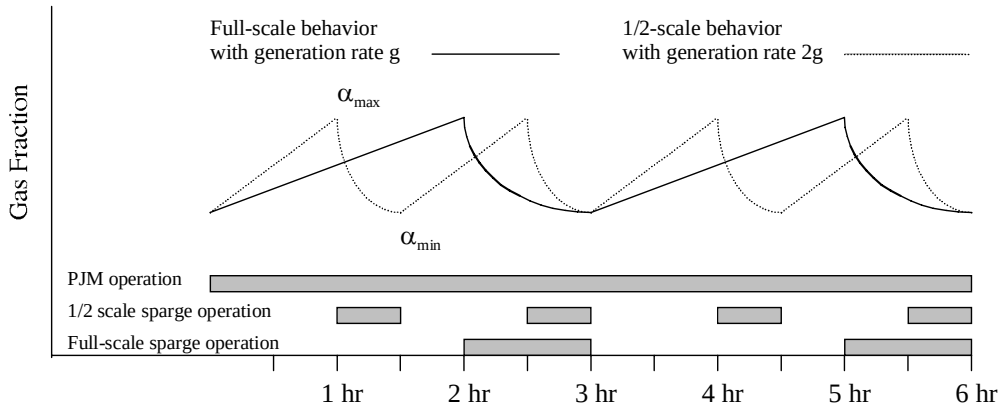

Figure 9.1. Illustration of the Scaling Relationship Between Half- and Full-Scale Gas Holdup Behavior During Normal Operation

fractions as the full-scale system over half the cycle time. However, the 6-hour idle period was reduced to 2 hours to accommodate rapid decomposition of hydrogen peroxide, as described in Section 9.2.2.

Each test was continued until a repeating periodic steady state was achieved, as defined by the calculated minimum and maximum gas volume fractions over a cycle. These values varied widely, and formal criteria to identify steady-state gas holdup behavior were not found to be practical. Instead, plots of the gas volume fractions derived from periodic static liquid level measurements, where the PJMs stopped and the spargers switched to idle flow for a brief time, were reviewed by the Steering Committee to determine whether an acceptable steady state was achieved or the test should be continued to differentiate slow transients from periodic oscillations in the data.

9.2.2 Strategy for Simulating Gas Generation with Hydrogen Peroxide

Ideally, the range of gas volume fractions over an operational cycle in the test should be approximately equal to those expected in the plant. However, it is more important to achieve a gas volume fraction high enough to be measured accurately in the test. Experience with previous tests showed that a practical minimum measurable gas volume fraction is on the order of 0.5 vol%, and gas volume fractions on the order of a few vol% were desired for the test. A nominal cycle-average hydrogen peroxide injection rate of 50 mL/min in the HSLS vessel: 0.7 to 1.3 vol% in the normal operation cycle and 1.0 to 2.5 vol% in the post-DBE and NTAR cycles.

It is very difficult to approximate continuous and uniform volumetric gas generation using hydrogen peroxide decomposition in the scaled tests in which the mixing system is cycled on and off. Because gas is generated in the test only where the decomposition reaction occurs, the hydrogen peroxide solution must be injected so that it is mixed throughout the vessel to approximate continuous and uniform gas generation. In the normal operation scenario, hydrogen peroxide was added continuously to the PJM cavern, which experiences continuous mixing from the PJMs. During idle sparging the hydrogen peroxide was mixed only within the PJM cavern, producing a somewhat higher gas generation rate there. At the same time, the slurry outside the cavern was not mixed, allowing more gas to accumulate. Even with this periodic spatial nonuniformity, gas generation was still effectively continuous and uniform overall.

For post-DBE and NTAR operation, however, the operation of the entire mixing system was intermittent. Because hydrogen peroxide could be added only while the mixing system operated, excess hydrogen peroxide had to be "spiked" during the short mixing period to provide gas generation during the idle-sparge period when mixing was off. Seven times the average flow of hydrogen peroxide solution would be required for a test with a 1-hour mixing period followed by a 6-hour idle-sparge, mixing-off period. Furthermore, the hydrogen peroxide solution was injected only for the first 55 minutes of the mixing period to ensure adequate mixing before starting the idle-sparge, mixing-off period. This increases the hydrogen peroxide flow rate to 7.6 times the average (i.e., a target injection rate of 382 mL/min under this regimen would provide an average of 50 mL/min of hydrogen peroxide solution for a 7-hour cycle).

The mixing-off times also had to be adjusted (shortened) to adequately simulate a constant gas generation rate during the post-DBE and NTAR operations. It was found that hydrogen peroxide decomposes fairly rapidly, and most of the excess injected during the mixing period was depleted long before the end of the 6-hour idle-sparge, mixing-off period. This would have resulted in an extended period of essentially static conditions with very low gas generation rates. To maintain an approximately uniform generation rate while achieving the desired maximum gas volume fraction, the idle-sparge, mixing-off period was shortened so the estimated gas generation rate at the end was roughly equal to the desired overall average. For HSLS test conditions, a 2-hour idle-sparge, mixing-off period was equivalent to the scaled 6 hours, as illustrated in Figure 9.2. The calculated gas generation rates for 2- and 6-hour mixing-off periods are compared in Figure 9.3.[(a)]

The two primary test results for the cyclic mixing operations were the maximum gas volume fraction, α_{MAX}, which occurs at the end of the mixing-off period, and the minimum gas volume fraction, α_{MIN}, which occurs at the end of the mixing period. However, the large gas generation rate resulting from the

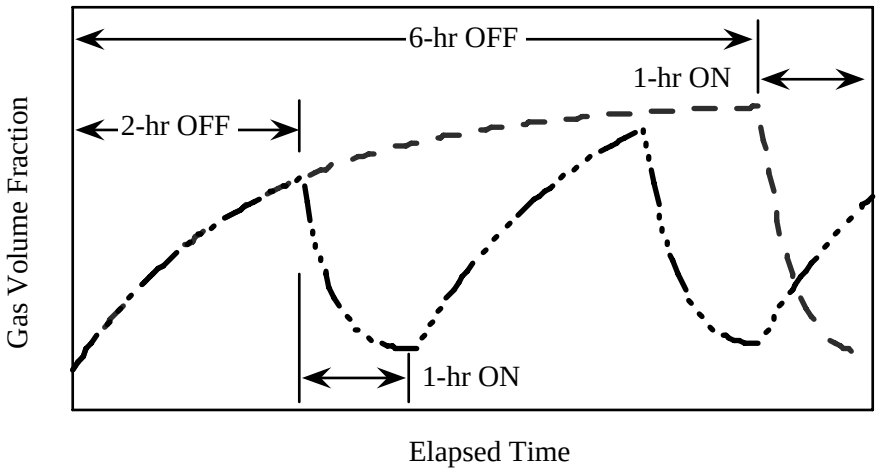

Figure 9.2. Strategy for Shortening the Off Period During Post-DBE and NTAR Testing

(a) An injection rate of 382 mL/min for 55 minutes of the shortened 3-hr cycle actually averages 116 mL/min, hence the last-cycle correction discussed in the next paragraph.

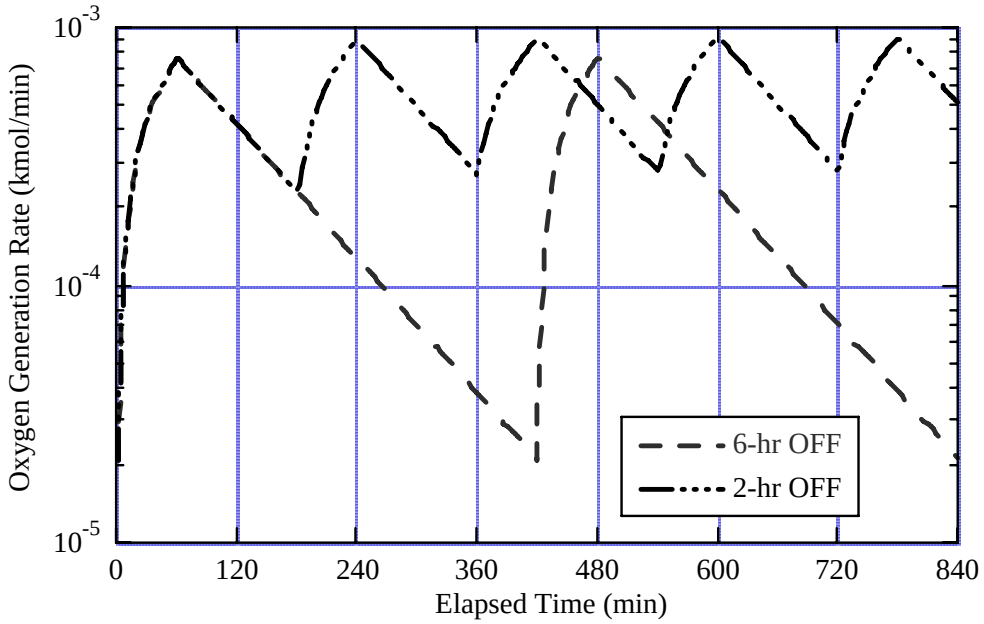

Figure 9.3. Oxygen Generation Rates for 2- and 6-hr Off Periods for Post-DBE Test

excess volume of hydrogen peroxide injected during the mixing period made α_{MIN} artificially large. To obtain the correct value of α_{MIN}, the hydrogen peroxide flow was reduced to the nominal target rate of 50 mL/min during the last mixing cycle after steady state was determined.

The gas volume fractions were calculated from the change in simulant volume derived from static surface level measurements and a level-volume relationship derived earlier by filling the tank with water. The calculation included manual measurements with a tape measure and automatically recorded data from laser level sensors. The calculated gas volume was corrected for the net volume change derived from changes in total tank weight due to hydrogen peroxide addition and evaporation.

9.2.3 Strategy for Mixing Tests

The objective of the mixing tests was to determine the unmixed volume and time to mix with full-flow sparging and PJMs at half-stroke and with full sparging only. Mixing was determined from the concentration of a chloride tracer (concentrated salt solution of ~20 to 25 wt% NaCl in water). To determine the chloride concentration, the aqueous phase was separated by centrifuging periodic grab samples of the clay simulant and analyzed using ion chromatography. Initially, the chloride tracer was introduced through the hydrogen peroxide injection lines, but this caused small amounts of chloride tracer to accumulate in the sparger heel and within the dead-volume of the pulse tubes during half-stroke operation. This problem was eliminated by adding tracer directly to the top of the simulant.

Each test began by mixing the tank completely for a minimum of two hours with PJMs at full stroke and spargers at full flow rate to homogenize and mobilize the simulant. Then the PJMs were turned off and the spargers switched to shutdown flow. A measured amount of chloride tracer salt solution was added to the simulant. After the tracer was added, the mixing system was started in the specified mode and periodic grab samples collected and analyzed to track the progress of the tracer through the simulant.

Grab samples were collected from four locations at three elevations using a 100-mL syringe mounted at one end of a long pipe that was guided to the appropriate location inside a fixed, 2-inch PVC tube. Grab samples were collected before the test started, approximately every 30 minutes for about 6 hours, and then every 1 to 2 hours. Samples were sent in batches of 16 to 24 for analysis, with a typical turnaround time of 12 hours. The chloride concentration versus time data were reviewed by the Steering Committee to determine whether an acceptable steady state was achieved or the test should be continued to further differentiate slow transients from analytical uncertainty in the data.

After the Steering Committee ascertained a steady state, the mixing mode was switched to PJMs at full stroke and spargers at full flow rate, and the tank was mixed for a minimum of 2½ hours while additional grab samples were collected every ½ to 1 hour. Final grab samples were then collected to determine the final chloride ion concentration with the simulant as fully mixed as possible.

9.3 HSLS Test Description and Results

The gas retention and release tests conducted in the HSLS vessel are summarized in Table 9.1 and the mixing tests in Table 9.2. The GR&R test series was completed before the mixing tests. The major tests are described and their results presented in Sections 9.3.1 through 9.3.5.

Table 9.1. HSLS Gas Retention and Release Tests

Test ID/Run	Engineering Purpose/Objectives	Configuration	Objective
HSLS-1, Run 1	Normal operations: Needed to make decision on removing recirculation mixing pumps from LS and blend vessels.	Holdup test with PJMs at ½ stroke + full sparging	1) Determine steady-state holdup for PJMs + full sparging
Run 2		Holdup test PJMs at ½ stroke + idle sparging	1) determine steady-state holdup for PJMs with idle sparging, 2) verify peroxide addition rate, 3) set start point for normal operation test
Run 3		Normal operation cycle	1) replicate intended normal operations, 2) demonstrate gas release by intermittent sparging, continuous PJMs, 3) demonstrate steady periodic behavior
HSLS-2, Run 1a	Post-DBE operations: Define sizing of backup ITS air compressors and diesel generators	Post-DBE operation cycle	1) replicate post-DBE operations, 2) demonstrate gas release by intermittent PJM/sparging, 3) demonstrate steady periodic behavior
Run 1b			Determine the alpha min (α_{min}) corresponding to a constant peroxide injection rate
HSLS-3, Run 1a	NTAR operations: Assess need for redundant racks, valves, compressors, and diesel generators for PJM operations.	NTAR operation cycle	1) replicate intended NTAR operations, 2) demonstrate gas release by intermittent sparging and no PJMs, 3) demonstrate steady periodic behavior
Run 1b			Determine the alpha min (α_{min}) corresponding to a constant peroxide injection rate
Run 2		Holdup test with full sparging only	Generate additional data to determine the gas holdup when only main spargers are operating.
HSLS-8	Gas release test	Gas release test: full sparging only	Obtain data on gas release with full sparging; estimate unmixed volume
HSLS-9	Gas release test	Gas release test: PJMs at ½ stroke + idle sparging	Obtain data on gas release with PJMs and spargers on idle; estimate unmixed volume

Table 9.2. HSLS Mixing Tests

Test ID/Run	Engineering Purpose/ Objectives	Configuration	Objective
HSLS-4, Run 1	Mixing runs: determine mixing times and quality of mixing	Full sparging only (high rheology ~45 Pa)	1) Determine mixing time with spargers only operating. 2) Determine unmixed heel volume. This run also had a long second step with PJMs at ½ stroke + full sparging
Run 2		PJMs @ ½ stroke + full sparging	Determine mixing time with PJMs and spargers operating.
Run 3		Full sparging only	1) Determine mixing time with spargers only operating. 2) Determine unmixed heel volume.
Run 4		Spargers only (repeat of Run 3)	1) Determine mixing time with spargers only operating. 2) Determine unmixed heel volume.
Run 5		Full sparging only (repeat #2 of Run 3)	1) Determine mixing time with spargers only operating. 2) Determine unmixed heel volume.
Run 6		PJMs @ ½ stroke + full sparging (variant of Run 2)	Determine mixing time with PJMs and spargers operating with dilution water and salt tracer added on top of simulant.

In addition to the tests summarized in Tables 9.1 and 9.2, a series of preparatory tests called HSLS-0 was performed to quantify some of the potential uncertainties inherent in calculating the gas volume fraction from changes in the simulant surface level and mass. The three main factors and results are described below.

- Simulant cakeout on tank walls and support structures. Continued deposition of clay simulant on tank walls and internals during testing could have had an adverse effect on the ability to measure gas fractions. HSLS-0 Run 0 determined the cakeout rate with PJMs at half-stroke and full sparging operating continuously for 6 hours starting with a relatively clean tank without hydrogen peroxide added. A static surface level measurement was made every 2 hours determined simulant volume. The cakeout mass was taken as the difference between the "live" simulant mass calculated from the volume and known density and the total simulant mass determined from the measured tank gross weight and empty weight. This and succeeding tests showed that the cakeout mass built quickly to a roughly constant value (1,000 to 1,200 lb), eliminating continuing simulant deposition as a problem in gas volume calculations.

- Retained gas due to PJMs and sparger operation. Retained air bubbles introduced by the PJMs and spargers could have influenced the measured gas fraction during the gas holdup and release tests, especially a long-term holdup of small bubbles. Therefore, initial gas holdup tests with no hydrogen peroxide injection determined the gas holdup for PJMs/full sparging (HSLS-0 Run 1), PJMs/idle sparging (HSLS-0 Run 2), and full sparging-only conditions (HSLS-0 Run 3). Each run lasted 3.5 to 5 hours with static levels measured at the start and approximately every 30 minutes throughout each run. The tests revealed a fluctuating but very repeatable short-term sparger holdup (i.e., present only during sparging) of approximately 0.5 vol% with full sparge air flow with or without PJMs operating. PJM operation did not appear to cause any short-term holdup and neither sparging nor PJMs produced a measurable long-term holdup.

- Water loss due to evaporation. During the HSLS gas holdup and mixing tests, water was lost from the tank due to evaporation and stripping by the sparger air. The rate of water loss was a function of the simulant temperature and the flow rate, temperature, and humidity of the sparger

air. Evaporation was investigated as part of each HSLS-0 test. Because the weight of simulant deposition or cakeout appeared to be approximately constant, and no long-term sparger or PJM holdup was present, net evaporation from both sparger air flow and from the simulant surface was fully accounted for in the tank weight. Later experience showed that evaporation was not negligible but roughly balanced by the hydrogen peroxide mass injected.

9.3.1 HSLS-1: Normal Operation Demonstration

The objective of HSLS-1 test was to demonstrate the normal operational cycle, which consists of continuous PJM operation at half-stroke with intermittent sparging at full air flow. The test had three runs, as follows:

- Run 1 verified that the planned ~90 mL/min hydrogen peroxide injection rate (actual flow averaged 94 mL/min) would create a measurable gas holdup when the PJMs and spargers were operating continuously.
- Run 2 established the holdup with continuous PJM and idle sparging with a hydrogen peroxide injection rate at ~90 mL/min.
- Run 3 demonstrated the actual normal operation cycle of ½ hour of full sparging followed by 1 hour of idle sparging (half-scale representation of 1 hour full sparging and 2 hours idle sparging in the plant) with the PJMs operating continuously at half-stroke. The hydrogen peroxide injection rate was continuous at ~90 mL/min.

Figure 9.4 plots the gas volume fraction versus time for the entire HSLS-1 test sequence. Both the gas volume fraction computed from the continuously recorded electronic simulant surface level data (solid line) and that recorded during static measurements with the spargers at idle and PJMs off (open circles) are shown.[(a)] The gas holdup during Run 1 (continuous PJMs and full sparging) varied from 0.22 to 0.41 vol% with an average of 0.36 vol% based on the last six static-level measurements. The short-term sparger holdup adds approximately 0.5 vol% to the gas fraction based on electronically recorded level data during this period. In Run 2 (continuous PJMs and idle sparging), the average steady-state gas holdup (α_{ss}) was 2.6 vol% based on the last six static level measurements. The gas volume fractions derived from static data match those from the electronic data in this run because sparger holdup was absent. During Run 3 (scaled normal operational cycle) the average minimum gas volume fraction (α_{MIN}) was 0.70 vol%, and the maximum average gas volume fraction (α_{MAX}) was 1.1 vol% based on the maximum and minimum static-level measurements for the last six cycles.

(a) Because of fluctuations in the sparger holdup, only static level measurements could be used for calculating steady-state holdup and the maximum and minimum gas volume fractions during cyclic operations. Only the gas volume fractions derived from static data will be shown in succeeding plots.

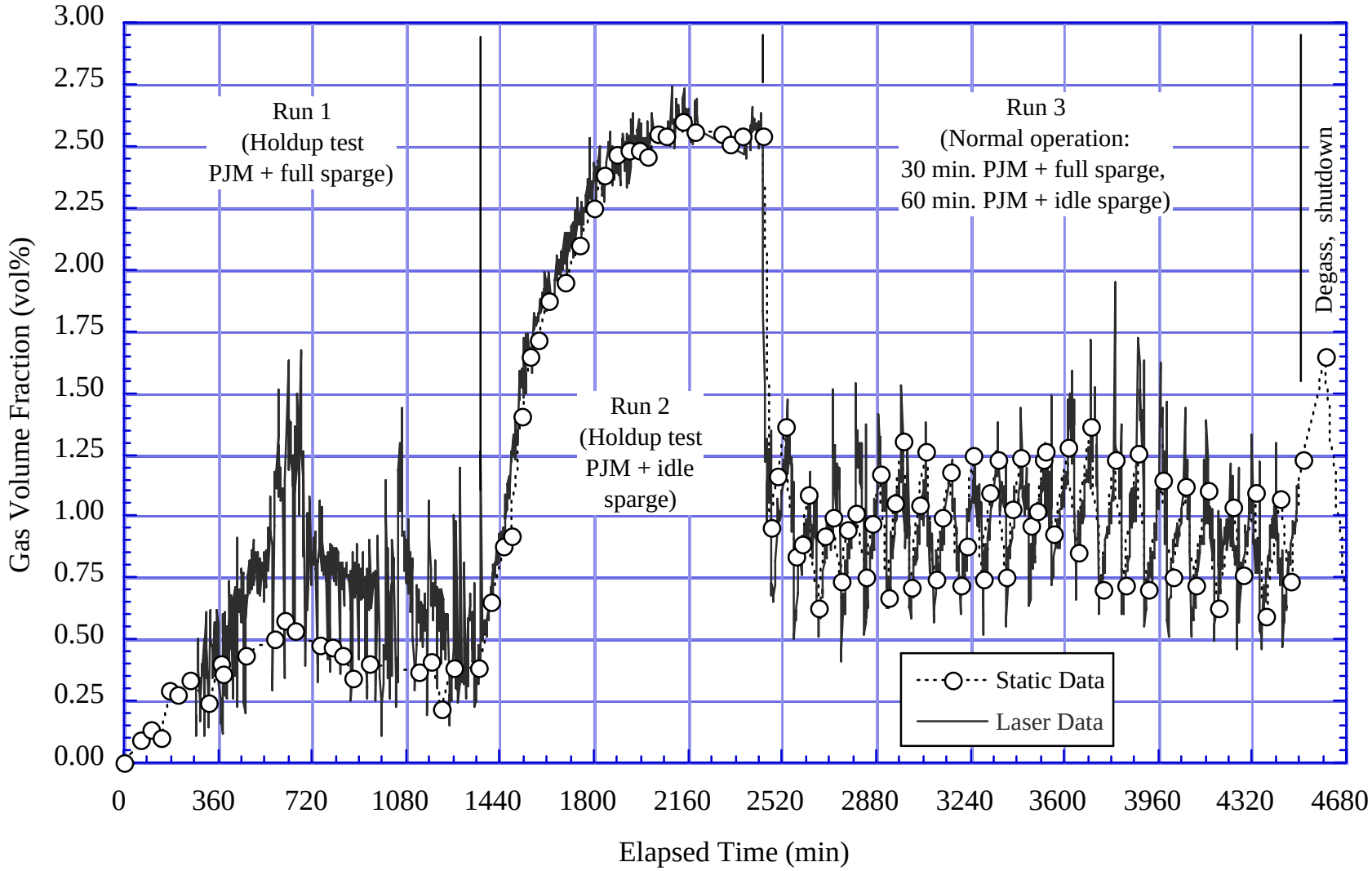

Figure 9.4. Gas Volume Fraction Versus Time for Entire HSLS-1 Test

9.3.2 Post-DBE Operations Demonstration

This test demonstrated the post-DBE operating cycle, which consists of intermittent PJM operation and sparge operation (2 hours full sparging and PJMs operating at half-stroke followed by 12 hours idle at plant scale). The scaled post-DBE cycle consisted of repeated cycles of 1 hr of full sparging and PJM operation followed by 2 hours of idle sparging (shortened from the scaled 6 hours as described in Section 9.1.2). Hydrogen peroxide was injected at ~382 mL/min during the first 55 min of the one-hour mixing period. After steady state was attained, the test concluded with a reduction in the hydrogen peroxide flow rate to 50 mL/min for one post-DBE mixing cycle to measure the correct α_{MIN}.

Figure 9.5 shows a plot of the gas volume fraction derived from static level measurements as a function of time during the HSLS-2 test. At 3751 minutes, the hydrogen peroxide flow rate was reduced to ~50 mL/min for one post-DBE cycle. The simulant was then degassed with full sparging and PJMs. The maximum gas fraction calculated from static levels (α_{MAX}) varied from 2.5 to 3.2 vol% with an average of 2.8 vol% based on the last 10 cycles. The minimum gas volume fraction (α_{MIN}) varied between 0.90 and 1.2 vol% with an average of 1.1 vol% based on the last 10 cycles. The final α_{MIN} measured during the last cycle with reduced gas generation was 0.6 vol%

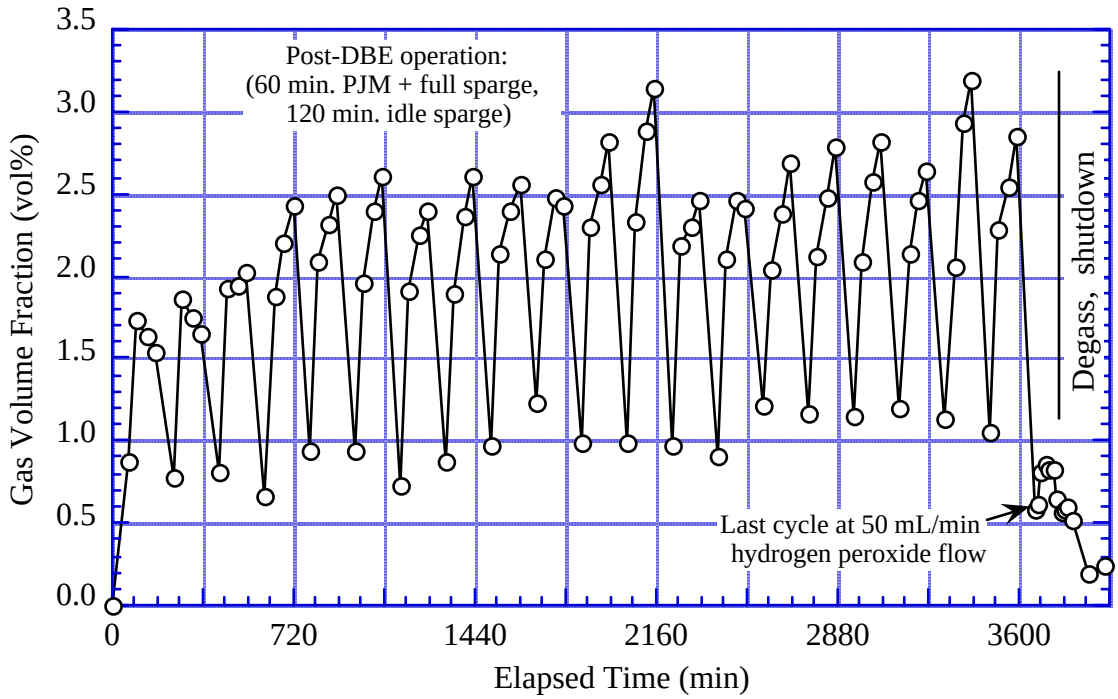

Figure 9.5. Gas Volume Fraction Versus Time for the HSLS-2 Test

9.3.3 NTAR Demonstration

The NTAR test demonstrated loss-of-PJM operating scenario, which consists of intermittent sparging (no PJM operation, full sparging for 2 hours, and idle sparging for 12 hours at plant scale). The scaled test used repeated cycles of 1 hour of full sparging followed by 2 hours (shortened from the scaled

6 hours discussed in Section 9.1.2) of idle sparging with hydrogen peroxide injected at ~382 mL/min during the first 55 minutes of each full sparging period. Eleven cycles were completed simulating 154 hours at full scale, over 150% of the 100 hours of planned NTAR operation. The last cycle was conducted with a reduced hydrogen peroxide flow of ~50 mL/min. The test concluded with a sparger only holdup run with a hydrogen peroxide flow rate of ~90 mL/min.

Figure 9.6 plots the gas volume fraction derived from static level measurements versus time for the entire HSLS-3 test. From 1980 to 2200 minutes elapsed time, an additional NTAR cycle was completed at a reduced hydrogen peroxide rate of 50 mL/min. At 2200 minutes, the hydrogen peroxide flow rate was increased to 90 mL/min with full sparging operation and continued until 3100 minutes. The maximum gas volume fraction (α_{MAX}) varied from 2.4 to 2.8 vol% with an average of 2.6 vol% based on the last three cycles. The minimum gas volume fraction (α_{MIN}) averaged of 1.3 vol% based on the last three cycles. The corrected (α_{MIN}) obtained in the last cycle with reduced gas generation is 0.87 vol%. The holdup test with full-flow sparging did not reach a steady state. The holdup during the last 10 cycles averaged less than 1 vol%.

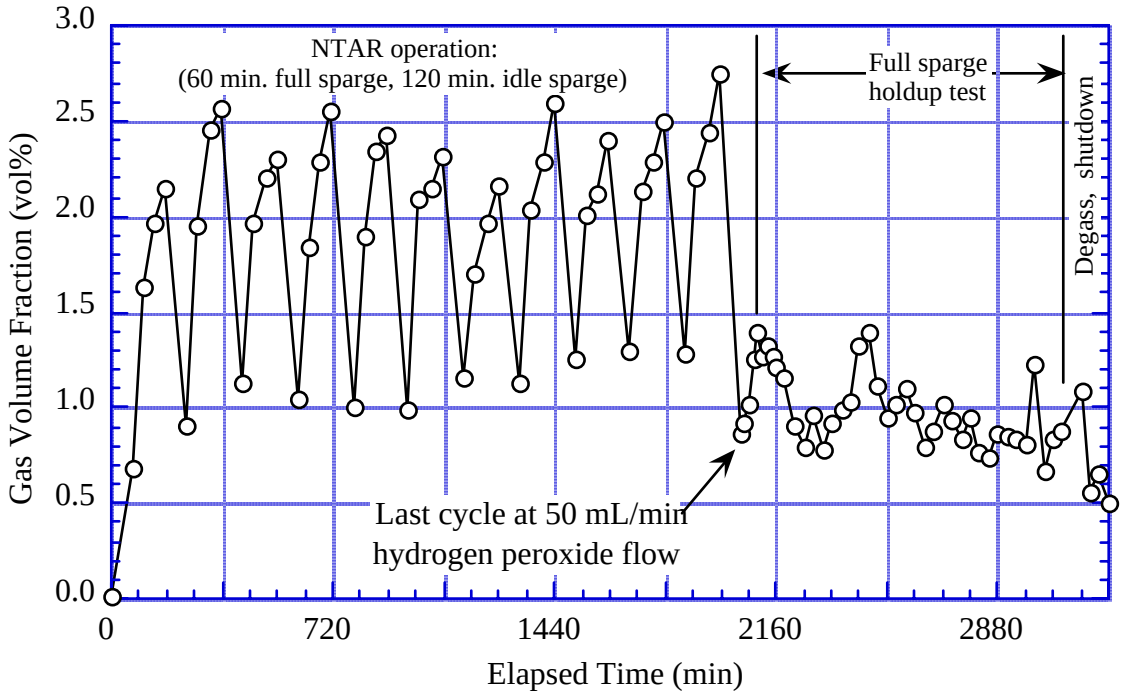

Figure 9.6. Gas Volume Fraction Versus Time for Entire HSLS-3 Test

9.3.4 Gas Release Tests

The HSLS-8 and 9 tests obtained gas release data with full sparging and with PJMs and idle sparging, respectively, to help define the unmixed sparger heel. The gas release test sequence was as follows:

- The simulant was mixed for 2 hours with PJMs and full sparging.

- Hydrogen peroxide was injected at ~200 mL/min for 2 hours while continuing PJMs and full sparging. The injection rate was increased to ~350 mL/min in HSLS-9 to provide a higher initial gas fraction.
- The mixing system was switched to shutdown sparging to allow gas to accumulate until a steady simulant level indicated most of the hydrogen peroxide had decomposed.
- Gas release was initiated with full-flow sparging (without PJMs) in HSLS-8, and PJMs operating at half-stroke with idle sparging in HSLS-9, for a minimum of 4 hours or until a steady simulant level indicated all gas was released.

Figure 9.7 presents the gas volume fraction versus elapsed time for both HSLS-8 and HSLS-9 gas release tests, including the mixing and gas growth periods. Based on the last four static level measurements taken just before the start of gas release, the initial gas volume fraction varied between 1.6 and 1.8 vol% with an average of 1.7 vol%. Gas release was quite rapid with full sparging only but incomplete due to lack of mixing in the sparger heel. The final gas fraction was 0.7 vol% based on the two static-level measurements at 344 and 374 minutes. The initial gas fraction for HSLS-9 averaged 3.8 vol%. The gas release rate induced by PJMs only was much slower than that due to sparging. At the time the test was terminated the average gas volume fraction was 0.4 vol%. But the long-term trend indicated that release would have been complete if carried on a few more hours.

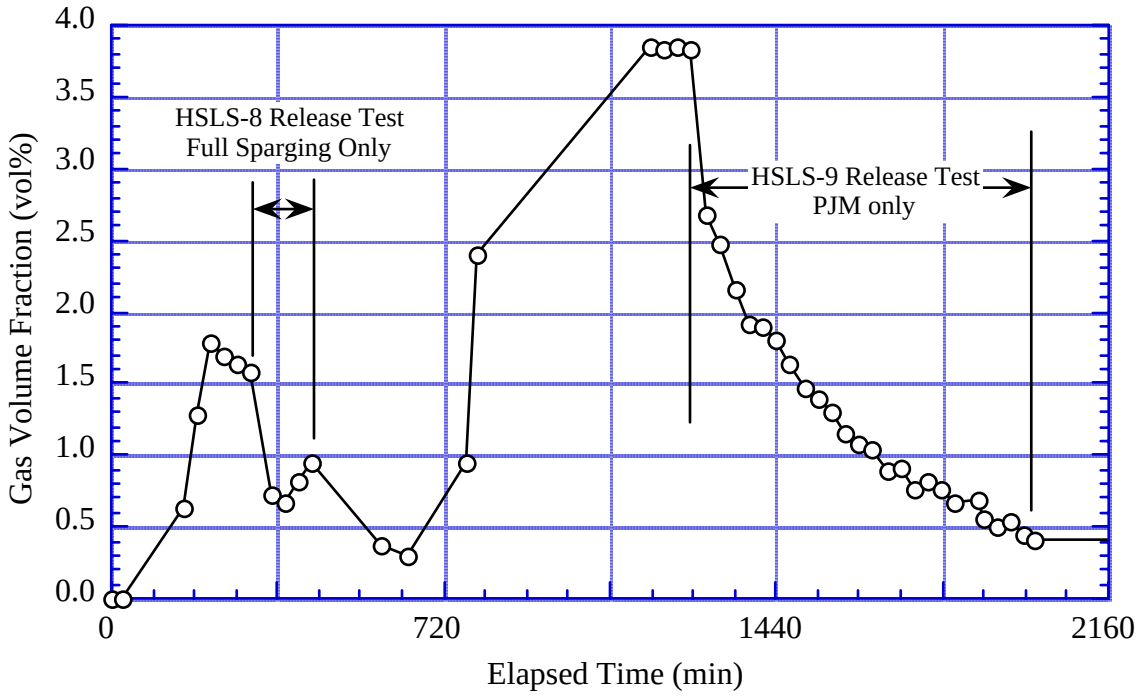

Figure 9.7. Gas Volume Fraction Versus Time for HSLS-8 and HSLS-9 Gas Release Tests

9.3.5 Mixing Tests

The objectives of the six mixing runs conducted during the HSLS-4 test were:

- Run 1: Determine time to mix and volume of the unmixed heel with only the spargers operating using a simulant with a yield stress of ~45 Pa and. Secondarily, determine whether the tank could be fully mixed with full sparging and PJMs operating at half stroke. Tracer added to PJM cavern through the hydrogen peroxide injection tubes.
- Run 2: Determine the time to mix and the effectiveness of mixing with PJMs operating at half stroke with full sparging (simulant yield stress reduced to ~35 Pa). Tracer was added to the PJM cavern through the hydrogen peroxide injection tubes.
- Run 3, 4, and 5: Determine the time to mix and the volume of the unmixed sparge heel with only full flow sparging using a simulant with a yield stress of ~34 Pa. Tracer was added to the simulant surface.
- Run 6: Determine the time to mix and the effectiveness of mixing of a low density material added to the top of the tank with the PJMs operating at half stroke with full sparging.

In addition, Runs 1 and 2 were conducted with a deep simulant above the top of the pulse tube domes (H/D = 0.93) and the rest with the simulant level in the cylindrical section below the pulse tube domes (H/D = 0.81).

The mixing test results are summarized in Table 9.3. The percent mixed is defined such that tracer concentrations greater than the final tracer concentration in the homogenized simulant result in percent mixed values less than 100%. Tracer concentrations greater than the final concentration occur in regions where the initial concentrated tracer is being mixed into regions of lower concentration. Tracer

Table 9.3. Summary of Mixing Results

Run	Time to 95% Mixed (hr)	Unmixed Volume (%)		Simulant H/D	Simulant Volume (L)[a]	Yield Stress (Pa)	Consistency (cP)
		MB	IC				
Spargers only on full flow							
1	> 5	ND[b]		0.93	35960	47	41
3	23-28	34	34	0.81	31460	38	34
4	5	39	38	0.81	31610	34	31
5	> 6	42	34	0.81	31630	34	31
PJMs @ half-stroke with full-flow sparging							
1	NA	6	6	0.93	35960	47	41
2	5	0	0	0.93	35850	35	35
6	9	0[c]		0.94	36270	34	33

(a) There are some differences between the simulant volume and the H/D due to round-off error.
(b) An unmixed volume estimate could not be determined because the test did not run long enough to reach a steady-state condition.
(c) Both the mass balance and IC approaches suggested there may have been some tracer that was not well mixed at the end of the run.

concentrations less than the final concentration occur in regions where the concentrated tracer has not yet arrived and result in apparent percent mixed values greater than 100%. The vol% mixed results are calculated two ways. In the "IC approach" the final chloride concentration is the average obtained from the IC analyses. In the "mass balance" approach the final chloride concentration is calculated from a mass balance on the known amount of tracer added. The time to mix is defined as the time required for the chloride ion concentration to reach and remain between 95 and 105% of the final equilibrium value, as determined using the log variance approach. Mixing times corresponding to 90 and 95% mixed are provided. Given the considerable variability in the results, the time to mix is rounded off to the nearest hour. There was some evidence of an unmixed volume in run 1 that is thought to be due to a slug of simulant moving up and down in the pulse tubes.

An example of the progress of mixing with spargers only is shown for HSLS-4, Run 5 in Figure 9.8. The volume percent mixed rises close to its final value of ~66% in two hours though it continues to vary such that the criterion for mixing time was not yet met at the end of the run in 6 hours. The unmixed simulant volume is thought to reside in the pulse tubes and in a sparge heel below the spargers. Final mixing with full sparging plus PJMs operating at full stroke quickly reached 100% mixed.

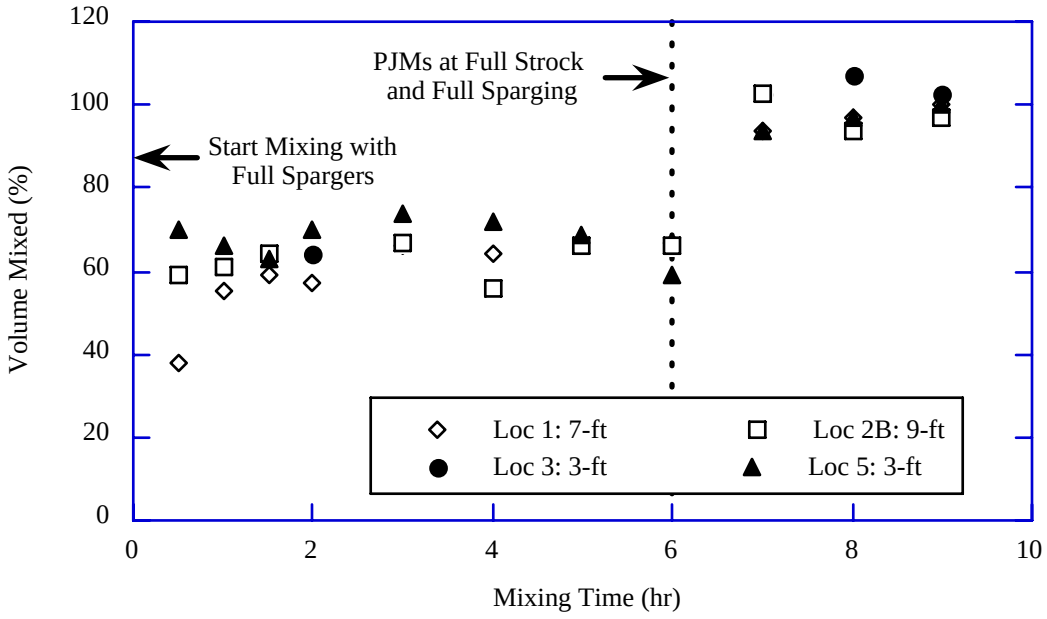

Figure 9.8. Volume Mixed Versus Time for HSLS-4, Run 5

9.4 Conclusions

The HSLS tests demonstrated and confirmed the performance of cyclic intermittent mixing for normal operations, post-DBE operations and the NTAR scenario. In each test a repeating periodic state was achieved with moderate fluctuations of the maximum and minimum cyclic retained gas volume fractions. Mixing was reestablished early in each mixing cycle, and the retained gas accumulated during the off cycle was released with no measurable long-term buildup.

Mixing tests showed that full-flow sparging mixed over 60% of the simulant volume with an unmixed heel on the order of 35%, including the PJM pulse tube volume. Mixing with both full-flow sparging and PJMs operating at half-stroke provided essentially 100% mixing. Mixing times ranged from 5 to 25 hours. In one mixing run with thick clay (~45 Pa yield stress), there was some evidence of an unmixed volume in the pulse tubes that were operating at half-stroke.

These tests also provided a firm technical basis from which to apply the scaling principles described in Section 3 to predict full-scale plant operation. This process is described in Section 10.

10.0 Scale-up to Plant Conditions

This section describes how the results of the HSLS tests and earlier tests of a 1:4.9-scale UFP vessel (Russell et al. 2005) can be applied to predict GR&R and mixing behavior at full plant scale. The GR&R scale-up process uses a gas mass conservation model fit to the HSLS test data and based on scaling relationships derived from the basic principles of gas bubble dynamics. Estimates of the unmixed volume and full-scale mixing times derived from HSLS tests are also given for the LS vessel. Estimates of the mixing times for the full scale UFP are derived from tests in the 1:4.9-scale UFP vessel (Johnson et al. 2005).

10.1 Scaling Model for Gas Retention and Release

The fundamental scaling assumption for GR&R is that the retained gas exists as relatively small, discrete bubbles whose behavior is determined by the condition of the simulant or waste slurry independent of scale. This assumption allows the scaling laws for gas holdup and release to be embodied in a gas inventory model that is the vehicle for analyzing the HSLS data and applying the scaling principles to predict full-scale plant behavior. It is based on global conservation of the total number of moles of gas existing as bubbles in the slurry. An additional conservation equation is needed to track the mass of hydrogen peroxide used to generate oxygen gas to analyze test data. This model is fit to the HSLS data in a Monte Carlo uncertainty analysis as the precursor to actual scale-up calculations.

10.1.1 Gas Inventory Model

During a test, hydrogen peroxide accumulates in the simulant until it is balanced by the increasing decomposition rate and resulting gas generation. The mass of unreacted hydrogen peroxide in the simulant must be tracked. Assuming the gas bubbles in the slurry consist only of oxygen, and all the oxygen in the simulant is generated by hydrogen peroxide decomposition with no losses to the atmosphere, finite difference conservation equations for hydrogen peroxide mass, W_p, and moles of oxygen gas retained, N_g, at time t_2 as a function of conditions at t_1 are expressed as

$$W_p(t_2) = W_p(t_1)e^{-2A_g(t_2-t_1)} + \frac{x_p \rho_{ps} Q_{ps}}{2A_g}\left[1 - e^{-2A_g(t_2-t_1)}\right] \tag{10.1}$$

$$N_g(t_2) = N_g(t_1)e^{-A_R(t_2-t_1)} + \frac{\bar{W}_p A_g}{M_p A_R}\left[1 - e^{-A_R(t_2-t_1)}\right] \tag{10.2}$$

where

A_g = hydrogen peroxide decay rate constant (1/min)
x_p = mass fraction of hydrogen peroxide in the injected solution
ρ_{ps} = density of the hydrogen peroxide solution (g/mL)
Q_{ps} = volumetric flow rate of the injected solution (mL/min)
A_R = gas release rate constant (1/min)
M_p = molecular weight of hydrogen peroxide (34 g/mole)

$\overline{\overline{W}}_p$ = the integral time average mass of hydrogen peroxide between t_1 and t_2, given by

$$\overline{\overline{W}}_p = \frac{x_p \rho_{ps} Q_{ps}}{2A_g} - \frac{W_p(t_2) - W_p(t_1)}{2A_g(t_2 - t_1)} \tag{10.3}$$

For simulating plant-scale operations using an assigned constant molar gas generation rate, G_m, a simplified version of Eq. (7.20) is used without having to solve for the hydrogen peroxide mass, as follows:

$$N_g(t_2) = N_g(t_1)e^{-A_R(t_2-t_1)} + \frac{G_m}{A_R}\left[1 - e^{-A_R(t_2-t_1)}\right] \tag{10.4}$$

The average gas volume fraction in the slurry is calculated from the number of moles of gas and slurry volume by the ideal gas law as follows:

$$\alpha = \frac{N_g}{V_{bs}}\frac{RT}{p} = \frac{1}{\frac{V_s}{N_g}\frac{p}{RT} + 1} \tag{10.5}$$

where

V_{bs} = the volume of bubbly slurry (L)
V_s = the total volume of gas-free slurry (L)
R = the gas constant (0.08206 L-atm/gram-mole-K)
T = the average slurry temperature (K)
p = the average gas pressure (atm).

10.1.2 Fitting the Model to HSLS Data

The gas release and gas generation rate constants, A_g and A_R in Eq. (10.1) and (10.2), were determined from HSLS test data by minimizing the sum of the squared difference between the predictions of the gas volume fractions from Eq. (10.2) and (10.5) and those calculated from simulant levels and tank weights recorded during the tests. Estimates for the two constants, A_g and A_R, were developed to represent each of the four operation modes of the HSLS tests (see Section 9.3). Constants for the PJMs + full sparge mode were derived from HSLS-1 Runs 1 and 3, and HSLS-2 data, constants for the PJM + idle sparge mode from HSLS-1, Run 3. HSLS-3 provided constants for the full-sparge-only mode, and constants for the idle-sparge mode were derived from HSLS-2 and HSLS-3 data. The four gas release rate constants (hydrogen peroxide decomposition rate constants are not needed) derived from the HSLS data are the primary variables that are scaled up for plant-scale predictions (Section 10.2).

The values of the four rate constants from the error minimization solution capture both the measurement uncertainty and variability of the data recorded from the tests. Measurement uncertainties were propagated through the gas inventory model using a Monte Carlo simulation. This simulation calculated 10,000 sets of gas volume fractions for all data points from corresponding realizations of the uncertainty distributions of the five level measurements (four laser readings and one manual tape

measurement) and tank weight. The least-squares error minimization fit the gas inventory model to each of these 10,000 data sets produced an uncertainty distribution of the gas release rate constants and hydrogen peroxide decomposition rate constants. The 95% confidence range of the gas release rate constant distributions are listed in Table 10.1, and histograms are shown in Figure 10.1.

Table 10.1. Gas Release Rate Constants Derived from HSLS Test Data

Mode	Gas Release Rate Constant, A_R (1/min)		
	2.5th percentile	**Median**	**97.5th percentile**
PJM + Full Sparge	0.0398	0.0478	0.0611
PJM + Idle Sparge	0.0111	0.0158	0.0248
Full Sparge	0.0353	0.0445	0.0578
Idle Sparge	0.0055	0.0071	0.0092

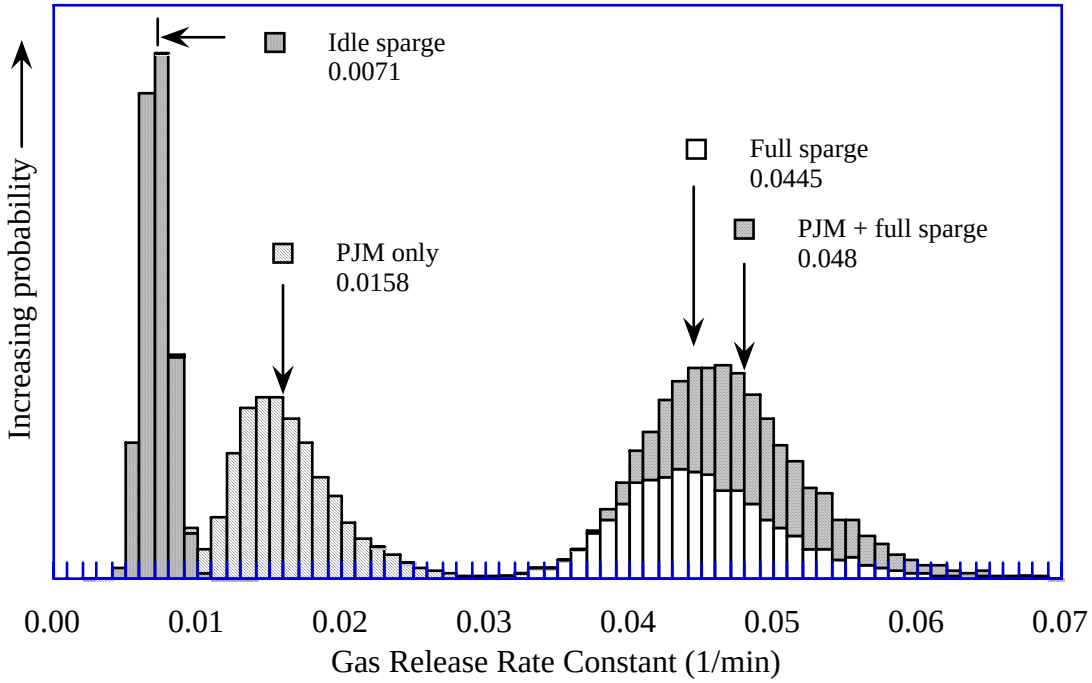

Figure 10.1. Histogram of Gas Release Rate Constants from HSLS Data

No independent data set is available to formally validate the model for the kinds of cyclic operations used in the HSLS tests. However, the fact that a single set of four constants fit the data in three different tests serves as reasonable validation that the gas inventory model captures the dominant physical processes occurring during the tests. The RMS errors in gas volume fraction for HSLS-1, -2, and -3 using these four constants were 0.09, 0.24, and 0.17 vol%, respectively, using these four values of the constant A_R. The corresponding R^2 values of the least squares fit were 0.81, 0.89, and 0.93, respectively. An example of the comparison of model predictions and the data for the HSLS-2 test is shown in Figure 10.2.

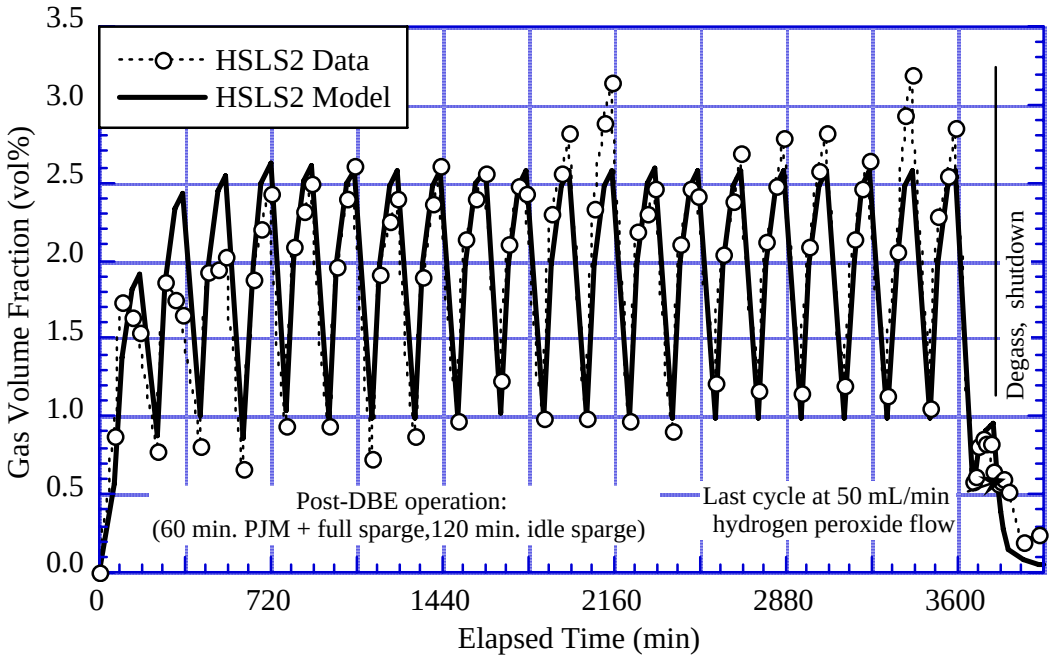

Figure 10.2. Comparison of Gas Inventory Prediction with HSLS-2 Data

10.2 Scale-up Methodology

Statistical analysis of the HSLS test data produced probability distributions for gas release rate constants representing four mixing modes: PJMs and full sparging, PJMs and idle sparging, full sparging only, and idle sparging only. This section describes a methodology to scale up these four parameters and apply them via the mass balance model to predict plant-scale GR&R behavior incorporating both the uncertainty in the reduced data and the uncertainty in the scaling process itself. Section 10.2.1 applies to the LS/blend vessels using HSLS data directly, and Section 10.2.2 extends this method to scale-up calculations for the UFP vessel for which no large-scale test data are available.

10.2.1 Scale-up Method for the LS/Blend Vessel

The gas release rate constants are equal to U_R/H, the empirical bubble rise velocity at the surface, U_R, divided by the simulant depth, H. If U_R were constant, the full-scale gas release rate constants would be inversely proportional to the scale factor, S (ratio of plant vessel to test vessel linear dimension). That is,

$$\left(\frac{U_R}{H}\right)_{plant} = \left(\frac{U_R}{H}\right)_{test}\left(\frac{H_{test}}{H_{plant}}\right) = \left(\frac{U_R}{H}\right)_{test} S_{test} \qquad (10.6)$$

However, the accumulated ¼ and ½ scale test data show that U_R varies with both slurry yield stress and the product of volumetric gas generation rate and simulant depth, $g_v H$. Additional calculations are postulated to account for these effects before Eq. (10.6) is applied.

Four gas holdup tests in the APEL 4PJM vessel had nearly the same gas generation rates with variations only in simulant rheology. The bubble rise velocity in these tests did not appear to be correlated to the consistency factor but clearly decreased with the yield stress, τ_y, according to

$$U_{R,4PJM}(\tau_y) = 0.3347 - 0.003587\tau_y \tag{10.7}$$

The bubble rise velocity obtained in a test, $U_{R,test}$, with a simulant with yield stress τ_{test} can be assumed related to plant conditions with a slurry of yield stress τ_{plant} by a factor, F_τ, equal to the ratio of $U_{R,4PJM}$ calculated from Eq. (10.7) at the two values of yield stress, or

$$U_{R,plant} = U_{R,test}F_\tau = U_{R,test}\frac{U_{R,4PJM}(\tau_{plant})}{U_{R,4PJM}(\tau_{test})} \tag{10.8}$$

The correction F_τ is uncertain because the relation between yield stress and U_R seen in the APEL 4PJM tests may not apply elsewhere, the consistency factor likely has a stronger effect on U_R than the APEL 4PJM data show, and bubbles may behave differently in waste slurry than in clay of the same rheology. This uncertainty may be at least partially captured by recasting F_τ in the following form:

$$F_\tau = 1 + C_\tau\left[\frac{U_{R,4PJM}(\tau_{plant})}{U_{R,4PJM}(\tau_{test})} - 1\right] \tag{10.9}$$

where C_τ is a constant with values following a normal distribution from zero (no influence of yield stress on U_R) to 2 (twice the effect of yield stress as derived from APEL 4PJM data) with a mean of 1 (same effect as APEL 4PJM data).

Bubble rise velocities derived from ¼-scale holdup tests in several vessels increase with both gas generation rate and slurry depth. Figure 10.3 plots U_R, adjusted to a 30-Pa yield stress using Eq. (10.8), versus the product, (g_vH), of the volumetric gas generation rate, g_v, and slurry depth, H. These data imply that linear extrapolation at the same slope, m, can be applied to determine the bubble rise velocity for plant-scale conditions, $U_{R,plant}$, from that derived from the test result, $U_{R,test}$, by

$$U_{R,plant} = U_{R,test} + m\left[(g_vH)_{plant} - (g_vH)_{test}\right] \tag{10.10}$$

where the slope, m, follows a normal distribution with mean and standard deviation equal to that of the four tests shown in Figure 10.3, truncated at ± three standard deviations. Extrapolation of U_R from the HSLS test (shown as X on the plot) using the mean and the upper and lower limits of the slope result in the range of bubble rise velocities for the plant-scale LS vessel (shown by "+" on the plot).[(a)] The uncertainty in the slope results in a relatively small variation in the result because the extrapolation from the half-scale data is short.

(a) In the figure, the plant-scale gas generation rate was 0.0336 L/L-day.

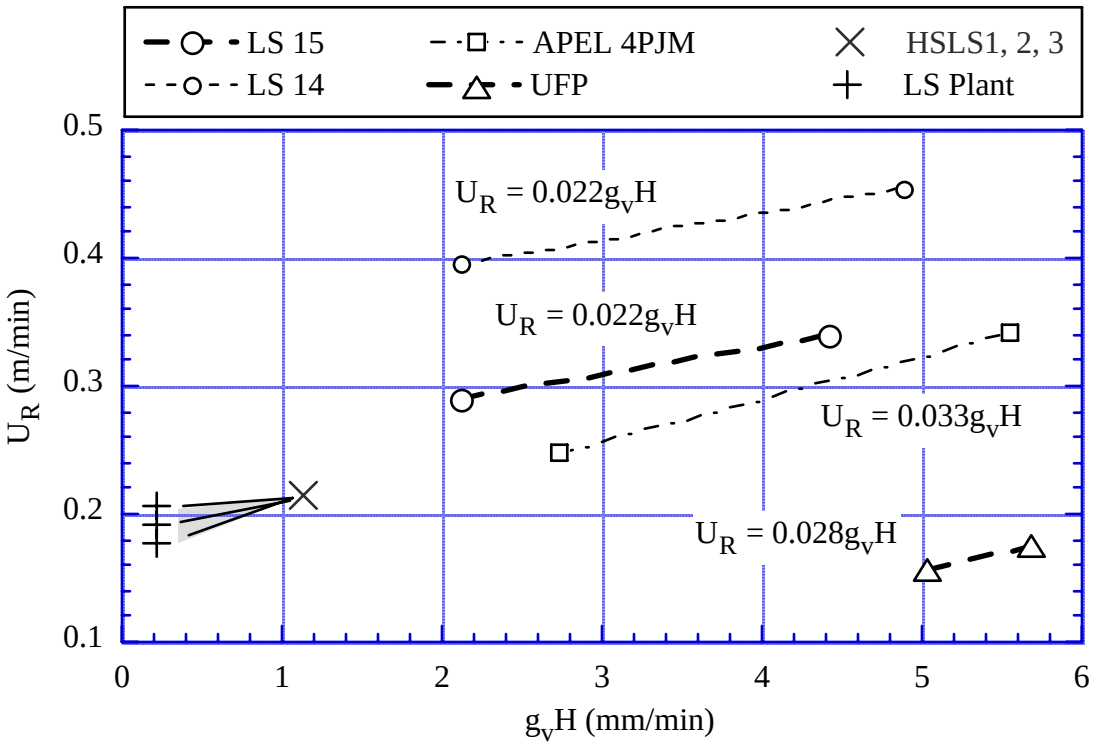

Figure 10.3. Variation of U_R Versus Gas Generation and Depth

The last but possibly largest source of uncertainty in scaling up the HSLS tests results to full-scale is the potentially different gas retention behavior of clay versus waste slurry containing an anti-foaming agent (AFA) and of bubbles with a significant fraction of hydrogen (generated by radio-thermal processes in the waste) versus bubbles with a large fraction of oxygen (generated by hydrogen peroxide decomposition in the tests).

The difference between clay simulant test results and actual waste behavior is accommodated in the scale-up calculation by dividing the final result of the foregoing calculations by a bubble rise velocity reduction factor, F_W. Since the value of F_W is unknown at this time, it is appropriate to represent it by a uniform probability distribution with a range from X to Y (bubble rise velocity in clay tests is X to Y times than in actual waste). Available evidence suggests that $X \cong 1$ and $Y > 1$ (Bontha et al. 2005).

Combining Eq. (10.9) and (10.10) with Eq. (10.6), and including the F_W factor yields an expression describing the overall scale-up calculation for the gas release rate constant is expressed as

$$\left(\frac{U_R}{H}\right)_{plant} = \left\{\begin{array}{l}\left(\frac{U_R}{H}\right)_{test}\left(1+C_\tau\left[\frac{U_{R,4PJM}(\tau_{plant})}{U_{R,4PJM}(\tau_{test})}-1\right]\right) \\ +m\left[(g_vH)_{plant}-(g_vH)_{test}\right]\end{array}\right\}\frac{S_{test}}{F_W} \qquad (10.11)$$

Finally, because there are gas release rate constants for four operating modes to scale up, it is more convenient to apply Eq. (10.11) to only one of them and compute the rest by the ratio of their test values. Applying Eq. (10.11) to scale up the largest rate constant, that of PJMs + full sparge (P+S), the (U_R/H) values for the other three modes (PJMs + idle sparging, full sparging only, and idle sparging only) can be computed by

$$\left(\frac{U_R}{H}\right)_{plant,other} = \left(\frac{U_R}{H}\right)_{plant,P+S} \frac{\left(\frac{U_R}{H}\right)_{test,other}}{\left(\frac{U_R}{H}\right)_{test,P+S}} \tag{10.12}$$

where the $(U_R/H)_{test,other}$ are output distributions from the Monte Carlo simulation for data reduction described in Section 10.1 (see Table 10.1 and Figure 10.1).

The actual plant-scale predictions of minimum and maximum gas volume fractions are made by using the scaled-up gas release rate constants above as input to the gas inventory model. For plant-scale predictions the model can be simplified considerably because gas generation rates are constant, and tracking the hydrogen peroxide inventory is not required. Only the gas inventory and gas volume fraction Eq. (10.4) and (10.5) must be solved. Also, because the gas inventory equation is closed, it need only be evaluated at the end points of the operating cycle, where the gas release rate constant changes to reflect different operating modes. It is recommended that the initial gas volume fractions for the post-DBE and NTAR simulations be set at the last α_{MAX} value from the normal operations calculation.

To obtain a scale-up prediction correctly incorporating all the uncertainties described above, it is recommended that a Monte Carlo simulation be performed where Eq. (10.11) and (10.12) are applied for each of the 10,000 sets of gas release rate constant data produced by the HSLS data uncertainty analysis, while values of the scale-up extrapolation parameters are chosen from their respective distributions. This will provide 10,000 sets of nine output values, α_{MAX}, α_{MIN}, and $\alpha_{MAX} - \alpha_{MIN}$, at the repeating steady state for normal operations and post-DBE and at the 100-hour point for the NTAR scenario. The 97.5th percentile from each distribution, which is the upper bound of the 95% confidence interval, is a standard level of conservatism recommended as the reported value.

10.2.2 Extension to UFP Vessel Scale-up

The method for scaling up test results for the UFP vessel would follow the same procedure as the LS vessel except that no data are available for a half-scale or other large-scale test that include the cyclic operation planned for the WTP. The only data representing the UFP tank were produced by steady-state holdup tests in a 1:4.9 scale prototype. The difference in scale, as well as the gas generation rate used in the test, greatly increases the distance the data must be extrapolated.

The available UFP test data also lack representative cyclic operation in the four operating modes designed for the plant. However, assuming the uncertainties and the relationships between the gas release rate constants are similar, the results of the LS scale up analysis can be applied to the small-scale UFP

data. Realizations of the nominal gas release rate constant, A_R, from UFP test data can be developed from the HSLS uncertainty analysis by the relationship:

$$\left(A_{R,UFP}\right)_{MC} = \left(A_{R,HSLS}\right)_{MC} \frac{\left(A_{R,UFP}\right)_{med}}{\left(A_{R,HSLS}\right)_{med}} \tag{10.13}$$

where

$(A_{R,UFP})_{MC}$ = realization of A_R for UFP scale-up analysis
$(A_{R,HSLS})_{MC}$ = realization of A_R from LS Monte Carlo analysis
$(A_{R,HSLS})_{med}$ = median value of A_R from recorded HSLS data (0.048 1/min for PJM + full sparging, 0.0159 1/min for PJM + idle sparging)
$(A_{R,UFP})_{med}$ = median value of A_R from recorded UFP data (A_R = 0.102 1/min from ~¼ scale UFP tests).

Assuming that the UFP small-scale test represented the PJM plus full sparger mode, the ratio of UFP to HSLS in Eq. (10.13) is

$$(A_{R,UFP})_{med}/(A_{R,HSLS})_{med} = 0.102/0.048 = 2.1$$

However, it is unclear whether the small-scale UFP test best represents the PJM + full sparging or the PJM + idle sparging operating mode. In the latter case, the ratio would be

$$(AR,UFP)data/(AR,HSLS)data = 0.102/0.0159 = 6.4$$

In an attempt to gain some insight, the four nominal A_R values from the HSLS tests were back-extrapolated using the same methods as the forward extrapolation in the LS scale-up calculation and compared to values derived from the ¼ scale UFP data. The comparison implies that the UFP tests probably fall somewhere between the two HSLS modes. To account for this uncertainty, the UFP/HSLS factor can be given a uniform distribution between 2.1 and 6.4 in the Monte Carlo scale-up analysis. Besides this additional uncertainty distribution, the method of analysis for UFP scale-up follows Eq. (10.11) and (10.12).

10.3 Scale-up of Mixing Results

Scale-up principles for predicting mixing times based on small-scale test results were applied to the data from the HSLS tests to predict plant-scale mixing times for the LS vessel. Mixing time scaling principles were developed and reported by Bamberger et al. (2005) for PJM operation and by Poloski et al. (2005) for sparger operation. The mixing time model described scaling of a dimensionless mixing time $t_m u_o/d_o$, where t_m, u_0, and d_0 are mixing time, nozzle velocity, and nozzle diameter, respectively. In accordance with these principles, the mixing times at plant scale should be twice those calculated for the test and the fraction of simulant volume unmixed should be the same as determined from the test.

Since mixing tests were conducted with continuous operation with a given mixing mode, the cyclic nature of the full-scale plant operations complicates the scale-up of mixing test results because the intermittent periods must be accounted for. The mixing times and unmixed volumes were determined in

the HSLS tests only for continuous operation in two modes, 1) full-flow sparge-only; and 2) PJMs operating at half-stroke with full-flow sparging. During intermittent normal operation, for example, the actual mixing time would be three times that of continuous operation of PJMs at half-stroke with full sparging if mixing in the sparger-only mode is discounted (the factor of 3 is the inverse of the one-third duty cycle for this mode). Allowing some credit for the sparge-only period, the mixing time would be less than three times that of combined mode. Also, because the mixing time is greater than the cycle period, the average unmixed volume should be between the values predicted for these two operating modes.

The scaled up mixing results for continuous operations plant scale are summarized in Table 10.2. The unmixed sparge heel at full scale is estimated to be 34 to 38% at H/D = 0.81, corresponding to unmixed volumes of 85,000–97,000 L of waste. Mixing times for sparger-only operation are estimated to be 10 to 50 hours at full scale (twice the result of the 1/2-scale test). For PJM operation at half-stroke with spargers, the unmixed volume in the vessel is estimated to be in the range of 0 to 6% or 0 to 17,260 L. This unmixed volume is assumed to be inside the PJMs. Mixing times for half-stroke PJMs and spargers are expected to be on the order of 10 hours at full scale; blending (homogenization) times for the addition of dilute liquid on top of the vessel contents are expected to be greater than 18 hours at full scale.

Table 10.2. Summary of Mixing Results Applied to Full-Scale LS

Time to 95% mixed (hr)	Unmixed volume (%)	Simulant H/D	Unmixed Volume (L)	Yield stress (Pa)	Consistency (cP)
Spargers only on full flow					
10-50	34-38	0.81-0.93	85000-97000	34-47	31-41
PJMs @ half stroke with full flow sparging					
10	0-6	0.93	0-17260	35-47	35-41
>18 (blend time)	0	0.94	0	34	33

A mixing test conducted with a chemical tracer was performed in the UFP scaled prototype (scale factor of 4.3) with PJMs operating at full-stroke (peak average nozzle velocity of 11.3 m/s) and full flow sparging (Johnson et al. 2005). The kaolin-bentonite clay simulant was used at an H/D of 1.4. The time to mix was less than 15 minutes as defined by the first sampling event. Mixing times generally increase with the geometric scale factor so the time to mix in the full scale vessel is estimated to be less than 75 minutes.

11.0 References

Bamberger JA, PA Meyer, JR Bontha, CW Enderlin, DA Wilson, AP Poloski, JA Fort, ST Yokuda, HD Smith, F Nigl, M Friedrich, DE Kurath, GL Smith, JM Bates, and MA Gerber. 2005. *Technical Basis for Testing Scaled Pulse Jet Mixing Systems for Non-Newtonian Slurries.* WTP-RPT-113 Rev. 0 (PNWD-3551), Battelle – Pacific Northwest Division, Richland, Washington.

Bates JM, JW Brothers, JM Alzheimer, and DE Wallace. 2004. *Test Results for Pulse Jet Mixers in Prototypic Ultrafiltration Feed Process and High-Level Waste Lag Storage Vessels*. WTP-RPT-110 Rev. 0 (PNWD-3496), Battelle – Pacific Northwest Division, Richland Washington.

Bontha JR, JM Bates, CW Enderlin, and MG Dodson. 2003. *Large Tank Experimental Data for Validation of the FLUENT CFD Model of Pulsed Jet Mixers.* PNWD-3303, Battelle – Pacific Northwest Division, Richland, Washington.

Bontha JR, CW Stewart, DE Kurath, PA Meyer, ST Arm, CE Guzman-Leong, MS Fountain, M Friedrich, SA Hartley, LK Jagoda, CD Johnson, KS Koschik, DL Lessor, F Nigl, RL Russell, GL Smith, W Yantasee, and ST Yokuda. 2005. *Technical Basis for Predicting Mixing and Flammable Gas behavior in the Ultrafiltration Feed Process and High-Level Waste Lag Storage Vessels with Non-Newtonian Slurries*. WTP-RPT-132 Rev. 0, Battelle – Pacific Northwest Division, Richland, Washington.

Edward PL, VA Atiemo-Obeng, and SM Kresta (eds.). 2004. *Handbook of Industrial Mixing—Science and Practice*, Ch. 4. Wiley and Sons, New York, pp. 167–178.

Enderlin CW, MG Dodson, F Nigl, J Bontha, and JM Bates. 2003. *Results of Small-Scale Particle Cloud Tests and Non-Newtonian Fluid Cavern Tests*. WTRPT-078 Rev. 0 (PNWD-3360), Battelle – Pacific Northwest Division, Richland, Washington.

Flury M and NN Wai. 2003. "Dyes as tracers for vadose zone hydrology." *Reviews of Geophysics*. 41(1):1002.

Gauglitz PA, SD Rassat, PR Bredt, JH Konynenbelt, JM Tingey, and DP Mendoza. 1996. *Mechanisms of Gas Bubble Retention and Release: Results for Hanford Waste Tanks 241-S-102 and 241-SY-103 and Single-Shell Tank Simulants.* PNNL-11298, Pacific Northwest National Laboratory, Richland, Washington.

Guerrero HN and KR Eberl. 2004a. *Final Report – Hybrid-Mixing Tests Supporting the Concentrate Receipt Vessel (CRV-VSL-00002A/2B) Configuration*. WSRC-TR-2004-00398 Rev. 0 (SRNL-RPP-2004-00060 Rev. 0), Savannah River National Laboratory, Aiken, South Carolina.

Guerrero HN and KR Eberl. 2004b. *Final Report – Gas Retention and Release Tests Supporting the Concentrate Receipt Vessel (CRV-VSL-00002A/2B) Configuration*. WSRC-TR-2004-00399 Rev. 0 (SRNL-RPP-2004-00062 Rev. 0), Savannah River National Laboratory, Aiken, South Carolina.

Johnson MD, JR Bontha, and JM Bates. 2003. *Demonstration of Ability to Mix in a Small-Scale Pulse-Jet Mixer Test Facility.* WTP-RPT-077 Rev. 0 (PNWD-3273), Battelle – Pacific Northwest Division, Richland, Washington.

Johnson MD, MA Gerber, JR Bontha, AP Poloski, RT Hallen, SK Sundaram, and DE Wallace. 2005. *Hybrid Mixing System Test Results for Prototype Ultrafiltration Feed Process and High-Level Waste Lag Storage Vessels*. WTP-RPT-128 Rev. 0, Battelle – Pacific Northwest Division, Richland, Washington.

Poloski AP. 2004. *Technical Basis for HLW Vitrification Stream Physical and Rheological Property Bounding Conditions*. WTP-RPT-100 Rev. 0, Battelle – Pacific Northwest Division, Richland, Washington.

Poloski AP, PA Meyer, LK Jagoda, and PR Hrma. 2004a. *Non-Newtonian Slurry Simulant Development and Selection for Pulsed Jet Mixer Testing.* WTP-RPT-111 Rev. 0 (PNWD-3495), Battelle – Pacific Northwest Division, Richland, Washington.

Poloski AP, LA Snow, and ST Arm. 2004b. *Chemical Tracer Techniques for Assessing Mixing Performance in Non-Newtonian Slurries for WTP Pulsed Jet Mixer Systems.* WTP-RPT-121 Rev. 0 (PNWD-3494), Battelle – Pacific Northwest Division, Richland, Washington.

Poloski AP, ST Arm, JA Bamberger, B Barnett, R Brown, BJ Cook, CW Enderlin, MS Fountain, M Friedrich, BG Fritz, RP Mueller, F Nigl, Y Onishi, LA Schienbein, LA Snow, S Tzemos, M White, and JA Vucelik. 2005. *Technical Basis for Scaling of Air Sparging Systems for Mixing in Non-Newtonian Slurries*. WTP-RPT-129 Rev. 0 (PNWD-3541), Battelle – Pacific Northwest Division, Richland, Washington.

Rassat SD, LM Bagaasen, LA Mahoney, RL Russell, DD Caldwell, and DP Mendoza. 2003. *Physical and Liquid Chemical Simulant Formulations for Transuranic Wastes in Hanford Single-Shell Tanks.* PNNL-14333, Pacific Northwest National Laboratory, Richland Washington.

Russell RL, SD Rassat, ST Arm, MS Fountain, BK Hatchell, CW Stewart, CD Johnson, PA Meyer, and CE Guzman-Leong. 2005. *Final Report: Gas Retention and Release in Hybrid Pulse Jet-Mixed Tanks Containing non-Newtonian Waste Simulants*. WTP-RPT-114 Rev. 1 (PNWD-3552), Battelle – Pacific Northwest Division, Richland, Washington.

Smith GL and K Prindiville. 2002. *Guidelines for Performing Chemical, Physical, and Rheological Properties Measurements.* 24590-WTP-GPG-RTD-001 Rev. 0, Bechtel National, Inc., Richland, Washington.

Speers RA, KR Holme, MA Tung, and WT Williamson. 1987. "Drilling fluid shear stress overshoot behavior." *Rheologica Acta,* Vol. 26, pp. 447-452.

Steffe JF. 1996. *Rheological Methods in Food Process Engineering*, 2nd Edition. Freeman Press. Available online at: http://www.egr.msu.edu/~steffe/freebook/offer.html.

Stone ME. 2005. *Yield Stress Reduction of Radioactive Waste Slurries by Addition of Surfactants.* WSRC-MS-2005-00097, Savannah River National Laboratory, Aikin, South Carolina.

Sundar PS. 2004. *Gas Retention and Release Tests in Non-Newtonian Simulants at the Florida International University in Support of the WTP Project.* 24590-PTF—RPT-RT-04-0005 Rev. 0, Bechtel National Inc., Richland, Washington.

Tilton HN and TWF Russell. November 29, 1982. "Designing Gas-Sparged Vessels for Mass Transfer." *Chemical Engineering,* pp. 61-68.

Wilson DA, ML Restivo, HN Guerrero, TJ Steeper, RE Eibling, EK Hansen, TM Jones, and KR Eberl. November 2004. *One-Eighth-Scale Pulse Jet Mixer (PJM) - Design Parameters Scale Law Testing.* WSRC-TR-2004-00430 Rev. 0 (SRNL-RPP-2004-00069 Rev. 0), Westinghouse Savannah River Company, Aiken, South Carolina.

Distribution

No. of Copies

OFFSITE

1 Savannah River National Laboratory
Richard Edwards
Savannah River National Laboratory
Westinghouse SA
Aiken, SC 29808-0001

No. of Copies

ONSITE

20 Battelle – Pacific Northwest Division

S. T. Arm	P7-28
J. R. Bontha	K6-24
M. Friedrich	K5-16
M. S. Fountain	P7-27
C. E. Guzman-Leong	K5-22
L. K. Jagoda	K6-24
C. D. Johnson	K6-96
D. E. Kurath	P7-28
K. S. Koschik	J2-09
P. A. Meyer	K7-15
F. Nigl	K7-15
R. L. Russell	K6-24
G. L. Smith	H4-02
C. W. Stewart	K7-15
W. Yantasee	K8-93
S. T. Yokuda	K7-15
Project Office (2)	P7-28
Information Release (2)	K1-06

7 Bechtel National, Inc.

H. A. Abodishish	H4-02
S. M. Barnes	H4-02
A. S. Bronner	H4-02
C. E. Corriveau Jr.	H4-02
J. C. Deckers (2)	H4-02
D. E. Larson	H4-02